Co-Channel Signal Separation Using Coupled Digital Phase-Locked Loops

by

Brad Allen Hedstrom
M.A.Sc., University of Victoria, 1989
B.S.E.E, University of Wyoming, 1986

A Dissertation Submitted in Partial Fulfillment of the Requirements for the Degree of

DOCTOR OF PHILOSOPHY

in the Department Electrical and Computer Engineering

We accept this dissertation as conforming to the required standard

Dr. R. Lynn Kirlin, Supervisor (Department Electrical and Computer Engineering)

Dr. Wu Sheng Lu, Department Member Department Electrical and Computer Engineering

Dr. Warren Little, Department Member Department Electrical and Computer Engineering

Dr. Inna Sharf, Outside Member (Department of Mechanical Engineering)

Dr. Wojciech J. Kolodziej, External Examiner (Oregon State University)

University of Victoria

Supervisor: Dr. R. Lynn Kirlin

Abstract

Side effects of frequency reuse are discussed, particularly co-channel interference in scalar measurement FM systems. Continuous and discrete time state-space models for multiple source angle modulated communications environments are developed and coupled digital phase-locked loop (CDPLL) estimator structures are derived based on the Extended Kalman Filter (EKF). Separability of two sources is investigated by examination of state observability and by simulations of the derived estimators. The relationship between the EKF and the CDPLL is presented and their linear and nonlinear behavior discussed. Acquisition and tracking characteristics are simulated and results presented. The new estimator is compared to related efforts found in the literature. The effects of time-varying signal multiplicity is briefly treated. An example of polarization diversity for frequency reuse (vector measurement) is also presented and is shown to be adequately modeled by the derived communications model.

Examiners

Dr. R. Lynn Kirlin, Supervisor (Department Electrical and Computer Engineering)

Dr. Wu Sheng Lu, Department Member Department Electrical and Computer Engineering

Dr. Warren Little, Department Member Department Electrical and Computer Engineering

Dr. Inna Sharf, Outside Member (Department of Mechanical Engineering)

Dr. Wojciech J. Kołodziej, External Examiner (Oregon State University)

Table of Contents

List of Tables

List of Figures

Acknowledgements

I would like to thank my supervisor, Dr. Kirlin, for talking me into staying at UVic after I completed my Master's. In addition to his guidance on this project, I would also like to thank him for providing me the opportunity to pursue other interests: giving me my first taste of consulting, including me in the DREP towfish project, working with him on the new and improved random signals course, and allowing me to teach microprocessor systems course for two summers—all of which detracted time away from my dissertation. The occasional "How's your research coming?" kick in the pants also helped.

I would also like to thank the Faculty of Graduate Studies for awarding me the University Fellowship for three years. Without it, I would not have been able to stay at UVic and complete my Doctorate.

Finally I would like to thank Dr. Stuchly for having enough faith in me to allow me to teach the fourth year microprocessor systems course. It has proven to be a very valuable experience.

Dedication

To Carole and Dane...

...it's finally time for me to get a "real" job now!

1. Introduction

The bandwidth allotted to mobile radios and mobile telephones has become insufficient to keep pace with demand [1]. As the air traffic around the world's major airports increases, it becomes increasingly difficult to track and separate their radar reflections. Submarine propellers are being designed to operate much quieter than in the past, making it more difficult to track them with sonar. As radio-astronomers peer to the edges of the known universe, separating distinct radio sources pushes the detection instrumentation to the limits due to the minute apparent spatial separation and the infinitesimal power levels.

On the surface these examples appear quite distinct and unrelated, however each may be reduced to the problem of spectral and spatial estimation. The estimation of temporal phases and of directions of arrival of multiple narrowband sources is one of the recent research topics in beamforming, tracking, and array signal processing. A number of spectral estimation methods have been developed which are based on the eigendecomposition of the covariance matrix of the received signal [2]. These methods yield good results, however they assume stationary statistics and their computational overhead is quite high. This makes them unlikely candidates for real-time applications.

A new method for tracking multiple narrowband sources which uses an array of coupled digital phase-locked loop pairs has recently been proposed [3]. Implementation of the digital phase-locked loop generally produces comparatively low computational burden, unlike modern eigendecomposition-based spectral estimation methods. Thus this new method facilitates the real-time implementation of a system which can continuously track both bearing angles and temporal phases of multiple uncorrelated sources.

1.1. Motivation: Mobile Cellular Communication

Mobile communications, especially mobile telephony, has experienced rapid growth during the last decade and the rate of growth is expected to increase well into the next century [1]. Current commercial mobile radio and telephone systems are primarily analog; however, the next generation of cellular technology will most probably be "digital" [4, Ch. 1]. The general assumption in the communication community is that digital transmission is to be the vehicle by which many of the current limitations on mobile telephony will be solved.

One phrase abounds in the current mobile communication literature: *spectral efficiency.* The bandwidth of wireless communication is inherently bounded by the "usable regions" of the electromagnetic spectrum. This finite resource is further restricted by regulatory bodies which parcel out bits and pieces to the various competing entities which each require "more Megahertz" [1]. A case in point is the first commercial American cellular system which was installed in Chicago in 1983 and by 1984 had saturated some of its cells [4]. The United States Federal Communications Commission (FCC), as well as regulating bodies in other countries, have been slow to release additional spectrum for cellular use. There are also technological limits. With current analog cellular technology's spectral efficiency, approximately 600 MHz of bandwidth would be required to support a 20% penetration level in a typical large metropolitan area [4]. Since all of the usable spectrum cannot be allocated for mobile radio and telephony, greater spectral efficiency is required.

It was this need for spectral efficiency that motivated the development of cellular mobile radio [5, Ch. 13]. One method of increasing the capacity of fixed number of channels is by re-using the same channels in different locations. Thus a geographical area is divided into cells; each cell operating in a particular portion of the total allocated spectrum. Adjacent cells necessarily use non-overlapping channels but cells which are separated by some distance may use the same channels (See Fig. 1–1). However, there are a few consequences of this method of frequency reuse.

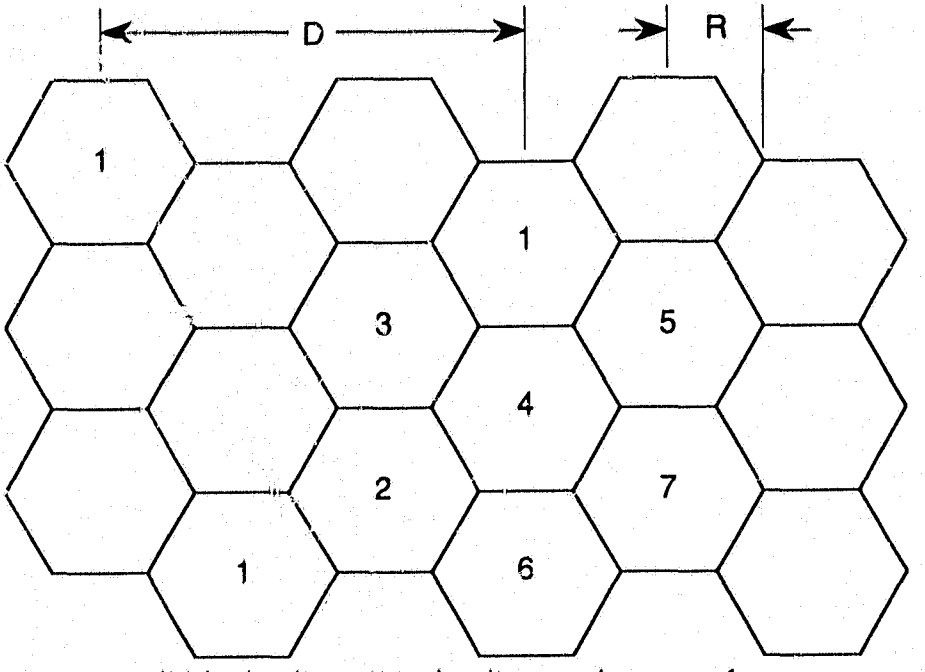

Figure 1–1 Basic cell block where *D* is the distance between frequency re-use cells and *R* is the radius of each cell [6].

Considering that the primary users of cellular are mobile, one of the most obvious ramifications of cellular division is maintaining communications with a mobile while it moves from cell to cell. Since adjacent cells operate on different channels, a mobile must be released from the cell it is leaving and be picked up by the cell it is entering. This process, known as *hand-off*, is carried out by a mobile switching center which determines to which cell to hand-off the mobile. There is a substantial amount of overhead in this operation [4, Ch. 4].

Cellular topologies also suffer from two related types of interference that have plagued wireless communication since its conception. *Adjacent channel interference* (ACI) is a result of energy in one channel leaking into a spectrally proximate channel (See Fig. 1–2a). *Co-channel interference* (CCI) is a similar phenomenon except that the leakage is from a transmitter in the same channel (see. Fig. 1–2b). The level of ACI and of CCI increases as the spectrum becomes more crowded, a result of increased spectral efficiency. This makes cellular an *interference limited* system [4, Ch. 9].

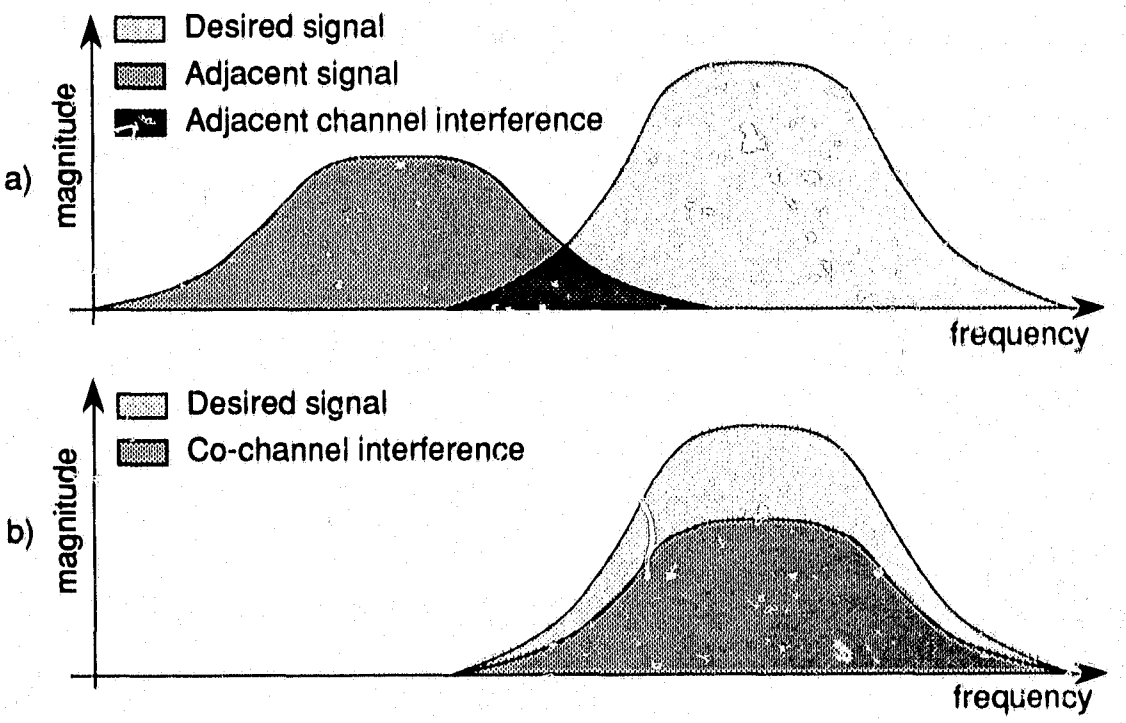

Figure 1–2 Adjacent and co-channel interference.

Bearing in mind this interference bound on frequency reuse, it becomes evident that large technical as well as economic gains may be realized if the effective levels of ACI and CCI can be reduced. The technical benefits would be in the form of higher quality transmission due to reduced levels of interference. This would allow greater spectral utilization since the channels could be packed closer together which is economically advantageous. Digital transmission tends to be less affected by interference than its analog counterpart. This is partly due to the inherent quantization and coding of digital transmission; an interfering signal will be perceived as noise, not as an intelligible signal. The net effect of the interference is to increase the bit error rate (BER) of the desired signal [4, Ch. 9]. Therefore emphasis is on digital communications systems.

1.2. Problem Formulation

We have shown the need for reduced ACI and CCI in the cellular communications scenario. These same types of interference manifest themselves in other applications as well. ACI and CCI are present in nearly every form of wireless communication as well as tracking applications like sonar arrays and radar systems. The problem can be generalized to the separations of signals in space and time. In signal processing terminology, this is referred to as spatial and temporal (or spatio-temporal) spectral estimation.

Two common examples of spatial estimation are sonar arrays and radar tracking stations. In each case the position of an object relative to the observer is desired. In the case of these two applications, the position is usually determined by the target's range and bearing (see Fig. 1–3). Sensors may be broadly classed as active or passive. An active system transmits a signal to and then receives a signal from the target. The range or distance may be estimated by the echo time. A passive system "listens" for signals emitted by or reflected from the target and estimates the bearing, or *angle of arrival* (AOA), by the relative phases of the wavefront at each of the sensors. Thus the sensor array acts as a spatial aperture or window through which the target may be "seen" via spectral estimation techniques.

Temporal spectral estimation differs little from spatial spectral estimation except that the spatial aperture is replaced by a temporal aperture usually implemented as a delay line. The same basic spectral estimation techniques used to find range and bearing in the spatial window can be used to find frequency and phase information in the temporal window. Thus spectral estimation provides the framework to separate signals in space and time be they airplanes tracked by radar, submarines tracked by sonar, or mobile telephones moving around a cellular network.

The previous two decades have seen a great deal of interest in spectral estimation theory with attendant improvements over "classical" spectral estimation [2, Ch. 1]. The cost of these "modern" techniques is in their complexity. Whereas classical Fourier transform techniques

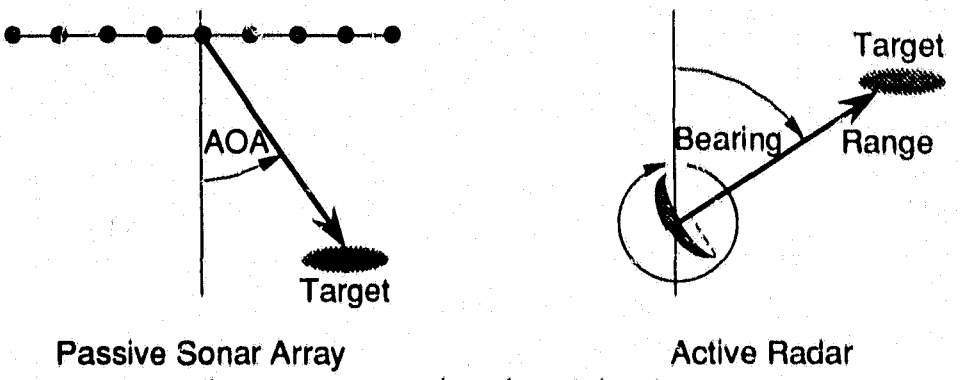

Figure 1–3 Examples of spatial estimators.

exhibit a computational complexity $O(N \log_2 N)$ where N is the number of samples comprising the aperture, recent methods based on covariance matrix eigenstructure evince relative complexity of $O(N^3)$ [2, Ch. 14]. This makes many of these new methods ill-suited for real-time applications.

Kirlin [7] has derived a maximum likelihood (ML) multiple source tracker which was formulated in the phase-locked loop (PLL) context. Two important ideas resulted in this work: 1) a computationally feasible receiver/detector and 2) a link between the well developed PLL theory and eigenstructure-based spectral estimation methods. The former facilitates implementation and can be directly mapped onto specific application areas. The latter allows PLL theory to facilitate the analysis of difficult problems like resolution, detection probability, and error variance in eigenstructure methods [7].

Although Kirlin's CPLL tracker has been shown to realize ML temporal and spatial spectral estimation, there remain many unsolved problems, especially when particular application areas (e.g. mobile cellular) are investigated.

1.3. Related Work in the Literature

The novelty in Kirlin's development lies in the "utilization of the well-developed theory of PLL's" [7] to derive a ML temporal and spatial spectral estimator. The majority of PLL theory that has been developed during the last thirty years is found in such classical reference

texts as Viterbi [8], Stiffler [9], Gardner [10], and Lindsey [11]. However, PLL's are inherently non-linear making their complete analysis difficult for low-order loops and nearly impossible for higher order loops. Much of the performance analysis is done by linearizing the loop's characteristics around the steady-state or locked operating point. This linearization is not valid during the capture or lock-in time. These classical references also treat only analog PLL's; digital phase-locked loop (DPLL) theory is still maturing. The last ten to fifteen years have seen a shift from analog implementation to digital implementation in nearly every type of technology from household appliances to automobiles. Telecommunications is certainly no exception. Therefore prime emphasis is placed on DPLL's in this work.

The problem of signal separation, be it separating a signal from unwanted noise or resolving multiple, interfering signals in space and time, is one of the fundamental aspects of signal processing. Equivalent problems are often cloaked in the guise of unrelated applications. A review of relevant articles in the literature provides a background for this project.

Kirlin and Su [3] have shown that two cross-coupled digital phase-locked loops (CDPLL) can track multiple narrowband sources impinging on an M element, uniform linear array, $[s_1(t) \quad s_2(t) \quad \cdots \quad s_M(t)]$. In this formulation, one PLL tracks the temporal phase ϕ of the source and the other PLL tracks the spatial bearing θ producing phase and bearing estimation errors ψ_ϕ and ψ_θ respectively (see Fig. 1–4). The Numerically Controlled Oscillator (NCO) then generates local estimate of the signal present at each sensor, $[\tilde{s}_1(t) \quad \tilde{s}_2(t) \quad \cdots \quad \tilde{s}_M(t)]$. By cascading multiple CDPLL pairs, multiple narrowband sources can be separated and tracked; each source is tracked by one CDPLL pair and its local estimates may be subtracted from the inputs to the other CDPLL pairs (see Fig. 1–5).

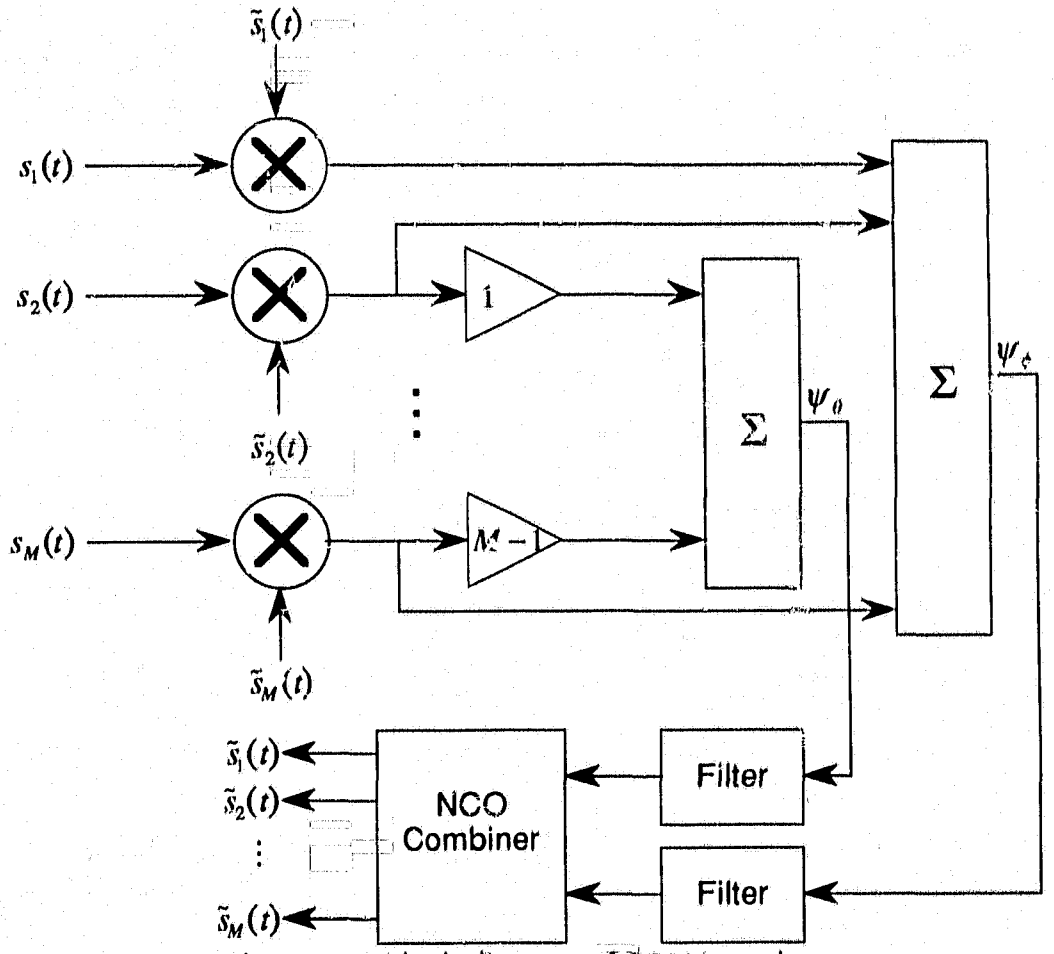

Figure 1–4 Block diagram of CDPLL tracker.

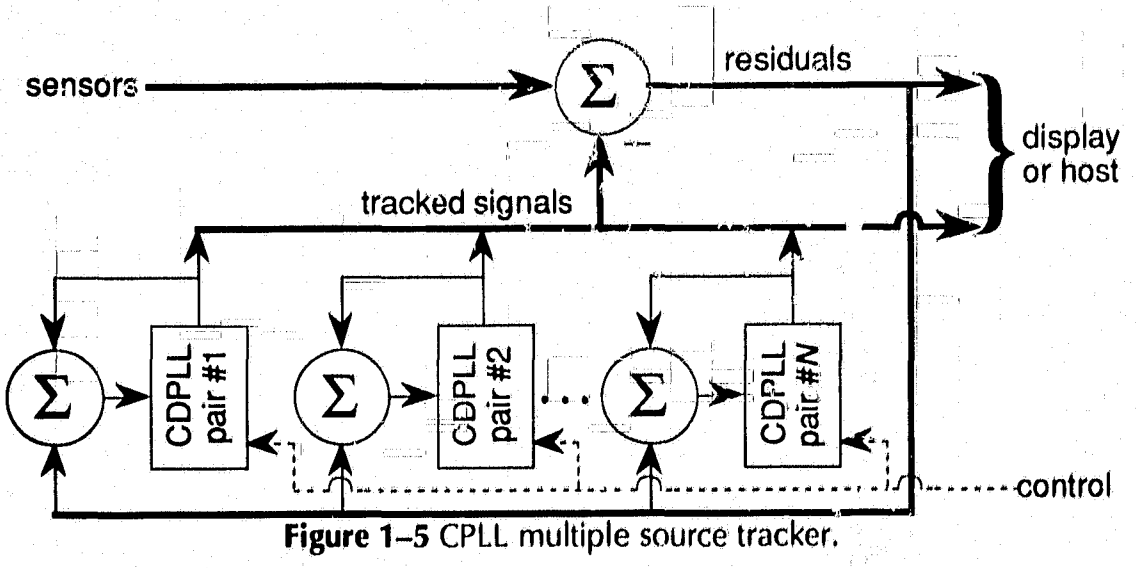

Figure 1–5 CPLL multiple source tracker.

Kirlin and Su also studied the performance of the CDPLL pair when implemented with a zero-crossing digital phase-locked loop (ZC-DPLL). Expressions for stability, convergence, noise bandwidth, and signal to noise ratio (SNR) of the linearized CDPLL where derived. Several two-signal baseband test cases were simulated for various loop parameters and initial conditions. All simulations compared favorably with established eigenstructure-based methods.

A similar problem has recently been treated by Parker and Anderson [12]. In this scenario, a nonsinusoidal periodic signal is tracked by estimating its fundamental frequency and its first m harmonics, both amplitude and phase. The estimator then follows the amplitudes and phases as they change over time. The estimator is based on the Extended Kalman Filter (EKF) and in certain situations, may be realized by CPLL's. This method differs from Kirlin's in that N harmonics of a single frequency are estimated as opposed to estimating N signals with unrelated frequencies. Thus some of the assumptions made in [12] are not valid for general signal separation which implies that Parker and Anderson's method is a special case of that proposed by Kirlin.

The method proposed by Kirlin is very similar to the receiver proposed by Cassara *et al.* [13, 14, 15, 16] to reduce interchannel interference in frequency modulation (FM) receivers. Here an optimal receiver is derived from maximum *a posteriori* (MAP) estimation theory. This optimal receiver is realized by two coupled analog phase locked loops. In this case the scalar measurement r is composed of the desired signal and an adjacent or co-channel interferer. Each loop locks on to and tracks one of the signals whose estimate is then canceled from the input to the other PLL (see Fig. 1–6). Since the measurement is scalar, no spatial estimation is carried out. Thus Cassara's FM receiver is a special case of Kirlin's multiple source tracker.

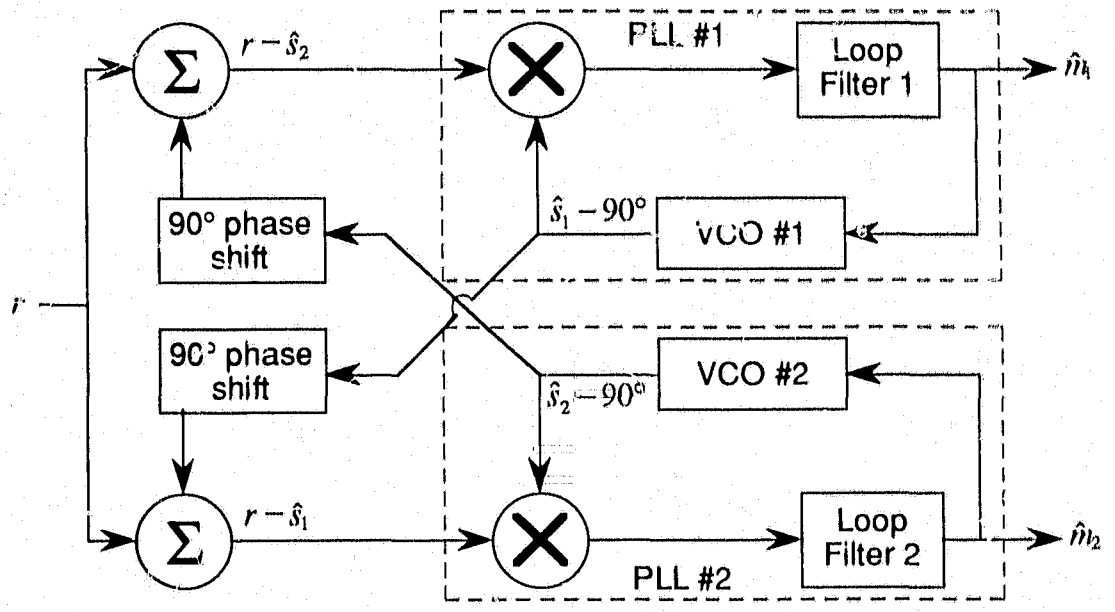

Figure 1–6 CCPLL demodulator [13].

In the study by Bradley [17], Cassara's analog PLL's were replaced by ZC-DPLL's. Computer simulation revealed that the use of the CDPLL allowed the weaker signal to be detected or extracted from the much stronger interferer for a wide range of signal to interference ratios (SIR). Loop parameters were chosen heuristically. In a more recent paper Bradley [18] derived a CDPLL based FM receiver from EKF theory but little analysis has been carried out on the resulting structure. In a similar but independent work Lagunas [19] derived a receiver structure similar to that of Bradley. Although their efforts yielded some promising results, they have also raised additional questions. It was discovered that in order to lock, the coupled loops required that their uncoupled closed-loop bandwidths had to be on the order of the carrier frequency as opposed to being on the order of the bandwidth of the modulated signal as is usually the case. A tractable model of the CDPLL is required to give insight into the design of the loop components.

This also raised the question, "What *type* of DPLL should be used?" The ZC-DPLL is by far the most common because it is relatively easy to implement and is the most studied of the DPLL's [20]. However the mapping from analog PLL's to digital DPLL's has been under

continued investigation, especially by Gardner [21]. So far the analysis of the CDPLL has only been carried out for the ZC-DPLL. It is highly desirable to be able to model the CDPLL independent of the actual DPLL implementation.

With this in mind, attention will now be focused on PLL's themselves. It is well known that the phase-locked loop is a realization of the optimum MAP estimator of a phase-modulated waveform. Van Trees [22, Ch. 2] derives the PLL demodulator first by an intuitive approach and then by using the MAP estimator derived in [23, Ch. 5]. He then also shows that the PLL, with properly designed filters, provides the minimum mean-square error (MMSE) estimate of the modulated signal when the loop error is small corresponding to the linear region of the loop's operating characteristics. This analysis considered only continuous time signals.

The 1960's saw great advances in digital technology. It was during this time digital PLL's made their debut. The transition from analog to digital has been gradual. Early "digital" loops may have had only one digital component. These types of loops are now referred to as hybrid phase-locked loops (HPLL) [24]. One of the first totally "digital" PLL's was proposed by Gill and Gupta [25] in which the analog multiplier, loop filter, and the voltage controlled oscillator (VCO) were replaced by a sampler, digital filter, and a digital clock respectively. This structure, the ZC-DPLL, is one of the most common forms of DPLL's and has been extensively studied [26, 20]. Most of the early DPLL formulations were intuitively derived from their analog PLL counterparts. Since the PLL is a realization of the MAP estimator, a DPLL derived from a PLL also yields an approximation of the MAP estimator, although not necessarily optimum [27].

Kelly and Gupta [28], Polk and Gupta [29], and McBride [30] have approached the estimation problem by deriving the DPLL structure from estimation theory instead of by approximating the analog PLL. Kelly and Gupta examined demodulation of continuous-time signals from discrete-time observations. They extended the state-variable communication

model to include discrete-time observations and derived realizable estimation structure from two different approximations of conditional mean (CM) estimation algorithms: the modified Gaussian and the modified truncated second-order approximations. From these results receiver structures for amplitude modulation (AM), phase modulation (PM), and FM were developed. As expected, receiver structures for PM and for FM were found to be DPLL's. Kelly and Gupta concluded "...[there was] the need to consider the digital receiver as a device in itself and not as an approximation to the continuous-time receiver." [28].

Polk and Gupta [29] followed this by examining two other non-linear approximations: the EKF and the MAP estimator. As in [28], Polk and Gupta derive the digital communication model from the analog angle-modulated model and, in this case, apply the EKF and MAP algorithms to the discrete communication model. The DPLL structure is then extracted from the two approximations and analyzed. It was discovered that the DPLL structures were identical to those found in [28]. However, by use of the EKF it was also discovered that in high SNR conditions the loop filter reduces to the standard discrete Kalman filter. This results in a simplified design procedure as compared to [28]. The relationship between the EKF and the DPLL will figure prominently in this project.

McBride [30] also tackles the optimum discrete demodulation problem by synthesizing the structure from discrete estimation theory. Although similar to [28] and [29], McBride's derivation exhibits some distinctions. Firstly, the in-phase and quadrature components of the continuous time signal are sampled at carrier or intermediate frequency (IF). This allows for complete characterization of the bandpass signal as a complex baseband signal [31]. McBride's discrete communication model is similar to Gupta's but adds another driving noise in the state equation to account for the possible difference between the frequencies of the receiver and of the transmitter. McBride found an approximate solution to the MAP estimator equations by a technique known as invariant imbedding [22]. The realizable de-

modulator structure obtained is a DPLL with a time-varying gain. For high SNR conditions this structure also reverts to the discrete Kalman filter.

Finally a note on the use of the term *digital* phase-locked loop is given. The exact denotation of digital in reference to PLLs seems to vary from author to author and from subject to subject. Many of the early papers classified a PLL as digital if it contained any digital components (e.g. a digital VCO). As DPLL's advanced the terminology became more specific. These first DPLL's were classed as HPLL's and structures like the ZC-DPLL were specified as *discrete* phase-locked loops. In a recent report Gardner [21] takes great care in formalizing the DPLL terminology to more accurately categorize the various implementations. By his definition a loop is a DPLL only if it samples the analog waveform's instantaneous frequency uniformly (that is, asynchronously). This differentiates the "true" DPLL from the discrete PLL where, when locked, the analog waveform's instantaneous frequency is sampled synchronously which results in non-uniform sampling intervals. Garnder's definitions are adhered to in the remainder of this report.

1.4. Contributions of this Project

Kirlin [7] has shown that a pair of coupled PLL's can track the spatial bearing and temporal phase of multiple narrowband sources. However, the design of these CPLL's has not been formalized and the analysis is incomplete. Kirlin and Su [3] have analyzed, both analytically and by simulation, a specific CDPLL pair where each DPLL is implemented by a ZC-DPLL. Stability criterion were established, but no general design guidelines were presented. Bradley [18] and Lagunas [19] have both derived CDPLL based receivers but little analysis has been carried out. Thus one of the major components of this effort is in the development of a general model of a CDPLL which is independent of the actual DPLL implementation and use this model to study CDPLL tracking behavior. Much of this development is an extension of the work done by Gupta et al. [28, 29], McBride [30], Bradley [18] and Lagunas [19].

Specific contributions of this thesis include:

- Development of a model for multiple co-channel sources
- Derivation of realizable estimator structures
- Investigation of the separability of co-channel signals
- Analysis of the behavior of the derived structures

1.5. Outline of Thesis

Chapter 2 is comprised of the development of the communication model, Extended Kalman Filter, and derivation of resulting estimator structures.

Chapter 3 examines the co-channel signal observability and separability issue based on the previously derived EKF.

Chapter 4 provides analysis of a CDPLL receiver, its relationship to the EKF, and its acquisition and tracking characteristics. Time-varying co-channel signal multiplicity is also investigated.

Chapter 5 using the models and estimators derived in the previous chapters the framework for polarization diversity crosstalk is presented

Chapter 6 summarizes the thesis.

2. Communication and Estimator Models

The first step in the development of an estimator is the modeling of the system of interest. The prime area of interest in this work is telecommunication, thus a meaningful model of a phase-modulated communication system is required. In this chapter the communication model used throughout this work is presented. It is based on the state-space communication model in Polk [29], Bradley [18], and Lagunas [19] but has been extended to the multiple source, multiple sensor scenario.

An Extended Kalman Filter estimator is derived based on this communication model. The EKF estimator provides the framework by which the problem can be studied.

2.1. Communication Model

The primary area of interest in this thesis is communication via angle modulation. A natural starting point is the development of the communication model for angle modulation, either phase modulation (PM) or frequency modulation (FM). Angle modulation is accomplished by instantaneously altering the phase of a sinusoidal carrier

$$s(\theta(t),t) = \sqrt{2}A\sin(\omega_c t + \theta(t)) \tag{2.1}$$

where A is the unmodulated carrier power, ω_c is the carrier frequency, and $\theta(t)$ is the instantaneous phase. In communication systems $\theta(t)$ is derived from the message process $m(t)$ by scaling in the case of PM

$$s(m(t),t) = \sqrt{2}A\sin\left(\omega_c t + d_p m(t)\right), \tag{2.2}$$

where d_p is the phase sensitivity, and by integration in the case of FM

$$s(m(t),t) = \sqrt{2}A\sin\left(\omega_c t + d_f \int_{T_i}^{t} m(\tau)\, d\tau\right), \tag{2.3}$$

where d_f is the frequency sensitivity. Angle modulation is a nonlinear modulation scheme, and FM in particular also exhibits memory due to the integration of the message process [23].

2.1.1. Message Process

In general the message process is baseband in nature, at least with respect to the carrier frequency. Speech is a common example. However, speech is nonstationary and relatively difficult to accurately model. Therefore it is common practice to model the message process by some stationary, bandlimited, random process. This is a first approximation to a "real" message process and simplifies the analysis. Modeling the message process as a linear dynamic system allows for various levels of complexity while maintaining analytic tractability and compact notation. State-space notation utilizes compact vector/matrix algebra and provides a convenient representation of differential equations. State-space notation will be used exclusively in this work. There are many excellent references including [23, 32] for readers who are unfamiliar with state-space.

The linear dynamic system (see Fig 2–1) is a recursive structure which is described by the n-dimensional first-order stochastic differential equation

$$\dot{\mathbf{x}}(t) = \mathbf{F}\mathbf{x}(t) + \mathbf{G}\mathbf{u}(t) \tag{2.4}$$

where $\mathbf{x}$ is the state vector, $\mathbf{F}$ is the state equation matrix, and $\mathbf{u}$ is a white noise driving process with mean $\mathbf{m}_u$ and covariance $\mathbf{R}_u$. The characteristics of the message process are determined by the state vector and the state equation matrix. A stationary Gauss-Markov random process is used to model the message process because it is essentially flat over a finite bandwidth and exhibits an exponentially decaying auto-correlation function [32]. The ensuing derivation of the communication and estimator models follows closely with that of Polk [29] with the noted additions.

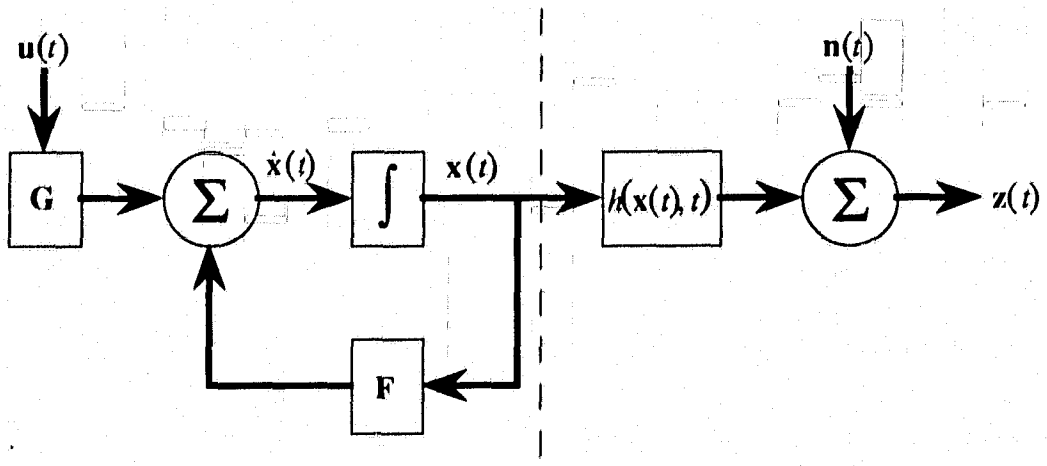

Figure 2–1 Analog communication model.

The message process is described by an N^{th}-order differential equation

$$\alpha_{N-1}\frac{d^{N-1}m(t)}{dt^{N-1}}+\cdots+\alpha_1\frac{dm(t)}{dt}+\alpha_0 m(t)=u(t) \tag{2.5}$$

which defines state vector for an N^{th}-order message model

$$\mathbf{x}_m(t)=\begin{bmatrix}x_1(t)\\x_2(t)\\\vdots\\x_N(t)\end{bmatrix}=\begin{bmatrix}m(t)\\\dfrac{dm(t)}{dt}\\\vdots\\\dfrac{d^{N-1}m(t)}{dt^{N-1}}\end{bmatrix}. \tag{2.6}$$

For PM, the phase state vector $\mathbf{x}_\theta$ is the same as the message state vector $\mathbf{x}_m$. However for FM, the phase state x_θ is separate from the message state vector so the augmented FM state vector is $\mathbf{x}_\theta=\begin{bmatrix}x_\theta & \mathbf{x}_m^{\mathrm{T}}\end{bmatrix}^{\mathrm{T}}$. Carrier amplitude may be included by augmenting the amplitude state $x_A=A$ with the phase state vector $\mathbf{x}_\theta$ forming

$$\mathbf{x}(t)=\begin{bmatrix}\mathbf{x}_\theta^{\mathrm{T}}(t) & x_A(t)\end{bmatrix}^{\mathrm{T}}. \tag{2.7}$$

The majority of this work will concentrate on a first order unit-energy lowpass message process described by

$$\dot{x}_m(t)=\dot{m}(t)=-\alpha m(t)+\sqrt{2\alpha}u(t), \tag{2.8}$$

where $u(t)$ is a zero-mean, unit variance, scalar white Gaussian process and α, derived from (2.5), is the 3 dB bandwidth of the message process.

2.1.2. Observation Process

The modulation, modeled in the observation process side of Fig. 2–1, is the measurement equation

$$\mathbf{z}(t) = h(\mathbf{x}(t), t) + \mathbf{n}(t), \tag{2.9}$$

where $h(\mathbf{x}(t), t)$ is some observation transformation of the state $\mathbf{x}$, and $\mathbf{n}$ is the measurement noise with mean $\mathbf{n}_v$ and covariance $\mathbf{R}_n$. The form of $h(\mathbf{x}(t), t)$ is defined by the type of modulation. For angle modulation the observation function is

$$h(\mathbf{x}(t), t) = \sqrt{2}A\sin(\omega_c t + \theta(t)), \tag{0}$$

wh<u>ere</u> where the phase angle $\theta(t) = \mathbf{c}_\theta^{\mathrm{T}}\mathbf{x}_\theta(t)$ is derived from the state vector (2.7) by the phase "sel<u>ection</u>" vector

$$\mathbf{c}_\theta^{\mathrm{T}} = [1 \quad 0 \quad \cdots \quad 0]. \tag{2.11}$$

The phase and amplitude state selection vector is

$$\mathbf{c}^{\mathrm{T}} = [\mathbf{c}_\theta^{\mathrm{T}} \quad 1]. \tag{2.12}$$

2.1.3. Continuous-Time Multiple Source Model

The scalar observation communication model in [29] may be expanded to accommodate multiple, independent message processes by augmenting the "total" state vector with the state vector for each source

$$\mathbf{x}(t) = \begin{bmatrix} \mathbf{x}_1(t) \\ \mathbf{x}_2(t) \\ \vdots \\ \mathbf{x}_N(t) \end{bmatrix} \begin{matrix} \leftarrow \text{First source's state vector} \\ \leftarrow \text{Second source's state vector} \\ \\ \leftarrow N^{th} \text{ source's state vector} \end{matrix}, \tag{2.13}$$

where $\mathbf{x}_i(t)$ denotes the state vector for the i^{th} source described by the i^{th} state equation

$$\dot{\mathbf{x}}_i(t) = \mathbf{F}_i\mathbf{x}_i(t) + \mathbf{G}_i\mathbf{u}_i(t). \tag{2.14}$$

The augmented state equation is in the form of (2.4) where the state vector is (2.13) and the augmented state matrix is

$$\mathbf{F} = \mathbf{F}_i \otimes \underset{N\times N}{\mathbf{I}}, \tag{2.15}$$

where $\otimes$ denotes the Kronecker matrix product[1] and $\underset{N\times N}{\mathbf{I}}$ is an N-dimensional identity matrix. Use of the identity ensures that the N different processes are uncoupled. Coupling between processes may be accomplished by non-zero off-diagonal elements in the state matrix or by coupled driving noise processes. The process driving noise vector is augmented with N independent noise vectors

$$\mathbf{u}(t) = \begin{bmatrix}\mathbf{u}_1(t) & \mathbf{u}_2(t) & \cdots & \mathbf{u}_N(t)\end{bmatrix}^{\mathrm{T}}, \tag{2.16}$$

and the augmented noise gain matrix is

$$\mathbf{G} = \mathbf{G}_i \otimes \underset{N\times N}{\mathbf{I}}. \tag{2.17}$$

The observation model also depends upon the type of sensor with which the measurement is made. For example, a measurement from a single antenna receiving multiple angle modulated sources is described by the scalar observation model

$$z(t) = \sqrt{2}\left[\sum_{i=1}^{N} A_i \sin\left(\omega_c t + \theta_i(t)\right)\right] + n(t); \tag{2.18}$$

whereas an array of M omnidirectional sensors makes the vector observation

$$\mathbf{z}(t) = \sqrt{2}\left[\sum_{i=1}^{N} A_i \sin\left(\omega_c t + \theta_i(t)\right)\mathbf{a}_i\right] + \mathbf{n}(t), \tag{2.19}$$

---

[1]The Kronecker matrix product $\mathbf{A}\otimes\mathbf{B}$ multiplies each element of matrix $\mathbf{B}$ by matrix $\mathbf{A}$. For example:

$$\mathbf{A} = \begin{bmatrix} a & b \\ c & d \end{bmatrix}, \mathbf{B} = \begin{bmatrix} e & 0 \\ 0 & f \end{bmatrix}; \mathbf{A}\otimes\mathbf{B} = \begin{bmatrix} ea & eb & & \mathbf{0} \\ ec & ed & & \\ & \mathbf{0} & fa & fb \\ & & fc & fd \end{bmatrix}.$$

where $\mathbf{a}_i$ is the source direction vector for the i^{th} source, and $\mathbf{n}$ is the noise vector for the array. For the uniform linear array, the source direction vector is defined by

$$\mathbf{a}_i = \begin{bmatrix} 1 & e^{j\phi_i} & e^{j2\phi_i} & \cdots & e^{j(M-1)\phi_i} \end{bmatrix}^{\mathrm{T}}. \tag{2.20}$$

The differential phase of a planar wavefront at two adjacent sensors for the i^{th} source is $\phi_i = \omega_i \Delta \sin(\psi_i)/C$ where ω_i is the frequency of ith source, Δ is the sensor spacing, ψ_i is the angle of arrival of the i^{th} source, and C is the propagation velocity of the medium. It is apparent that (2.18) is simply the single sensor case of (2.19).

Whereas it is assumed in [29] that the amplitude of the carrier is known, it is a parameter to be estimated in our system and therefore will be included in the state vector. The form of the state vector depends on the type of angle modulation. The state variable notation x_A and A for example, will be used interchangeably for the stake of readability.

Phase Modulation

In phase modulation, the phase process is the message process. Thus the extended state vector for the N^{th}-order PM source becomes

$$\mathbf{x}_i(t) = \begin{bmatrix} x_{\theta,i}(t) \\ \vdots \\ x_{A,i}(t) \end{bmatrix} = \begin{bmatrix} \theta_i(t) \\ \vdots \\ A_i(t) \end{bmatrix} \begin{matrix} \leftarrow \text{Carrier phase} \\ \leftarrow \text{Higher order states.} \\ \leftarrow \text{Carrier Amplitude} \end{matrix} \tag{2.21}$$

The number of state variables for each source is $N+1$ where N is the order of the message process.

For the first order message process (2.8), the resulting state equation for the i^{th} source's phase process is

$$x_\theta(t) = \dot{\theta}(t) = -\alpha\theta(t) + \sqrt{2\alpha}u(t) \tag{2.22}$$

and the augmented state equation is

$$\mathbf{x}(t) = \begin{bmatrix} \dot{x}_{\theta,i}(t) \\ \cdots\cdots \\ \dot{x}_{A,i}(t) \end{bmatrix} = \begin{bmatrix} -\alpha_i & \vdots & 0 \\ \cdots & \cdots & \cdots \\ 0 & \vdots & 0 \end{bmatrix} \begin{bmatrix} x_{\theta,i}(t) \\ \cdots\cdots \\ x_{A,i}(t) \end{bmatrix} + \begin{bmatrix} \sqrt{2\alpha_i} \\ \cdots \\ 0 \end{bmatrix} u_i(t). \tag{2.23}$$

In frequency modulation, the phase is the integral of the message process so an additional state variable is required. The extended state vector for the N^{th}-order FM source where the instantaneous frequency is equal to the message process is

$$\mathbf{x}_i(t) = \begin{bmatrix} x_{0,i}(t) \\ x_{f,i}(t) \\ \vdots \\ x_{A,i}(t) \end{bmatrix} = \begin{bmatrix} \theta_i(t) \\ f_i(t) \\ \vdots \\ A_i \end{bmatrix} \begin{matrix} \leftarrow \text{Carrier phase} \\ \leftarrow \text{Message} \\ \leftarrow \text{Higher order states} \\ \leftarrow \text{Carrier Amplitude} \end{matrix} \tag{2.24}$$

The number of state variables for each source is $N+2$ where N is the order of the message process.

A first-order low-pass FM message process is completely described by combining (2.3), (2.8), and (2.24) into

$$\mathbf{x}_\theta(t) = \begin{bmatrix} \dot{\theta}(t) \\ \dot{f}(t) \end{bmatrix} = \begin{bmatrix} 0 & d_f \\ 0 & -\alpha \end{bmatrix} \begin{bmatrix} \theta(t) \\ f(t) \end{bmatrix} + \begin{bmatrix} 0 \\ \sqrt{2\alpha} \end{bmatrix} u(t). \tag{2.25}$$

The augmented state vector for the i^{th} first-order FM source is

$$\mathbf{x}(t) = \begin{bmatrix} \dot{x}_{\theta,i}(t) \\ \dot{x}_{f,i}(t) \\ \dot{x}_{A,i}(t) \end{bmatrix} = \left[\begin{array}{cc:c} 0 & d_{f_i} & 0 \\ 0 & -\alpha_i & 0 \\ \hdashline 0 & 0 & 0 \end{array}\right] \begin{bmatrix} x_{\theta,i}(t) \\ x_{f,i}(t) \\ x_{A,i}(t) \end{bmatrix} + \begin{bmatrix} 0 \\ \sqrt{2\alpha_i} \\ 0 \end{bmatrix} u_i(t). \tag{2.26}$$

2.1.4. Discrete-Time Multiple Source Model

The system will ultimately be implemented digitally, so the observations will be accomplished by sampling (2.19) at times $t_k = kT_s$ where T_s is the uniform sampling interval. Thus an equivalent discrete communication model is required (see Fig 2–2).

The general form of a discrete state-space system is

$$\mathbf{x}(k+1) = \Phi(k+1,k)\mathbf{x}(k) + \Gamma\mathbf{w}(k), \tag{2.27}$$

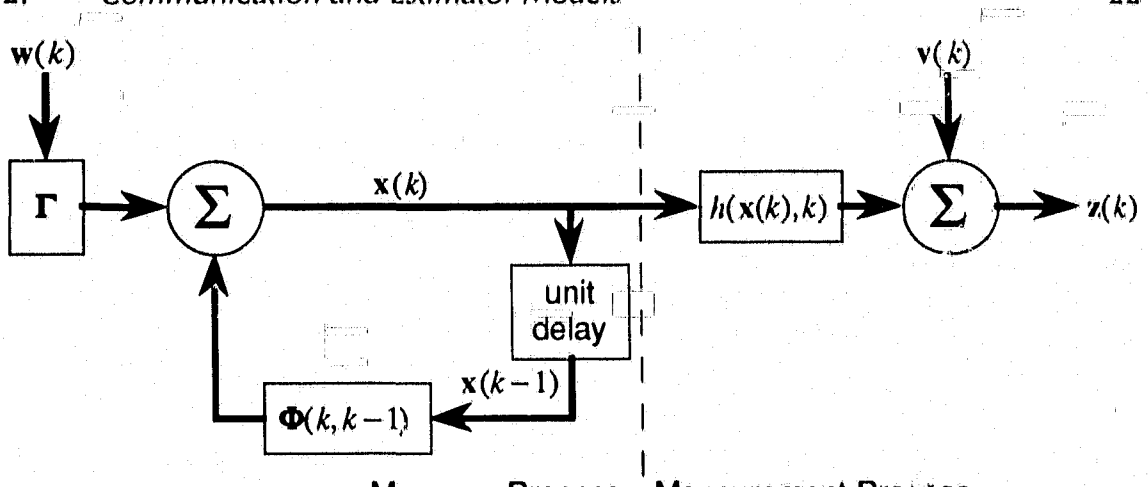

Figure 2–2 Discrete communication model.

where $\mathbf{w}(k)$ is a vector of independent zero mean, unit variance ($N:[0,1]$) Gaussian samples, $E\{\mathbf{w}\mathbf{w}^{\mathrm{T}}\} = \mathbf{I}$.[2] Since the message and amplitude processes are independent, (2.27) may be partitioned into the two separate state vectors $\mathbf{x}(k) = [\mathbf{x}_\theta(k) \vdots x_A(k)]^{\mathrm{T}}$

$$\begin{bmatrix} \mathbf{x}_\theta(k+1) \\ \cdots\cdots \\ x_A(k+1) \end{bmatrix} = \begin{bmatrix} \mathbf{\Phi}_\theta & \vdots & \mathbf{0} \\ \cdots & \vdots & \cdots \\ \mathbf{0} & \vdots & 1 \end{bmatrix} \begin{bmatrix} \mathbf{x}_\theta(k) \\ \cdots\cdots \\ x_A(k) \end{bmatrix} + \begin{bmatrix} \mathbf{\Gamma}_\theta & \vdots & \mathbf{0} \\ \cdots & \vdots & \cdots \\ \mathbf{0} & \vdots & 0 \end{bmatrix} \begin{bmatrix} \mathbf{w}(k) \\ \cdots\cdots \\ 0 \end{bmatrix}. \tag{2.28}$$

The measurement equation is

$$\mathbf{z}(k) = h(\mathbf{x}(k),k) + \mathbf{v}(k). \tag{2.29}$$

where the measurement noise $\mathbf{v}$ has covariance $\mathbf{R}_{\mathbf{v}}$. In (2.27) the state equation matrix $\mathbf{F}$ has been replaced by the state transition matrix $\mathbf{\Phi}$. The state transition matrix is the solution of the unforced homogeneous state equation $\dot{\mathbf{x}}(t) = \mathbf{F}\mathbf{x}(t)$. If the linear system is stationary, that is if $\mathbf{F}$ is time invariant, then the state transition matrix is

$$\mathbf{\Phi}(k) = \mathbf{\Phi}(k+1,k) = \mathbf{\Phi}(t_{k+1} - t_k) = e^{\mathbf{F}(t_{k+1}-t_k)} = e^{\mathbf{F}(T_s)}. \tag{2.30}$$

---

[2] In general state models generate non-stationary processes whose statistics depend on the distribution of the initial conditions. If the initial conditions are drawn from the steady-state state covariance, then the process is stationary [39]. The state covariance is discussed in Chapter 3.

Thus the state transition matrix may be found from [23, Chapter 6]

$$\mathbf{\Phi}(k) = \mathcal{L}^{-1}\{\mathbf{\Phi}(s)\} = \mathcal{L}^{-1}\left\{(s\mathbf{I} - \mathbf{F})^{-1}\right\} \tag{2.31}$$

where $\mathcal{L}^{-1}\{\cdot\}$ denotes the inverse Laplace transform.

The continuous-time process driving noise of (2.4) may be discretized by use of the matrix superposition integral[32]

$$\mathbf{\Gamma}(k)\mathbf{w}(k) = \int_{t_{k-1}}^{t_k} \mathbf{\Phi}(t_k, \tau)\mathbf{G}(\tau)d(\tau)\, d\tau, \tag{2.32}$$

The resulting discrete process driving noise has covariance

$$\mathbf{Q}_{\Gamma\mathbf{w}} = \int_{t_{k-1}}^{t_k} \mathbf{\Phi}(t_k, \tau)\mathbf{G}(\tau)\mathbf{R}_{\mathbf{d}}(\tau)\mathbf{G}^{\mathrm{T}}(\tau)\mathbf{\Phi}^{\mathrm{T}}(t_k, \tau)\, d\tau. \tag{2.33}$$

The discrete angle modulation observation function from (2.19) is

$$h(\mathbf{x}(k), k) = \sqrt{2}A\sin(\omega_c k T_s + \theta(k))\mathbf{a}. \tag{2.34}$$

The discrete first-order message process is obtained from (2.8) by substituting (2.31) and (2.32) into (2.27) yielding

$$x_m(k+1) = m(k+1) = e^{-\alpha T_s} m(k) + \left(1 - e^{-2\alpha T_s}\right)^{\frac{1}{2}} w(k). \tag{2.35}$$

As in the continuous case, multiple signals are formed by augmenting their individual state equations. The discrete equivalent of (2.13) is

$$\mathbf{x}(k) = \left[\mathbf{x}_1(k) \quad \mathbf{x}_2(k) \quad \cdots \quad \mathbf{x}_N(k)\right]^{\mathrm{T}}, \tag{2.36}$$

the augmented state transition matrix is

$$\mathbf{\Phi} = \mathbf{\Phi}_i \otimes \underset{N\times N}{\mathbf{I}}, \tag{2.37}$$

(2.16) becomes

$$\mathbf{w}(k) = \left[\mathbf{w}_1(k) \quad \mathbf{w}_2(k) \quad \cdots \quad \mathbf{w}_N(k)\right]^{\mathrm{T}}, \tag{2.38}$$

and (2.17) is

$$\mathbf{\Gamma} = \mathbf{\Gamma}_i \otimes \underset{N\times N}{\mathbf{I}}. \tag{2.39}$$

The same holds true with the state and noise covariance matrices where the augmented process noise covariance is

$$\mathbf{Q}_{\mathbf{W}} = \mathbf{Q}_{\mathbf{W},i} \otimes \underset{N\times N}{\mathbf{I}}. \tag{2.40}$$

Phase Modulation

For the discrete, first-order message process, the state transition matrix for the i^{th} source is

$$\mathbf{\Phi}_i(k) = \mathbf{\Phi}_i = \left[\begin{array}{c|c} \phi_{\theta,i} & 0 \\ \hline 0 & 1 \end{array}\right], \tag{2.41}$$

where the phase transition constant is

$$\mathbf{\Phi}_\theta = \phi_{\theta,i} = e^{-\alpha_i T_s}. \tag{2.42}$$

For the first-order model defined in (2.23), the process driving noise covariance from (2.33) is

$$\mathbf{Q}_{\mathrm{rw},i} = \left[\begin{array}{c|c} 1-e^{-2a_i T_s} & 0 \\ \hline 0 & 0 \end{array}\right]. \tag{2.43}$$

The discrete state equation for the i^{th} first-order PM source is

$$\left[\begin{array}{c} x_{\theta,i}(k+1) \\ \hline x_{A,i}(k+1) \end{array}\right] = \left[\begin{array}{c|c} \phi_{\theta,i} & 0 \\ \hline 0 & 1 \end{array}\right]\left[\begin{array}{c} x_{\theta,i}(k) \\ \hline x_{A,i}(k) \end{array}\right] + \left[\begin{array}{c} \gamma_{\theta,i} \\ \hline 0 \end{array}\right] w_i(t), \tag{2.44}$$

where the phase process driving noise standard deviation is

$$\gamma_{\theta,i} = \left(1-e^{-2a_i T_s}\right)^{\frac{1}{2}}. \tag{2.45}$$

A complete derivation may be found in Appendix A.

Frequency Modulation

For the discrete, first-order message process where $x_f = x_m$, the state transition matrix for the i^{th} source is

$$\mathbf{\Phi}_i(k) = \mathbf{\Phi}_i = \left[\begin{array}{cc|c} 1 & \phi_{\theta f,i} & 0 \\ 0 & \phi_{f,i} & 0 \\ \hline 0 & 0 & 1 \end{array}\right] \tag{2.46}$$

where

$$\phi_{\theta f,1} = \frac{d_{f_i}}{\alpha_i}\left(1 - e^{-\alpha_i T_s}\right) \tag{2.47}$$

$$\phi_{f,i} = e^{-\alpha_i T_s} \tag{2.48}$$

Using (2.33) the driving noise covariance the first-order model defined in (2.26) is,

$$\mathbf{Q}_{\Gamma w,i} = \left[\begin{array}{cc:c} q_{\theta,i} & q_{\theta f,i} & \mathbf{0} \\ q_{f\theta,i} & q_{f,i} & \\ \hdashline \multicolumn{2}{c:}{\mathbf{0}} & 0 \end{array}\right] \tag{2.49}$$

where

$$q_{\theta,i} = \beta_i^2\left(2\alpha_i T_s + 4e^{-\alpha_i T_s} - e^{-2\alpha_i T_s} - 3\right) \tag{2.50}$$

$$q_{\theta f,i} = q_{f\theta,i} = \beta_i\left(1 - e^{-\alpha_i T_s}\right)^2 \tag{2.51}$$

$$q_{f,i} = 1 - e^{-2\alpha_i T_s} \tag{2.52}$$

where $\beta_i \equiv d_{f_i}/\alpha_i$ is the bandwidth expansion ratio as defined in [22, p. 88].

The discrete state equation for the i^{th} first-order FM source is

$$\left[\begin{array}{c} x_{\theta,i}(k+1) \\ x_{f,i}(k+1) \\ \hdashline x_{A,i}(k+1) \end{array}\right] = \left[\begin{array}{cc:c} 1 & \phi_{\theta f,i} & 0 \\ 0 & \phi_{f,i} & 0 \\ \hdashline 0 & 0 & 1 \end{array}\right]\left[\begin{array}{c} x_{\theta,i}(k) \\ x_{f,i}(k) \\ \hdashline x_{A,i}(k) \end{array}\right] + \left[\begin{array}{cc:c} \gamma_{\theta,i} & \gamma_{\theta f,i} & \mathbf{0} \\ \gamma_{f\theta,i} & \gamma_{f,i} & \\ \hdashline \multicolumn{2}{c:}{\mathbf{0}} & 0 \end{array}\right]\left[\begin{array}{c} w_{\theta,i}(k) \\ w_{f,i}(k) \\ \hdashline 0 \end{array}\right], \tag{2.53}$$

where

$$\gamma_{\theta,i} = \beta_i\left(2\alpha_i T_s + 4e^{-\alpha_i T_s} - e^{-2\alpha_i T_s} - 3\right)^{\frac{1}{2}}, \tag{2.54}$$

$$\gamma_{\theta f,i} = \gamma_{f\theta,i} = \sqrt{\beta_i}\left(1 - e^{-\alpha_i T_s}\right) \tag{2.55}$$

$$\gamma_{f,i} = \left(1 - e^{-2\alpha_i T_s}\right)^{\frac{1}{2}}. \tag{2.56}$$

A complete derivation may be found in Appendix A.

2.1.5. Deterministic Modulation

In digital data communications it is common to have deterministic message processes as opposed to stochastic ones like (2.35). An example is the pseudo-noise (PN) sequence used in spread-spectrum communications [33]. Here the deterministic sequence, called the spreading sequence, is used by the transmitter to *spread* the bandwidth of the message such that the spectrum of the transmitted signal is nearly independent of the message. The receiver then uses the same spreading sequence to despread the received signal so the original message may be recovered.

An example of a spreading sequence would be that generated by a maximal-length linear feedback shift register where the sequence is of length or period $L = 2^n - 1$ where n is the length of the shift register and N is the number of elements comprising the Galois field (see Fig. 2–3). A single cycle of the spreading sequence of phase or cyclic shift k is

$$\mathbf{s}(k) = \begin{bmatrix} s(k) & s(k-1) & \cdots & s(k-L+1) \end{bmatrix}^{\mathrm{T}}, \tag{2.57}$$

and the entire spreading sequence is the continuous repetition of (2.57)

$$\mathbf{s} = \begin{bmatrix} \mathbf{s}(k)^{\mathrm{T}} & \mathbf{s}(k)^{\mathrm{T}} & \cdots & \mathbf{s}(k)^{\mathrm{T}} \end{bmatrix}^{\mathrm{T}}. \tag{2.58}$$

In order for the received signal to be correctly recovered, the spreading sequences at the transmitter and receiver must be synchronized. Since the transmission channel will introduce a time delay in the received signal, this delay will have to be estimated by the receiver so the spreading sequences may be synchronized. In addition the receiver may not have *a priori* information as to when the transmitters spreading sequence began so the relative phase k of the spreading sequences may also have to be estimated.

One of the benefits of spread-spectrum communication is the ability to have numerous users share the same channel; co-channel interference is an inherent part of the system. Thus we require a model which adequately describes this situation.

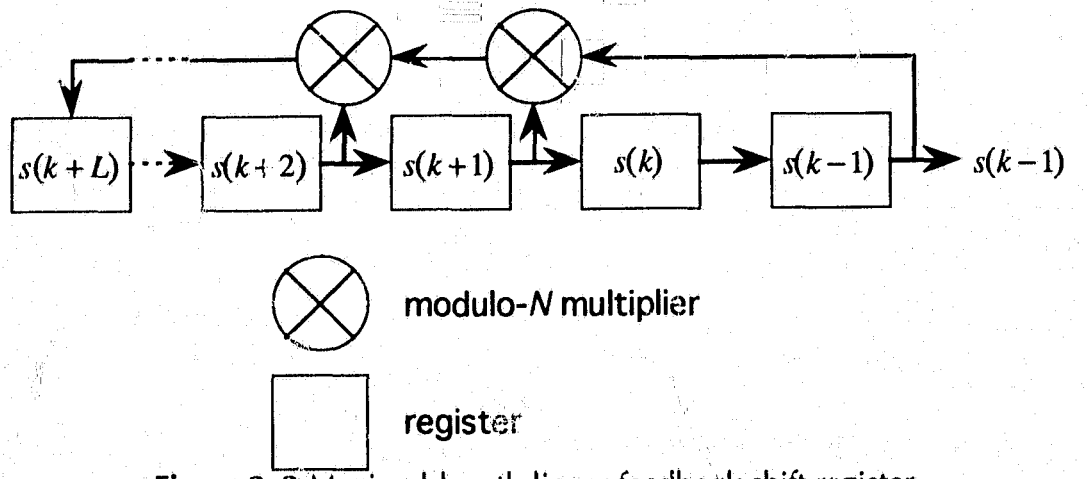

Figure 2–3 Maximal-length linear feedback shift register.

Consider several users sharing the same channel and employing the same spreading sequence $\mathbf{s}$ of length L. Each transmitter's spreading code will be received with a different phase relative to the receiver which translated into an unknown cyclic shift of $\mathbf{s}$. Thus for each cyclic shift of $\mathbf{s}$ there may or may not be a transmitter with that phase. The $L \times 1$ state vector for the i^{th} source is composed of delay states

$$\mathbf{x}_i = \begin{bmatrix} 0 & \cdots & 0 & \underset{d}{\alpha_i} & 0 & \cdots & 0 \end{bmatrix}^{\mathrm{T}} = \alpha_i \mathbf{1}_d, \tag{2.59}$$

where d is the sequence delay or phase for that source. The delay for the i^{th} source does not change with time so the state equation is

$$\mathbf{x}_i(k+1) = \mathbf{\Phi}\mathbf{x}_i(k) = \mathbf{x}_i(k), \tag{2.60}$$

so $\mathbf{\Phi} = \mathbf{I}$. Since all of the sources are using the same spreading sequence, the multiple source state vector is not augmented as in the previous chapter but simply added for each additional source

$$\mathbf{x} = \begin{bmatrix} 0 & \underset{1}{\alpha_1} & 0 & \underset{4}{\alpha_4} & \underset{5}{\alpha_5} & \cdots & 0 & \underset{j}{\alpha_j} & \cdots & 0 \end{bmatrix}^{\mathrm{T}} = \sum_{i=0}^{L-1} \alpha_i \mathbf{1}_i. \tag{2.61}$$

The state observation is one cycle of the spreading sequence

$$z(k) = \mathbf{H}(k)\mathbf{x}(k) + v(k)$$
$$= \mathbf{s}^{\mathrm{T}}(k)\mathbf{x}(k) + v(k) \tag{2.62}$$

so after L measurements each phase of the sequence has been observed.

2.2. Extended Kalman Filter Estimator

There are numerous references on the Kalman filter and the Extended Kalman filter. Very little introduction will be provided here; complete treatments are readily available in the literature [34, 32, 35].

The Kalman filter is a "linear minimum error variance sequential state estimation algorithm" [34, Chapter 7]. For a time-varying linear system it is the optimum (in the minimum error variance sense) linear filter for any distribution and the best of any linear or nonlinear filters for conditionally-Gaussian distributions. The Kalman filter has significant computational advantages over other optimal linear filters like the Wiener-Kolmogorov filter. Thus the Kalman filter has been used in applications from radar tracking to economic forecasting.

The discrete Kalman filter equations for the system model (2.27) and measurement equation

$$\mathbf{z}(k) = \mathbf{H}(k)\mathbf{x}(k) + \mathbf{v}(k) \tag{2.63}$$

where $\mathbf{H}(k)$ is the observation matrix, are [34, 32]

Next state prediction	$\hat{\mathbf{x}}(k \mid k-1) = \mathbf{\Phi}(k)\hat{\mathbf{x}}(k-1)$	(2.64)
Error covariance prediction	$\mathbf{P}(k \mid k-1) = \mathbf{\Phi}(k)\mathbf{P}(k-1)\mathbf{\Phi}^{\mathrm{T}}(k) + \mathbf{\Gamma Q}(k)\mathbf{\Gamma}^{\mathrm{T}}$	(2.65)
State update	$\hat{\mathbf{x}}(k) = \hat{\mathbf{x}}(k \mid k-1) + \mathbf{K}(k)\left[\mathbf{z}(k) - \mathbf{H}(k)\hat{\mathbf{x}}(k \mid k-1)\right]$	(2.66)
Error covariance update	$\mathbf{P}(k) = \left[\mathbf{I} - \mathbf{K}(k)\mathbf{H}(k)\right]\mathbf{P}(k \mid k-1)$	(2.67)
Kalman gain update	$\mathbf{K}(k) = \mathbf{P}(k)\mathbf{H}^{\mathrm{T}}(k)\mathbf{R}_{v}^{-1}(k)$	(2.68)

Table 2–1 Discrete Kalman Filter equations.

where the notation $\hat{\mathbf{x}}(k \mid k-1)$ indicates the predicted value of $\mathbf{x}$ at time k given the measurement taken at time $k-1$. The Kalman filter first estimates the next state of the system given the current measurement, Eqs. (2.64) and (2.65). The Kalman algorithm then adjusts

the error covariance $\mathbf{P}$ (2.67) and the gain matrix $\mathbf{K}$ (2.68) to properly weight the new measurement. The state for the new measurement is then estimated (2.66).

Although the message process (2.27) is linear, the discrete measurement equation for the communication model (2.34) is nonlinear; the linear observation matrix $\mathbf{H}(k)$ of (2.63) has been replaced by the non-linear observation function $h(\hat{\mathbf{x}}(k \mid k-1),k)$ which is the same as $h(\mathbf{x}(k),k)$ in (2.29) except the state has been replaced by the *predicted* state This implies that the update equations (2.66), (2.67), and (2.68) may not be valid.

The discrete Kalman filter of (2.64)–(2.68) may be extended to approximate the optimum minimum error variance estimator of a nonlinear system. In summary the nonlinear function $h(\mathbf{x}(k \mid k-1),k)$ in our case, is expanded into a power series about the current prediction $\hat{\mathbf{x}}(k \mid k-1)$,

$$h(\mathbf{x}(k),k) = h(\hat{\mathbf{x}}(k \mid k-1),k) + \mathbf{H}(\hat{\mathbf{x}}(k \mid k-1),k)(\mathbf{x}(k) - \hat{\mathbf{x}}(k \mid k-1)) + \cdots \tag{2.69}$$

where

$$\mathbf{H}(\hat{\mathbf{x}}(k \mid k-1),k) = \left.\frac{\partial h(\mathbf{x},k)}{\partial \mathbf{x}}\right|_{\mathbf{x}=\hat{\mathbf{x}}(k|k-1)} \tag{2.70}$$

Truncating all but the first two terms of (2.69) and combining with (2.66), (2.67), and (2.68) yields the Extended Kalman Filter equations. Full derivations are presented in [34, 32].

Next state prediction	$\hat{\mathbf{x}}(k \mid k-1) = \mathbf{\Phi}(k)\hat{\mathbf{x}}(k-1)$	(2.71)
Error covariance prediction	$\mathbf{P}(k \mid k-1) = \mathbf{\Phi}(k)\mathbf{P}(k-1)\mathbf{\Phi}^{\mathbf{T}}(k) + \mathbf{\Gamma Q}(k)\mathbf{\Gamma}^{\mathbf{T}}$	(2.72)
State update	$\hat{\mathbf{x}}(k) = \hat{\mathbf{x}}(k \mid k-1) + \mathbf{K}(k)\left[\mathbf{z}(k) - h(\hat{\mathbf{x}}(k \mid k-1),k)\right]$	(2.73)
Error covariance update	$\mathbf{P}(k) = \left[\mathbf{I} - \mathbf{K}(k)\mathbf{H}(\hat{\mathbf{x}}(k \mid k-1),k)\right]\mathbf{P}(k \mid k-1)$	(2.74)
Kalman gain update	$\mathbf{K}(k) = \mathbf{P}(k)\mathbf{H}^{\mathbf{T}}(\hat{\mathbf{x}}(k \mid k-1),k)\mathbf{R}_{\nu}^{-1}(k)$	(2.75)

Table 2–2 Discrete Extended Kalman Filter equations.

2.2.1. Scalar Observation

If the observation is scalar, say from a single antenna, $\mathbf{a}_i = 1$ in (2.34), which when combined with (2.28) may be written

$$z(k) = \sqrt{2}\sum_{i=1}^{N} h\left(\mathbf{x}_i(k), k\right) + v(k), \tag{2.76}$$

where the observation function for the i^{th} source is

$$h\left(\mathbf{x}_i(k), k\right) = x_{A,i} \sin\left(\omega_c k T_s + \mathbf{c}_\theta^{\mathrm{T}} \mathbf{x}_{\theta,i}\right). \tag{2.77}$$

Since the measurement is a scalar, so is the measurement noise and $\mathbf{R}_v = R_v$. Each source will be tracked by one estimator (or one EKF), thus the predicted observation for the i^{th} source is

$$h_i\left(\hat{\mathbf{x}}(k \mid k-1), k\right) = \sqrt{2}\hat{A}_i(k \mid k-1)\sin\left(\hat{\Theta}_i(k)\right) \tag{2.78}$$

where

$$\hat{\Theta}_i(k) = \omega_c k T_s + \theta_i(k \mid k-1) \tag{2.79}$$

and the corresponding gradient of the i^{th} source's predicted observation, as defined in (2.70), is

$$\mathbf{H}_i^{\mathrm{T}}\left(\hat{\mathbf{x}}(k \mid k-1), k\right) = \begin{bmatrix} \mathbf{H}_\theta^{\mathrm{T}}\left(\hat{\mathbf{x}}(k \mid k-1), k\right) \\ \hdashline \mathbf{H}_A\left(\hat{\mathbf{x}}(k \mid k-1), k\right) \end{bmatrix} = \begin{bmatrix} \sqrt{2}\hat{A}_i(k \mid k-1)\cos\left(\hat{\Theta}_i(k)\right) \\ 0 \\ \hdashline \sqrt{2}\sin\left(\hat{\Theta}_i(k)\right) \end{bmatrix}. \tag{2.80}$$

In the scalar observation case the measurement noise v is also a scalar. Thus $\mathbf{R}^{-1}$ in (2.75) is simply the reciprocal of the measurement noise covariance $\mathbf{R}$.

2.2.2. Vector Observation, Uniform Linear Array

For a vector observation from a uniform linear array of M sensors, the source direction vector $\mathbf{a}_i$ in (2.34) is as defined in (2.20):

$$\mathbf{a}_i = \begin{bmatrix} 1 & e^{j\phi_i} & e^{j2\phi_i} & \cdots & e^{j(M-1)\phi_i} \end{bmatrix}^{\mathrm{T}}, \tag{2.81}$$

where $\phi_i = \omega_i \Delta \sin(\psi_i)/C$ for the i^{th} source. Again each source will be tracked by one estimator so the predicted vector observation for the i^{th} source is

$$h_i(\hat{\mathbf{x}}(k \mid k-1), k) = \sqrt{2}\hat{A}_i(k \mid k-1)\sin\left(\hat{\Theta}_i\right)\hat{\mathbf{a}}_i(k), \tag{2.82}$$

where the predicted source direction vector is

$$\hat{\mathbf{a}}_i = \begin{bmatrix} 1 & e^{j\hat{\phi}_i} & e^{j2\hat{\phi}_i} & \cdots & e^{j(M-1)\hat{\phi}_i} \end{bmatrix}^{\mathrm{T}} \tag{2.83}$$

and

$$\hat{\phi}_i = \left(\omega_c + \hat{x}_{2,i}(k \mid k-1)\right)\Delta \sin(\psi_i)/C \tag{2.84}$$

is the predicted phase between adjacent sensors. The resulting gradient of (2.82) is

$$\mathbf{H}_i^{\mathrm{T}}(\hat{\mathbf{x}}(k \mid k-1), k) = \begin{bmatrix} \mathbf{H}_\theta^{\mathrm{T}}(\hat{\mathbf{x}}(k \mid k-1), k) \\ \hdashline \mathbf{H}_A^{\mathrm{T}}(\hat{\mathbf{x}}(k \mid k-1), k) \end{bmatrix} = \begin{bmatrix} \sqrt{2}\hat{A}_i(k \mid k-1)\cos\left(\hat{\Theta}_i\right)\hat{\mathbf{a}}_i(k) \\ 0 \\ \vdots \\ \hdashline \sqrt{2}\sin\left(\hat{\Theta}_i\right)\hat{\mathbf{a}}_i(k) \end{bmatrix}. \tag{2.85}$$

2.3. Estimator Formulation

The Extended Kalman Filter algorithms have been derived for the multiple source, discrete communication model. The next task is to examine these equations to find practical estimator structures.

Polk and Gupta [29] originally derived a digital phase-lock loop from an EKF estimator. Using the same methodology, we will formulate DPLL-based receiver structures from the EKF estimator derived in the previous section. Our contribution to Polk's work is two-fold: inclusion of amplitude estimation and expansion to include multiple sources.

Based on the communication model of Fig. 2–2 and the EKF equations (2.71)–(2.75), Polk and Gupta [29] have shown that the EKF may be realized by a DPLL. The form of the structure is arrived at by substituting (2.71) and (2.75) into (2.73) thus forming the Kalman filter equation

$$\hat{\mathbf{x}}(k) = \Phi\hat{\mathbf{x}}(k-1) + \mathbf{P}(k)\mathbf{H}^{\mathrm{T}}\big(\hat{\mathbf{x}}(k\,|\,k-1)\big)R_{\nu}^{-1}(k)\nu(k), \tag{2.86}$$

where

$$\nu(k) = z(k) - h\big(\hat{\mathbf{x}}(k\,|\,k-1)\big) \tag{2.87}$$

is the so-called *innovations process.* This is actually an approximation of the true innovations since the nonlinear measurement function is based on the predicted state. If the prediction is poor, $\nu(k)$ is not the true innovations. Henceforth $\nu(k)$ will refer to the approximate innovations process. The error covariance matrix is updated by combining (2.73) and (2.75) to form

$$\mathbf{P}(k) = \mathbf{P}(k\,|\,k-1) - \frac{\mathbf{P}(k\,|\,k-1)\mathbf{H}^{\mathrm{T}}\big(\hat{\mathbf{x}}(k\,|\,k-1)\big)\mathbf{H}\big(\hat{\mathbf{x}}(k\,|\,k-1)\big)\mathbf{P}(k\,|\,k-1)}{R_{\nu}(k) + \mathbf{H}\big(\hat{\mathbf{x}}(k\,|\,k-1)\big)\mathbf{P}(k\,|\,k-1)\mathbf{H}^{\mathrm{T}}\big(\hat{\mathbf{x}}(k\,|\,k-1)\big)}, \tag{2.88}$$

where the prior covariance update is (2.72).

2.3.1. Phase Estimation

In [29] the Kalman filter equation is further decomposed by substituting $\mathbf{c}_{\theta}^{\mathrm{T}}\mathbf{H}_{\theta}^{\mathrm{T}}\big(\hat{\mathbf{x}}_{\theta}(k\,|\,k-1),k\big)$ for $\mathbf{H}\big(\hat{\mathbf{x}}(k\,|\,k-1),k\big)$ where the vector $\mathbf{c}_{\theta}$ from (2.11) selects the phase from the state vector. The resulting estimator takes the form shown in Fig. 2–4.

Rewrite (2.86) as

$$\hat{\mathbf{x}}_{\theta}(k) = \Phi_{\theta}\hat{\mathbf{x}}_{\theta}(k-1) + \mathbf{P}_{\theta}(k)\mathbf{c}_{\theta}R_{\nu}^{-1}(k)\varphi_{\theta}(k), \tag{2.89}$$

where

$$\varphi_{\theta}(k) = \mathbf{c}_{\theta}^{\mathrm{T}}\mathbf{H}_{\theta}^{\mathrm{T}}\big(\hat{\mathbf{x}}_{\theta}(k\,|\,k-1)\big)\nu(k) \tag{2.90}$$

is the output of the phase detector. Expanding (2.90) yields

$$\varphi_{\theta}(k) = \mathbf{c}_{\theta}^{\mathrm{T}}\mathbf{H}_{\theta}^{\mathrm{T}}\big(\hat{\mathbf{x}}_{\theta}(k\,|\,k-1)\big)z(k) - \mathbf{c}_{\theta}^{\mathrm{T}}\mathbf{H}_{\theta}^{\mathrm{T}}\big(\hat{\mathbf{x}}_{\theta}(k\,|\,k-1)\big)h\big(\hat{\mathbf{x}}_{\theta}(k\,|\,k-1)\big). \tag{2.91}$$

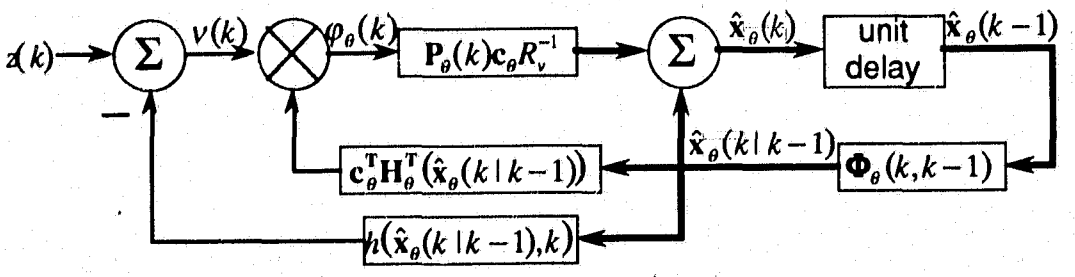

Figure 2–4 Direct EKF realization.

$\mathbf{H}_\theta(\cdot)$ and $h_\theta(\cdot)$ as defined in (2.80) and (2.77) are composed of sines and cosines at nearly the same frequency. Their product produces both sum and difference frequencies. In [29] the second order harmonics are neglected[3] reducing (2.91) to

$$\begin{aligned}\varphi_\theta(k) &= \sqrt{2}A\cos\left(\hat{\Theta}(k)\right)z(k) - 2A^2\cos\left(\hat{\Theta}(k)\right)\sin\left(\hat{\Theta}(k)\right)\\ &= \sqrt{2}A\cos\left(\hat{\Theta}(k)\right)z(k) - A^2\sin\left(2\hat{\Theta}(k)\right)\\ &\approx \sqrt{2}A\cos\left(\hat{\Theta}(k)\right)z(k)\\ \varphi'_\theta(k) &\equiv \mathbf{c}_\theta^{\mathrm{T}}\mathbf{H}_\theta^{\mathrm{T}}\left(\hat{\mathbf{x}}_\theta(k\,|\,k-1)\right)z(k).\end{aligned} \tag{2.92}$$

Eq. (2.86) becomes

$$\hat{\mathbf{x}}_\theta(k) = \mathbf{\Phi}_\theta\hat{\mathbf{x}}_\theta(k-1) + \mathbf{P}_\theta(k)\mathbf{c}_\theta R_\nu^{-1}(k)\mathbf{c}_\theta^{\mathrm{T}}\mathbf{H}_\theta^{\mathrm{T}}\left(\hat{\mathbf{x}}_\theta(k\,|\,k-1)\right)z(k). \tag{2.93}$$

The DPLL structure of Fig. 2–5 results directly from (2.93). This shows that the only contribution of the innovations process is the $A^2\sin\left(2\hat{\Theta}(k)\right)$ term which is effectively filtered out by the loop filter.

The realization of Fig. 2–5 has a slightly lower computational cost than that of Fig. 2–4.

Unlike conventional PLLs and DPLLs, the gain $\mathbf{P}_\theta(k)\mathbf{c}_\theta R_\nu^{-1}(k)$ comprising the loop filter is variable and is a function of the input $z(k)$. Thus the EKF-derived DPLL is able to re-

---

[3]The double frequency image is filtered by the loop filter and may be further be removed by filtering the output of the DPLL.

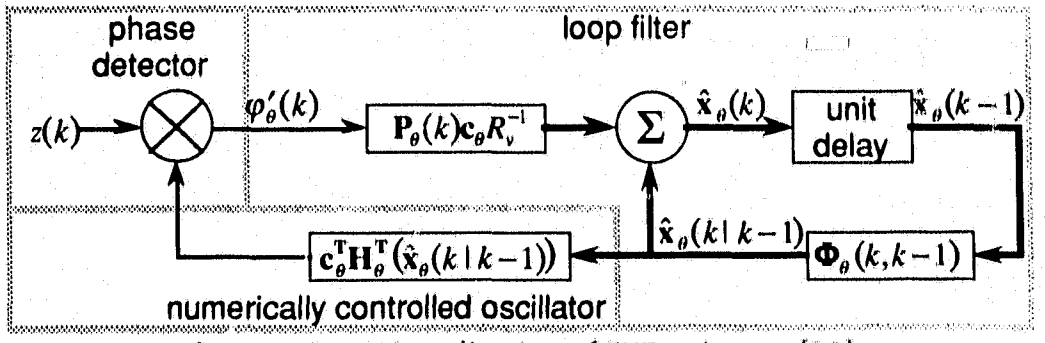

Figure 2–5 DPLL realization of EKF estimator [29].

cursively approach the minimum variance estimator. As will be shown later, this is one of the main advantages of this approach.

Using this foundation, DPLL structures are now derived for amplitude and phase estimation for single and multiple sources.

2.3.2. Inclusion of Amplitude Estimation

Amplitude estimation may be included by augmenting the amplitude state x_A with the phase state vector $\mathbf{x}_\theta$ as in (2.28). When (2.28) is substituted into (2.86)

$$\begin{bmatrix}\hat{\mathbf{x}}_\theta(k)\\ \hat{x}_A(k)\end{bmatrix}=\begin{bmatrix}\mathbf{\Phi}_\theta & \mathbf{0}\\ \mathbf{0} & 1\end{bmatrix}\begin{bmatrix}\hat{\mathbf{x}}_\theta(k-1)\\ \hat{x}_A(k-1)\end{bmatrix}+\begin{bmatrix}\mathbf{P}_\theta & \mathbf{P}_{\theta A}\\ \mathbf{P}_{\theta A}^T & P_A\end{bmatrix}R_v^{-1}\begin{bmatrix}\mathbf{c}_\theta\varphi_\theta(k)\\ \varphi_A(k)\end{bmatrix}, \tag{2.94}$$

where

$$\varphi(k)=\begin{bmatrix}\mathbf{c}_\theta\varphi_\theta(k)\\ \varphi_A(k)\end{bmatrix}=\begin{bmatrix}\mathbf{c}_\theta\mathbf{c}_\theta^T\mathbf{H}_\theta^T(\hat{\mathbf{x}}(k|k-1))v(k)\\ \mathbf{H}_A^T(\hat{\mathbf{x}}(k|k-1))v(k)\end{bmatrix}, \tag{2.95}$$

two separate but coupled Kalman filter equations result. The coupling results from the cross-covariance vectors $\mathbf{P}_{\theta A}$ as shown in Fig. 2–6.

Substituting (2.77), (2.80), and (2.87) into (2.95) and expanding results in double frequency term in the Kalman filter equation for both $\hat{\mathbf{x}}_\theta$ and $\hat{x}_A$. As previously, the loop filter of the DPLL will remove the double frequency components from $\hat{\mathbf{x}}_\theta$, however the loop filter for $\hat{x}_A$ is all-pass and thus the double frequency components present in the amplitude esti-

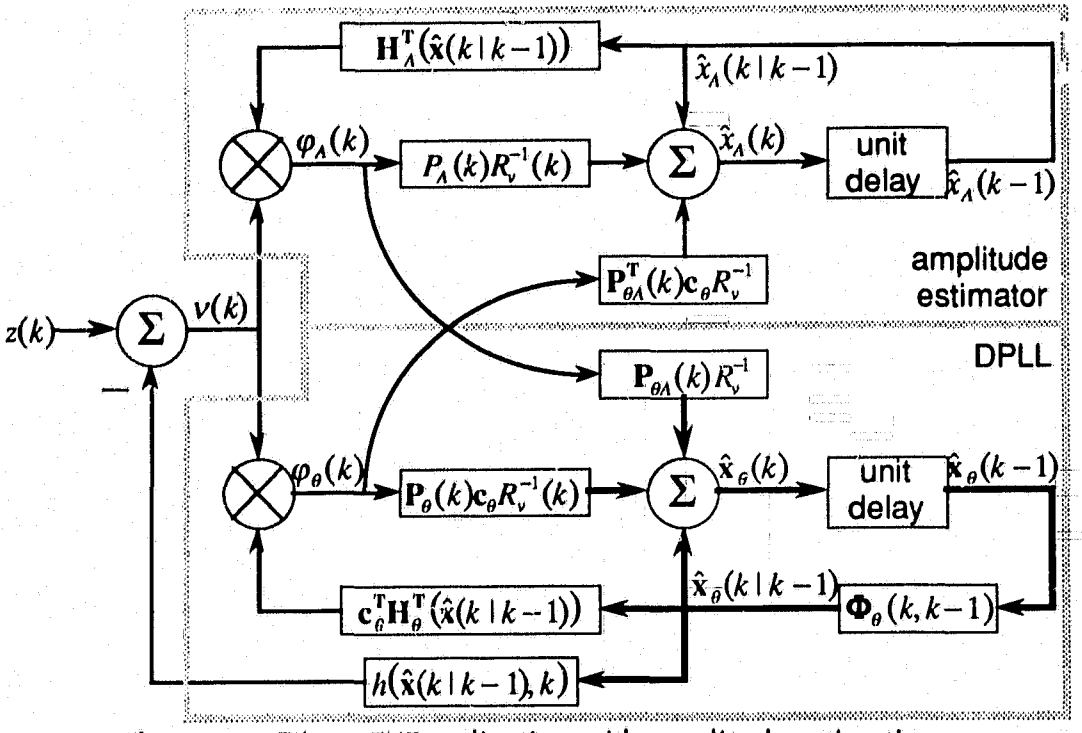

Figure 2–6 Direct EKF realization with amplitude estimation.

mator cannot be neglected. Neglecting the second order harmonics for $\hat{\mathbf{x}}_\theta$ in (2.95) yields the approximation

$$\begin{bmatrix} \mathbf{c}_\theta\varphi'_\theta(k) \\ \hline \varphi'_A(k) \end{bmatrix} = \begin{bmatrix} \mathbf{c}_\theta\mathbf{c}_\theta^T\mathbf{H}_\theta^T(\hat{\mathbf{x}}(k|k-1))z(k) \\ \hline \mathbf{H}_A^T(\hat{\mathbf{x}}(k|k-1))z(k) - \hat{x}_A(k|k-1) \end{bmatrix}, \tag{2.96}$$

where $\varphi'_\theta(k)$ is from (2.92) and $\varphi'_A(k)$ is from

$$\begin{aligned} \varphi_A(k) &= \sqrt{2}\sin\left(\hat{\Theta}(k)\right)z(k) - 2\hat{x}_A(k|k-1)\sin^2\left(\hat{\Theta}(k)\right) \\ &= \sqrt{2}\sin\left(\hat{\Theta}(k)\right)z(k) - \hat{x}_A(k|k-1)\left[1-\cos\left(2\hat{\Theta}(k)\right)\right] \\ &\approx \sqrt{2}\sin\left(\hat{\Theta}(k)\right)z(k) - \hat{x}_A(k|k-1) \\ \varphi'_A(k) &\equiv \mathbf{H}_A^T(x(k|k-1),k)z(k) - \hat{x}_A(k|k-1), \end{aligned} \tag{2.97}$$

which results in the realization of Fig. 2–7. Here the innovations process contributes the $\hat{x}_A(k|k-1)\left[1-\cos\left(2\hat{\Theta}(k)\right)\right]$ term which even after being filtered by the loop filter leaves the residual amplitude estimate $\hat{x}_A(k|k-1)$.

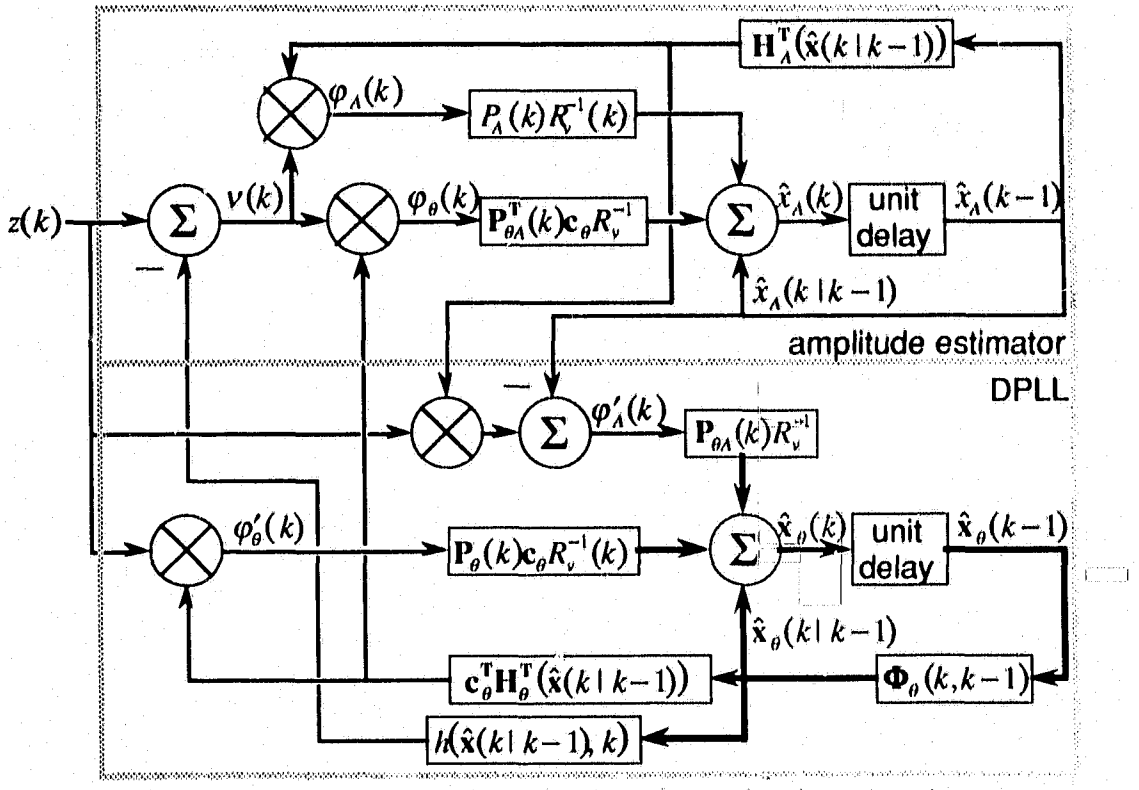

Figure 2–7 DPLL realization of EKF with amplitude estimation.

In the case where only phase estimation is required, neglecting the double frequency terms results in a simplified realization. However, where amplitude estimation is included, the requirement of double frequency terms in the amplitude estimator obviates the benefits of ignoring the double frequency terms and actually results in a computationally less efficient realization as evident by the number of multipliers and summers.

The coupling of the two estimators occurs by the cross-covariance elements P_{ij} where $i \neq j$. Since the phase and amplitude processes of (2.44) are not coupled, investigation into the nature of the cross-covariance coupling is required. We begin by examining the error covariance update (2.88) for the angle modulation observation matrix (2.80).

In keeping with the assumption that $\mathbf{P}_{\theta A} = \mathbf{0}$, make the initial error covariance diagonal

$$\mathbf{P}(0) = \left[\begin{array}{c:c} \mathbf{P}_\theta(0) & \mathbf{0} \\ \hdashline \mathbf{0} & P_A(0) \end{array}\right] \tag{2.98}$$

and form the prior covariance estimate (2.72)

$$\mathbf{P}(1|0)=\left[\begin{array}{c|c}\boldsymbol{\Phi}_\theta\mathbf{P}_\theta(0)\boldsymbol{\Phi}_\theta^{\mathrm{T}}+\Gamma_\theta\Gamma_\theta^{\mathrm{T}} & \mathbf{0}\\ \hline \mathbf{0} & P_\Lambda(0)\end{array}\right], \tag{2.99}$$

which remains block diagonal. Applying (2.88) and abbreviating $\mathbf{H}_y\left(\hat{\mathbf{x}}_y(k|k-1),k\right)$ as $\mathbf{H}_y$ yields

$$\mathbf{P}(1)=\left[\begin{array}{c|c}\mathbf{P}_\theta(1|0)-\mu\mathbf{P}_\theta(1|0)\mathbf{H}_\theta^{\mathrm{T}}\mathbf{H}_\theta\mathbf{P}_\theta(1|0) & -\mu\mathbf{P}_\theta(1|0)\mathbf{H}_\theta^{\mathrm{T}}\mathbf{H}_\Lambda P_\Lambda(0)\\ \hline -\mu\mathbf{P}_\theta^{\mathrm{T}}(1|0)\mathbf{H}_\theta\mathbf{H}_\Lambda^{\mathrm{T}}P_\Lambda(0) & P_\Lambda(0)-\mu P_\Lambda(1|0)\mathbf{H}_\Lambda^{\mathrm{T}}\mathbf{H}_\Lambda P_\Lambda(0)\end{array}\right], \tag{2.100}$$

where

$$\mu=\left[R_v+\mathbf{H}_\theta\mathbf{P}_\theta(1|0)\mathbf{H}_\theta^{\mathrm{T}}+\mathbf{H}_\Lambda\mathbf{P}_\Lambda(0)\mathbf{H}_\Lambda^{\mathrm{T}}\right]^{-1}. \tag{2.101}$$

Further study of $\mu\mathbf{P}_\theta(1|0)\mathbf{H}_\theta^{\mathrm{T}}\mathbf{H}_\Lambda P_\Lambda(0)$ requires specific knowledge of $\boldsymbol{\Phi}_\theta\mathbf{P}_\theta(0)\boldsymbol{\Phi}_\theta^{\mathrm{T}}+\Gamma_\theta\Gamma_\theta^{\mathrm{T}}$ and will be examined in subsequent sections.

2.3.3. Inclusion of Multiple Sources

By using the multiple source state vector, (2.89) may be written

$$\begin{bmatrix}\hat{\mathbf{x}}_1(k)\\ \hat{\mathbf{x}}_2(k)\\ \vdots\\ \hat{\mathbf{x}}_N(k)\end{bmatrix}=\begin{bmatrix}\boldsymbol{\Phi}_1 & & & \mathbf{0}\\ & \boldsymbol{\Phi}_2 & & \\ & & \ddots & \\ \mathbf{0} & & & \boldsymbol{\Phi}_N\end{bmatrix}\begin{bmatrix}\hat{\mathbf{x}}_1(k-1)\\ \hat{\mathbf{x}}_2(k-1)\\ \vdots\\ \hat{\mathbf{x}}_N(k-1)\end{bmatrix}+\mathbf{P}(k)R_v^{-1}\varphi(k), \tag{2.102}$$

where

$$\mathbf{P}(k)R_v^{-1}\varphi(k)=\begin{bmatrix}\mathbf{P}_{11}(k) & \mathbf{P}_{12}(k) & \cdots & \mathbf{P}_{1N}(k)\\ \mathbf{P}_{21}(k) & \mathbf{P}_{22}(k) & \cdots & \mathbf{P}_{2N}(k)\\ \vdots & \vdots & \ddots & \vdots\\ \mathbf{P}_{N1}(k) & \mathbf{P}_{N2}(k) & \cdots & \mathbf{P}_{NN}(k)\end{bmatrix}R_v^{-1}\begin{bmatrix}\varphi_1(k)\\ \varphi_2(k)\\ \vdots\\ \varphi_N(k)\end{bmatrix}, \tag{2.103}$$

and also

$$\boldsymbol{\varphi}_i(k)=\boldsymbol{\varphi}_{\theta,i}(k)=\mathbf{c}_{\theta,i}\mathbf{c}_{\theta,i}^{\mathrm{T}}\mathbf{H}_{\theta,i}^{\mathrm{T}}\left(\hat{\mathbf{x}}_i(k|k-1),k\right)\nu(k), \tag{2.104}$$

where the innovations process is

$$\nu(k)=z(k)-\sum_{i=1}^{N}h_i\left(\hat{\mathbf{x}}_i(k|k-1),k\right). \tag{2.105}$$

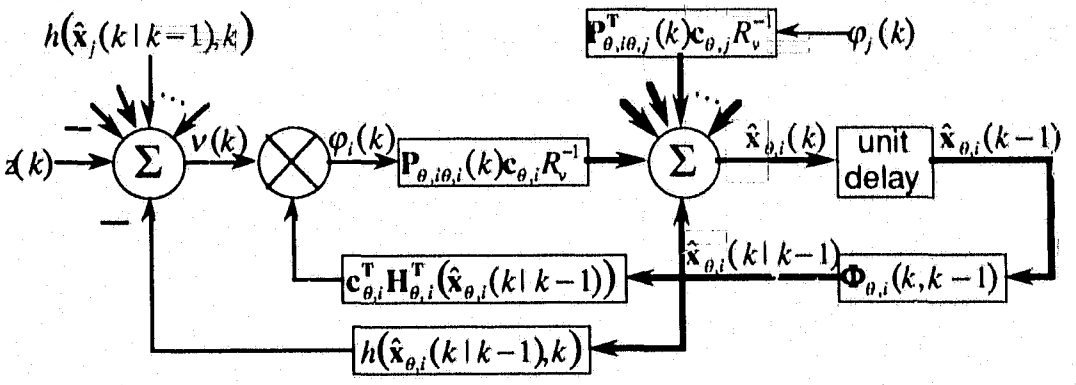

Figure 2–8 Direct realization of i^{th} EKF estimator (amplitudes known).

Thus Kalman filter equation for the i^{th} estimator is

$$\hat{\mathbf{x}}_i(k) = \Phi_i\hat{\mathbf{x}}_i(k-1) + \mathbf{P}(k)R_v^{-1}(k)\varphi(k). \tag{2.106}$$

For known carrier amplitudes, the direct implementation of (2.106) is shown in Fig. 2–8.

Expanding (2.104) yields

$$\begin{aligned}\varphi_{\theta,i}(k) &= \mathbf{c}_{\theta,i}\mathbf{c}^{\mathrm{T}}_{\theta,i}\left[\mathbf{H}^{\mathrm{T}}_{\theta,i}(\hat{\mathbf{x}}_i)z(k) - \mathbf{H}^{\mathrm{T}}_{\theta,i}(\hat{\mathbf{x}}_i)\sum_{j=1}^{N}h_{\theta,j}(\hat{\mathbf{x}}_j)\right] \\ &= \mathbf{c}_{\theta,i}\mathbf{c}^{\mathrm{T}}_{\theta,i}\left[\mathbf{H}^{\mathrm{T}}_{\theta,i}(\hat{\mathbf{x}}_i)z(k) - \mathbf{H}^{\mathrm{T}}_{\theta,i}(\hat{\mathbf{x}}_i)h_{\theta,i}(\hat{\mathbf{x}}_i) - \mathbf{H}^{\mathrm{T}}_{\theta,i}(\hat{\mathbf{x}}_i)\sum_{j=1,j\neq i}^{N}h_{\theta,j}(\hat{\mathbf{x}}_j)\right].\end{aligned} \tag{2.107}$$

Substituting $\mathbf{H}^{\mathrm{T}}_{\theta}(\hat{\mathbf{x}}(k|k-1),k)$ from (2.80) gives

$$\boldsymbol{\varphi}_{\theta,i}(k) = \mathbf{c}_{\theta,i}\left[\sqrt{2}A_i\cos(\hat{\Theta}_i)z(k) - 2A_i^2\cos(\hat{\Theta}_i)\sin(\hat{\Theta}_i) - 2A_i\cos(\hat{\Theta}_i)\sum_{j=1,j\neq i}^{N}A_j\sin(\hat{\Theta}_j)\right]. \tag{2.108}$$

The middle term of (2.108) simplifies to $A_i^2\sin(2\omega_c k + 2\hat{\theta}_i(k))$ and, as it is solely composed of double frequency terms, will be removed by the loop filter and may be neglected leaving

$$\boldsymbol{\varphi}'_{\theta,i}(k) = \mathbf{c}_{\theta,i}\left[\sqrt{2}A_i\cos(\hat{\Theta}_i(k))z(k) - 2A_i\cos(\hat{\Theta}_i(k))\sum_{j=1,j\neq i}^{N}A_j\sin(\hat{\Theta}_j(k))\right]. \tag{2.109}$$

The last term of which reduces to

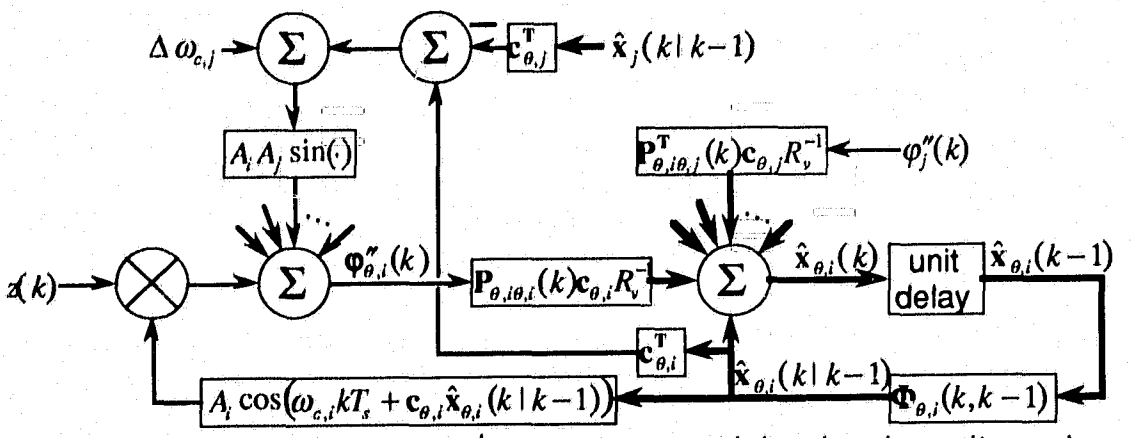

Figure 2–9 DPLL realization of i^{th} EKF estimator with baseband coupling only (amplitudes known).

$$2A_i\cos\left(\hat{\Theta}_i(k)\right)\sum_{j=1,j\neq i}^{N}A_j\sin\left(\hat{\Theta}_j(k)\right)= A_i\sum_{j=1,j\neq i}^{N}A_j\left[\sin\left(\hat{\Theta}_i(k)+\hat{\Theta}_j(k)\right)-\sin\left(\hat{\Theta}_i(k)-\hat{\Theta}_j(k)\right)\right] \tag{2.110}$$

To allow (2.110) to describe both ACI and CCI, assume that the carriers need not have the same carrier frequency, that is $\hat{\Theta}_i(k)=\omega_{c,i}kT_s+\hat{\theta}_i(k)$ and $\hat{\Theta}_j(k)=\omega_{c,j}kT_s+\hat{\vartheta}_j(k)$ where $\omega_{c,i}$ and $\omega_{c,j}$ are not necessarily equal. In (2.110) $\sin\left(\hat{\Theta}_i(k)+\hat{\Theta}_j(k)\right)=\sin\left(\left(\omega_{c,i}+\omega_{c,j}\right)kT_s+\hat{\theta}_i(k)+\hat{\theta}_j(k)\right)$ may be neglected since $\omega_{c,i}+\omega_{c,j}$ will always be substantially greater than the bandwidth of the loop filter. The other term in (2.110) is

$$\sin\left(\hat{\Theta}_i(k)-\hat{\Theta}_j(k)\right)=\sin\left(\Delta\omega_{c,j}kT_s+\hat{\theta}_i(k)-\hat{\theta}_j(k)\right), \tag{2.111}$$

where $\Delta\omega_{c,j}=\omega_{c,i}-\omega_{c,j}$ is the carrier frequency offset between the two sources. If $\left|\Delta\omega_{c,j}\right|$ is within the bandwidth of the loop filter, (2.111) cannot be neglected and (2.108) becomes

$$\boldsymbol{\varphi}'_{\theta,i}(k)=\mathbf{c}_{\theta,i}\left[\sqrt{2}A_i\cos\left(\hat{\Theta}_i(k)\right)z(k)-A_i\sum_{j=1,j\neq i}^{N}A_j\sin\left(\Delta\omega_{c,j}kT_s+\hat{\theta}_i(k)-\hat{\theta}_j(k)\right)\right], \tag{2.112}$$

the resulting CDPLL realization is shown in Fig. 2–9. If $\Delta\omega_{c,j}=0$ then $\sin\left(\hat{\Theta}_i(k)-\hat{\Theta}_j(k)\right)=\sin\left(\hat{\theta}_i(k)-\hat{\theta}_j(k)\right)$ in which case the coupling between the two source

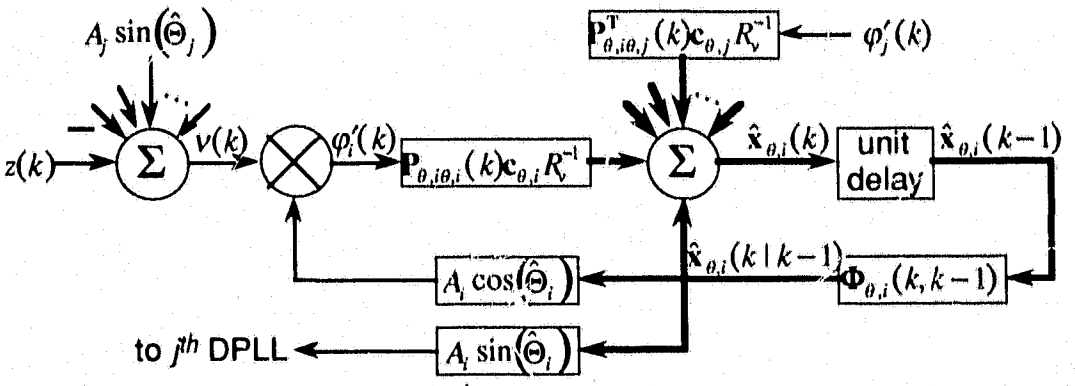

Figure 2–10 DPLL realization of i^{th} EKF estimator with baseband and passband coupling (amplitudes known).

estimators is strictly baseband. However, if $\Delta\omega_{c,j} \neq 0$ then the coupling due to (2.111) is a bandpass process. As $|\Delta\omega_{c,j}|$ increases, it begins to be removed by the loop filter and once $|\Delta\omega_{c,j}|$ is much greater than the bandwidth of the loop filter, (2.111) may be neglected in which case (2.108) becomes simply $\mathbf{c}_{\theta,i}\left[\sqrt{2}A\cos\left(\hat{\Theta}_i(k)\right)z(k)\right]$ which is identical to (2.92), an uncoupled DPLL. This is intuitively satisfying since increasing $|\Delta\omega_{c,j}|$ means that the two signals are moving out of the same channel and once $|\Delta\omega_{c,j}|$ is greater than the bandwidths of the sources, the two signals are no longer effecting each other; that is to say, neither ACI not CCI are present.

It may be more efficient to implement (2.109) directly as opposed to generating (2.112). This is equivalent to moving the innovations coupling from baseband (2.112) to passband (2.109) centered at the RF or IF. Fig. 2–10 shows this passband coupled scheme which is functionally equivalent to that of Fig. 2–9.

If the carrier amplitude is to be estimated, then (2.106) is partitioned as in (2.94) resulting in

$$\begin{bmatrix}\hat{\mathbf{x}}_{\theta,i}(k)\\ \hat{x}_{A,i}(k)\end{bmatrix} = \begin{bmatrix}\Phi_{\theta,i} & \mathbf{0}\\ \mathbf{0} & 1\end{bmatrix}\begin{bmatrix}\hat{\mathbf{x}}_{\theta,i}(k-1)\\ \hat{x}_{A,i}(k-1)\end{bmatrix} + \mathbf{P}(k)R_v^{-1}\varphi(k), \tag{2.113}$$

where from (2.103)

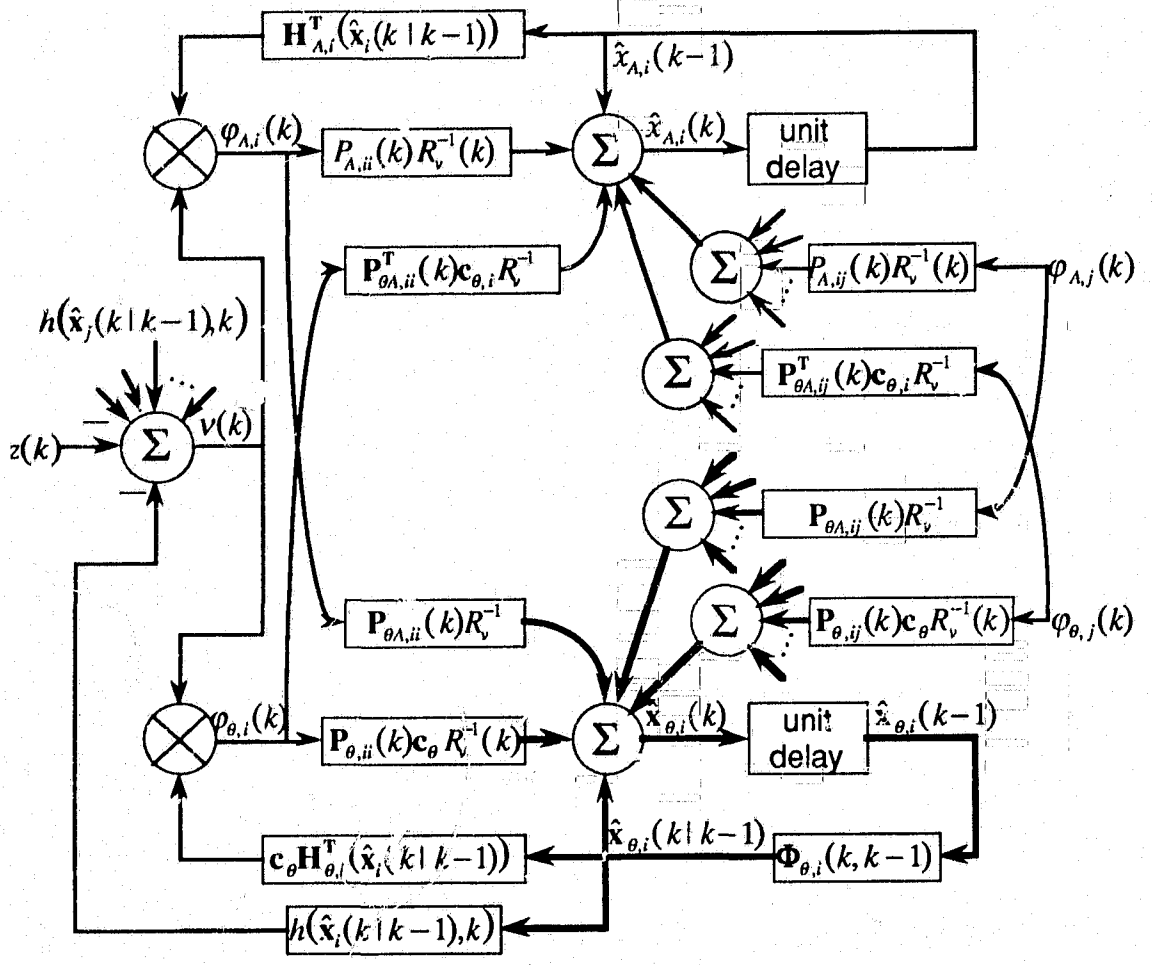

Figure 2–11 Direct realization of i^{th} EKF estimator with amplitude estimation.

$$\mathbf{P}_{ij}(k)=\left[\begin{array}{c|c}\mathbf{P}_{\theta,ij}(k) & \mathbf{P}_{\theta\Lambda,ij}(k)\\ \hline \mathbf{P}^{\mathrm{T}}_{\theta\Lambda,ij}(k) & P_{\Lambda,ij}(k)\end{array}\right], \tag{2.114}$$

and

$$\varphi_i(k)=\left[\begin{array}{c}\mathbf{c}_{\theta,i}\varphi_{\theta,i}(k)\\ \hline \varphi_{\Lambda,i}(k)\end{array}\right]=\left[\begin{array}{c}\mathbf{c}_{\theta,i}\mathbf{H}^{\mathrm{T}}_{\theta,i}(\hat{\mathbf{x}}_i(k\mid k-1))\nu(k)\\ \hline \mathbf{H}^{\mathrm{T}}_{\Lambda,i}(\hat{\mathbf{x}}_i(k\mid k-1))\nu(k)\end{array}\right]. \tag{2.115}$$

The direct implementation of the i^{th} amplitude and phase estimator takes the form of Fig. 2–11. It quickly becomes obvious that the complexity of the estimator of Fig. 2–11 increases drastically with the increase in the number of sources. Since the coupling is due to the error

covariance matrix, the number of cross-couple connections increases as N^2 where N is the number of sources.

As before, the double frequency terms in phase estimation may be neglected. Substituting (2.80) into (2.115), expanding, and neglecting double frequency terms gives

$$\boldsymbol{\varphi}_i'(k)=\begin{bmatrix}\boldsymbol{\varphi}_{\theta,i}'(k)\\ \varphi_{A,i}'(k)\end{bmatrix}=\begin{bmatrix}\mathbf{c}_i\left[\sqrt{2}\hat{A}_i\cos\left(\hat{\Theta}_i(k)\right)z(k)+2\hat{A}_i\cos\left(\hat{\Theta}_i(k)\right)\sum_{j=1,j\neq i}^{N}\hat{A}_j\sin\left(\hat{\Theta}_j(k)\right)\right]\\ \sqrt{2}\sin\left(\hat{\Theta}_i(k)\right)z(k)-\hat{A}_i-2\sin\left(\hat{\Theta}_i(k)\right)\sum_{j=1,j\neq i}^{N}\hat{A}_j\sin\left(\hat{\Theta}_j(k)\right)\end{bmatrix}, \quad (2.116)$$

where $\hat{A}_i=\hat{A}_i(k\,|\,k-1)$ and where $\varphi_{\theta,i}'(k)$ is from (2.109). $\varphi_{A,i}(k)$ results from (2.115) by expanding $\varphi_{A,i}(k)$

$$\varphi_{A,i}(k)=\sqrt{2}\sin\left(\hat{\Theta}_i(k)\right)z(k)-2\hat{A}_i\sin^2\left(\hat{\Theta}_i(k)\right)-2\sin\left(\hat{\Theta}_i(k)\right)\sum_{j=1,j\neq i}^{N}\hat{A}_i\sin\left(\hat{\Theta}_j(k)\right) \quad (2.117)$$

and using the trigonometric identity

$$2\sin^2(\zeta)=1-\cos(2\zeta), \quad (2.118)$$

and neglecting double frequency terms gives

$$\varphi_{A,i}'(k)\equiv\sqrt{2}\sin\left(\hat{\Theta}_i(k)\right)z(k)-\hat{A}_i-\sum_{j=1,j\neq i}^{N}\hat{A}_j\cos\left(\hat{\Theta}_i(k)-\hat{\Theta}_j(k)\right). \quad (2.119)$$

So DPLL realization of the estimation of $\mathbf{x}_{\theta,i}(k)$ utilizes (2.116) whereas the estimation of $x_{A,i}(k)$ utilizes (2.115) as shown in Fig. 2–12.

When $i=j$ in the estimation error covariance matrix of (2.113), $\mathbf{P}_{ij}(k)$ is the auto-covariance of the estimation error in $\hat{\mathbf{x}}_i(k)$ which has been studied in Section 2.3.2. Of interest at this point is the contribution of the cross-covariance matrices in the coupling of the DPLLs. Using the same procedure as before, set

$$\mathbf{P}_{ii}(0)=\begin{bmatrix}\mathbf{P}_{\theta,i}(0) & \mathbf{0}\\ \mathbf{0} & P_{A,i}(0)\end{bmatrix} \quad (2.120)$$

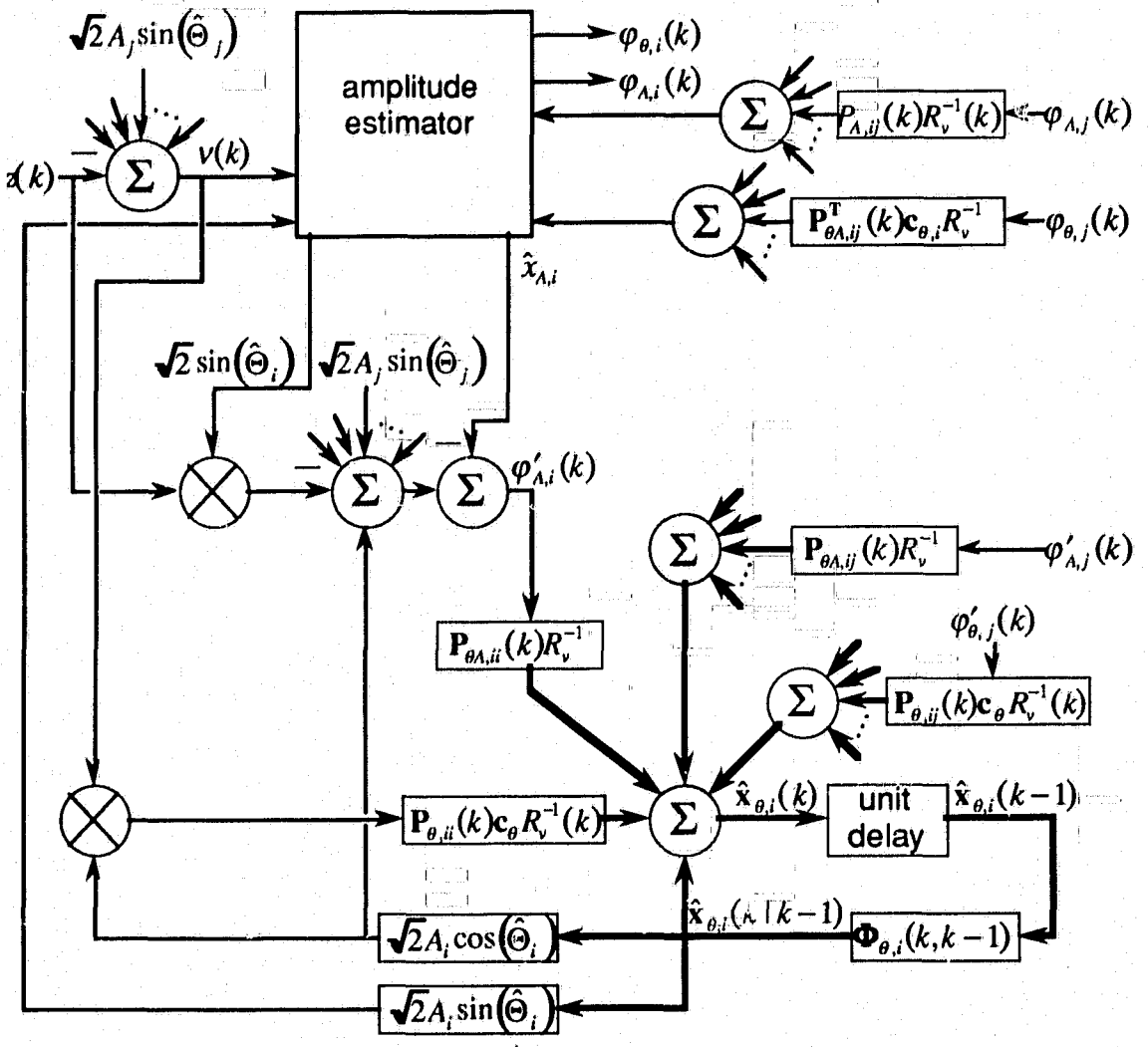

Figure 2–12 DPLL realization of i^{th} EKF estimator with amplitude estimation.

and set $\mathbf{P}_{ij}(0) = \mathbf{0}$. The prior error covariance estimate from (2.72) remains block diagonal

$$\mathbf{P}(1|0) = \begin{bmatrix} \mathbf{P}_{11}(1|0) & & & \mathbf{0} \\ & \mathbf{P}_{22}(1|0) & & \\ & & \ddots & \\ \mathbf{0} & & & \mathbf{P}_{NN}(1|0) \end{bmatrix}. \tag{2.121}$$

Substituting (2.121) into (2.88) and examining the off-diagonal matrices reveals that

$$\mathbf{P}_{ij}(1) = \frac{\mathbf{P}_{ii}(1|0)\mathbf{H}_i(\mathbf{x}_i(1|0))\mathbf{H}_j^{\mathrm{T}}(\mathbf{x}_i(1|0))\mathbf{P}_{jj}^{\mathrm{T}}(1|0)}{R_v + \sum_{l=1}^{N}\mathbf{H}_l(\mathbf{x}_l(1|0))\mathbf{P}_{ll}(1|0)\mathbf{H}_l^{\mathrm{T}}(\mathbf{x}_l(1|0))}, \tag{2.122}$$

indicating that the cross-covariance terms may not in general be neglected. The relative magnitude of the cross-covariance matrices determines the "strength" of the coupling between the DPLLs.

Further examination of the direct and DPLL realizations is possible but is dependent on the particular state vector and modulation process. Much of the subsequent work focuses on the first-order phase process (2.44) for a PM source. Therefore a PM receiver example will be presented. Bradley [18] derived an estimator for the FM case described by (2.53) which will also be presented.

2.3.4. PM Receiver Structure

Example structures from Sections. 2.3.2 and 2.3.3 are presented for phase modulated first order phase processes. First the single source case is examined and then a two source receiver is presented.

Single Source

For a phase modulate first order phase process, (2.28) is

$$\begin{bmatrix} x_\theta(k+1) \\ x_A(k+1) \end{bmatrix} = \begin{bmatrix} \theta(k+1) \\ A(k+1) \end{bmatrix} = \begin{bmatrix} \phi_\theta & 0 \\ 0 & 1 \end{bmatrix} \begin{bmatrix} \theta(k) \\ A(k) \end{bmatrix} + \begin{bmatrix} \gamma_\theta \\ 0 \end{bmatrix} w(k). \tag{2.123}$$

and the measurement is

$$z(k) = \sqrt{2}A(k)\sin\left(\omega_c k T_s + \theta(k)\right) + v(k). \tag{2.124}$$

From the observation function

$$h\left(\hat{\mathbf{x}}(k \mid k-1), k\right) = \sqrt{2}\hat{A}(k \mid k-1)\cos\left(\hat{\Theta}(k)\right), \tag{2.125}$$

the observation matrix (2.80) is

$$\mathbf{H}\left(\hat{\mathbf{x}}(k \mid k-1), k\right)^{\mathrm{T}} = \begin{bmatrix} \sqrt{2}\hat{A}(k \mid k-1)\cos\left(\hat{\Theta}(k)\right) \\ \sqrt{2}\sin\left(\hat{\Theta}(k)\right) \end{bmatrix}. \tag{2.126}$$

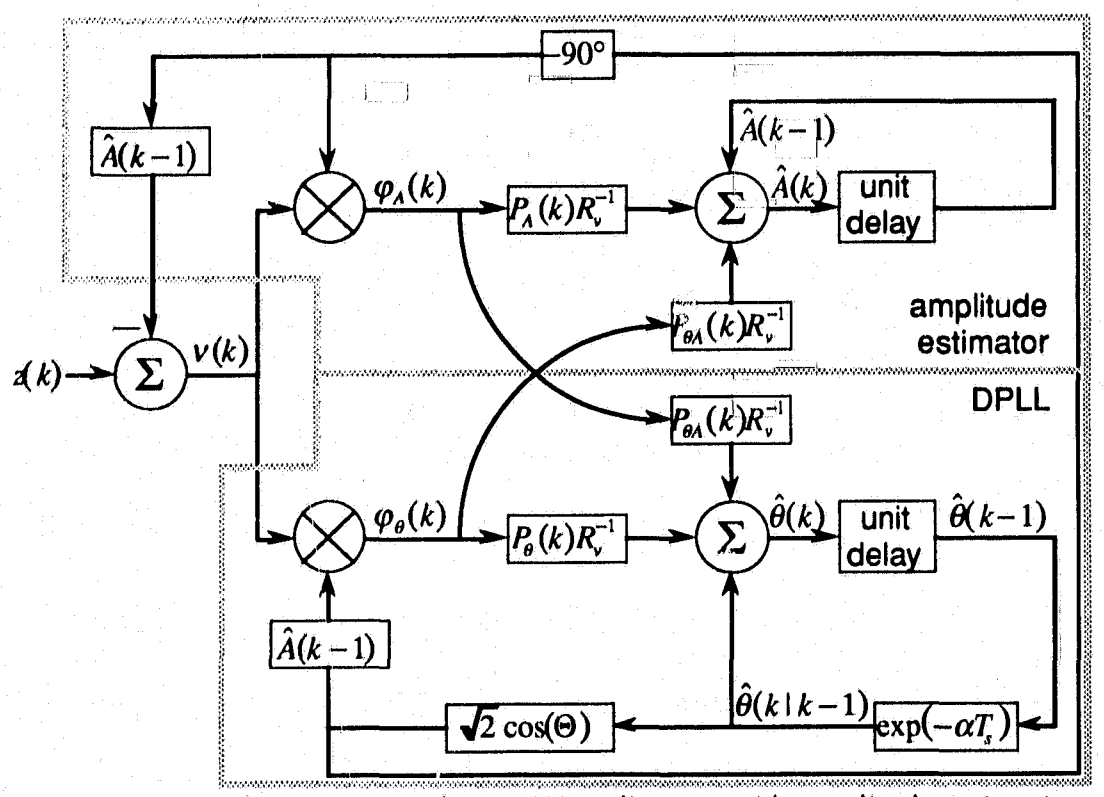

Figure 2–13 Single source PM direct EKF realization with amplitude estimation.

Substituting (2.126) and (2.125) into (2.94) gives the EKF equation

$$\begin{bmatrix}\hat{\theta}(k)\\ \hat{A}(k)\end{bmatrix}=\begin{bmatrix}\phi_\theta & 0\\ 0 & 1\end{bmatrix}\begin{bmatrix}\hat{\theta}(k-1)\\ \hat{A}(k-1)\end{bmatrix}+\begin{bmatrix}P_\theta(k) & P_{\theta A}(k)\\ P_{\theta A}(k) & P_A(k)\end{bmatrix}R_v^{-1}\begin{bmatrix}\varphi_\theta(k)\\ \varphi_A(k)\end{bmatrix}, \tag{2.127}$$

where from (2.95)

$$\begin{bmatrix}\varphi_\theta(k)\\ \varphi_A(k)\end{bmatrix}=\begin{bmatrix}\sqrt{2}\hat{A}(k|k-1)\cos\left(\hat{\Theta}(k)\right)v(k)\\ \sqrt{2}\sin\left(\hat{\Theta}(k)\right)v(k)\end{bmatrix}, \tag{2.128}$$

where the innovations process

$$v(k)=z(k)-\sqrt{2}\hat{A}(k|k-1)\sin\left(\hat{\Theta}(k)\right). \tag{2.129}$$

The elements of (2.127) give the phase estimate

$$\hat{\theta}(k)=\phi_\theta\hat{\theta}(k-1)+P_\theta(k)R_v^{-1}\varphi_\theta(k)+P_{\theta A}(k)R_v^{-1}\varphi_A(k), \tag{2.130}$$

and amplitude estimate

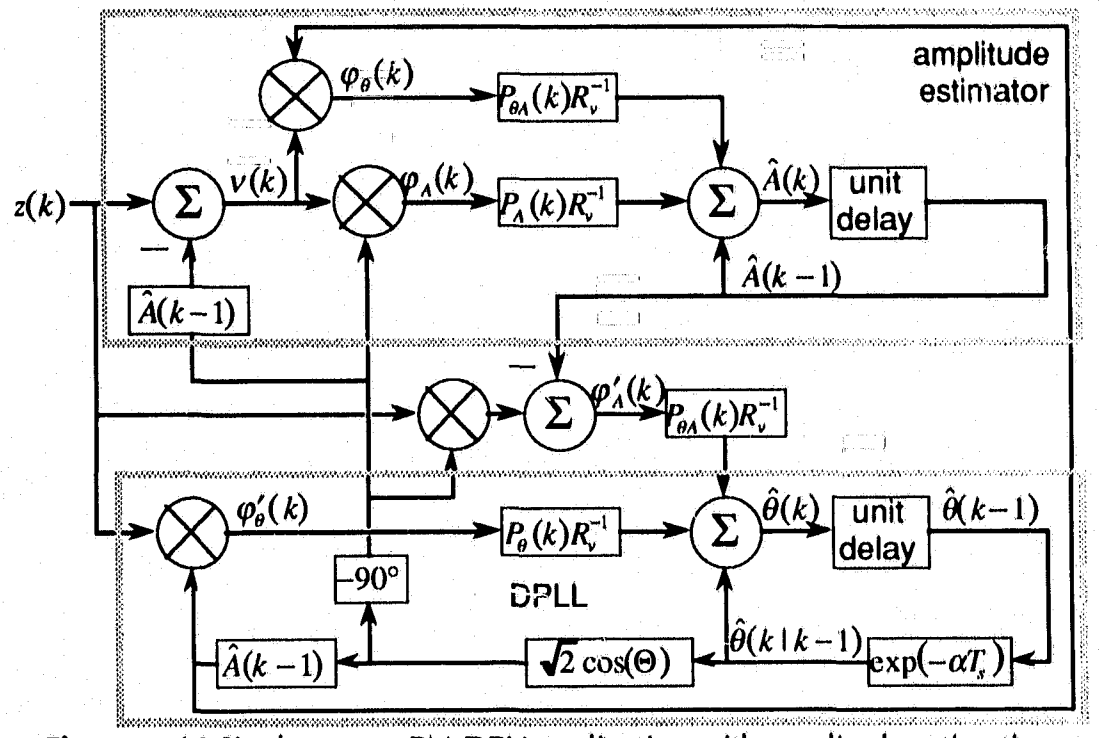

Figure 2–14 Single source PM DPLL realization with amplitude estimation.

$$\hat{A}(k) = \hat{A}(k-1) + P_{\theta A}(k)R_v^{-1}\varphi_\theta(k) + P_A(k)R_v^{-1}\varphi_A(k). \tag{2.131}$$

The direct realization of (2.130) and (2.131) is shown in Fig. 2–13, which is simply a special case of Fig. 2–6. The separate amplitude and phase estimators may easily be seen. The phase estimator is that of Fig. 2–4 which is basically a DPLL with the addition of the innovations process input into the phase detector.

From (2.96) the double frequency terms of the phase estate estimate (2.130) may be neglected in (2.128)

$$\begin{bmatrix}\varphi'_\theta(k)\\ \varphi'_A(k)\end{bmatrix} = \begin{bmatrix}\sqrt{2}\hat{A}(k\,|\,k-1)\cos\left(\hat{\Theta}(k)\right)z(k)\\ \sqrt{2}\sin\left(\hat{\Theta}(k)\right)z(k) - \hat{A}(k\,|\,k-1)\end{bmatrix}. \tag{2.132}$$

However, the double frequency terms may not be neglected in amplitude estimation since the loop filter for the amplitude state is essentially all-pass. Thus only the phase state estimate (2.130) may be simplified as

$$\hat{\theta}(k) = \phi_\theta \hat{\theta}(k-1) + P_\theta(k) R_v^{-1} \varphi_\theta'(k) + P_{\theta\Lambda}(k) R_v^{-1} \varphi_\Lambda'(k). \tag{2.133}$$

The resulting receiver structure of Fig. 2–14 is composed of coupled phase and amplitude estimators where the phase estimator is the DPLL of Fig. 2–4 with the addition of the coupling of the amplitude estimator.

The coupling of the two estimators occurs by the cross-covariance elements $P_{\theta\Lambda}$. Since the phase and amplitude processes of (2.123) are not coupled, investigation into the nature of the cross-covariance coupling is required.

At this time we are interested only in the off-diagonal elements of (2.100) into which we substitute (2.126) to find

$$P_{\theta\Lambda}(1) = \frac{2P_\theta(1|0)P_\Lambda(0)\hat{x}_\Lambda(1|0)\cos(\Theta(k))\sin(\Theta(k))}{R_v + 2P_\theta(1|0)\hat{x}_\Lambda(1|0)\cos^2(\Theta(k)) + 2P_\Lambda(0)\sin^2(\Theta(k))}, \tag{2.134}$$

which after use of the trigonometry identities

$$2\cos(\zeta)\sin(\zeta) = \sin(2\zeta), \tag{2.135}$$

and (2.118) (2.134) becomes

$$P_{\theta\Lambda}(1) = \frac{P_\theta(1|0)P_\Lambda(0)\hat{x}_\Lambda(1|0)\sin(2\Theta(k))}{R_v + P_\theta(1|0)\hat{x}_\Lambda(1|0)\big(1+\cos(2\Theta(k))\big) + P_\Lambda(0)\big(1-\cos(2\Theta(k))\big)}. \tag{2.136}$$

The off-diagonal elements are zero if the numerator of (2.136) is zero. The conditions which result in a zero denominator are if $P_\Lambda(0) = 0$ or if $P_\theta(1|0) = 0$ which is unlikely since the prior error covariance of the estimates is zero only if $\hat{A}(k|k-1) = A(k)$ or if $\hat{\theta}(k|k-1) = \theta(k)$ which will definitely not be the case during acquisition when the states are being estimated. $P_\theta(1|0) > 0$ since $0 < \phi_\theta^2 = \exp(-2\alpha T_s) < 1$ and $0 < \gamma_\theta^2 = 1 - \phi_\theta^2$. Thus the error covariance update (2.88) reveals that $P_{\theta\Lambda}$ may not be zero during the acquisition stage. Once the states have been accurately estimated, then $P_{\theta\Lambda}$ may become less significant and may then possibly be neglected.

Two Sources, Known Amplitudes

We now expand the development the single source DPLL to that for two sources. For the case where the amplitudes of the carriers are known, the state equation is

$$\begin{bmatrix} x_{\theta,1}(k+1) \\ x_{\theta,2}(k+1) \end{bmatrix} = \begin{bmatrix} \theta_1(k+1) \\ \theta_2(k+1) \end{bmatrix} = \begin{bmatrix} \phi_{\theta,1} & 0 \\ 0 & \phi_{\theta,2} \end{bmatrix} \begin{bmatrix} \theta_1(k) \\ \theta_2(k) \end{bmatrix} + \begin{bmatrix} \gamma_{\theta,1} & 0 \\ 0 & \gamma_{\theta,2} \end{bmatrix} \begin{bmatrix} w_{\theta,1}(k) \\ w_{\theta,2}(k) \end{bmatrix}, \tag{2.137}$$

and the PM measurement is

$$z(k) = \sqrt{2}\left[A_1 \sin\left(\omega_c k T_s + \theta_1(k)\right) + A_2 \sin\left(\omega_c k T_s + \theta_2(k)\right)\right] + v(k), \tag{2.138}$$

where A_1 and A_2 are both known constants. The EKF equation is

$$\begin{bmatrix} \hat{\theta}_1(k) \\ \hat{\theta}_2(k) \end{bmatrix} = \begin{bmatrix} \phi_{\theta,1} & 0 \\ 0 & \phi_{\theta,2} \end{bmatrix} \begin{bmatrix} \hat{\theta}_1(k-1) \\ \hat{\theta}_2(k-1) \end{bmatrix} + \begin{bmatrix} P_{\theta,1}(k) & P_{\theta,1\theta,2}(k) \\ P_{\theta,1\theta,2}(k) & P_{\theta,2}(k) \end{bmatrix} R_v^{-1} \begin{bmatrix} \varphi_{\theta,1}(k) \\ \varphi_{\theta,2}(k) \end{bmatrix}, \tag{2.139}$$

where

$$\begin{bmatrix} \varphi_{\theta,1}(k) \\ \varphi_{\theta,2}(k) \end{bmatrix} = \begin{bmatrix} \sqrt{2}A_1 \cos\left(\hat{\Theta}_1(k)\right) v(k) \\ \sqrt{2}A_2 \cos\left(\hat{\Theta}_2(k)\right) v(k) \end{bmatrix}. \tag{2.140}$$

with innovations process

$$v(k) = z(k) - \sqrt{2}\left[A_1 \sin\left(\hat{\Theta}_1(k)\right) + A_2 \sin\left(\hat{\Theta}_2(k)\right)\right]. \tag{2.141}$$

The phase estimates may be rewritten as

$$\hat{\theta}_1(k) = \phi_{\theta,1}\hat{\theta}_1(k-1) + P_{\theta,1}(k) R_v^{-1} \varphi_{\theta,1}(k) + P_{\theta,1\theta,2}(k) R_v^{-1} \varphi_{\theta,2}(k), \tag{2.142}$$

$$\hat{\theta}_2(k) = \phi_{\theta,2}\hat{\theta}_2(k-1) + P_{\theta,1\theta,2}(k) R_v^{-1} \varphi_{\theta,1}(k) + P_{\theta,2}(k) R_v^{-1} \varphi_{\theta,2}(k), \tag{2.143}$$

The resulting receiver structure is composed of two coupled phase estimators (see Fig. 2–15).

Neglecting the double frequency terms, (2.109) for this case becomes

$$\begin{bmatrix} \varphi'_{\theta,1}(k) \\ \varphi'_{\theta,2}(k) \end{bmatrix} = \begin{bmatrix} \sqrt{2}A_1 \cos\left(\hat{\Theta}_1(k)\right) z(k) - 2A_1 \cos\left(\hat{\Theta}_1(k)\right) A_2 \sin\left(\hat{\Theta}_2(k)\right) \\ \sqrt{2}A_2 \cos\left(\hat{\Theta}_2(k)\right) z(k) - 2A_2 \cos\left(\hat{\Theta}_2(k)\right) A_1 \sin\left(\hat{\Theta}_1(k)\right) \end{bmatrix}, \tag{2.144}$$

which may be implemented as shown in Fig. 2–16. The simplified innovations process is

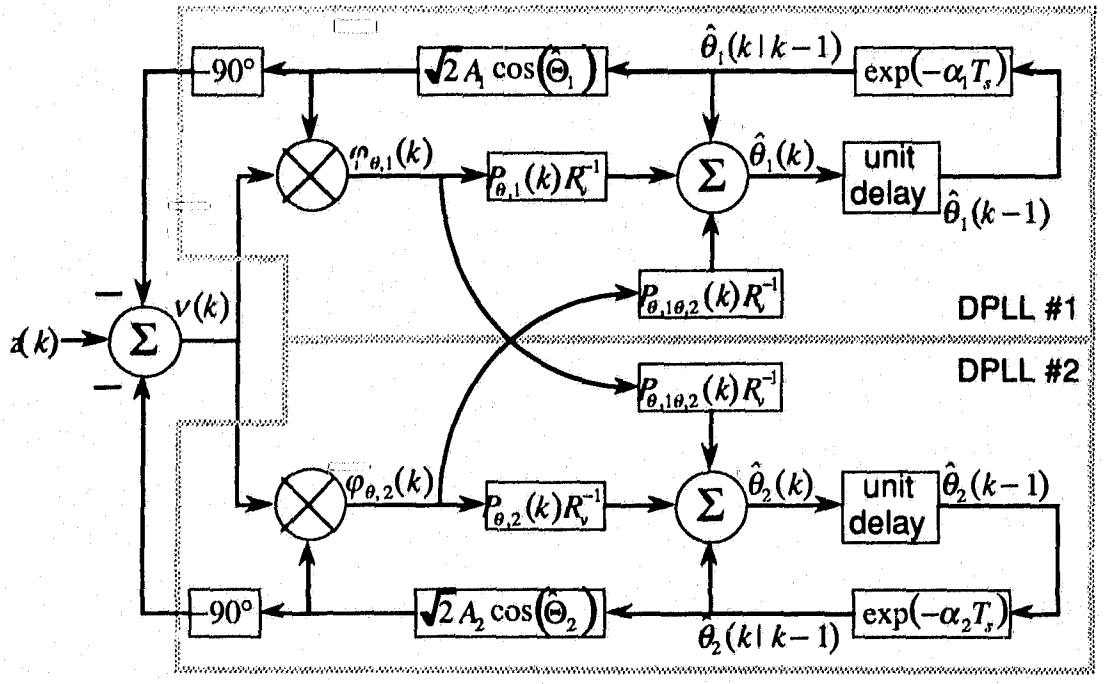

Figure 2–15 Direct realization of two source EKF estimator.

$$\begin{bmatrix} v_1(k) \\ v_2(k) \end{bmatrix} = \begin{bmatrix} z(k) - \sqrt{2}A_2 \sin\left(\hat{\Theta}_2(k)\right) \\ z(k) - \sqrt{2}A_1 \sin\left(\hat{\Theta}_1(k)\right) \end{bmatrix}. \tag{2.145}$$

Although the two phase processes are independent, they are coupled. This is intuitively satisfying since the ability to correctly estimate one of the phases directly affects the ability to estimate the other. Here (2.122) becomes

$$P_{\theta,1\theta,2}(1) = \frac{A_1 A_2 \left[\cos\left(\hat{\theta}_1 - \hat{\theta}_2\right) + \cos\left(\hat{\Theta}_1(k) + \hat{\Theta}_2(k)\right)\right] P_{\theta,1}(1|0) P_{\theta,2}(1|0)}{R_v + A_1^2\left(1 + \cos\left(2\hat{\Theta}_1(k)\right)\right) P_{\theta,1}(1|0) + A_2^2\left(1 + \cos\left(2\hat{\Theta}_2(k)\right)\right) P_{\theta,2}(1|0)}. \tag{2.146}$$

If the amplitude of either one of the carriers is zero, then the cross-covariance is zero. This makes sense since if one of the amplitudes is zero, then we have but a single source. The only other way that (2.146) may be zero is if one of the $P_{\theta,i}(1|0) = \phi_{\theta,i}^2 P_{\theta,i}(0) + \gamma_{\theta,i}^2$ terms is zero. Since $0 < \phi_{\theta,i}^2 = \exp(-2\alpha_i T_s) < 1$ and $0 < \gamma_{\theta,i}^2 = 1 - \phi_{\theta,i}^2$ then $P_{\theta,i}(1|0) > 0$. Therefore the cross-covariance elements may not simply be neglected.

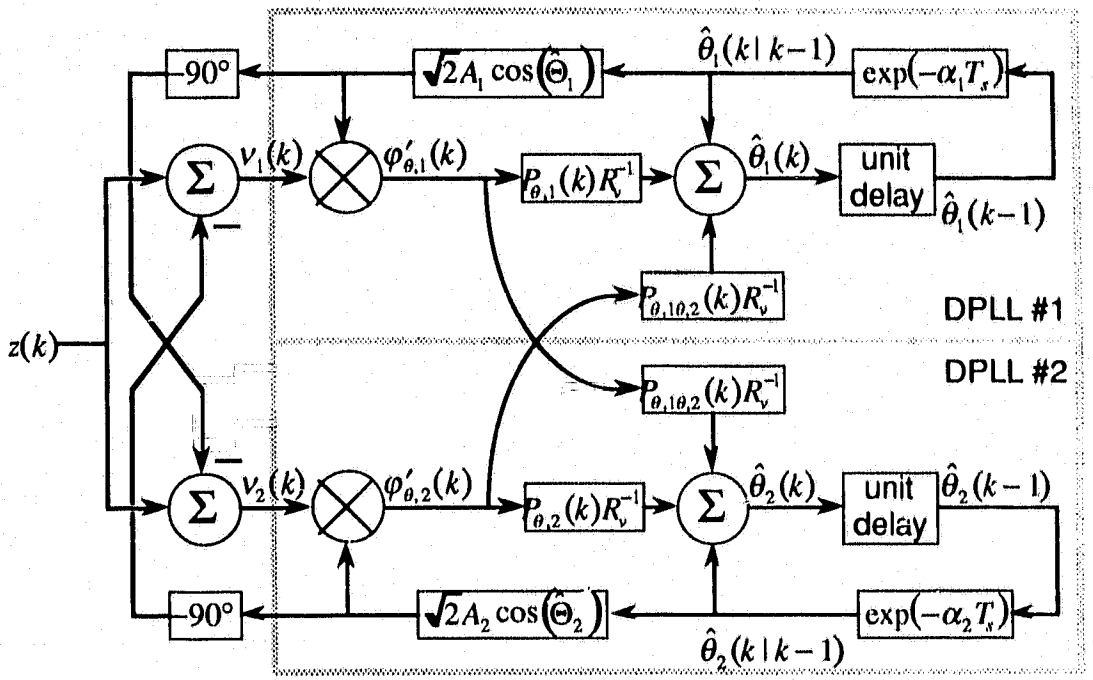

Figure 2–16 Two source PM CDPLL.

If the baseband coupling of Fig. 2–16 is removed, that is $P_{\theta 1,\theta 2}(k)=0$, the case of the analog MAP derived CPLL estimator [13] and in the subsequent works [14] [15] results. In their estimator the estimate of θ_2 is removed from the input of DPLL #1 and vice versa (see Fig. 1–6). However, as their MAP estimator simply uses independent stationary Gaussian processes to model the modulation, the baseband coupling between the states that result from the EKF are not present in the MAP derivation.

Another approach is to look at each DPLL as a separate estimator, each described by (2.93). This is accomplished by creating a separate innovations process for each of the two EKFs. In (2.141) the predicted state measurement is

$$h(\hat{\mathbf{x}}(k),k)=\sqrt{2}\left[A_1\sin\left(\hat{\Theta}_1(k)\right)+A_2\sin\left(\hat{\Theta}_2(k)\right)\right]. \tag{2.147}$$

However, the predicted state measurement for θ_1 is $h\left(\hat{\theta}_1(k|k-1),k\right)=\sqrt{2}A_1\sin\left(\hat{\Theta}_1(k)\right)$ and similarly for θ_2. In this manner (2.141) becomes

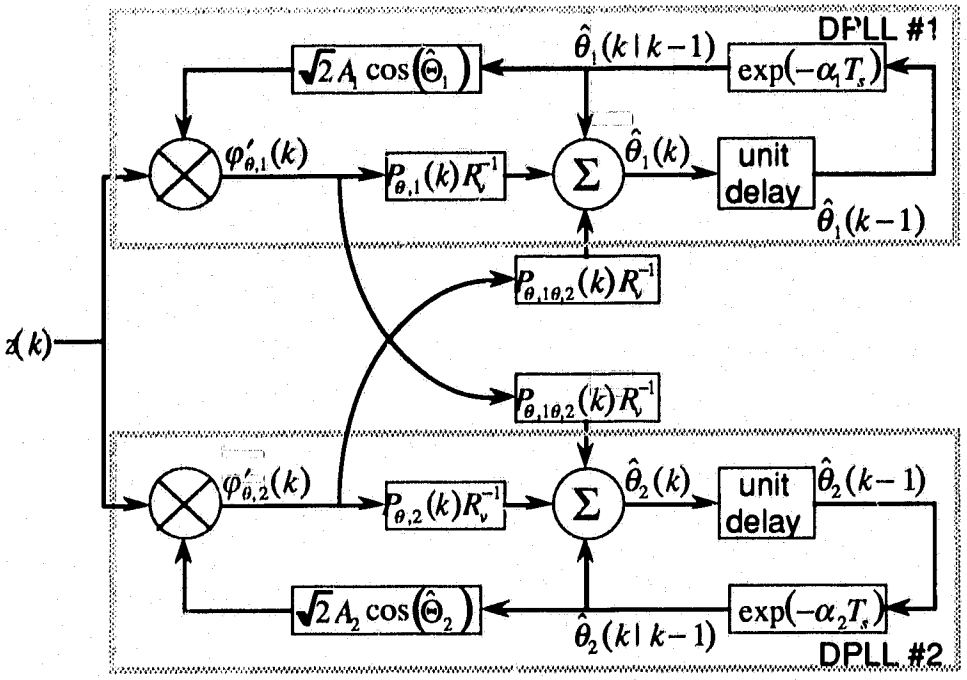

Figure 2–17 Two source PM CDPLL with no innovations process.

$$\begin{bmatrix} v_1(k) \\ v_2(k) \end{bmatrix} = \begin{bmatrix} z(k) - \sqrt{2}A_1 \sin\left(\hat{\Theta}_1(k)\right) \\ z(k) - \sqrt{2}A_2 \sin\left(\hat{\Theta}_2(k)\right) \end{bmatrix}. \tag{2.148}$$

Substituting (2.148) into (2.140) and neglecting double frequency terms leaves

$$\begin{bmatrix} \varphi'_1(k) \\ \varphi'_2(k) \end{bmatrix} = \begin{bmatrix} \sqrt{2}A_1 \cos\left(\hat{\Theta}_1(k)\right) z(k) \\ \sqrt{2}A_2 \cos\left(\hat{\Theta}_2(k)\right) z(k) \end{bmatrix}. \tag{2.149}$$

This is equivalent to replacing the innovations process with the measurement as in (2.93) which is realized by Fig. 2–17. This is similar to the receiver developed by Kumar [36, 37].

Two sources, unknown amplitude

Finally amplitude estimation is included in the two-source estimator. The state equation from (2.44) is

$$\begin{bmatrix}\theta_1(k+1)\\ A_1(k+1)\\ \theta_2(k+1)\\ A_2(k+1)\end{bmatrix}=\begin{bmatrix}\phi_{\theta,1} & 0 & \mathbf{0} & \\ 0 & 1 & & \\ & \mathbf{0} & \phi_{\theta,2} & 0\\ & & 0 & 1\end{bmatrix}\begin{bmatrix}\theta_1(k)\\ A_1(k)\\ \theta_2(k)\\ A_2(k)\end{bmatrix}+\begin{bmatrix}\gamma_{\theta,1} & 0 & \mathbf{0} & \\ 0 & 0 & & \\ & \mathbf{0} & \gamma_{\theta,2} & 0\\ & & 0 & 0\end{bmatrix}\begin{bmatrix}w_{\theta,1}(k)\\ 0\\ w_{\theta,2}(k)\\ 0\end{bmatrix}, \tag{2.150}$$

with corresponding measurement

$$z(k)=\sqrt{2}\left[A_1(k)\sin\left(\omega_c kT_s+\theta_1(k)\right)+A_2(k)\sin\left(\omega_c kT_s+\theta_2(k)\right)\right]+v(k), \tag{2.151}$$

resulting in the observation matrix

$$\mathbf{H}\left(\hat{\mathbf{x}}(k\mid k-1),k\right)^{\mathrm{T}}=\begin{bmatrix}\sqrt{2}\hat{A}_1(k\mid k-1)\cos\left(\hat{\Theta}_1(k)\right)\\ \sqrt{2}\sin\left(\hat{\Theta}_1(k)\right)\\ \sqrt{2}\hat{A}_2(k\mid k-1)\cos\left(\hat{\Theta}_2(k)\right)\\ \sqrt{2}\sin\left(\hat{\Theta}_2(k)\right)\end{bmatrix}. \tag{2.152}$$

From the observation function of (2.151), the innovations process is

$$v(k)=z(k)-\sqrt{2}\left[\hat{A}_1(k\mid k-1)\sin\left(\hat{\Theta}_1(k)\right)+\hat{A}_2(k\mid k-1)\sin\left(\hat{\Theta}_2(k)\right)\right]. \tag{2.153}$$

The Kalman Filter equation from (2.113) is

$$\begin{bmatrix}\hat{\theta}_1(k+1)\\ \hat{A}_1(k+1)\\ \hat{\theta}_2(k+1)\\ \hat{A}_2(k+1)\end{bmatrix}=\begin{bmatrix}\phi_{\theta,1} & 0 & \mathbf{0} & \\ 0 & 1 & & \\ & \mathbf{0} & \phi_{\theta,2} & 0\\ & & 0 & 1\end{bmatrix}\begin{bmatrix}\hat{\theta}_1(k)\\ \hat{A}_1(k)\\ \hat{\theta}_2(k)\\ \hat{A}_2(k)\end{bmatrix}+\begin{bmatrix}\mathbf{P}_{11}(k) & \mathbf{P}_{12}(k)\\ \mathbf{P}_{21}(k) & \mathbf{P}_{22}(k)\end{bmatrix}R_v^{-1}\begin{bmatrix}\varphi_1(k)\\ \varphi_2(k)\end{bmatrix} \tag{2.154}$$

where $\mathbf{P}_{ij}(k)$ are defined in (2.114) and from (2.128)

$$\boldsymbol{\varphi}_i(k)=\begin{bmatrix}\sqrt{2}\hat{A}_i(k\mid k-1)\cos\left(\hat{\Theta}_i(k)\right)v(k)\\ \sqrt{2}\sin\left(\hat{\Theta}_i(k)\right)v(k)\end{bmatrix}. \tag{2.155}$$

which may be simplified via (2.116)

$$\boldsymbol{\varphi}_i'(k)=\begin{bmatrix}\boldsymbol{\varphi}_{\theta,i}'(k)\\ \varphi_{A,i}'(k)\end{bmatrix}=\begin{bmatrix}\mathbf{c}_i\left[\sqrt{2}\hat{A}_i\cos\left(\hat{\Theta}_i(k)\right)z(k)+2\hat{A}_i\cos\left(\hat{\Theta}_i(k)\right)\hat{A}_j\sin\left(\hat{\Theta}_j(k)\right)\right]\\ \sqrt{2}\sin\left(\hat{\Theta}_i(k)\right)z(k)-\hat{A}_i-2\sin\left(\hat{\Theta}_i(k)\right)\hat{A}_j\sin\left(\hat{\Theta}_j(k)\right)\end{bmatrix}. \tag{2.156}$$

The realization of (2.156) and the EKF equation is shown in Fig. 2–18.

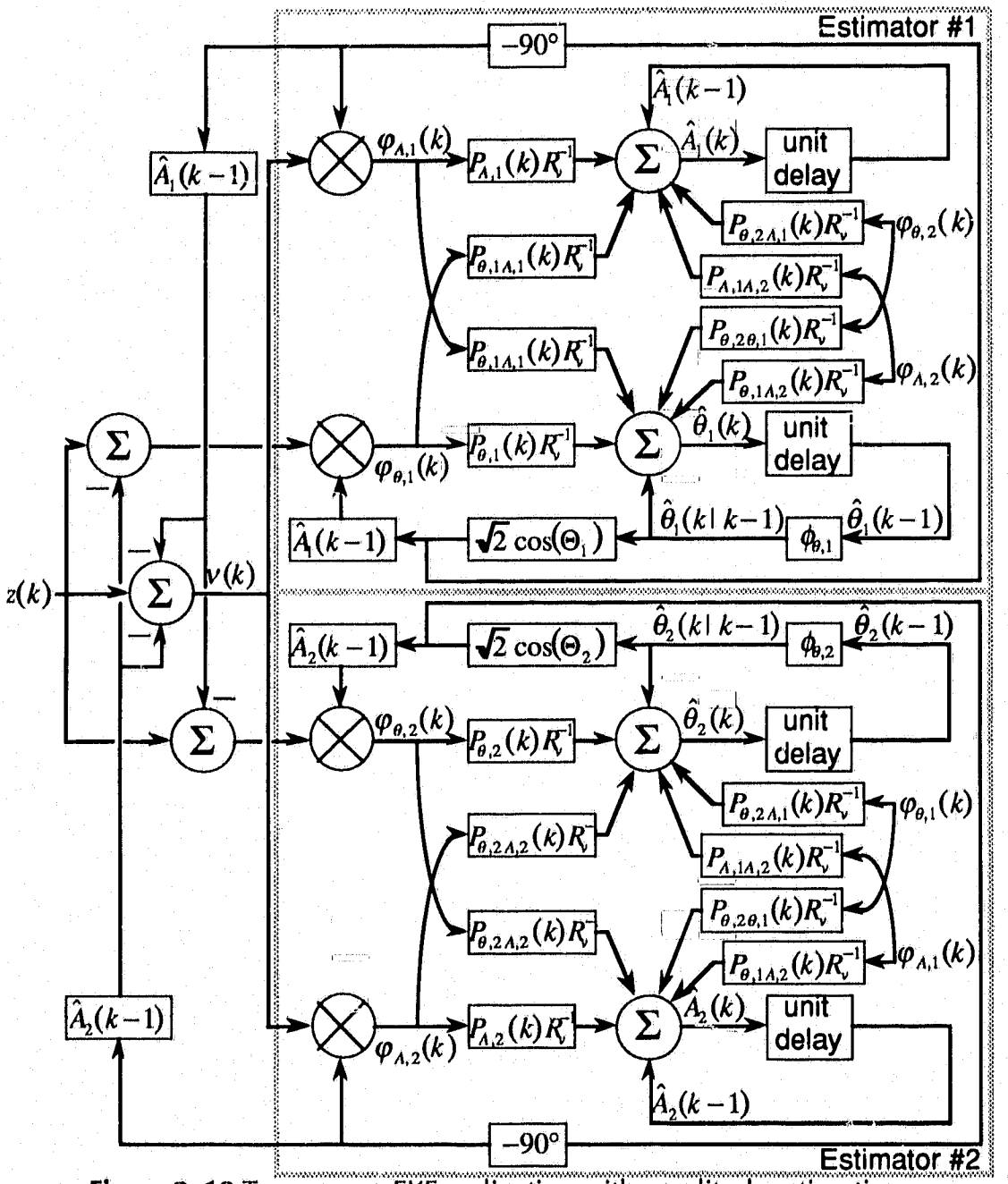

Figure 2–18 Two source EKF realization with amplitude estimation.

The coupling between A and θ in $\mathbf{P}_{ii}(k)$ was presented in (2.134). However the coupling between the two process estimators has not been studied. From (2.122) the elements of $\mathbf{P}_{\theta,iA,j}(k)$ are found to be

$$P_{\theta,iA,j}(1)=\frac{\hat{A}_i(1|0)\left[\sin\left(\hat{\Theta}_i(k)+\hat{\Theta}_j(k)\right)-\sin\left(\hat{\theta}_i(k)-\hat{\theta}_j(k)\right)\right]P_{\theta,i}(1|0)P_{A,j}(1|0)}{R_v+\sum_{l=1}^{2}\hat{A}_l^2(1|0)\left(1+\cos\left(2\hat{\Theta}_1(k)\right)\right)P_{\theta,l}(1|0)+\left(1-\cos\left(2\hat{\Theta}_1(k)\right)\right)P_{A,l}(1|0)}, \quad (2.157)$$

$$P_{A,1A,2}(1)=\frac{\left[\cos\left(\hat{\Theta}_1(k)+\hat{\Theta}_2(k)\right)-\cos\left(\hat{\theta}_1(k)-\hat{\theta}_2(k)\right)\right]P_{A,1}(1|0)P_{A,2}(1|0)}{R_v+\sum_{l=1}^{2}\hat{A}_l^2(1|0)\left(1+\cos\left(2\hat{\Theta}_1(k)\right)\right)P_{\theta,l}(1|0)+\left(1-\cos\left(2\hat{\Theta}_1(k)\right)\right)P_{A,l}(1|0)}, \quad (2.158)$$

and $P_{\theta,1\theta,2}(1)$ is as in (2.146). Again it is evident that the coupling cannot be dismissed especially during acquisition.

2.3.5. FM Receiver Structure

The first example of angle modulation presented was phase modulation. Since the message process is the same as the phase process, PM is a convenient modulation scheme to examine. However, frequency modulation is the most common form of angle modulation and is commonly the modulation scheme examined in the literature. Therefore the FM equivalents of the PM structures derived in the previous section will be presented.

Single Source

Since FM demodulation requires the estimation of an additional state when compared to PM, the single source FM receiver with amplitude estimation is presented first.

The state equation for a first-order FM source from (2.53) is

$$\begin{bmatrix}x_\theta(k+1)\\ x_f(k+1)\\ \hdashline x_A(k+1)\end{bmatrix}=\begin{bmatrix}\theta(k+1)\\ f(k+1)\\ \hdashline A(k+1)\end{bmatrix}=\left[\begin{array}{cc:c}1 & \phi_{\theta f} & 0\\ 0 & \phi_f & 0\\ \hdashline 0 & 0 & 1\end{array}\right]\begin{bmatrix}\theta(k)\\ f(k)\\ \hdashline A(k)\end{bmatrix}+\left[\begin{array}{cc:c}\gamma_\theta & \gamma_{\theta f} & \\ \gamma_{f\theta} & \gamma_f & \mathbf{0}\\ \hdashline \multicolumn{2}{c:}{\mathbf{0}} & 0\end{array}\right]\begin{bmatrix}w_\theta(k)\\ w_f(k)\\ \hdashline 0\end{bmatrix}, \quad (2.159)$$

where $\phi_{\theta f}$ and ϕ_f are defined in (2.47) and (2.48) respectively. The state selection vector is

$$\mathbf{c}=\left[\mathbf{c}_\theta^T \vdots 0\right]^T=\left[1 \quad 0 \vdots 0\right]^T, \quad (2.160)$$

resulting in the same measurement equation as for PM, (2.124). From (2.80) the observation matrix is

$$\mathbf{H}^{\mathrm{T}}(\hat{\mathbf{x}}(k\,|\,k-1),k)=\begin{bmatrix}\mathbf{c}_\theta^{\mathrm{T}}\mathbf{H}_\theta^{\mathrm{T}}(\hat{\mathbf{x}}(k\,|\,k-1),k)\\ \cdots\cdots\cdots\cdots\cdots\cdots\\ \mathbf{H}_A(\hat{\mathbf{x}}(k\,|\,k-1),k)\end{bmatrix}=\begin{bmatrix}\sqrt{2}\hat{A}(k\,|\,k-1)\cos\left(\hat{\Theta}(k)\right)\\ 0\\ \cdots\cdots\cdots\cdots\\ \sqrt{2}\sin\left(\hat{\Theta}(k)\right)\end{bmatrix}. \tag{2.161}$$

The estimator is formed by substituting (2.159), (2.160), and (2.161) into (2.94) which becomes

$$\begin{bmatrix}\hat{\theta}(k)\\ \hat{f}(k)\\ \hat{A}(k)\end{bmatrix}=\begin{bmatrix}1 & \phi_{\theta f} & 0\\ 0 & \phi_f & 0\\ 0 & 0 & 1\end{bmatrix}\begin{bmatrix}\hat{\theta}(k-1)\\ \hat{f}(k-1)\\ \hat{A}(k-1)\end{bmatrix}+\begin{bmatrix}P_\theta(k) & P_{\theta f}(k) & P_{\theta A}(k)\\ P_{f\theta}(k) & P_f(k) & P_{fA}(k)\\ P_{A\theta}(k) & P_{Af}(k) & P_A(k)\end{bmatrix}R_v^{-1}\begin{bmatrix}\varphi_\theta(k)\\ \varphi_f(k)\\ \varphi_A(k)\end{bmatrix}, \tag{2.162}$$

where from (2.95)

$$\boldsymbol{\varphi}(k)=\begin{bmatrix}\varphi_\theta(k)\\ \varphi_f(k)\\ \varphi_A(k)\end{bmatrix}=\begin{bmatrix}\sqrt{2}\hat{A}(k\,|\,k-1)\cos\left(\hat{\Theta}(k)\right)v(k)\\ 0\\ \sqrt{2}\sin\left(\hat{\Theta}(k)\right)v(k)\end{bmatrix}, \tag{2.163}$$

and the innovations process is the same as (2.129).

Since $\varphi_f(k)=0$ the elements of the middle column of $\mathbf{P}$ do not contribute to the receiver and may be neglected. The resulting individual state estimates are

$$\hat{\theta}(k)=\hat{\theta}(k-1)+\phi_{\theta f}\hat{f}(k-1)+P_\theta(k)R_v^{-1}\varphi_\theta(k)+P_{\theta A}(k)R_v^{-1}\varphi_A(k) \tag{2.164}$$

$$\hat{f}(k)=\phi_f\hat{f}(k-1)+P_{f\theta}(k)R_v^{-1}\varphi_\theta(k)+P_{fA}(k)R_v^{-1}\varphi_A(k) \tag{2.165}$$

$$\hat{A}(k)=\hat{A}(k-1)+P_{A\theta}(k)R_v^{-1}\varphi_\theta(k)+P_A(k)R_v^{-1}\varphi_A(k). \tag{2.166}$$

To facilitate a more compact diagram and also to better show the structure of the loop filter, z-transform notation will be used for the state predictions. From [38] the causal difference equation $y(n)=ay(n-1)+x(n)$ has a corresponding system function of

$$H(z)=\frac{1}{1-az^{-1}} \tag{2.167}$$

where the region of convergence is $|z|>|a|$. The single source FM receiver is shown in Fig. 2–19.

If the double frequency terms are neglected, from (2.96) (2.163) becomes

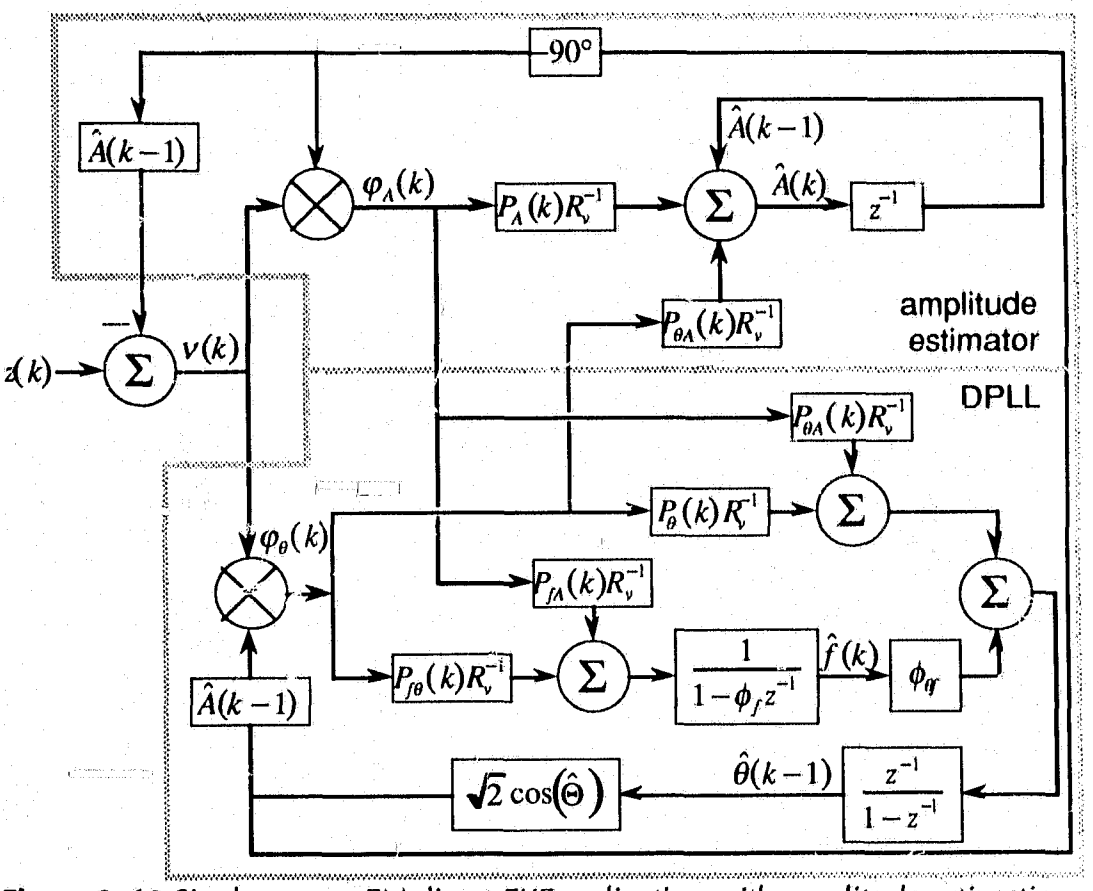

Figure 2–19 Single source FM direct EKF realization with amplitude estimation.

$$\begin{bmatrix}\varphi'_\theta(k)\\ \varphi'_f(k)\\ \varphi'_A(k)\end{bmatrix}=\begin{bmatrix}\sqrt{2}\hat{A}(k\,|\,k-1)\cos\left(\hat{\Theta}(k)\right)z(k)\\ 0\\ \sqrt{2}\sin\left(\hat{\Theta}(k)\right)z(k)-\hat{A}(k\,|\,k-1)\end{bmatrix}, \tag{2.168}$$

realized by the receiver of Fig. 2–20.

The state coupling again needs to be investigated with the addition of the frequency state. As previously mentioned, the middle column of **P** may be neglected so only the two outer columns need to be examined. Starting with an initial error covariance

$$P(0)=\begin{bmatrix}P_\theta(0) & 0 & 0\\ 0 & P_f(0) & 0\\ 0 & 0 & P_A(0)\end{bmatrix} \tag{2.169}$$

the error covariance prediction (2.72) is

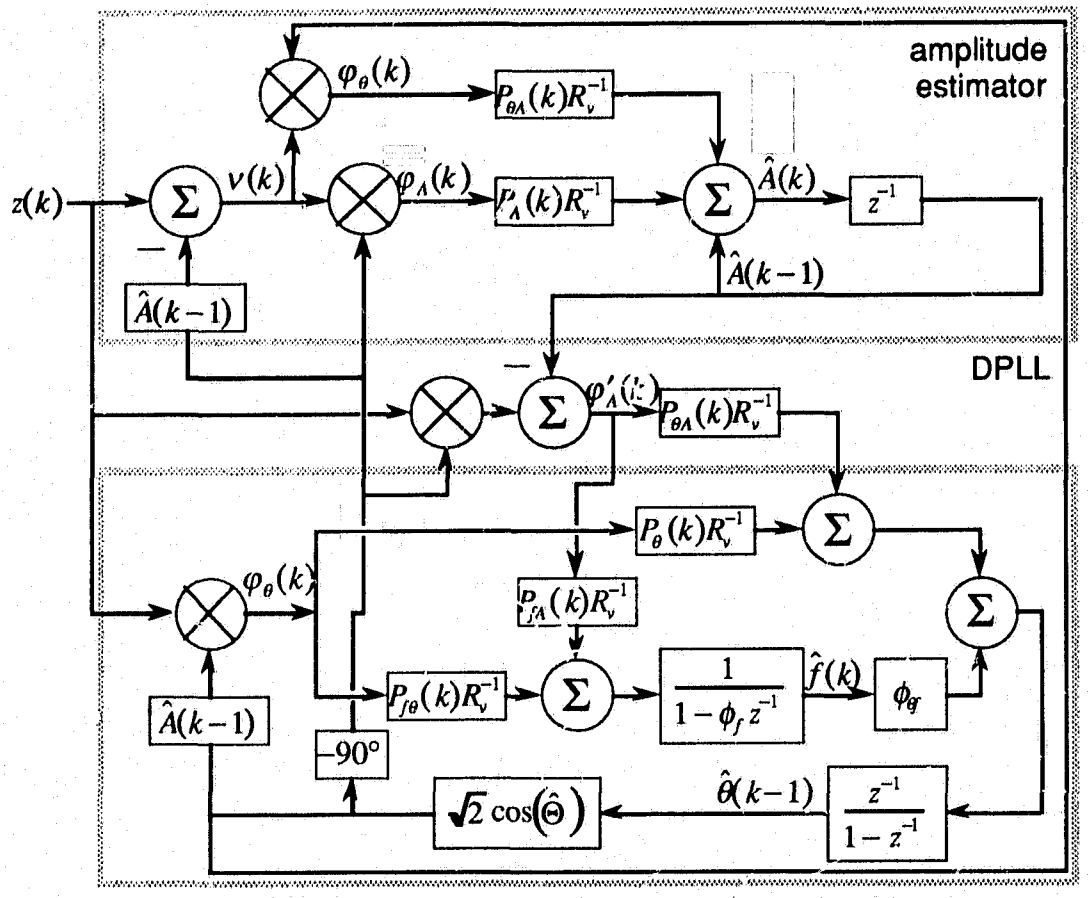

Figure 2–20 Single source FM DPLL realization with amplitude estimation.

$$P(1|0)=\begin{bmatrix} P_\theta(0)+\phi_{ff}^2P_f(0)+\gamma_\theta^2+\gamma_{ff}^2 & \phi_{ff}\phi_fP_f(0)+\gamma_\theta\gamma_{f\theta}+\gamma_{ff}\gamma_f & 0 \\ \phi_{ff}\phi_fP_f(0)+\gamma_\theta\gamma_{f\theta}+\gamma_{ff}\gamma_f & \phi_f^2P_f(0)+\gamma_{f\theta}^2+\gamma_f^2 & 0 \\ 0 & 0 & P_A(0) \end{bmatrix}. \tag{2.170}$$

Thus it is immediately apparent that the coupling between the phase and frequency states, via $P_{f\theta}$, may not be neglected. This is intuitively satisfying since the two states are coupled in the state equation. The coupling between the amplitude and the phase and frequency states is due to $\mu\mathbf{P}_\theta(1|0)\mathbf{H}_\theta^{\mathrm{T}}\mathbf{H}_A P_A(0)$ in (2.100) after substitution of (2.161) and (2.170) becomes

$$\mu\mathbf{P}_\theta(1|0)\mathbf{H}_\theta^{\mathrm{T}}\mathbf{H}_A P_A(0)=\mu\begin{bmatrix} 2\hat{A}(0)\cos\left(\hat{\Theta}(k)\right)P_\theta(1|0)\sin\left(\hat{\Theta}(k)\right)P_A(0) \\ 2\hat{A}(0)\cos\left(\hat{\Theta}(k)\right)P_{f\theta}(1|0)\sin\left(\hat{\Theta}(k)\right)P_A(0) \end{bmatrix} \tag{2.171}$$

where

$$\mu = \left[R_v + 2\hat{A}^2(0)\cos^2\left(\hat{\Theta}(k)\right)P_\theta(1|0) + 2\sin^2\left(\hat{\Theta}(k)\right)P_\lambda(1|0)\right]^{-1}. \tag{2.172}$$

Since none of the terms in the numerator of (2.171) are initially zero, again the state coupling cannot be neglected especially during acquisition.

Two Sources, Known Amplitudes

Nearly all of the related CPLL and CDPLL literature [13, 14, 15, 18, 19] has been developed with the two FM source scenario. The latter three have included some form of amplitude estimation. Therefore as a final example we present the two FM source EKF derived receiver structures. First we present the case where the amplitudes are known and then when they are unknown.

The state equation describing the two sources is

$$\begin{bmatrix}\theta_1(k+1)\\ f_1(k+1)\\ \theta_2(k+1)\\ f_2(k+1)\end{bmatrix} = \begin{bmatrix}\boldsymbol{\Phi}_{\theta,1} & \mathbf{0}\\ \mathbf{0} & \boldsymbol{\Phi}_{\theta,2}\end{bmatrix}\begin{bmatrix}\theta_1(k)\\ f_1(k)\\ \theta_2(k)\\ f_2(k)\end{bmatrix} + \begin{bmatrix}\boldsymbol{\Gamma}_{\theta,1} & \mathbf{0}\\ \mathbf{0} & \boldsymbol{\Gamma}_{\theta,2}\end{bmatrix}\begin{bmatrix}w_{\theta,1}(k)\\ w_{f,1}(k)\\ w_{\theta,2}(k)\\ w_{f,2}(k)\end{bmatrix}, \tag{2.173}$$

and the measurement equation is the same as (2.138). The observation matrix is

$$\mathbf{H}\left(\hat{\mathbf{x}}(k|k-1),k\right)^{\mathrm{T}} = \begin{bmatrix}\sqrt{2}\hat{A}_1(k|k-1)\cos\left(\hat{\Theta}_1(k)\right)\\ \sqrt{2}\sin\left(\hat{\Theta}_1(k)\right)\\ \sqrt{2}\hat{A}_2(k|k-1)\cos\left(\hat{\Theta}_2(k)\right)\\ \sqrt{2}\sin\left(\hat{\Theta}_2(k)\right)\end{bmatrix}. \tag{2.174}$$

The innovations process is the same as (2.141). The Kalman Filter equation from (2.106) is

$$\begin{bmatrix}\hat{\theta}_1(k)\\ \hat{f}_1(k)\\ \hat{\theta}_2(k)\\ \hat{f}_2(k)\end{bmatrix} = \begin{bmatrix}\boldsymbol{\Phi}_{\theta,1} & \mathbf{0}\\ \mathbf{0} & \boldsymbol{\Phi}_{\theta,2}\end{bmatrix}\begin{bmatrix}\hat{\theta}_1(k-1)\\ \hat{f}_1(k-1)\\ \hat{\theta}_2(k-1)\\ \hat{f}_2(k-1)\end{bmatrix} + \begin{bmatrix}\mathbf{P}_{11}(k) & \mathbf{P}_{12}(k)\\ \mathbf{P}_{21}(k) & \mathbf{P}_{22}(k)\end{bmatrix}R_v^{-1}\begin{bmatrix}\boldsymbol{\varphi}_1(k)\\ \boldsymbol{\varphi}_2(k)\end{bmatrix}, \tag{2.175}$$

where $\mathbf{P}_{ij}(k)$ are defined in (2.114) and from (2.163)

$$\boldsymbol{\varphi}_i(k) = \begin{bmatrix}\sqrt{2}A_i\cos\left(\hat{\Theta}_i(k)\right)v(k)\\ 0\end{bmatrix}. \tag{2.176}$$

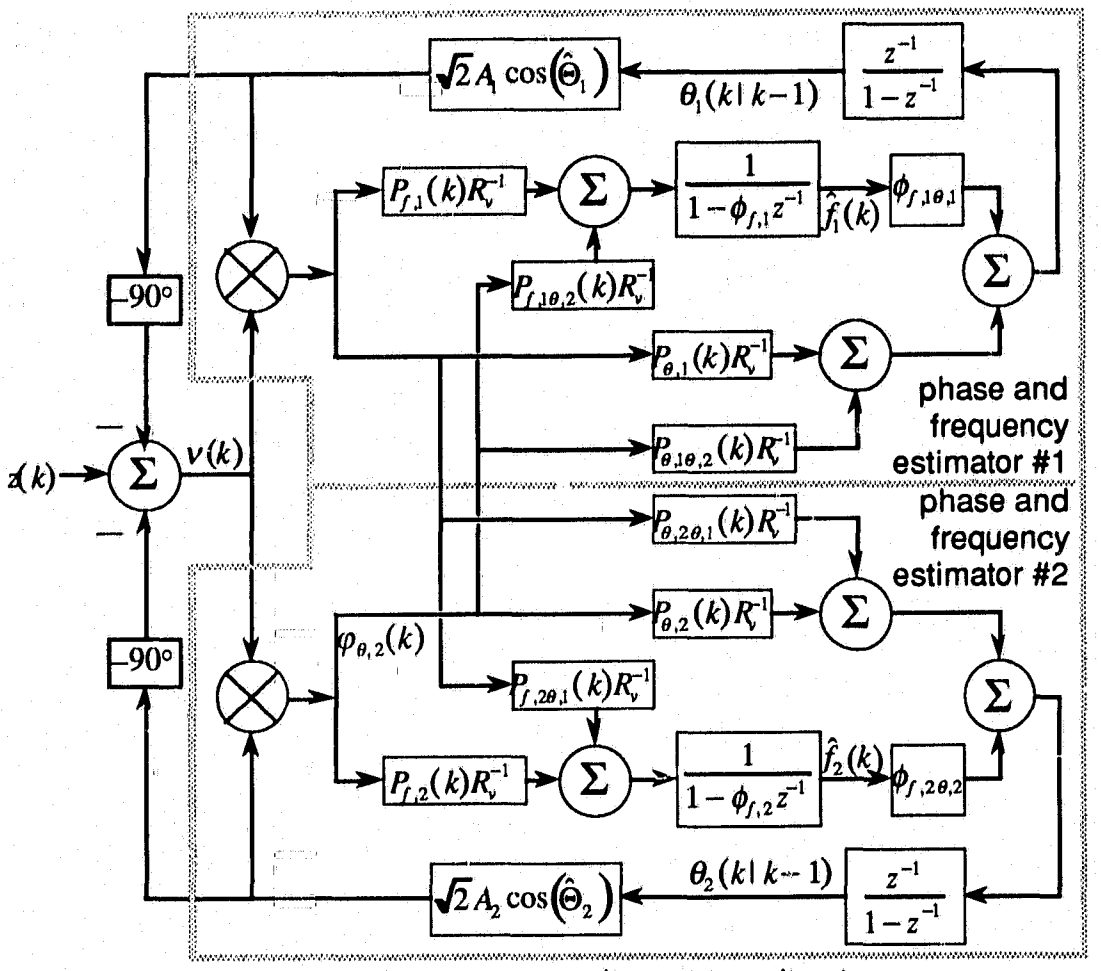

Figure 2–21 Two-source FM direct EKF realization.

The baseband approximation of (2.176) from (2.109) is

$$\boldsymbol{\varphi}_i'(k) = \left[\boldsymbol{\varphi}_{\theta,i}'(k)\right] = \begin{bmatrix} \sqrt{2}A_i\cos\left(\hat{\Theta}_i(k)\right)z(k) - 2A_i\cos\left(\hat{\Theta}_i(k)\right)\sum_{j=1,j\neq i}^{N} A_j\sin\left(\hat{\Theta}_j(k)\right) \\ 0 \end{bmatrix}. \qquad (2.177)$$

The block diagram of the direct realization of the resulting EKF equation is shown in Fig. 2–21. The CDPLL realization using (2.177) is nearly the same except that the innovations process of Fig. 2–21 is replaced by those of Fig. 2–16.

The coupling between θ and f and in $\mathbf{P}_{ii}(k)$ was presented in (2.171). However the coupling between the two process estimators has not been studied for FM. The cross-covariance matrix from (2.122) is

$$\mathbf{P}_{12}(k) = \begin{bmatrix} P_{\theta,1\theta,2}(k) & P_{\theta,1f,2}(k) \\ P_{f,1\theta,2}(k) & P_{f,1f,2}(k) \end{bmatrix}. \tag{2.178}$$

$P_{\theta,1\theta,2}(1)$ was presented in Section 2.3.4. The elements of the last column of (2.178) do not contribute to the coupling since they are multiplied by $\varphi_{f,i}(k) = 0$. The addition of the frequency state has thus introduced a new cross-covariance terms

$$P_{f,1\theta,2}(1) = \mu A_1 A_2 \left[\cos\left(\hat{\Theta}_1(1) + \hat{\Theta}_2(1)\right) + \cos\left(\hat{\theta}_1(1) - \hat{\theta}_2(1)\right)\right] P_{\theta,1f,1}(1|0) P_{\theta,2}(1|0), \tag{2.179}$$

where

$$\mu = \left\{ R_v^{-1} + \sum_{l=2}^{2} A_l \left[1 + \cos\left(2\hat{\Theta}_l(1)\right)\right] P_{\theta,l}(1|0) \right\}^{-1}. \tag{2.180}$$

It is clear that the cross-covariance terms may not be zero and should not be neglected at this point.

Two Sources, Unknown Amplitudes

Inclusion of unknown amplitudes is a direct extension of the above results. The state equation describing the two sources is

$$\begin{bmatrix} \theta_1(k+1) \\ f_1(k+1) \\ A_1(k+1) \\ \theta_2(k+1) \\ f_2(k+1) \\ A_2(k+1) \end{bmatrix} = \begin{bmatrix} \Phi_{\theta,1} & \mathbf{0} & & \mathbf{0} \\ \mathbf{0} & 1 & & \\ & & \Phi_{\theta,2} & \mathbf{0} \\ \mathbf{0} & & \mathbf{0} & 1 \end{bmatrix} \begin{bmatrix} \theta_1(k) \\ f_1(k) \\ A_1(k) \\ \theta_2(k) \\ f_2(k) \\ A_2(k) \end{bmatrix} + \begin{bmatrix} \Gamma_{\theta,1} & \mathbf{0} & & \mathbf{0} \\ \mathbf{0} & 0 & & \\ & & \Gamma_{\theta,2} & \mathbf{0} \\ \mathbf{0} & & \mathbf{0} & 0 \end{bmatrix} \begin{bmatrix} w_{\theta,1}(k) \\ w_{f,1}(k) \\ 0 \\ w_{\theta,2}(k) \\ w_{f,2}(k) \\ 0 \end{bmatrix}, \tag{2.181}$$

the observation matrix is

$$\mathbf{H}\left(\hat{\mathbf{x}}(k|k-1), k\right)^{\mathrm{T}} = \begin{bmatrix} \sqrt{2}\hat{A}_1(k|k-1)\cos\left(\hat{\Theta}_1(k)\right) \\ 0 \\ \sqrt{2}\sin\left(\hat{\Theta}_1(k)\right) \\ \sqrt{2}\hat{A}_2(k|k-1)\cos\left(\hat{\Theta}_2(k)\right) \\ 0 \\ \sqrt{2}\sin\left(\hat{\Theta}_2(k)\right) \end{bmatrix}. \tag{2.182}$$

The innovations process is the same as (2.153). The Kalman Filter equation from (2.113) is

$$\begin{bmatrix}\hat{\theta}_1(k)\\ \hat{f}_1(k)\\ \hat{A}_1(k)\\ \hat{\theta}_2(k)\\ \hat{f}_2(k)\\ \hat{A}_2(k)\end{bmatrix}=\begin{bmatrix}\boldsymbol{\Phi}_{\theta,1} & \mathbf{0} & & \mathbf{0} & & \\ \mathbf{0} & 1 & & & & \\ & & \boldsymbol{\Phi}_{\theta,2} & \mathbf{0} & & \\ \mathbf{0} & & \mathbf{0} & 1 & & \end{bmatrix}\begin{bmatrix}\hat{\theta}_1(k-1)\\ \hat{f}_1(k-1)\\ \hat{A}_1(k-1)\\ \hat{\theta}_2(k-1)\\ \hat{f}_2(k-1)\\ \hat{A}_2(k-1)\end{bmatrix}+\begin{bmatrix}\mathbf{P}_{11}(k) & \mathbf{P}_{12}(k)\\ \mathbf{P}_{21}(k) & \mathbf{P}_{22}(k)\end{bmatrix}R_v^{-1}\begin{bmatrix}\boldsymbol{\varphi}_1(k)\\ \boldsymbol{\varphi}_2(k)\end{bmatrix}, \tag{2.183}$$

where $\mathbf{P}_{ij}(k)$ are defined in (2.114) and from (2.163)

$$\boldsymbol{\varphi}_i(k)=\begin{bmatrix}\sqrt{2}\hat{A}_i(k\,|\,k-1)\cos\left(\hat{\Theta}_i(k)\right)v(k)\\ 0\\ \sqrt{2}\sin\left(\hat{\Theta}_i(k)\right)v(k)\end{bmatrix}. \tag{2.184}$$

The baseband approximation of (2.184) from (2.116) is

$$\boldsymbol{\varphi}_i'(k)=\begin{bmatrix}\boldsymbol{\varphi}'_{\theta,i}(k)\\ \cdots\cdots\\ \varphi'_{A,i}(k)\end{bmatrix}=\begin{bmatrix}\mathbf{c}_i\left[\sqrt{2}\hat{A}_i\cos\left(\hat{\Theta}_i(k)\right)z(k)+2\hat{A}_i\cos\left(\hat{\Theta}_i(k)\right)\hat{A}_j\sin\left(\hat{\Theta}_j(k)\right)\right]\\ \cdots\cdots\cdots\cdots\cdots\cdots\cdots\cdots\cdots\cdots\cdots\cdots\cdots\cdots\cdots\cdots\cdots\cdots\cdots\cdots\cdots\cdots\\ \sqrt{2}\sin\left(\hat{\Theta}_i(k)\right)z(k)-\hat{A}_i-2\sin\left(\hat{\Theta}_i(k)\right)\hat{A}_j\sin\left(\hat{\Theta}_j(k)\right)\end{bmatrix}. \tag{2.185}$$

The block diagram of the direct realization of the resulting EKF equation is shown in Fig. 2–22 where the amplitude and phase estimators are as shown in Fig. 2–19.

The coupling between θ, f, and A in $\mathbf{P}_{ii}(k)$ was presented in (2.171). However the coupling between the two process estimators has not been studied for FM. The cross-covariance matrix from (2.122) is

$$\mathbf{P}_{12}(k)=\begin{bmatrix}P_{\theta,1\theta,2}(k) & P_{\theta,1f,2}(k) & P_{\theta,1A,2}(k)\\ P_{f,1\theta,2}(k) & P_{f,1f,2}(k) & P_{f,1A,2}(k)\\ P_{A,1\theta,2}(k) & P_{A,1f,2}(k) & P_{A,1A,2}(k)\end{bmatrix}. \tag{2.186}$$

$P_{\theta,1\theta,2}(1)$, $P_{\theta,1A,2}(1)$, $P_{A,1\theta,2}(1)$, and $P_{A,1A,2}(1)$ were presented in Section 2.3.4. The elements of the middle column of (2.186) do not contribute to the coupling since they are multiplied by $\varphi_{f,i}(k)=0$. The addition of the frequency state has thus introduced two new cross-covariance terms

$$P_{f,1\theta,2}(1)=\mu\hat{A}_1(0)\hat{A}_2(0)\left[\cos\left(\hat{\Theta}_1(1)+\hat{\Theta}_2(1)\right)+\cos\left(\hat{\theta}_1(1)-\hat{\theta}_2(1)\right)\right]P_{\theta,1f,1}(1\,|\,0)P_{\theta,2}(1\,|\,0) \tag{2.187}$$

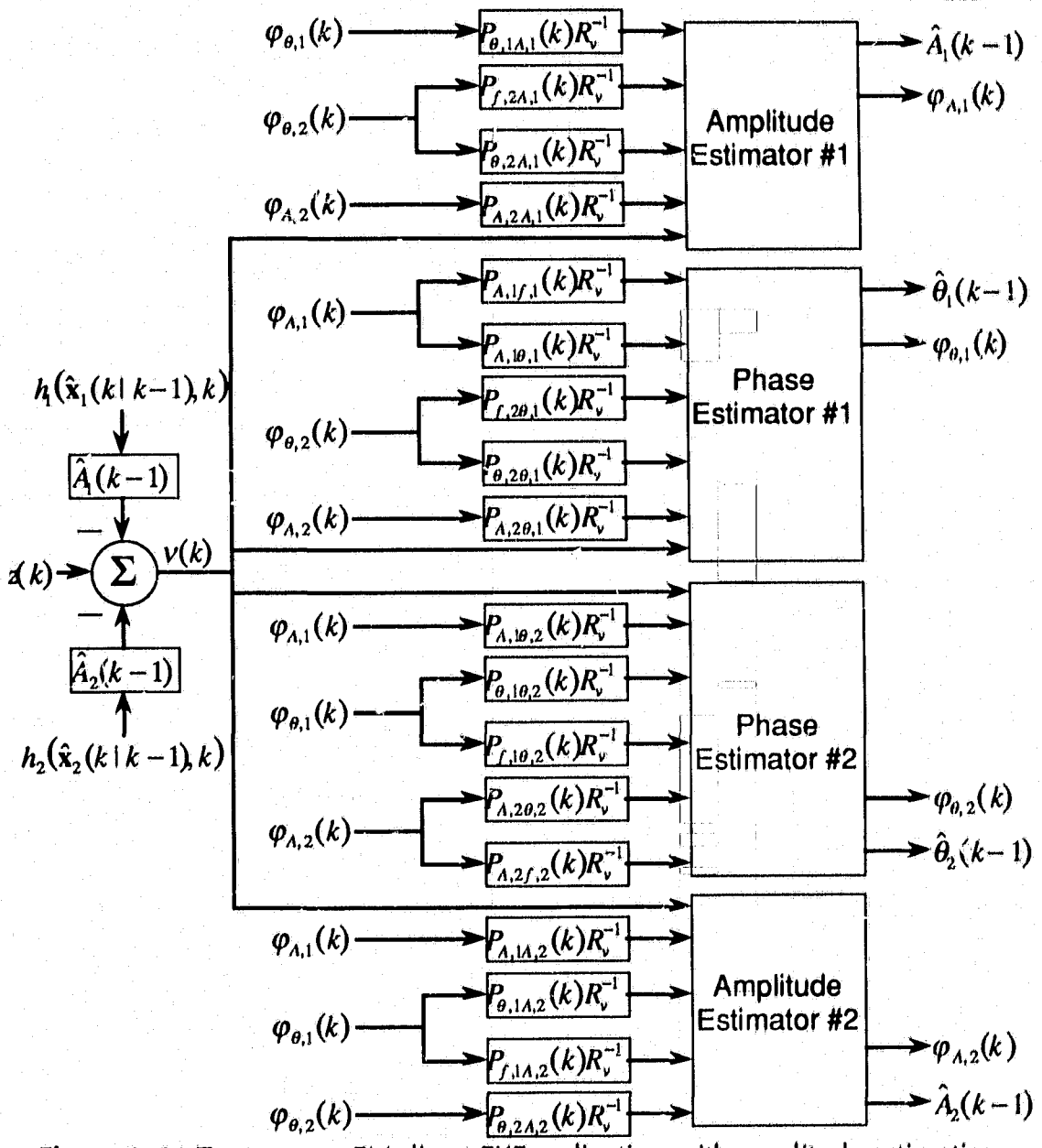

Figure 2–22 Two-source FM direct EKF realization with amplitude estimation.

and

$$P_{f,1A,2}(1) = \mu\hat{A}_1(0)\hat{A}_2(0)\left[\sin\left(\hat{\Theta}_1(1)+\hat{\Theta}_2(1)\right)-\sin\left(\hat{\theta}_1(1)-\hat{\theta}_2(1)\right)\right]P_{\theta,1f,1}(1|0)P_{A,2}(1|0) \quad (2.188)$$

where

$$\mu = \left\{R_v^{-1}+\sum_{l=1}^{2}\hat{A}_l(0)\left[1+\cos\left(2\hat{\Theta}_l(1)\right)\right]P_{\theta,l}(1|0)+\left[1-\cos\left(2\hat{\Theta}_l(1)\right)\right]P_{A,l}(1|0)\right\}^{-1}. \quad (2.189)$$

It is again clear that the cross-covariance terms may not be zero and should not be neglected at this point.

2.5. Summary

In this chapter we have derived a model to describe the problem at hand. State-space notation has been chosen for its ability to accurately and compactly describe the problem. State-space notation also facilitates the creation of a multiple source model by simply augmenting state vectors and matrices. A general N^{th}-order Gauss-Markov stochastic model has been chosen and described to model random modulating processes. From this a first-order Gauss-Markov message process has been derived and will be used throughout much of the remaining work. Both FM and PM first order message processes have also been derived.

From the continuous-time state-space model of the communication system a discrete model was derived as necessitated by the eventual digital implementation of the resulting receiver structures. This allowed for the development of a discrete Extended Kalman Filter which form the foundation for the formulation of a CDPLL receiver.

Several PM and FM receiver structures have been defined formulated and some preliminary analysis has been presented. Single and two source PM and FM examples with first-order message processes were illustrated. Further analysis follows in subsequent chapters.

Interference and improvement ratios have been defined for estimator performance comparisons in subsequent chapters.

3. Observation, Estimation, and State Separability

In this chapter the issue of signal separability is addressed. Due to the nonlinear nature of the angle modulation and demodulation processes, strict analytic solutions do not present themselves especially in the multiple signal scenario presented here. Additionally, the EKFs formulated in the previous chapter may only be studied by computer simulation as the estimator structures employ time-varying gains [29]. Therefore the methodology employed in this work is to break the general problem down into its various related aspects and examining these topics individually. Each topic is then further simplified as to allow the models derived in the previous chapter to be employed. Although this method does not provide convenient closed form solutions, valuable insights into the problem as a whole are gained through computer simulation.

The state separability and estimation issue is addressed item by item each built on the preceding. In the simplest case the co-channel interference problem is couched as the separation of two similar stochastic message processes. So as a foundation the non-linear PM observation function is grossly simplified by a linear observation model. The state separability is quantified by use of the state observability Gramian. We then replace the linear approximation with a non-linear one and examine state separability for first single and then two source cases, much the same manner as the EKF estimator was formulated in Section 2.3.

As mentioned in Chapter 2, estimation the amplitude as well as phase states are required. Since these are two distinct parameters, their observability and estimation will be treated separately. Phase estimation will be considered first, followed by phase and amplitude estimation, and finally phase, frequency, and amplitude estimation. In all estimator simulations the

measurement noise is small relative to the signal power (high SNR) to facilitate the study of the multi-source signal separation.

3.1. Message Process Characterization

As in the proceeding chapter, the message process (2.35) will be modeled by a first order unit-energy lowpass process described by

$$x_m(k+1) = m(k+1) = e^{-\alpha T_s} m(k) + \left(1 - e^{-2\alpha T_s}\right)^{\frac{1}{2}} w(k). \tag{3.1}$$

Since the goal is the investigation of similar signal separability, two independent, similar processes, m_1 and m_2, may be defined by the state equation

$$\begin{bmatrix} m_1(k+1) \\ m_2(k+1) \end{bmatrix} = \begin{bmatrix} e^{-\alpha_1 T_s} & 0 \\ 0 & e^{-\alpha_2 T_s} \end{bmatrix} \begin{bmatrix} m_1(k) \\ m_2(k) \end{bmatrix} + \begin{bmatrix} \left(1 - e^{-2\alpha_1 T_s}\right)^{\frac{1}{2}} & 0 \\ 0 & \left(1 - e^{-2\alpha_2 T_s}\right)^{\frac{1}{2}} \end{bmatrix} \begin{bmatrix} w_1(k) \\ w_2(k) \end{bmatrix}, \tag{3.2}$$

where w_1 and w_2 are identical independent $N:[0,1]$ discrete random processes. (3.2) may be written more compactly as

$$\mathbf{x}(k+1) = \mathbf{\Phi x}(k) + \mathbf{\Gamma w}(k). \tag{3.3}$$

The state covariance matrix $\mathbf{Q}_x$ for a linear, time-invariant system is described by the Lyapunov equation [39]

$$\mathbf{Q}_x = \mathbf{\Phi Q}_x \mathbf{\Phi}^T + \mathbf{\Gamma Q}_w \mathbf{\Gamma}^T, \tag{3.4}$$

where $\mathbf{Q}_w$ is the covariance of the process driving noise $\mathbf{w}$. For the first order case described by (3.2), the state covariance matrix is

$$\mathbf{Q}_x = \begin{bmatrix} 1 & 0 \\ 0 & 1 \end{bmatrix}, \tag{3.5}$$

since the message processes are independent and each is unit-energy.

The two processes are both first-order lowpass processes whose spectral characteristics are solely defined by the parameter α as well as being independent since $E[w_1(k)w_2(k)] = 0$. If $\alpha_1 = \alpha_2$ then the two processes are statistically identical although they are still independent.

In time varying processes like speech, $\alpha_1 \neq \alpha_2$, however with mobile data $\alpha_1 = \alpha_2$. Thus it is desirable to qualify and quantify the degree of similarity between the two processes.

One measure of similarity may be contained in the state transition matrix $\mathbf{\Phi}$ in (3.3). In the simple case of (3.2), $\mathbf{\Phi} = diag\left\{e^{-\alpha_1 Ts}, e^{-\alpha_2 Ts}\right\}$ and since $\mathbf{\Phi}$ is diagonal, its eigenvalues are simply its diagonal elements. Thus if $\alpha_i >> \alpha_j$, then α_j becomes the dominant eigenvalue of $\mathbf{\Phi}$ and the eigenvalue ratio $\lambda_{max}/\lambda_{min}$ becomes a crude measure of process similarity. Also, the signal processes are asymptotically stable if all of the eigenvalues of $\mathbf{\Phi}$ are less than unity [35].

3.2. Linear Time-Invariant Observation and Estimation

The crux of this work lies in the observation of the state variables. In general state-space notation the state observation is described by (repeated from Chapter 2)

$$\mathbf{z}(k) = h(\mathbf{x}(k), k) + \mathbf{v}(k), \tag{3.6}$$

where $h(\mathbf{x}(k), k)$ is an observation function possibly dependent on the state $\mathbf{x}$ and possibly dependent on the time k. As stated in Chapter 2, the observation function describing the process of phase modulation is inherently nonlinear. Thus the observation function plays a key role in the problem of the separation of signals.

In the investigation of nonlinear observation, we begin by examining the signal separability issue for linear observations of the state to gain some insight into the problem of how to treat the nonlinear case.

3.2.1. State Observation

In the case of linear, time invariant (LTI) state observation, $h(\mathbf{x}(k), k)$ may be replaced by the constant observation matrix $\mathbf{H}$ which results in the state observation equation

$$\mathbf{z}(k) = \mathbf{H}\mathbf{x}(k) + \mathbf{v}(k), \tag{3.7}$$

where $\mathbf{z}$ is the measurement of the state $\mathbf{x}$.

The co-channel communication problem can be grossly simplified by removing the modulation process completely and replacing it with the LTI observation matrix. Thus receiving the two processes of (3.2) on the same sensor, the scalar state measurement becomes

$$z(k) = [1 \quad 1]\begin{bmatrix} x_1(k) \\ x_2(k) \end{bmatrix} + v(k), \tag{3.8}$$

which is simply the sum of the two states plus measurement noise. Having made this gross simplification, we may now use the plethora of linear system theory in the initial investigation of the observation of similar signals.

The observability of a system is the relationship between the measurement $\mathbf{z}$ and the state $\mathbf{x}$. If every state $\mathbf{x}(k)$ may be determined from knowledge of $\mathbf{\Phi}$, $\mathbf{H}$, and the initial state $\mathbf{x}(0)$, then the system is said to be *uniformly completely observable.* In the case of LTI systems, the system is completely observable if the $n \times nm$ *observability matrix* [32]

$$\Xi = \left[\mathbf{H}^{\mathrm{T}} \;\vdots\; \mathbf{\Phi}^{\mathrm{T}}\mathbf{H}^{\mathrm{T}} \;\vdots\; \cdots \;\vdots\; \left(\mathbf{\Phi}^{\mathrm{T}}\right)^{n-1}\mathbf{H}^{\mathrm{T}}\right] \tag{3.9}$$

has rank n where n is the dimension of the state vector and m is the dimension of the measurement vector. In the case of scalar observations, Ξ is square and the system is completely observable if Ξ is of full rank. Substituting (3.2) and (3.8) into (3.9) yields

$$\Xi = \begin{bmatrix} 1 & e^{-\alpha_1 T_s} \\ 1 & e^{-\alpha_2 T_s} \end{bmatrix}. \tag{3.10}$$

Since the rank is defined as the dimension of the column space (the number of linearly independent columns), it is obvious that if $\alpha_1 = \alpha_2$ then Ξ is not full rank and therefore the system is not completely observable. Analytically if $\alpha_1 \neq \alpha_2$ then the two columns are linearly independent and the matrix is of full rank. However, numerically there is a transition when $\alpha_1 \approx \alpha_2$ where it is difficult to define the rank. The rank of the observability matrix will be investigated by examining the singular values of the observability matrix which, for (3.10), are

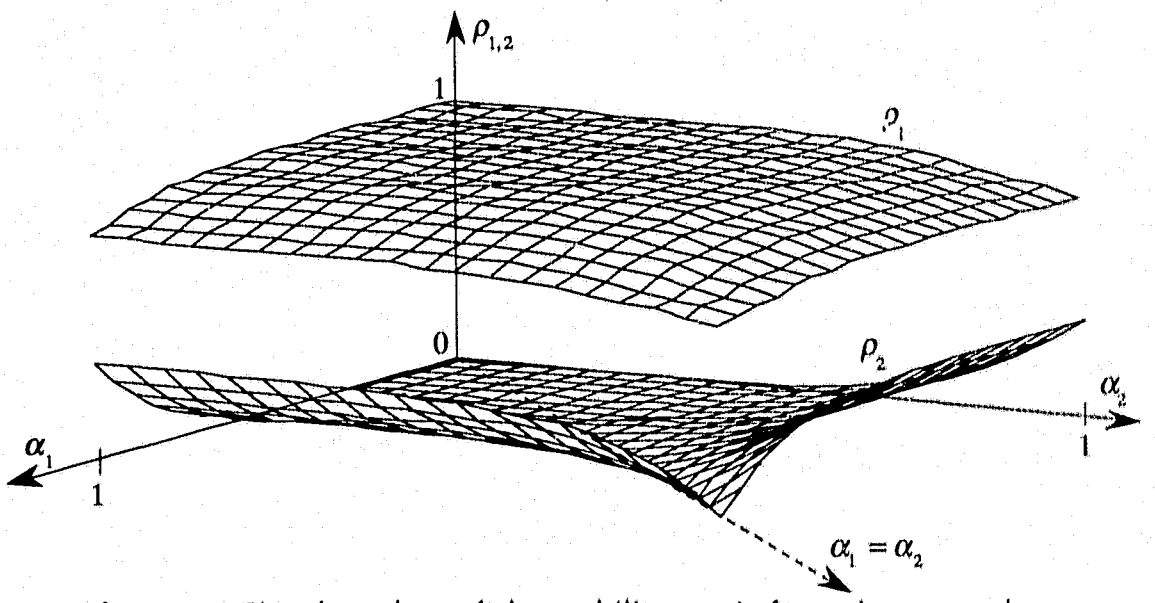

Figure 3–1 Singular values of observability matrix for various a_1 and α_2.

$$\rho_{1,2} = 1 + \tfrac{1}{2}e^{-2\alpha_1 T_s} + \tfrac{1}{2}e^{-2\alpha_2 T_s} \pm \tfrac{1}{2}\left(4 + e^{-4\alpha_1 T_s} + 2e^{-2(\alpha_1+\alpha_2)T_s} + e^{-4\alpha_2 T_s} + 8e^{-(\alpha_1+\alpha_2)T_s}\right)^{\frac{1}{2}} \tag{3.11}$$

and have been plotted in Fig. 3–1 with axes scaling $10^{-3} \le \alpha_1 \le 1$, $10^{-3} \le \alpha_2 \le 1$ where the α axes are logarithmic and $\sigma_{w,1}^2 = \sigma_{w,2}^2$. When $\alpha_1 = \alpha_2$, $\lambda_2 = 0$ which indicates that Ξ is singular (not full rank) and the state variables are not distinguishable. As a_1 and a_2 become less equal, Ξ is still ill conditioned but becomes better conditioned as ρ_2 increases. Thus the system becomes "more observable" as a_1 and a_2 diverge.

3.2.2. State Estimation

The effect of this varying observability on state estimation (and separability) may be investigated by examining a discrete Kalman filter's ability to separate similar processes for various α's. Since the LTI system is stationary, this may be accomplished by examining the solutions to the Kalman gain matrix, the prior (prediction) error covariance (Riccati equation), and the post (estimation) error covariance.

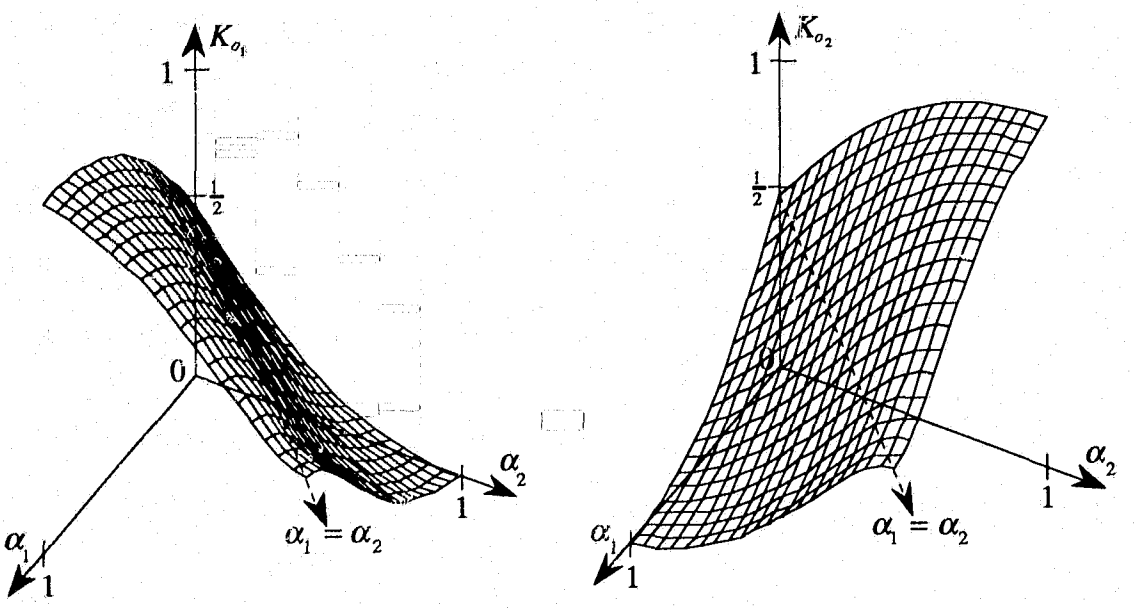

Figure 3–2 Kalman gains for various a_1 and α_2.

The effect of $\mathbf{K}_o$, the steady-state optimum Kalman gain, the filter equation (from (2.66))

$$\hat{\mathbf{x}}(k) = \hat{\mathbf{x}}(k \mid k-1) + \mathbf{K}_o[\mathbf{z}(k) - \mathbf{H}\hat{\mathbf{x}}(k \mid k-1)] \tag{3.12}$$

is to weight the information from the new measurement $\mathbf{z}(k) - \mathbf{H}\hat{\mathbf{x}}(k \mid k-1)$, also known as the innovations process, against the prediction of the state $\hat{\mathbf{x}}(k \mid k-1)$. Thus if $\mathbf{K}_o$ is small, very little information is present in the new measurement resulting in the state estimate is based almost completely on the previous prediction. On the other hand, if $\mathbf{K}_o$ is large, the new measurement contains more information than the prediction resulting in the state estimate is based almost completely on the measurement. The gain matrix is proportional to the uncertainty in the estimate (expressed in the error covariance $\mathbf{P}$) and inversely proportional to the uncertainly of the measurement (expressed in the measurement noise covariance $\mathbf{R}_v$). Thus $\mathbf{K}$ increases if the uncertainty in the estimate increases (indicating a poor state prediction) or if the measurement noise covariance decreases (indicating good state measurements).

In the simple system of (3.2) and (3.8), the Kalman filter equation (3.12) is

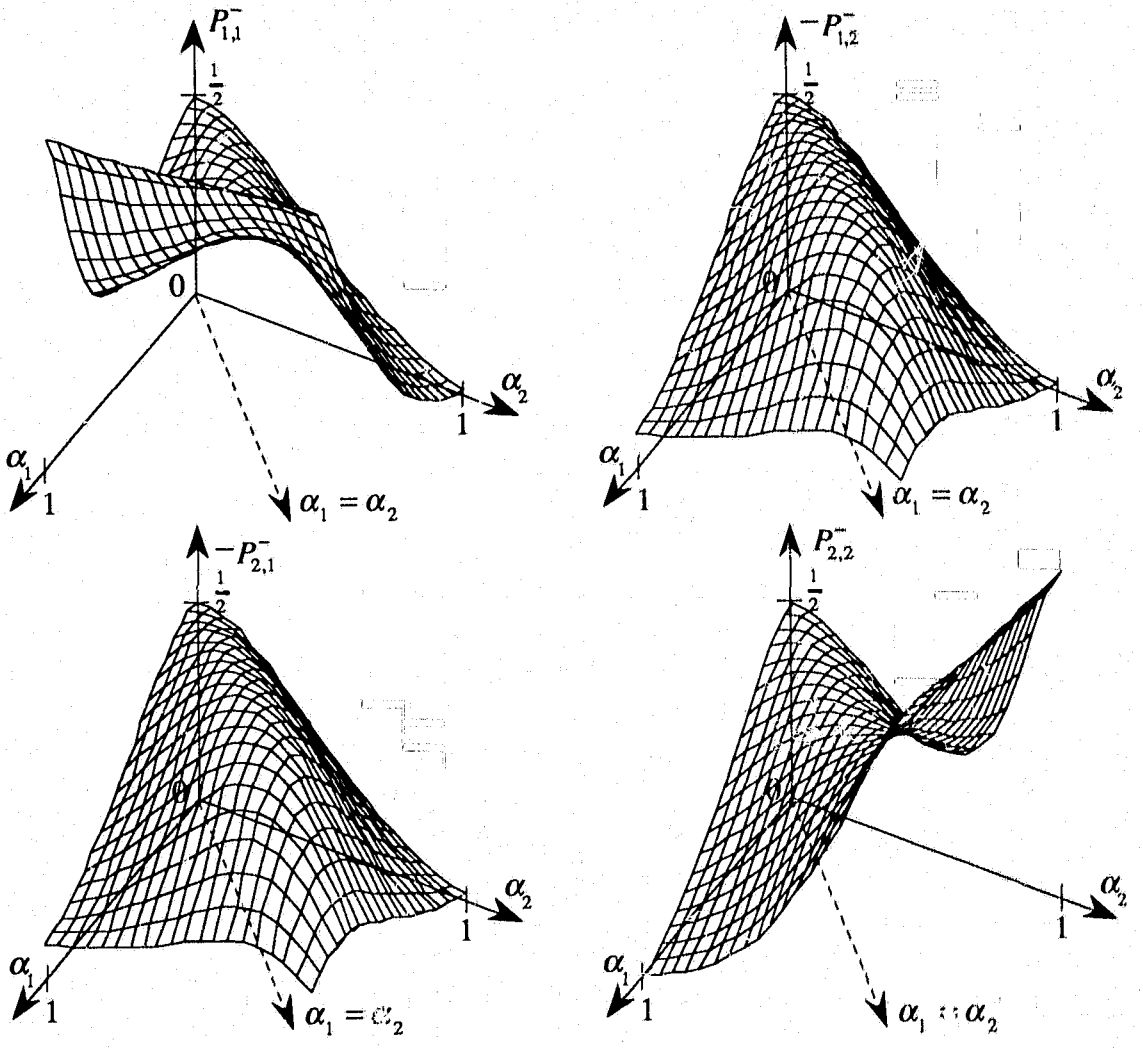

Figure 3–3 Prior error covariances for various a_1 and α_2.

$$\begin{bmatrix}\hat{x}_1(k)\\ \hat{x}_2(k)\end{bmatrix}=\begin{bmatrix}\hat{x}_1(k\mid k-1)\\ \hat{x}_2(k\mid k-1)\end{bmatrix}+\begin{bmatrix}K_{o,1}\\ K_{o,2}\end{bmatrix}\left[z(k)-\begin{bmatrix}1 & 1\end{bmatrix}\begin{bmatrix}\hat{x}_1(k\mid k-1)\\ \hat{x}_2(k\mid k-1)\end{bmatrix}\right], \tag{3.13}$$

where $\mathbf{K}_{o,1}$ and $\mathbf{K}_{o,2}$ are the optimal gains for the estimation of states x_1 and x_2 respectively. By examining these gains for various α's we can determine how much information is determined in the measurement of these states (see Fig. 3–2). When $\alpha_1 = \alpha_2$, $K_{o,1} = K_{o,2} = \frac{1}{2}$ which indicates that equal information is available from the measurement of x_1 and x_2. As $\alpha_1 > \alpha_2$, $K_{o,1}$ increases and $K_{o,2}$ decreases indicating that the measurements contain more information about x_1 than about x_2 since the measurement noise is constant. Similarly

when $\alpha_1 < \alpha_2$. When α is small (3.2), the transition from one state to the next is nearly unity since $e^{-\alpha T_s} \approx 1$ for small α, and the contribution from the driving noise is nearly zero because of the $\left(1-e^{-2\alpha T_s}\right)^{\frac{1}{2}}$ term. Since the Kalman filter assumes *a priori* knowledge of the state transition matrix, it is able to make very accurate predictions in this case, thus the measurement provides very little additional information. On the other hand, when α is large, the driving noise is the dominant factor in the state transitions so the Kalman filter cannot accurately predict the state and must rely on the measurements for state information. This is also related to the variance of each state which increases with α, resulting in a commensurate increase in the divergence between the state covariances.

Examination of the prior estimation error covariance matrix reveals the error in predicting $\hat{\mathbf{x}}(k \mid k-1)$ given the previous estimate. The covariance of the prediction error is given by the discrete-time Riccati recursion [35]

$$\mathbf{P}(k+1 \mid k) = \mathbf{\Phi}\mathbf{P}(k \mid k-1)\left(\mathbf{I} - \mathbf{H}\left(\mathbf{H}^{\mathrm{T}}\mathbf{P}(k \mid k-1)\mathbf{H} + \mathbf{R}_{\mathrm{v}}\right)^{-1}\mathbf{H}^{\mathrm{T}}\mathbf{P}(k \mid k-1)\right)\mathbf{\Phi}^{\mathrm{T}} + \mathbf{\Gamma}\mathbf{Q}_{\mathrm{w}}\mathbf{\Gamma}^{\mathrm{T}} \tag{3.14}$$

For an asymptotically stable LTI system, there exists some $\mathbf{P}^{-} = \lim_{k\to\infty}\mathbf{P}(k+1 \mid k)$ which satisfies the steady-state version of (3.14). By examining $\mathbf{P}^{-}$ for various α's we can determine the Kalman filter's ability to predict independent but statistically similar states given an observation of only their sum (see Fig. 3–3), where $P_{i,j}^{-}$ is the steady-state prediction error covariance of x_i based on x_j. In all four cases prediction error is large when $\alpha_1 \approx \alpha_2$. As a_1 increases with respect to a_2, we see that the prediction error covariance elements decrease monotonically except for $P_{1,1}^{-}$. This is due to the fact that the state prediction is almost entirely based on the state transition matrix and in the case when $\alpha_1 >> \alpha_2$, the state transition of x_1 is dominated by the process driving noise. Thus when $\alpha_1 >> \alpha_2$, it is more difficult to predict x_1 than it is to predict x_2, as shown by comparing $P_{1,1}^{-}$ with $P_{2,2}^{-}$. A similar argument applies when $\alpha_1 << \alpha_2$.

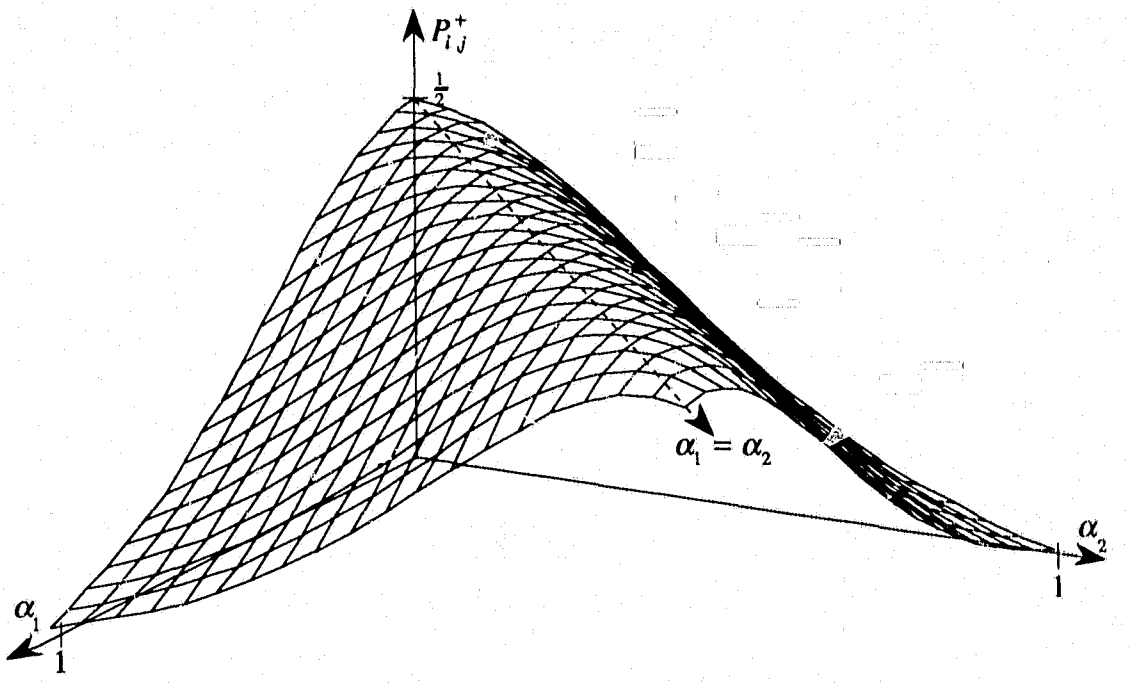

Figure 3–4 Post error covariances, $P^+_{1,1}$, $-P^+_{1,2}$, $-P^+_{2,1}$, and $P^+_{2,2}$, for various a_1 and α_2.

Finally examination of the post error covariance, where $\mathbf{P}^+ = E\left[(\hat{\mathbf{x}} - \mathbf{x})(\hat{\mathbf{x}} - \mathbf{x})^T\right]$, reveals that little improvement is made in estimation when $\alpha_1 \approx \alpha_2$ (see Fig. 3–4). However, as a_1 and a_2 diverge the estimation error variance decreases. When $\alpha_1 >> \alpha_2$, the correction from the innovations process provides substantial improvement in the estimation of x_1 implying that the measurement has valuable information (compare Fig. 3–3, $P^-_{1,1}$ to Fig. 3–4). Again this is due to the nature of the state transition of x_1 for large $\alpha_1 >> \alpha_2$ and similarly holds for x_2 when $\alpha_1 << \alpha_2$.

To get an idea of the absolute values involved, "slices" of Figs. 3–1– 3–4 are presented. a_1 was held constant at 0.0263665, the midpoint between 0.001 and 1 on the log scale, and a_2 varied from 0.001 to 1.

In Fig. 3–5 it is may be seen that when $\alpha_1 = \alpha_2$, the smaller singular value of the observability matrix is zero, indicating that Ξ is singular. Ξ becomes better conditioned as a_1 and a_2 diverge.

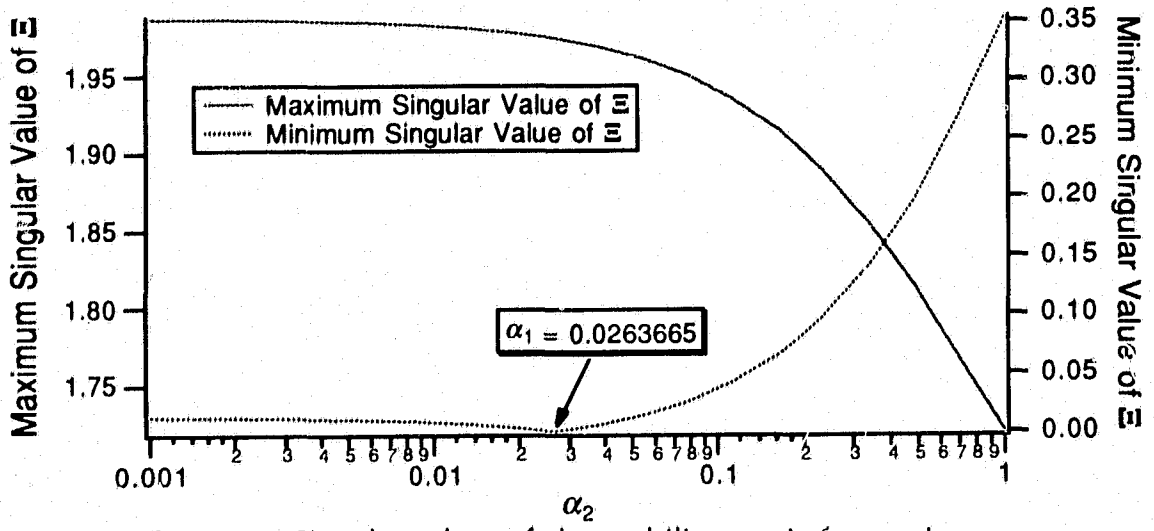

Figure 3–5 Singular values of observability matrix for varying a_2.

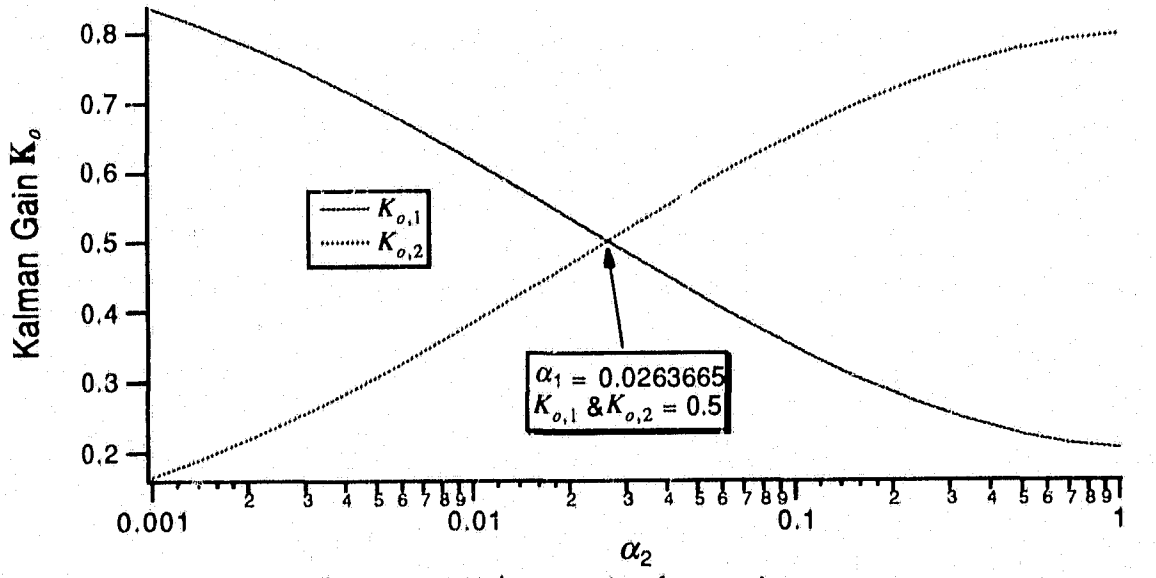

Figure 3–6 Kalman gains for varying a_2.

Fig. 3–6 demonstrates that the Kalman gains give greater weight to the process with the greater process driving noise contribution (larger α). When the α's are equal, so are the Kalman weights. In Fig. 3–7 the prediction error $P_{2,2}^-$ increases as a_2 increases indicating the dominating effect of the process driving noise on x_2. Finally, Fig. 3–8 shows that the prediction error peaks when $\alpha_1 = \alpha_2$.

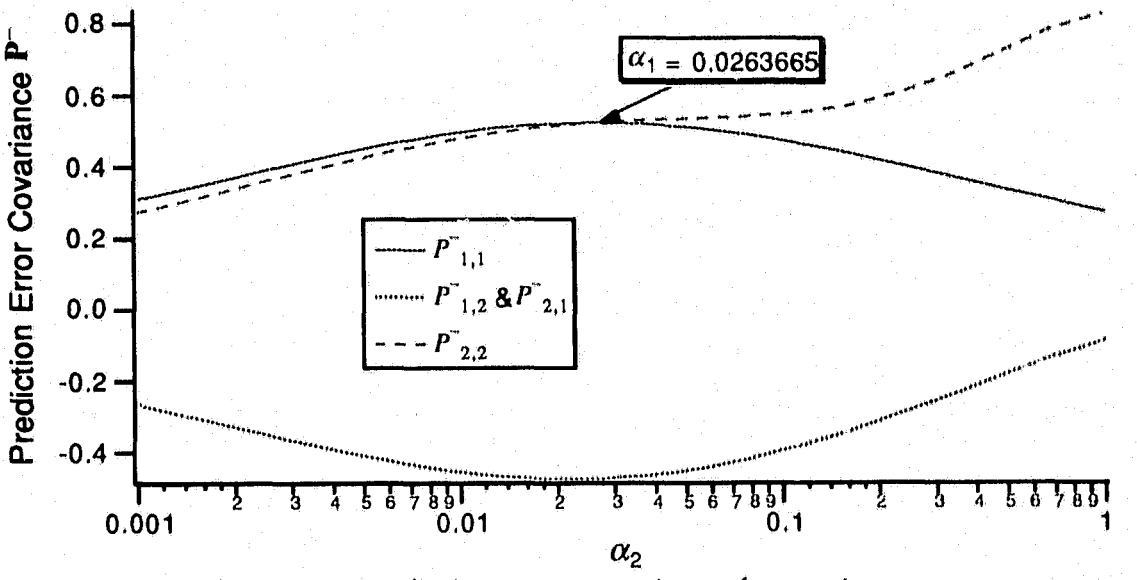

Figure 3–7 Prediction error covariance for varying a_2.

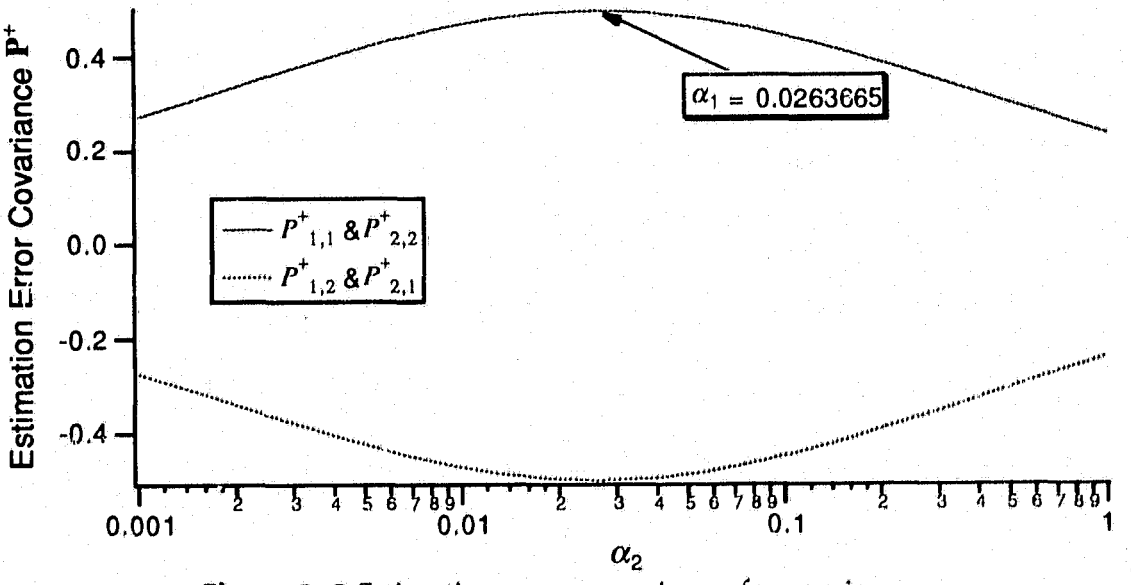

Figure 3–8 Estimation error covariance for varying a_2.

3.2.3. Summary and Interpretation

This exercise has shown that, to some degree, it is possible to separate two linearly combined states measured with a LTI observation function as long as there is some difference in their

state covariances. Holding the noise powers identical, this translates to the requirement that the state transition matrices must differ for different processes.

The degree or success of separation could be measured by setting a threshold on the post error covariance by defining an "acceptable" level of separation. The choice of this threshold would depend on the application area.

Armed with this knowledge, we now tackle the interesting part: nonlinear observations of the states.

3.3. Nonlinear Observation and Estimation

Now we examine the effects of phase modulation and the resulting nonlinear observation function on state observability and separability. First we will examine the observability for a single phase modulated first-order random process. Then we will extend this to multiple phase modulated processes. We will also look at IF and in-phase/quadrature (I-Q) sampling.

3.3.1. Single Source Phase Observability

The single sensor observation function for a single angle modulated source from (2.34) is

$$h(\mathbf{x}(k), k) = \sqrt{2}A\sin\left(\omega_c k\tau + \mathbf{c}^{\mathrm{T}}\mathbf{x}(k)\right), \tag{3.15}$$

where A is the amplitude, ω_c is the carrier frequency, $\mathbf{c}$ is a state selection vector (2.12), and $\mathbf{x}(k)$ is the current state. Since $h(\mathbf{x}(k),k)$ is a nonlinear function of both state and time, it cannot be expressed as a constant observation matrix $\mathbf{H}$ as it was in the LTI system. In order to examine observability as defined above, a linear approximation of $h(\mathbf{x}(k),k)$ is required. Two cases will be examined: passband and baseband (I-Q) observation functions.

Passband Sampling

The phase process for the single source phase modulated signal is the same as the message process (3.1) so

$$\mathbf{x}_\theta(k+1) = \theta(k+1) = e^{-\alpha T_s}\theta(k) + \left(1 - e^{-\alpha 2T_s}\right)^{\frac{1}{2}} w(k), \tag{3.16}$$

where $\theta(k)$ is the instantaneous phase. Since the phase selection vector $\mathbf{c}_\theta = 1$ in this case the phase modulated observation y of θ is simply

$$y(k) = h(\theta(k), k) = \sqrt{2}A\sin\left(\omega_c kT_s + \theta(k)\right), \tag{3.17}$$

and the resulting measurement is

$$z(k) = y(k) + v(k), \tag{3.18}$$

where v is the $N:\left[0,\sigma_v^2\right]$ measurement noise.

The following is similar to the related work of Lagunas [40, 19]. Now define $\hat{z}$ to be an estimate of the measurement based on the *a posteriori* phase estimate,

$$\hat{z}(k) = \hat{y}(k) = \sqrt{2}A\sin\left(\omega_c kT_s + \hat{\theta}(k)\right), \tag{3.19}$$

where $\hat{\theta}$ is the estimation of the instantaneous phase. Define the measurement estimation error as

$$\tilde{z}(k) = z(k) - \hat{z}(k) = y(k) - \hat{y}(k) + v(k) \tag{3.20}$$

and define the phase estimation error as $\tilde{\theta}(k) = \theta(k) - \hat{\theta}(k)$. Using the small angle approximations $\cos(\phi) \approx 1$ and $\sin(\phi) \approx \phi$ for $\phi << 1$, it may be shown that[1]

$$\begin{aligned} y(k) - \hat{y}(k) &= \sqrt{2}A\sin\left(\omega_c kT_s + \theta(k)\right) - \sqrt{2}A\sin\left(\omega_c kT_s + \hat{\theta}(k)\right) \\ &\approx \sqrt{2}A\cos\left(\omega_c kT_s + \hat{\theta}(k)\right)\tilde{\theta}(k) \end{aligned} \tag{3.21}$$

for $\tilde{\theta} << 1$. Combining (3.20) and (3.21) yields

$$\tilde{z}(k) \approx \sqrt{2}A\cos\left(\omega_c kT_s + \hat{\theta}(k)\right)\tilde{\theta}(k) + v(k) \tag{3.22}$$

which is in the same form as (3.7) where the state $\mathbf{x}$ is $\hat{\theta}$ and the observation matrix $\mathbf{H}$ is $\sqrt{2}A\cos\left(\omega_c kT_s + \hat{\theta}(k)\right)$. Thus the observability of the estimation error may be studied by linearizing the observation function around each phase estimate. This is similar to the development of the Extended Kalman Filter where the observation matrix used in the EKF equa-

---

[1]This is valid only after acquisition (phase lock) has been achieved. Acquisition behavior will be examined later.

tions is formed by expanding the nonlinear observation function $h(\mathbf{x}(k),k)$ by a truncated Taylor series around the current prediction as in (2.70). Applying (2.70) to (3.17) yields

$$\mathbf{H}\left(\hat{\theta}(k\mid k-1),k\right)=\left.\frac{\partial h(\theta(k),k)}{\partial\theta(k)}\right|_{\theta(k)=\hat{\theta}(k\mid k-1)}=\sqrt{2}A\cos\left(\omega_c kT_s+\hat{\theta}(k\mid k-1)\right), \tag{3.23}$$

where the cosine term is the same form as in (3.21) but the prediction has replaced the estimation. Formulating the new state $\tilde{\theta}$ and its phase modulated observation $\mathbf{H}\left(\hat{\theta}(k),k\right)$ in this manner allows for the study of the observability *of the estimation* error of phase modulated signals *for small estimation error.* Although this is fairly restrictive, it is hoped that this will shed some much needed light on the observability of phase modulated states in general.

Firstly the state update equation of the new state $\tilde{\theta}$ needs to be examined. The state estimation from the Extended Kalman Filter equations is (from Chapter 2)

$$\hat{\theta}(k)=\hat{\theta}(k\mid k-1)+\mathbf{K}(k)\left[z(k)-h\left(\hat{\theta}(k\mid k-1),k\right)\right]. \tag{3.24}$$

Examination of the state estimation error update

$$\begin{aligned}\tilde{\theta}(k)&=\theta(k)-\hat{\theta}(k)\\&=\mathbf{\Phi}\theta(k-1)+\mathbf{\Gamma}w(k)-\hat{\theta}(k\mid k-1)-\mathbf{K}(k)\left[z(k)-h\left(\hat{\theta}(k\mid k-1),k\right)\right]\\&=\mathbf{\Phi}\left(\theta(k-1)-\hat{\theta}(k-1)\right)+\mathbf{\Gamma}w(k)-\mathbf{K}(k)\left[z(k)-h\left(\hat{\theta}(k\mid k-1),k\right)\right]\\&=\mathbf{\Phi}\tilde{\theta}(k\quad 1)+\mathbf{\Gamma}w(k)-\mathbf{K}(k)\left[z(k)-h\left(\hat{\theta}(k\mid k-1),k\right)\right],\end{aligned} \tag{3.25}$$

demonstrates that the state prediction error has the same transition matrix as the phase state as defined in (3.16). So, in summary we have defined a new process, the state estimation error, defined by the state-space equations

$$\tilde{\theta}(k)=\mathbf{\Phi}\tilde{\theta}(k-1)-\mathbf{\Phi K}(k)\left[z(k)-h\left(\hat{\theta}(k\mid k-1),k\right)\right]+\mathbf{\Gamma}w(k) \tag{3.26}$$

$$\tilde{z}(k)=\mathbf{H}\left(\hat{\theta}(k),k\right)\tilde{\theta}(k)+v(k). \tag{3.27}$$

Bear in mind that (3.26) and (3.27) are only valid for $\tilde{\theta}<<1$.

We now diverge from Lagunas [40, 19] by addressing state observability using the above derivation. Although the state dependence has been removed from the observation function, it is still a function of time, and thus the observability matrix of (3.9) cannot be directly applied. However, a similar observability criteria exists for time varying observation matrices; actually (3.9) is a special case of the following. A system is *uniformly completely observable* if there exists an interval $k_f > k_0$ such that the matrix, often called the *observability* c*ramian* [41],

$$\mathcal{M}(k_0, k_f) = \sum_{k=k_0}^{k_f} \mathbf{\Phi}^{\mathrm{T}}(k_0, k)\mathbf{H}^{\mathrm{T}}(k)\mathbf{H}(k)\mathbf{\Phi}(k_0, k) \tag{3.28}$$

is positive definite [34]. The Gramian $\mathbf{\Phi}^{\mathrm{T}}\mathbf{H}^{\mathrm{T}}\mathbf{H}\mathbf{\Phi}$ is symmetric and since $\mathbf{\Phi}$ and $\mathbf{H}$ are real, $\mathbf{\Phi}^{\mathrm{T}}\mathbf{H}^{\mathrm{T}}\mathbf{H}\mathbf{\Phi}$ is Hermitian. A Hermitian matrix is positive definite (semidefinite) if and only if its eigenvalues are positive (nonnegative) [42]. Thus the positive definateness of $\mathcal{M}$ may be determined by looking at its eigenvalues.

Substituting the state transition matrix from (3.16) and the observation matrix (3.23) into (3.28) yields

$$\mathcal{M}(k_0, k_f) = \sqrt{2}A\sum_{k=k_0}^{k_f} e^{-2\alpha T_s(k-k_0)} \cos^2\left(\omega_c kT_s + \hat{\theta}(k)\right). \tag{3.29}$$

The observability condition will be satisfied if there exists some $k_f > k_0$ such that $\mathcal{M}(k_0, k_f) > 0$ since $\mathcal{M}$ is a scalar in this case. The exponential term will always be greater than zero as long as its argument is finite. The $\cos^2\left(\omega_c kT_s + \hat{\theta}(k)\right)$ term is always greater than or equal to zero and is zero only when $\left|\omega_c kT_s + \hat{\theta}(k)\right| = \frac{\pi}{2}n$ where $n = \pm 1, 3, 5, \cdots$. In communications, the bandwidth of the message process is substantially lower than the carrier frequency. Thus over a few cycles of the carrier, $\hat{\theta}$ will be nearly constant. Assuming that more than one sample is taken per carrier cycle, $\omega_c kT_s + \hat{\theta}(k)$ will not remain constant from sample to sample, thus it is clear that there exists some interval $k_f > k_0$ where

$\left|\omega_c k T_s + \hat{\theta}(k)\right| = \frac{\pi}{2} n$ which satisfies the $\mathcal{M}(k_0, k_f) > 0$ requirement for complete observability for a scalar sampled single phase modulated source.

Baseband Sampling

By sampling the signal's true in-phase and quadrature components[2], the bandpass signal can be completely described by two baseband signals. The I-Q observation function is

$$h(\theta(k), k) = \sqrt{2}A\begin{bmatrix}\cos\theta(k)\\ -\sin\theta(k)\end{bmatrix} \tag{3.30}$$

Substituting (3.30) into (3.17) through (3.23) reveals that

$$\mathbf{H}(\hat{\theta}(k), k) = \left.\frac{\partial h(\theta(k), k)}{\partial\theta(k)}\right|_{\theta(k)=\hat{\theta}(k)} = \sqrt{2}A\begin{bmatrix}-\sin\hat{\theta}(k) & -\cos\hat{\theta}(k)\end{bmatrix} \tag{3.31}$$

for $\tilde{\theta} << 1$. The resulting observability Gramian from (3.28) is

$$\mathcal{M}(k_0, k_f) = \sqrt{2}A\sum_{k=k_0}^{k_f} e^{-2\alpha T_s(k-k_0)}\begin{bmatrix}\cos^2\hat{\theta}(k) & \cos\hat{\theta}(k)\sin\hat{\theta}(k)\\ \cos\hat{\theta}(k)\sin\hat{\theta}(k) & \sin^2\hat{\theta}(k)\end{bmatrix}. \tag{3.32}$$

For only one sample observation ($k_0 = k_f = 0$) the eigenvalues of $\mathcal{M}(k_0, k_f)$ are $\begin{bmatrix}1 & 0\end{bmatrix}$ which is also consistent with the definition of $\mathcal{M}(k_0, k_f)$ which specifies that the observation interval must be $k_f > k_0$. If two observations are taken then

$$\begin{aligned}\mathcal{M}(0,1) = &\begin{bmatrix}\cos^2\hat{\theta}(0) & \cos\hat{\theta}(0)\sin\hat{\theta}(0)\\ \cos\hat{\theta}(0)\sin\hat{\theta}(0) & \sin^2\hat{\theta}(0)\end{bmatrix}\\ &+\phi^2\begin{bmatrix}\cos^2\hat{\theta}(1) & \cos\hat{\theta}(1)\sin\hat{\theta}(1)\\ \cos\hat{\theta}(1)\sin\hat{\theta}(1) & \sin^2\hat{\theta}(1)\end{bmatrix}\end{aligned} \tag{3.33}$$

The worst case is where the phase estimate does not change during the observation interval so that $\hat{\theta}(1) = \hat{\theta}(0)$. This is unlikely but not impossible if the change due to the state transition is exactly balanced by the change do to the driving noise. In this case, the eigenvalues of $\mathcal{M}(0,1)$ are $\begin{bmatrix}1 + e^{-2\alpha T_s} & 0\end{bmatrix}$ and the eigenvalues of the N^{th} sample are

---

[2]Again this assumes that aquisition has been achieved.

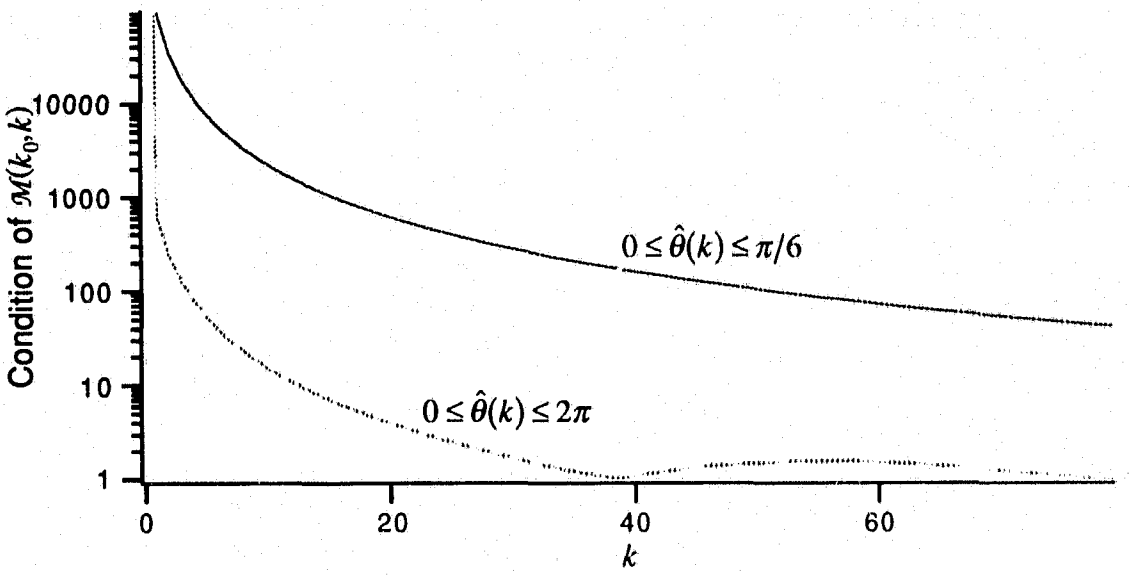

Figure 3–9 Condition of observability Gramian as the observation interval increases.

$$\lambda_{1,2} = \left[\sum_{i=0}^{N} e^{-2i\alpha T_s} \quad 0 \right]. \tag{3.34}$$

This is somewhat of an artificial case since in general $\hat{\theta}(N) \neq \cdots \hat{\theta}(1) \neq \hat{\theta}(0)$ due to the process driving noise w. The point is that as long as the phase estimate does change with time, the phase states are observable.

The rate of phase change does effect the observability. If $\hat{\theta}(i+1) \approx \hat{\theta}(i)$ then the eigenvalues will not be zero but the $\mathcal{M}$ will be ill-conditioned[3]. Two cases are illustrated: one where $\hat{\theta}$ varies slowly with respect to the sampling rate and one where $\hat{\theta}$ varies rapidly with respect to the sampling rate. As may be expected, the states become "more observable" with fewer samples when $\hat{\theta}$ varies rapidly with respect to the sampling rate.

---

[3]The condition of a matrix is the ratio of the largest to the smallest singular value. For Hermitian matrices, the singular values are equal to the absolute values of the eigenvalues..

3.3.2. Single Source Phase Estimation

To help tie in the observability issue with state estimation, the Extended Kalman Filter will be used to estimate (demodulate) the phase of a single phase modulated source. Since the analysis in the previous section is based on small phase estimation error, the EKF will be started with perfect knowledge of the signal's true phase, thus no acquisition is required.

Passband Sampling

In the scalar sampling case, the state and EKF equations reduce to scalars, repeated here for convenience. The state and measurement equations are

$$\theta(k+1) = e^{-\alpha T_s}\theta(k) + \left(1 - e^{-\alpha T_s}\right)^{\frac{1}{2}} w(k) \tag{3.35}$$

$$z(k) = \sqrt{2}A\sin\left(\omega_c k T_s + \theta(k)\right) + v(k), \tag{3.36}$$

and the single source EKF reduces to

$$\hat{\theta}(k) = \hat{\theta}(k \mid k-1) + K(k)\left[z(k) - \sqrt{2}A\sin\left(\omega_c k T_s + \hat{\theta}(k)\right)\right] \tag{3.37}$$

$$\hat{\theta}(k+1 \mid k) = e^{-\alpha T_s}\hat{\theta}(k) \tag{3.38}$$

$$P(k+1 \mid k) = e^{-2\alpha T_s}P(k) + 1 - e^{-\alpha T_s} \tag{3.39}$$

$$P(k) = \left[1 - K(k)\sqrt{2}A\cos\left(\omega_c k T_s + \hat{\theta}(k)\right)\right]P(k \mid k-1) \tag{3.40}$$

$$K(k) = P(k)\sqrt{2}A\cos\left(\omega_c k T_s + \hat{\theta}(k)\right)\frac{1}{\sigma_v^2}. \tag{3.41}$$

The steady-state values of the Kalman gain K, observation matrix H, estimation error covariance P, and mean-square error (MSE) in phase estimation are shown in Fig. 3–10 for an ensemble average of 100 runs. The cyclic nature of the observation matrix $H(k) = \sqrt{2}A\cos\left(\omega_c k T_s + \hat{\theta}(k)\right)$ results in periods during which little or no information is contained in the innovations process, thus the filter "goes with" the prediction by reducing the Kalman gain to zero. As a consequence the prediction error increases during these times indicating that the state, the phase in the case of PM, is not observable. However as $|H(k)|$

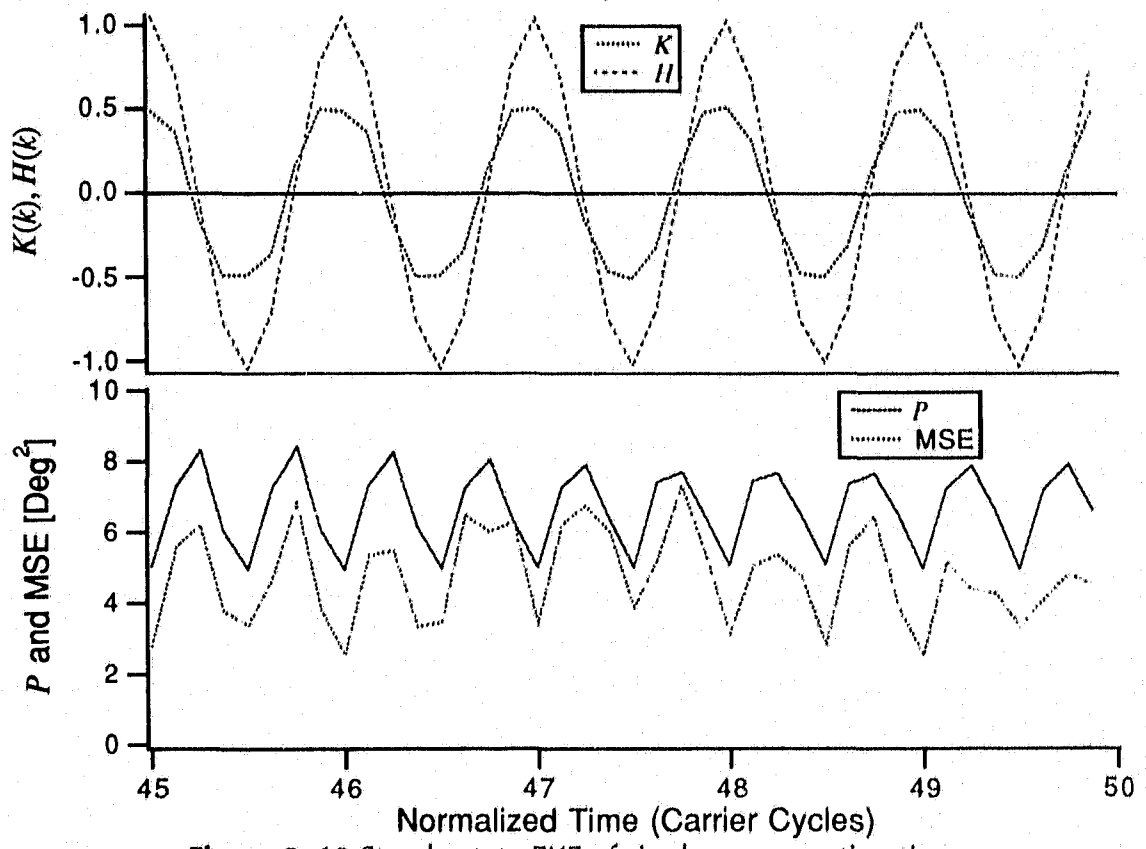

Figure 3–10 Steady-state EKF of single source estimation.

becomes greater than zero, more state information is available innovations process which is indicated by an increase in the magnitude of the Kalman gain. Given this additional information, the EKF is better able to estimate the state and the estimation error decreases. It should also be noted that the "ripple" in P is at twice the carrier frequency due to the multiplication of H and K in (3.40). It will be shown later that this is precisely how the phase-lock loop operates.

3.3.3. Single Source Phase and Amplitude Estimation

In addition to estimating the phase of a PM source, an estimate of the amplitude is also required. Following the approach of previous two sections, the observability and estimation of amplitude *and* phase will be examined.

The phase and amplitude processes as defined in (2.123)

$$\begin{bmatrix}\theta(k+1)\\ A(k+1)\end{bmatrix}=\begin{bmatrix}\phi_\theta & 0\\ 0 & 1\end{bmatrix}\begin{bmatrix}\theta(k)\\ A(k)\end{bmatrix}+\begin{bmatrix}\gamma_\theta\\ 0\end{bmatrix}w(k). \tag{3.42}$$

The scalar measurement from (2.124) is

$$z(k)=\sqrt{2}A(k)\sin\left(\omega_c kT_s+\theta(k)\right)+v(k) \tag{3.43}$$

and from (3.19) the measurement estimate is

$$\hat{z}(k)=\sqrt{2}\hat{A}(k)\sin\left(\omega_c kT_s+\hat{\theta}(k)\right), \tag{3.44}$$

with the resulting small angle estimation error

$$\begin{aligned}\tilde{z}(k)&=z(k)-\hat{z}(k)\\ &=\sqrt{2}A(k)\sin\left(\omega_c kT_s+\theta(k)\right)+v(k)-\sqrt{2}\hat{A}(k)\sin\left(\omega_c kT_s+\hat{\theta}(k)\right)\\ &\approx\sqrt{2}\left[\hat{A}(k)\cos\left(\omega_c kT_s+\hat{\theta}(k)\right)\tilde{\theta}(k)+\tilde{A}(k)\sin\left(\omega_c kT_s+\hat{\theta}(k)\right)\right]+v(k)\end{aligned} \tag{3.45}$$

for $\tilde{\theta}<<1$ and where $\tilde{A}(k)=A(k)-\hat{A}(k)$. By forming the prediction error state vector $\tilde{\mathbf{x}}(k)=\left[\tilde{\theta}(k)\quad\tilde{A}(k)\right]^{\mathrm{T}}$, (3.45) may be expressed in vector form as

$$\tilde{z}(k)=\begin{bmatrix}\sqrt{2}\hat{A}(k)\cos\left(\omega_c kT_s+\hat{\theta}(k)\right)\\ \sqrt{2}\sin\left(\omega_c kT_s+\hat{\theta}(k)\right)\end{bmatrix}^{\mathrm{T}}\tilde{\mathbf{x}}(k)+v(k). \tag{3.46}$$

As shown in (3.25)

$$\begin{aligned}\tilde{\mathbf{x}}(k)&=\mathbf{x}(k)-\hat{\mathbf{x}}(k)\\ &=\mathbf{\Phi}\mathbf{x}(k-1)+\mathbf{\Gamma}w(k)-\hat{\mathbf{x}}(k\mid k-1)-\mathbf{K}(k)\left[z(k)-h\left(\hat{\mathbf{x}}(k\mid k-1),k\right)\right]\\ &=\mathbf{\Phi}\left(\mathbf{x}(k-1)-\hat{\mathbf{x}}(k-1)\right)+\mathbf{\Gamma}w(k)-\mathbf{K}(k)\left[z(k)-h\left(\hat{\mathbf{x}}(k\mid k-1),k\right)\right]\\ &=\mathbf{\Phi}\tilde{\mathbf{x}}(k-1)+\mathbf{\Gamma}w(k)-\mathbf{K}(k)\left[z(k)-h\left(\hat{\mathbf{x}}(k\mid k-1),k\right)\right]\end{aligned} \tag{3.47}$$

which demonstrates that the state prediction error has the same transition matrix as the phase and amplitude state vector. This will be used to examine the observability of the state prediction errors.

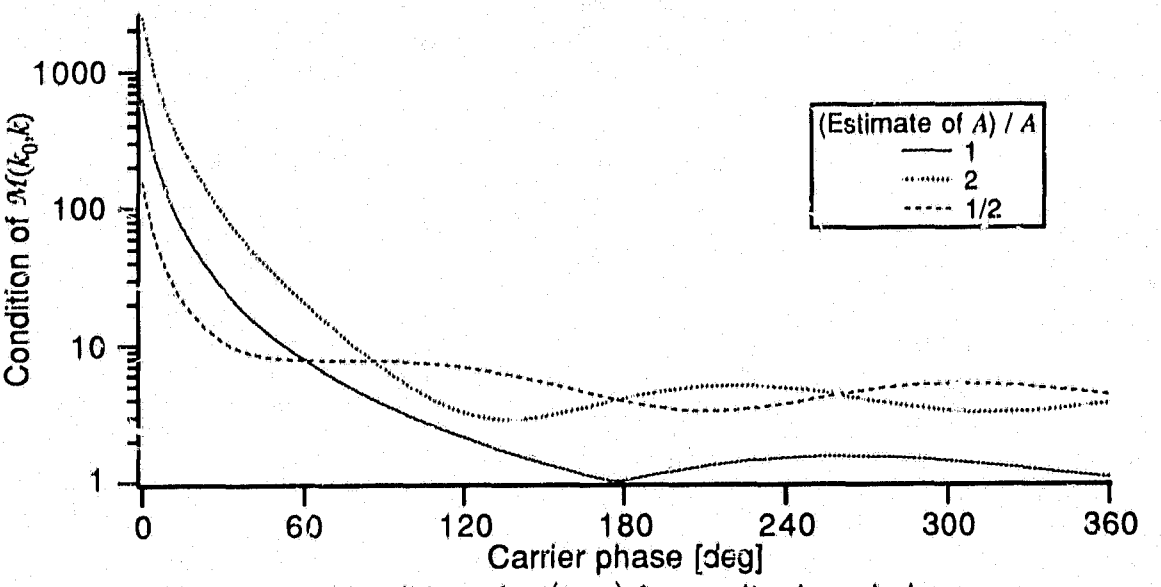

Figure 3–11 Condition of $\mathcal{M}(k_0, k)$ for amplitude and phase.

As in the previous section, the observability Gramian is singular for one sample but the condition of $\mathcal{M}(k_0, k)$ again improves as the observation interval increases. However, with the inclusion of the amplitude state, the $\mathcal{M}(k_0, k)$ becomes a function of both state variables. Fig. 3–11 shows the condition of $\mathcal{M}(k_0, k)$ for one cycle of the carrier for various $\hat{A}(k)$. Fig. 3–11 shows that, as in the previous section, an interval does exist such that $\tilde{\mathbf{x}}(k)$ is observable.

Simulation of the EKF estimator derived in Section 2.3.4 shows that both states may also be accurately estimated. The addition of amplitude estimation bears further examination. The linearized Kalman observation matrix (2.126) for single source phase and amplitude estimation is

$$\mathbf{H}\left(\hat{\mathbf{x}}(k\,|\,k-1),k\right)=\begin{bmatrix}\hat{A}(k\,|\,k-1)\cos\left(\omega_c kT_s+\hat{\theta}(k\,|\,k-1)\right)\\ \sin\left(\omega_c kT_s+\hat{\theta}(k\,|\,k-1)\right)\end{bmatrix}^{\mathrm{T}}. \tag{3.48}$$

The behavior of the phase estimation part of the EKF is nearly identical to that shown in Fig. 3–10. Fig. 3–12 shows the EKF state observation matrix and Kalman gain responsible for

amplitude estimation. It is interesting to note the Kalman gain for the amplitude state K_A is essentially zero once the EKF has converged. This is due to the random constant model of the carrier amplitude; once the EKF has accurately estimated the carrier amplitude, very little additional state information is present in the innovations process and the estimator goes with the state prediction. The small corrections are mostly due to the measurement noise $\sigma_v^2 = 10^{-3}$.

The estimation error covariance matrix $\mathbf{P}$, defined as

$$\mathbf{P}(k) \equiv E\left\{(\mathbf{x}(k) - \hat{\mathbf{x}}(k))(\mathbf{x}(k) - \hat{\mathbf{x}}(k))^{\mathrm{T}}\right\}, \tag{3.49}$$

which in this case has the familiar form

$$\mathbf{P}(k) = \begin{bmatrix} P_\theta(k) & P_{\theta A}(k) \\ P_{A\theta}(k) & P_A(k) \end{bmatrix}, \tag{3.50}$$

where the diagonal elements P_θ and P_A correspond to the estimation error variance of θ and A respectively and off-diagonal elements represent the cross-covariance in the estimation error of θ and A. The magnitude of the off-diagonal elements relative to the diagonal elements give an indication of the estimated coupling of the states. As shown in (2.136) the off-diagonal elements are not necessarily zero. Using the small state error condition of the EKF, the relative magnitudes of the error covariance terms and the resulting coupling between state estimators may be examined for estimator tracking. As shown in Fig. 3–13 the magnitudes of $P_{\theta A}$, $P_{A\theta}$, and P_A are five orders of magnitude smaller than that of P_θ indicating that *during tracking*, the states are essentially decoupled and the cross-covariance gains need not be included in the estimator *once acquisition has occurred.*

Unlike in phase estimation which converges within a few carrier cycles, the amplitude estimate converges much slower as do the cross-covariances (see Fig. 3–14). This slow convergence can be attributed to the small Kalman gain; the innovations process yields little information for each additional sample thus the MMSE is slowly achieved. Fig. 3–14 shows that the cross-covariance terms approach zero as is expected.

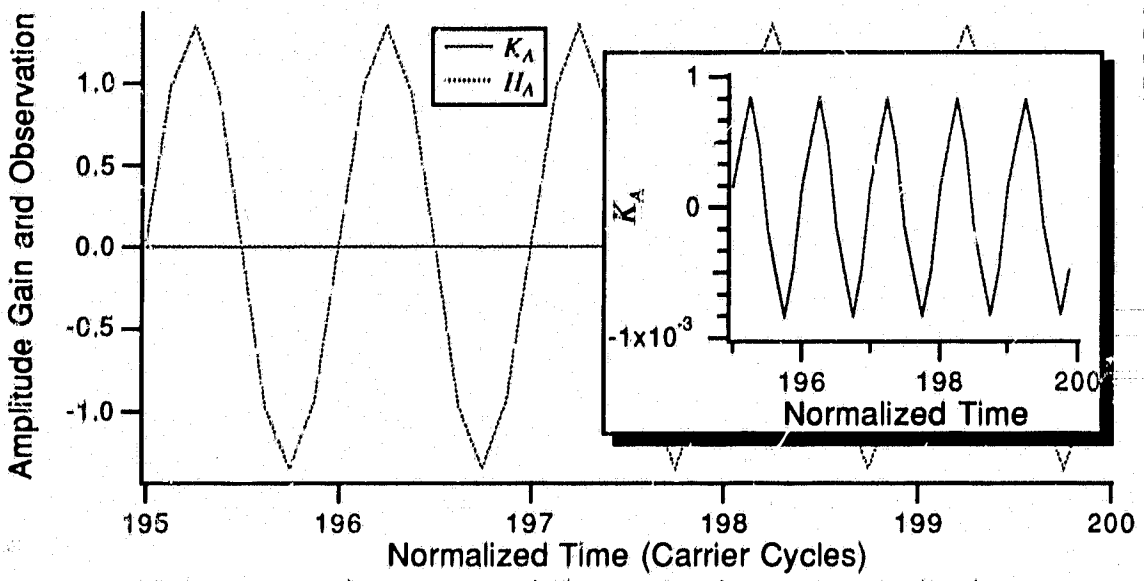

Figure 3–12 Kalman gain and observation for carrier amplitude.

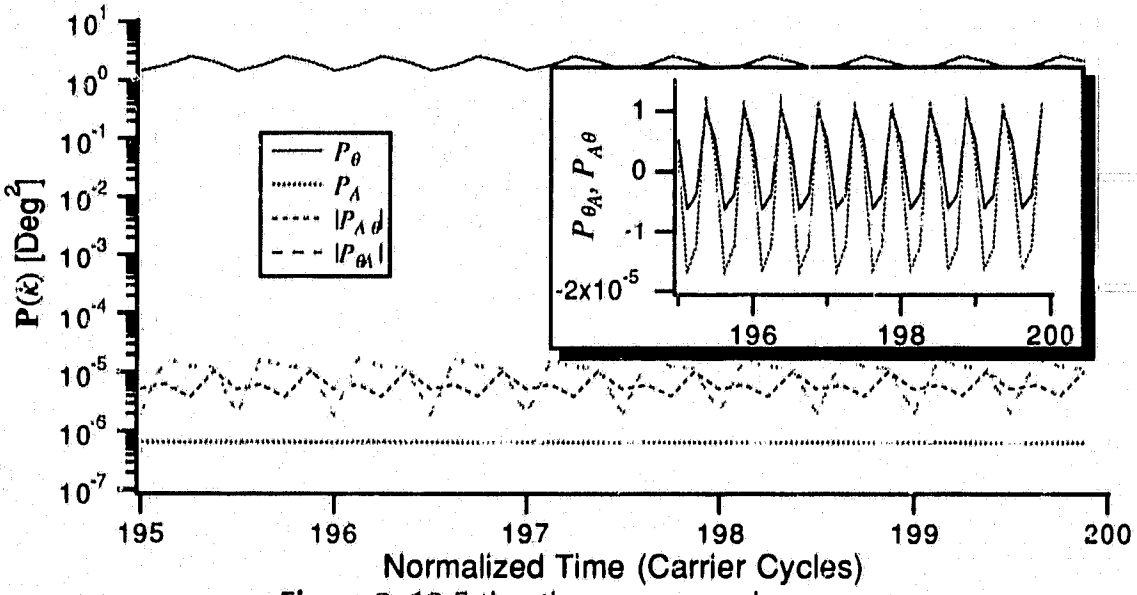

Figure 3–13 Estimation error covariances.

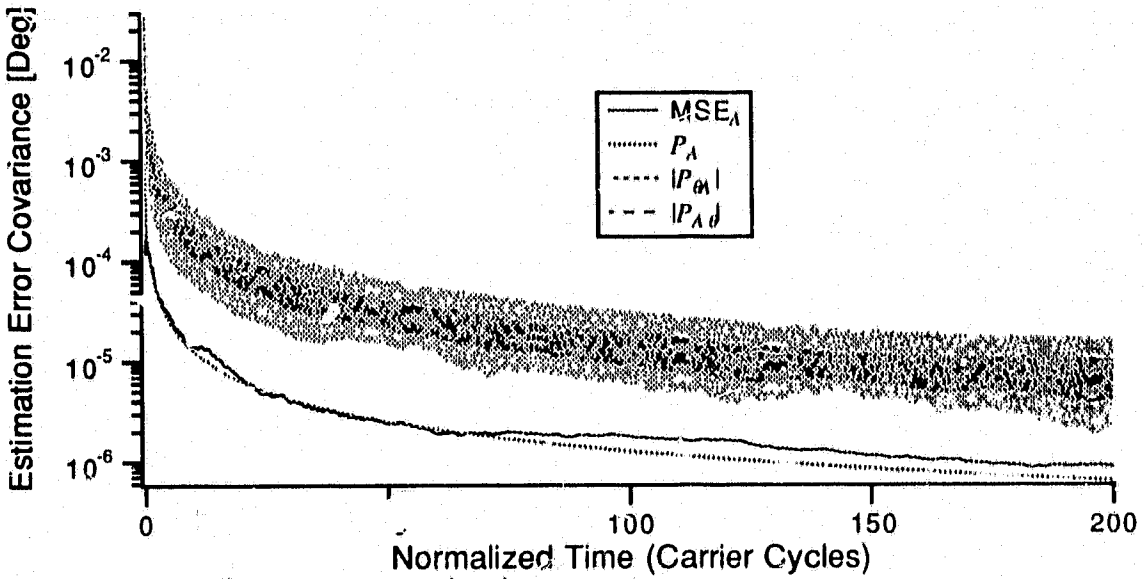

Figure 3–14 Amplitude estimation error convergence.

3.3.4. Two Source Phase Observability

The analysis carried out in the previous section will now be extended to examine the separability of multiple PM sources. The two source scenario will be examined.

Passband Sampling

As shown in (2.137), two independent message processes may be represented by

$$\begin{bmatrix}\theta_1(k+1)\\ \theta_2(k+1)\end{bmatrix}=\begin{bmatrix}\phi_{\theta,1} & 0\\ 0 & \phi_{\theta,2}\end{bmatrix}\begin{bmatrix}\theta_1(k)\\ \theta_2(k)\end{bmatrix}+\begin{bmatrix}\gamma_{\theta,1} & 0\\ 0 & \gamma_{\theta,2}\end{bmatrix}\begin{bmatrix}w_{\theta,1}(k)\\ w_{\theta,2}(k)\end{bmatrix}, \tag{3.51}$$

where θ_1 and θ_2 are two independent random phase processes and may be written more compactly as

$$\boldsymbol{\theta}(k+1)=\boldsymbol{\Phi}\boldsymbol{\theta}(k)+\boldsymbol{\Gamma}\mathbf{w}(k). \tag{3.52}$$

The scalar observation of the combination of the two phase modulated sources is

$$y(k)=h(\boldsymbol{\theta}(k),k)=\sqrt{2}\left[A_1\sin(\omega_c kT_s+\theta_1(k))+A_2\sin(\omega_c kT_s+\theta_2(k))\right] \tag{3.53}$$

with the resulting measurement as described by (2.138).

Again define the $\hat{z}$ to be an estimate of the measurement based on the *a posteriori* phase estimate,

$$\hat{z}(k) = \hat{y}(k) = \sqrt{2}\left[A_1 \sin\left(\omega_c kT_s + \hat{\theta}_1(k)\right) + A_2 \sin\left(\omega_c kT_s + \hat{\theta}_2(k)\right)\right], \tag{3.54}$$

and the resulting measurement estimation error is as defined in (3.20). Under the small estimation error condition, it may be shown that

$$\begin{aligned} y(k) - \hat{y}(k) &= \sqrt{2}\left[A_1 \sin\left(\omega_c kT_s + \theta_1(k)\right) + A_2 \sin\left(\omega_c kT_s + \theta_2(k)\right)\right] \\ &\quad -\sqrt{2}\left[A_1 \sin\left(\omega_c kT_s + \hat{\theta}_1(k)\right) + A_2 \sin\left(\omega_c kT_s + \hat{\theta}_2(k)\right)\right] \\ &\approx \sqrt{2}\left[A_1 \cos\left(\omega_c kT_s + \hat{\theta}_1(k)\right)\tilde{\theta}_1(k) + A_2 \cos\left(\omega_c kT_s + \hat{\theta}_2(k)\right)\tilde{\theta}_2(k)\right], \end{aligned} \tag{3.55}$$

which may be expressed more compactly as

$$\tilde{z}(k) = \sqrt{2}\begin{bmatrix} A_1 \cos\left(\hat{\Theta}_1\right) \\ A_2 \cos\left(\hat{\Theta}_2\right) \end{bmatrix}^{\mathrm{T}} \begin{bmatrix} \tilde{\theta}_1(k) \\ \tilde{\theta}_2(k) \end{bmatrix} + v(k). \tag{3.56}$$

It is apparent that (3.56) is in the same form as (3.27) where, in this case, (3.56) takes the form

$$\tilde{z}(k) = \mathbf{H}\left(\hat{\theta}(k), k\right)\tilde{\theta}(k) + v(k). \tag{3.57}$$

The observability Gramian of the two source case given one sample is

$$\begin{aligned} &\mathbf{\Phi}^{\mathrm{T}}(k,k_0)\mathbf{H}^{\mathrm{T}}\left(\hat{\theta}(k),k\right)\mathbf{H}\left(\hat{\theta}(k),k\right)\mathbf{\Phi}(k,k_0) = \\ &\begin{bmatrix} 2A_1^2\phi_{\theta,1}^2 \cos^2\left(\hat{\Theta}_1(k)\right) & 2A_1A_2\phi_{\theta,1}\phi_{\theta,2}\cos\left(\hat{\Theta}_1(k)\right)\cos\left(\hat{\Theta}_2(k)\right) \\ 2A_1A_2\phi_{\theta,1}\phi_{\theta,2}\cos\left(\hat{\Theta}_1(k)\right)\cos\left(\hat{\Theta}_2(k)\right) & 2A_2^2\phi_{\theta,2}^2\cos^2\left(\hat{\Theta}_2(k)\right) \end{bmatrix} \end{aligned} \tag{3.58}$$

with eigenvalues

$$\lambda_{1,2} = \left[0 \quad 2A_1^2\phi_1^2\cos^2\left(\hat{\Theta}_1(k)\right) + 2A_2^2\phi_2^2\cos^2\left(\hat{\Theta}_2(k)\right)\right], \tag{3.59}$$

indicating that the states are not uniformly completely observable given one measurement. Following the same approach as in the previous section, the observability based on two consecutive samples is examined. For $k = 0, 1$

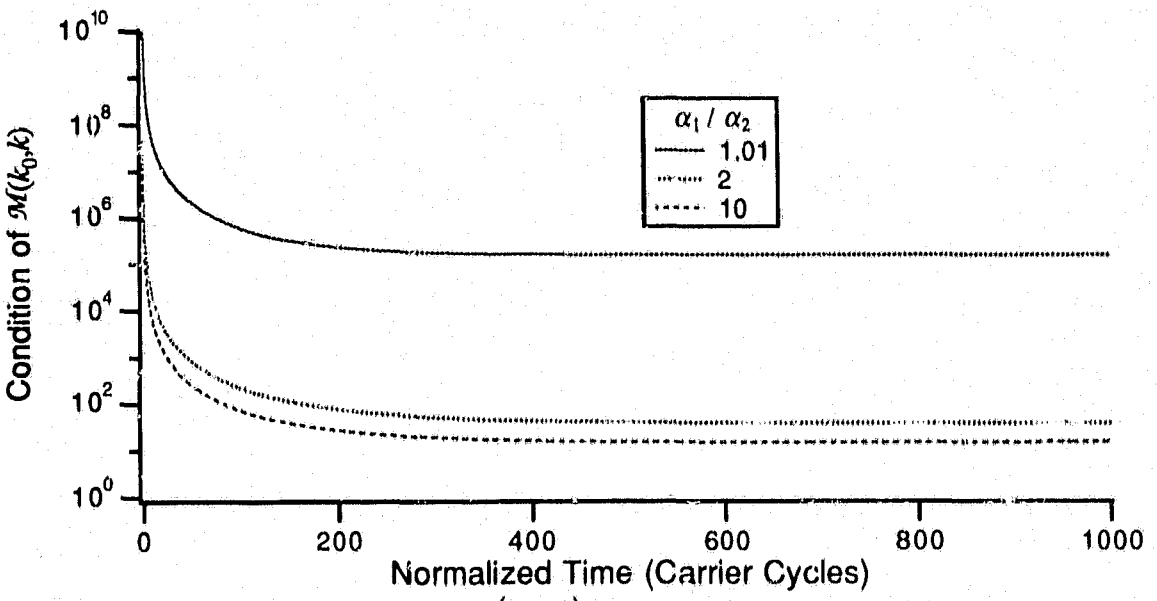

Figure 3–15 Condition of $\mathcal{M}(k_0,k_f)$ for zero carrier phase difference.

$$\mathbf{H}^{\mathrm{T}}\left(\hat{\boldsymbol{\theta}}(0),0\right)\mathbf{H}\left(\hat{\boldsymbol{\theta}}(0),0\right)+\boldsymbol{\Phi}^{\mathrm{T}}(1,0)\mathbf{H}^{\mathrm{T}}\left(\hat{\boldsymbol{\theta}}(1),1\right)\mathbf{H}\left(\hat{\boldsymbol{\theta}}(1),1\right)\boldsymbol{\Phi}(1,0)=\begin{bmatrix} m_{11} & m_{12} \\ m_{21} & m_{22}\end{bmatrix}, \tag{3.60}$$

where

$$m_{11}=2A_1^2\left\{\cos^2\left(\hat{\Theta}_1(0)\right)+\phi_1^2\cos^2\left(\hat{\Theta}_1(1)\right)\right\} \tag{3.61}$$

$$m_{12}=m_{21}=2A_1A_2\left\{\cos\left(\hat{\Theta}_1(0)\right)\cos\left(\hat{\Theta}_2(0)\right)+\phi_{\theta,1}\phi_{\theta,2}\cos\left(\hat{\Theta}_1(1)\right)\cos\left(\hat{\Theta}_2(1)\right)\right\} \tag{3.62}$$

$$m_{22}=2A_2^2\left\{\cos^2\left(\hat{\Theta}_2(0)\right)+\phi_2^2\cos^2\left(\hat{\Theta}_2(1)\right)\right\} \tag{3.63}$$

the eigenvalues of which are quite messy and will not be expressed in closed form here. It may be shown that the only condition under which (3.60) is not positive definite is where $\alpha_1=\alpha_2$ *and* where $\hat{\Theta}_1(k)=\hat{\Theta}_2(k)$ regardless of the relative carrier power (except in the limiting case where one of the carriers has zero power in which case there is only a single source). This indicates that unless the signals are spectrally identical, they are observable. However, as previously discussed, the condition of $\mathcal{M}$ may also shed some light on the state observability. This will be examined numerically by computer simulation. Unless otherwise noted, $A_1=A_2=1$ in subsequent work.

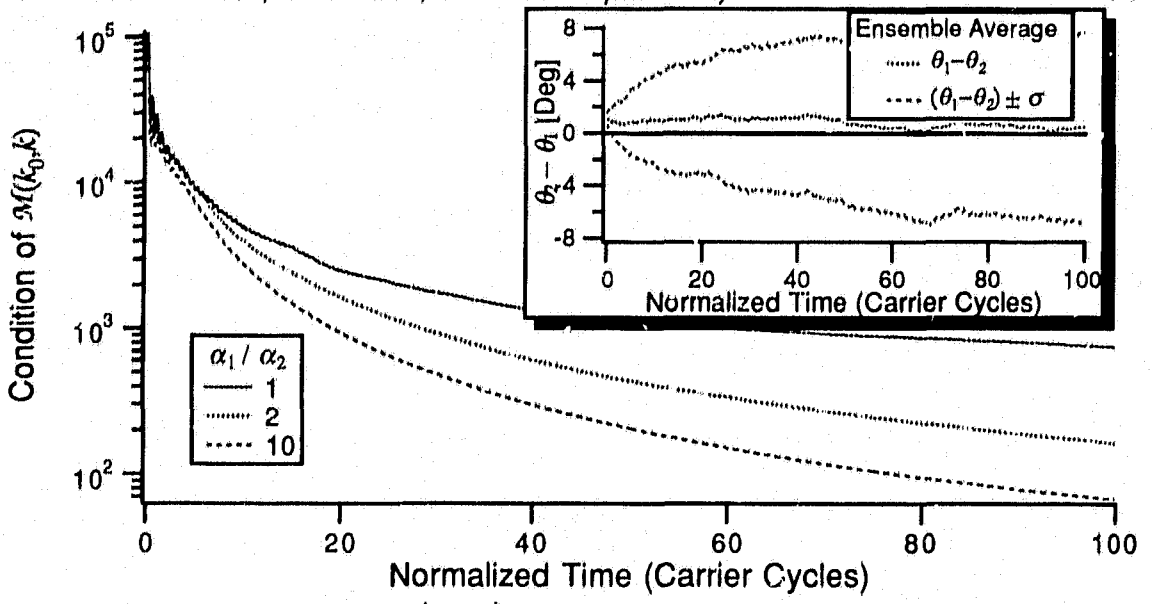

Figure 3–16 Condition of $\mathcal{M}(k_0,k_f)$ for nominally zero carrier phase difference.

To examine the effects of the interrelationships between α_i and $\hat{\Theta}_i(k)$ on observability, the condition of $\mathcal{M}(k_0,k)$, as defined in (3.28), is numerically evaluated for various cases. Since it is has been shown that $\mathcal{M}(k_0,k_0)$ is singular, the first point plotted in the following plots is $\mathcal{M}(k_0,k_0+1)$. In the first simulation, the length of the observation interval is increased (by taking more samples) for three different α ratios *while the carriers remain in phase.* As expected, when $\alpha_1=\alpha_2$ and $\hat{\Theta}_1(k)=\hat{\Theta}_2(k)$. ($\alpha_1/\alpha_2=1.01$ in this case since when $\alpha_1=\alpha_2$ the condition of $\mathcal{M}(k_0,k)$ remains about 10^{16}) the observability Gramian shows that it remains ill conditioned throughout the observation interval (see Fig. 3–15). However, when $\alpha_1\neq\alpha_2$ $\mathcal{M}(k_0,k)$ becomes better conditioned as the observation interval increases. There is a limit to the amount of state information available from additional measurements which is reflected in the leveling off of the condition of the observability matrix which is due to the decaying exponential nature of the state transition term $\phi_i=e^{-\alpha_i T_s}$.

Maintaining $\hat{\Theta}_1(k)=\hat{\Theta}_2(k)$ is a bit artificial since $\hat{\Theta}_i(k)$ is dependent on the stochastic process defined by α and thus $\hat{\Theta}_1(k)=\hat{\Theta}_2(k)$ would only happen "occasionally." Therefore the same experiment is repeated save that $\left|\hat{\Theta}_1(k)-\hat{\Theta}_2(k)\right|$ is *nominally* zero but not exactly

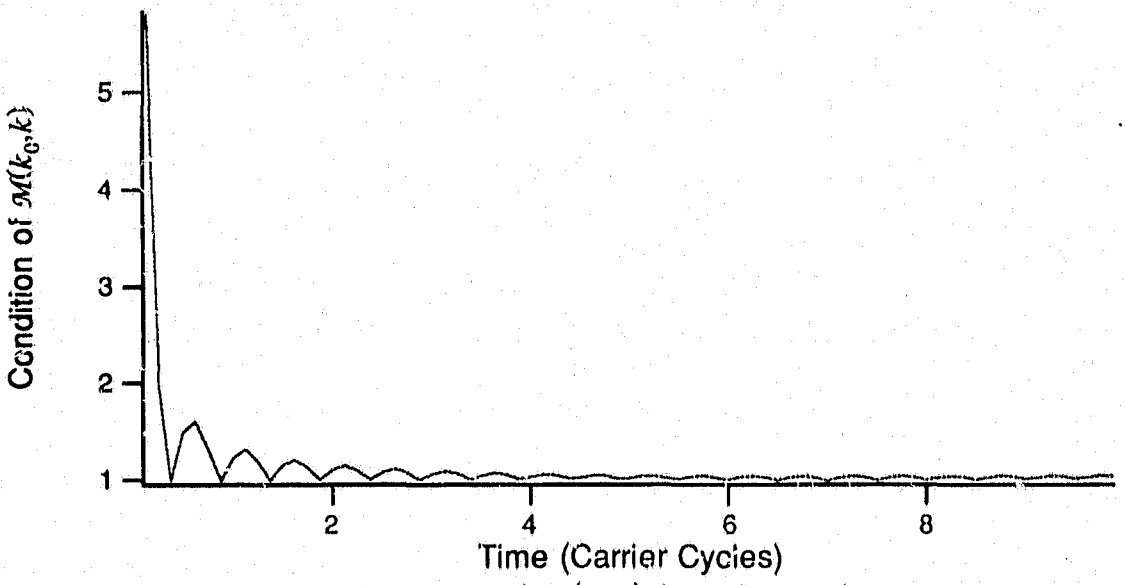

Figure 3–17 Condition of $\mathcal{M}(k_0,k)$ for orthogonal carriers.

zero since the phase difference is also stochastic (see Fig. 3–16). In an effort to keep the phase difference relatively constant, the phase sensivity described in (2.2) of each carrier is reduced from unity to $d_p = 0.1$. Here it is evident that the carrier phase difference has a far greater effect on state observability than the phase processes themselves. Even when $\alpha_1 = \alpha_2$ the observability Gramian is well conditioned due to the non-zero carrier phase difference. When the initial carrier phases are orthogonal, quite a different behavior emerges. The observability Gramian is well conditioned after the first two samples and is essentially independent of the message process bandwidth (see Fig. 3–17).

The observability as a function of effective sampling rate (the number of samples per carrier cycle) is also of interest. Four plots are shown corresponding to four different sampling rates with respect to the carrier in Fig. 3–18. The carriers are orthogonal. In all four cases, the observability matrix becomes well-conditioned after two samples indicating that, over a carrier cycle, the number of samples has little effect on state observability. This is due to the $e^{-\alpha T_s}$ term in the state transition matrix; as $T_s \to 0$, $e^{-\alpha T_s} \to 1$ which means that the state changes little between two adjacent channels and little if any additional state information is

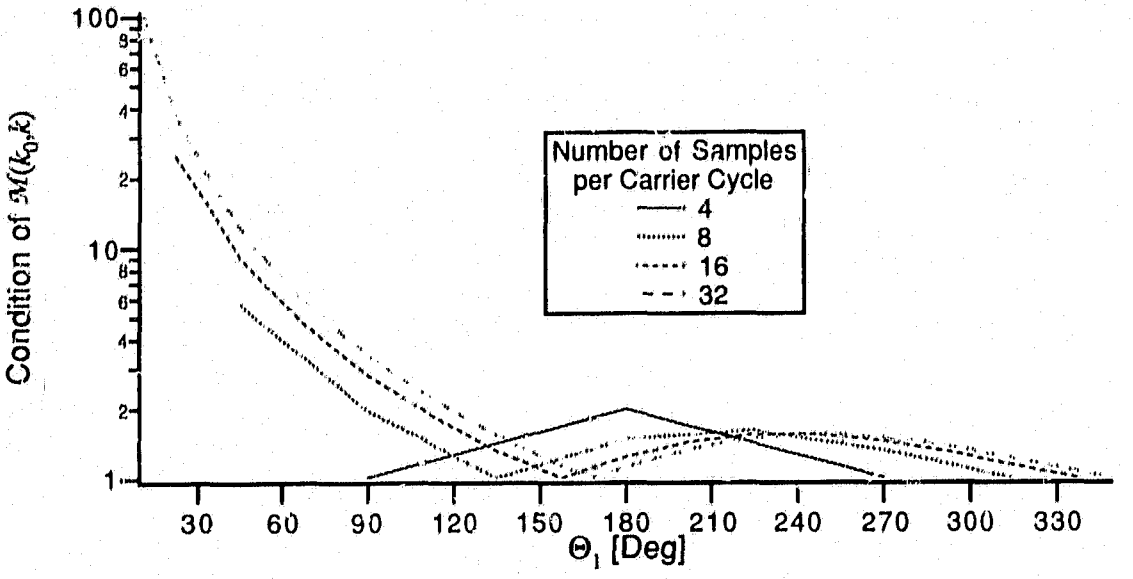

Figure 3–18 Condition of $\mathcal{M}(k_0,k)$ for various carrier sampling rates.

gained from the additional sample. In Figs. 3–15 and 3–17 and for much of the following, work unless otherwise noted, eight samples per cycle are used so that the cyclic nature of the signals may be shown.

Next the effect of the phase difference between the two carriers on the state observability is further examined by looking at the observability as a function of carrier phase difference. In Fig. 3–19, the eigenvalues of $\mathcal{M}(k_0,k_f)$ are shown for $0 \le |\hat{\theta}_1 - \hat{\theta}_2| \le 2\pi$. When the carriers are orthogonal, the eigenvalues are nearly equal and $\mathcal{M}(k_0,k_f)$ is close to the identity matrix, very well conditioned and positive definite. This would indicate the best condition for state observability. When the carriers are in-phase or anti-phase, $\mathcal{M}(k_0,k_f)$ becomes ill conditioned indicating poor state observability. The inset graph shows the effect of various α ratios. When the α's are equal and the carriers are in-phase or anti-phase, $\mathcal{M}(k_0,k_f)$ is singular which agrees with the above analysis. Even if the α's are not equal, $\mathcal{M}(k_0,k_f)$ is still ill-conditioned when the carriers are in-phase or anti-phase.

Fig. 3–20 shows the condition of $\mathcal{M}(k_0,k_f)$ as a function of carrier amplitude ratio. Although $\mathcal{M}(k_0,k_f)$ is generally well conditioned in Fig. 3–20, as the power of once carrier

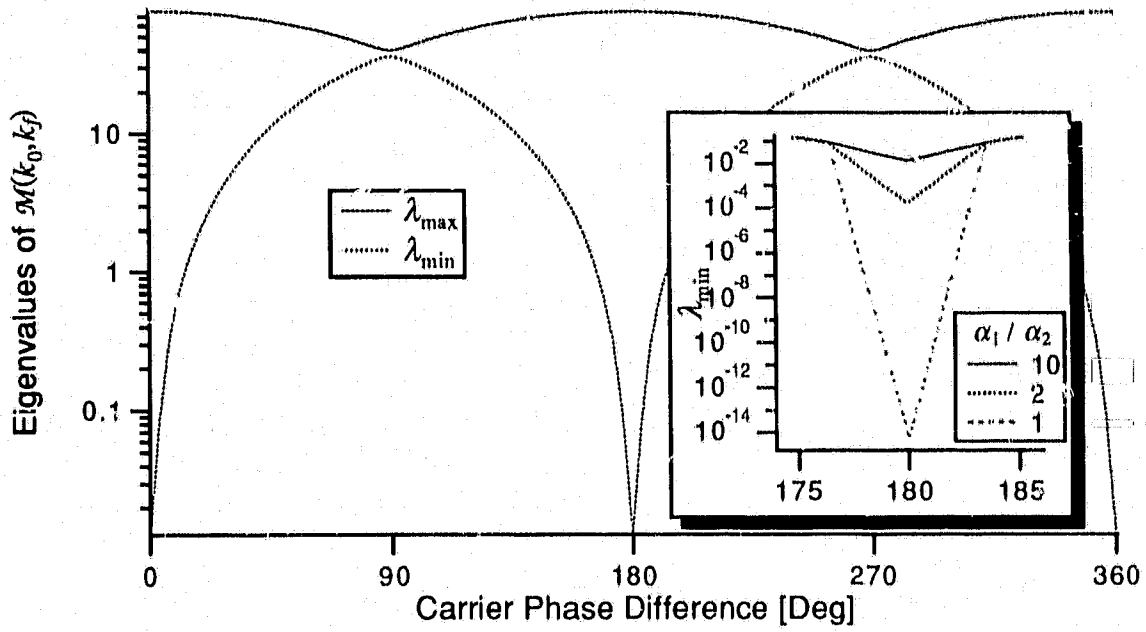

Figure 3–19 Eigenvalues of $\mathcal{M}(k_0,k_f)$ as a function of carrier phase difference and α.

overwhelms the second, the total state observability decreases since the states of the lower powered carrier are less observable.

Given the problems associated with nonlinear systems, we have, in a round about way, shown that two combined phase modulated signals may be separated unless their phases are equal. This hypothesis will now be tested.

3.3.5. Two Source Phase Estimation

To further explore the relationship between observability and separability, the ability of the EKF derived in Section 2.2 to separate the two signals is studied. The work in the previous section assumes that the phase estimation error is small. In a phase locked loop, this corresponds to the locked condition. Similarly, in the Kalman filer, this would require that the filter has already accurately estimated the states and the filter has reached steady-state. In the following simulation results, the EKF is initialized with perfect knowledge of the phase and the plots are shown in the steady-state condition. The two signals also have the same power,

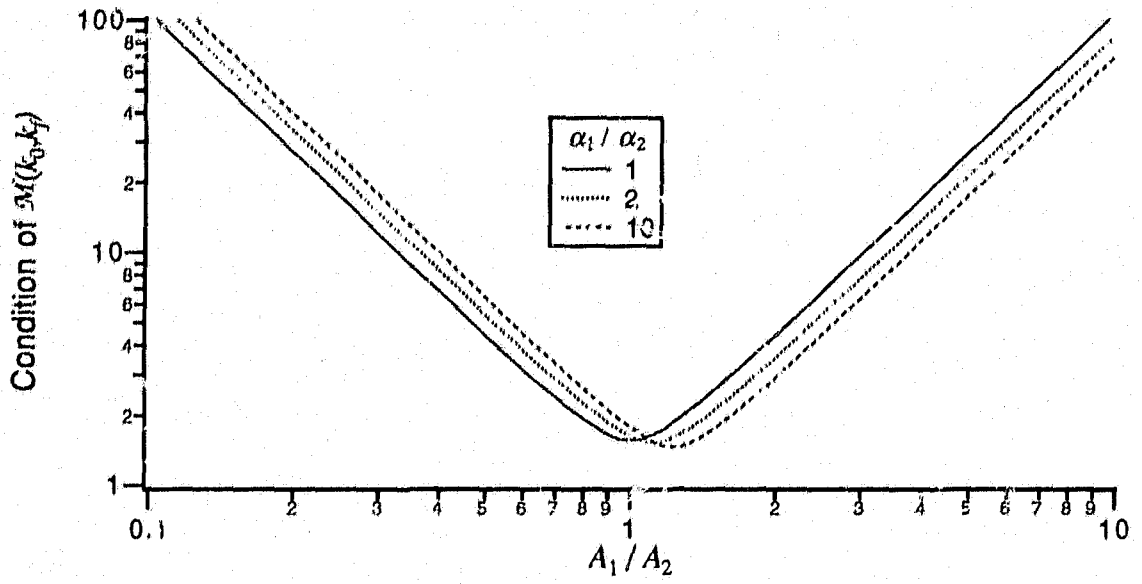

Figure 3–20 Condition of $\mathcal{M}(k_0,k_f)$ as a function of carrier amplitude ratio.

$A_1 = A_2 = 1$, and bandwidths $\alpha_1 = 2\alpha_2 = f_c/100$. The carriers are sampled at eight samples per cycle[4].

Carriers Nominally in Quadrature

As a first test the ability of the EKF to track modulations on two orthogonal carriers is examined. As shown in Fig. 3–21 the EKF is able to track each phase process. Examination of $\mathbf{K}(k)$, $\mathbf{H}\left(\hat{\boldsymbol{\theta}}(k\,|\,k-1),k\right)$, $\mathbf{P}(k)$, and the phase estimation MSE also provides insight into the EKF's behavior. The graphs in Fig. 3–22 through 3–24 are the ensemble average of the estimation error of 100 separate runs. The EKF generally achieves steady-state within a few carrier cycles.

The effect of state observability on state estimation manifests itself in the Kalman gain matrix, $\mathbf{K}$ (see Fig. 3–22). The Kalman gain K_i of phase θ_i is cyclic. The magnitude of K_i

---

[4]The effective sampling rate was increased solely for the purpose of graphing to better illustrate the subsequent discussions.

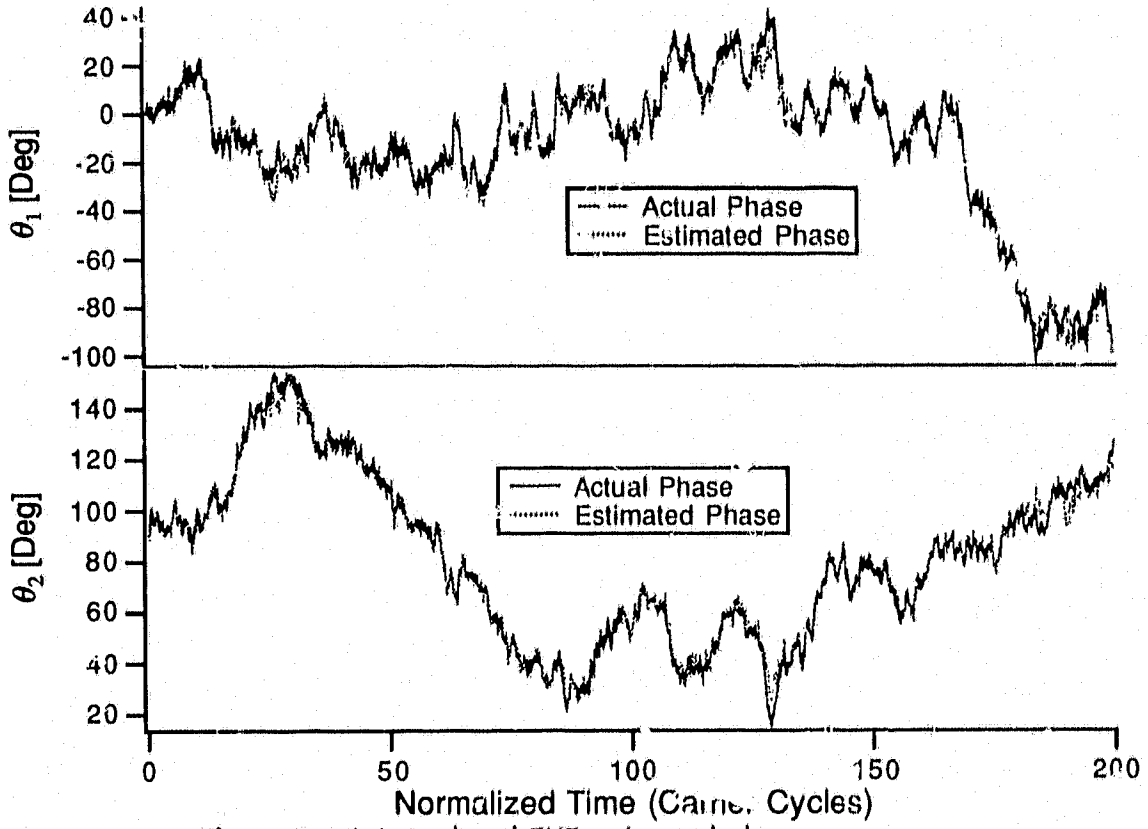

Figure 3–21 Actual and EKF estimated phase processes.

decreases as θ_i becomes less observable, $|K_i| \to 0$ as $\left|\mathbf{H}\left(\hat{\theta}_i(k|k-1),k\right)\right| \to 0$ from (2.80), resulting in a cyclic K_i. Also the RMS value of K_i decreases when $|\theta_1(k) - \theta_2(k)|$ is near zero. This is due to the reduced amount of state information available in the measurement and corresponding innovations process causing the EKF to weight the prediction more than the measurement. This results in an attendant increase in the estimation error covariance and MSE during these periods of time (see $P_{\theta,1}$ and $P_{\theta,2}$ in Fig. 3–23).

As in Section 3.3.3, the estimation error covariance matrix $\mathbf{P}$, has the form

$$\mathbf{P}(k) = \begin{bmatrix} P_{\theta,1}(k) & P_{\theta,1\theta,2}(k) \\ P_{\theta,2\theta,1}(k) & P_{\theta,2}(k) \end{bmatrix}, \tag{3.64}$$

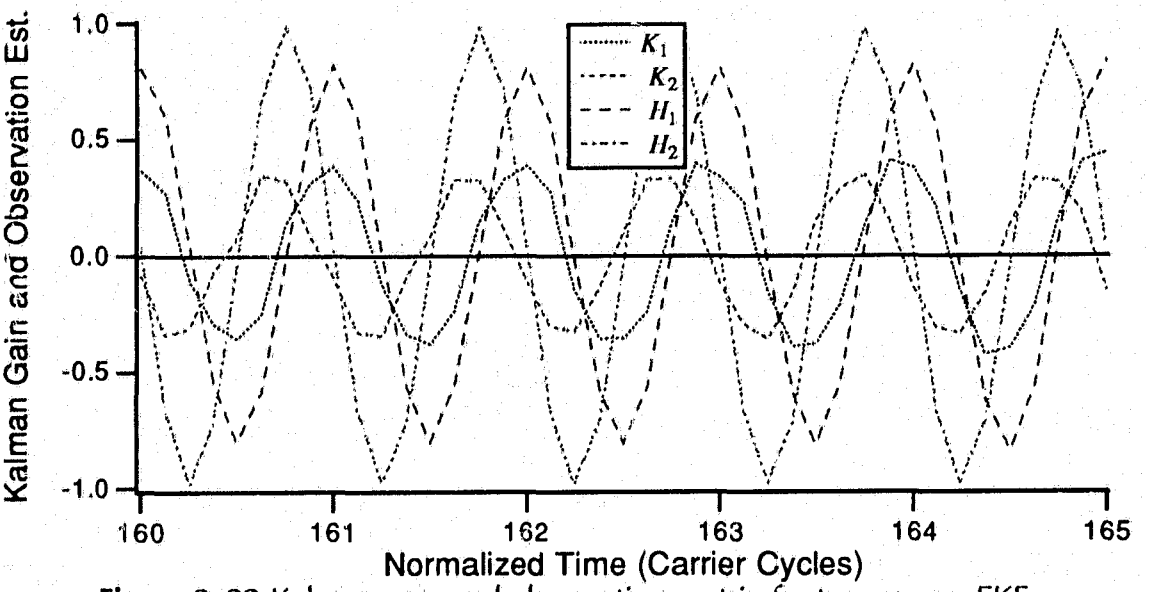

Figure 3–22 Kalman gain and observation matrix for two source EKF.

where, in this case, the diagonal elements $P_{\theta,1}$ and $P_{\theta,2}$ correspond to the estimation error variance of θ_1 and θ_2 respectively. The off-diagonal elements represent the cross-covariance in the estimation error of θ_1 and θ_2. Again we would *expect* that the off-diagonal elements of (3.64) to be zero in preserving the uncoupled nature of states but as shown in (2.146) the cross-covariance terms are generally not zero especially during acquisition. Fig. 3–23 reveals that the time-average cross-covariances are near zero when compared with the auto-covariances. However, since the phases are random processes, the carrier phase difference changes with time and as it changes, so does the "instantaneous" observability and separability. This can be readily observed in Fig. 3–24 where both the auto and cross-covariances increase as the carriers approach in-phase and anti-phase (0° and ±180°).

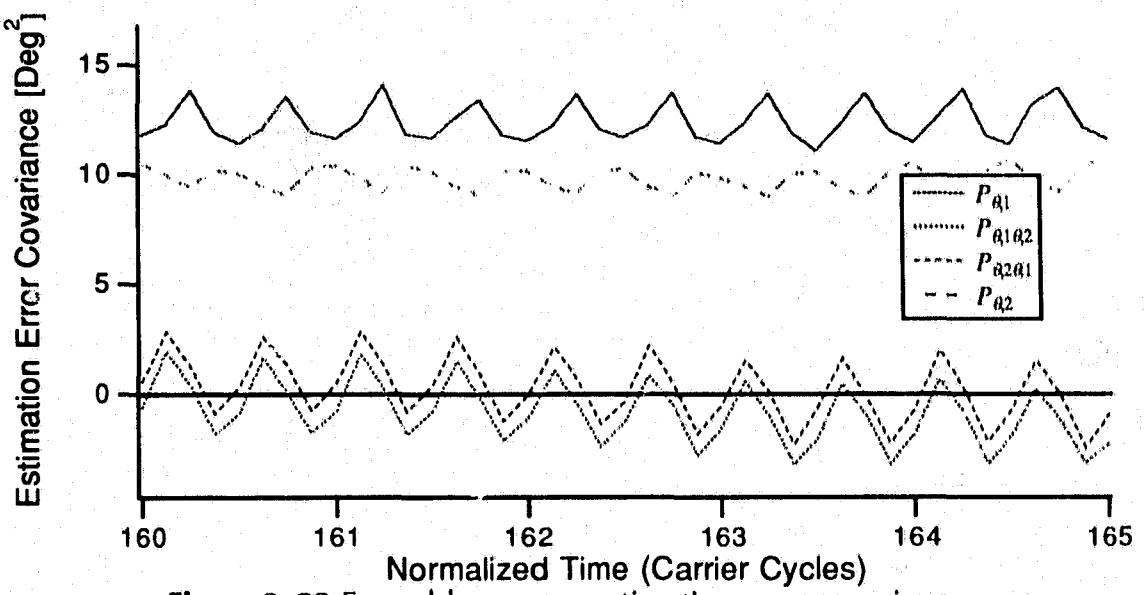

Figure 3–23 Ensemble average estimation error covariance.

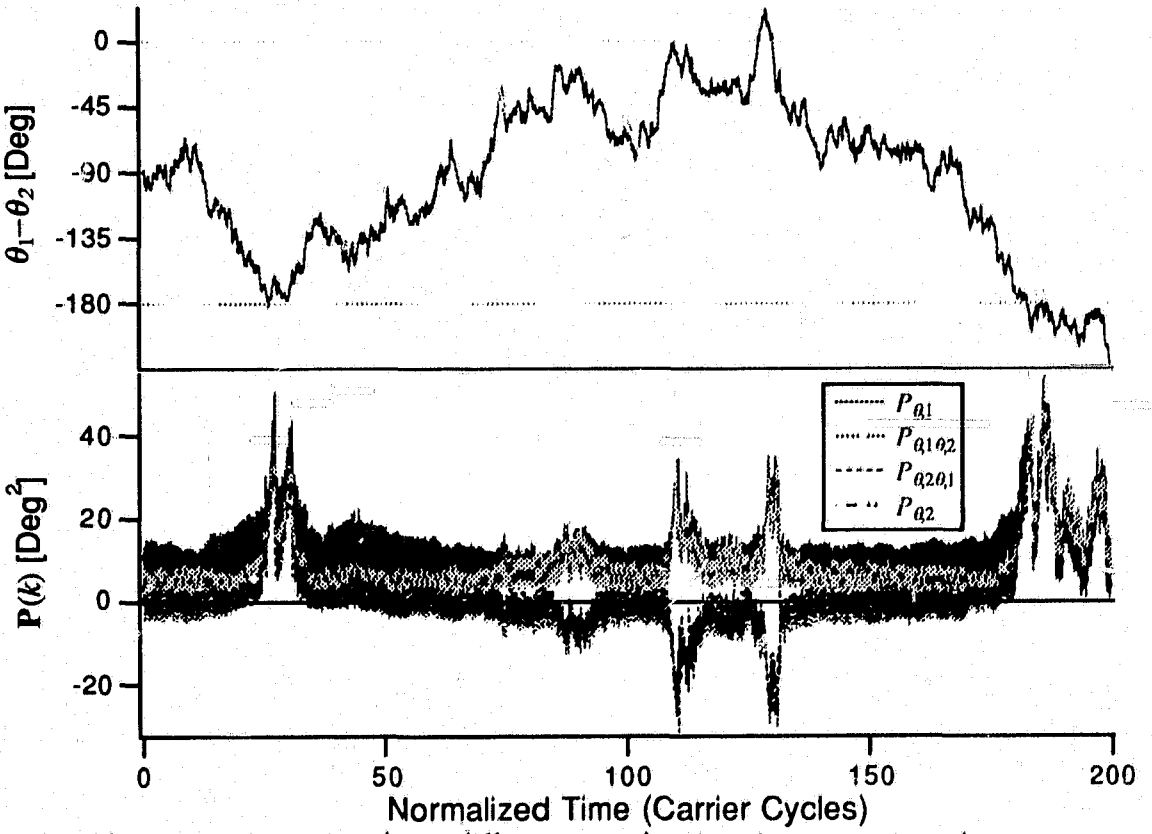

Figure 3–24 Carrier phase difference and estimation error covariances.

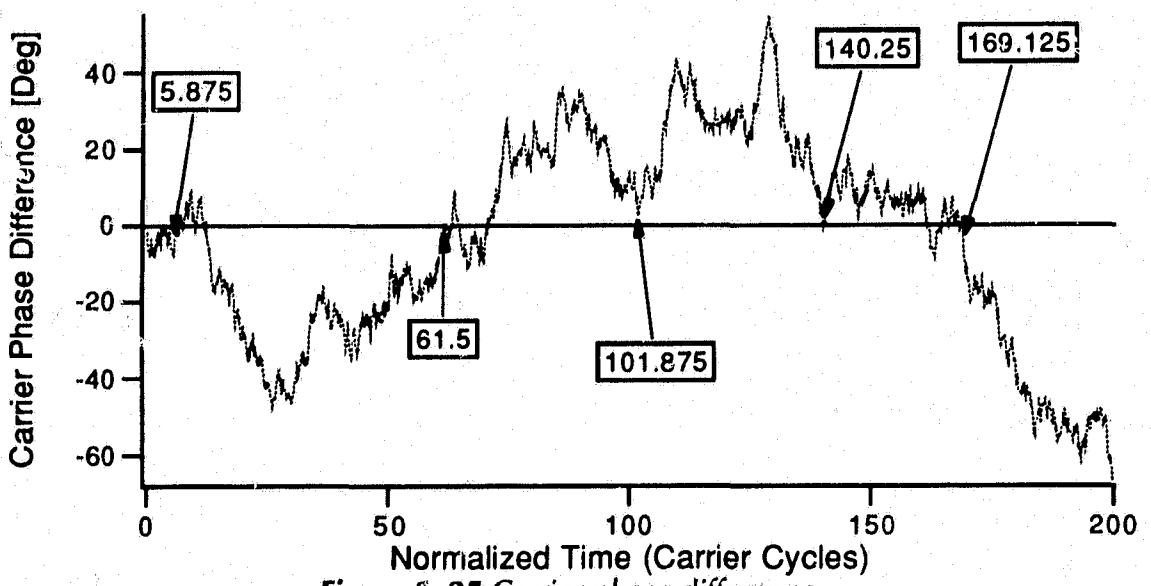

Figure 3–25 Carrier phase difference.

Carriers Nominally in Phase

As shown above when the carriers are not in phase the EKF is able to accurately track the two sources. However the situation is quite different when the carriers are in phase (or nearly so) and warrants additional investigation. The same simulations as above are carried out for the two sources nearly in phase. Since the carrier phases are random processes, it is not possible to maintain the in-phase condition. However the time over which the carriers are in phase may be increased by reducing the bandwidths of the PM sources and initializing the processes nearly in-phase (see Fig. 3–25 where $k_p = 0.5$ and where $\alpha_1 = 2\alpha_2$). Here there are four intervals during which the carriers are nearly in phase. Since only tracking behavior is presently under study, the processes cannot be started exactly in-phase because the EKF is not able to acquire (initially separate) them. Acquisition behavior is studied in a subsequent chapter.

As shown in Fig 3–26 the EKF is able to accurately track the two phase processes some of the time, initially and during the interval 100–160. Looking at the time intervals starting at 6 and again at 160 it may be seen that the phases are no longer being accurately tracked. This

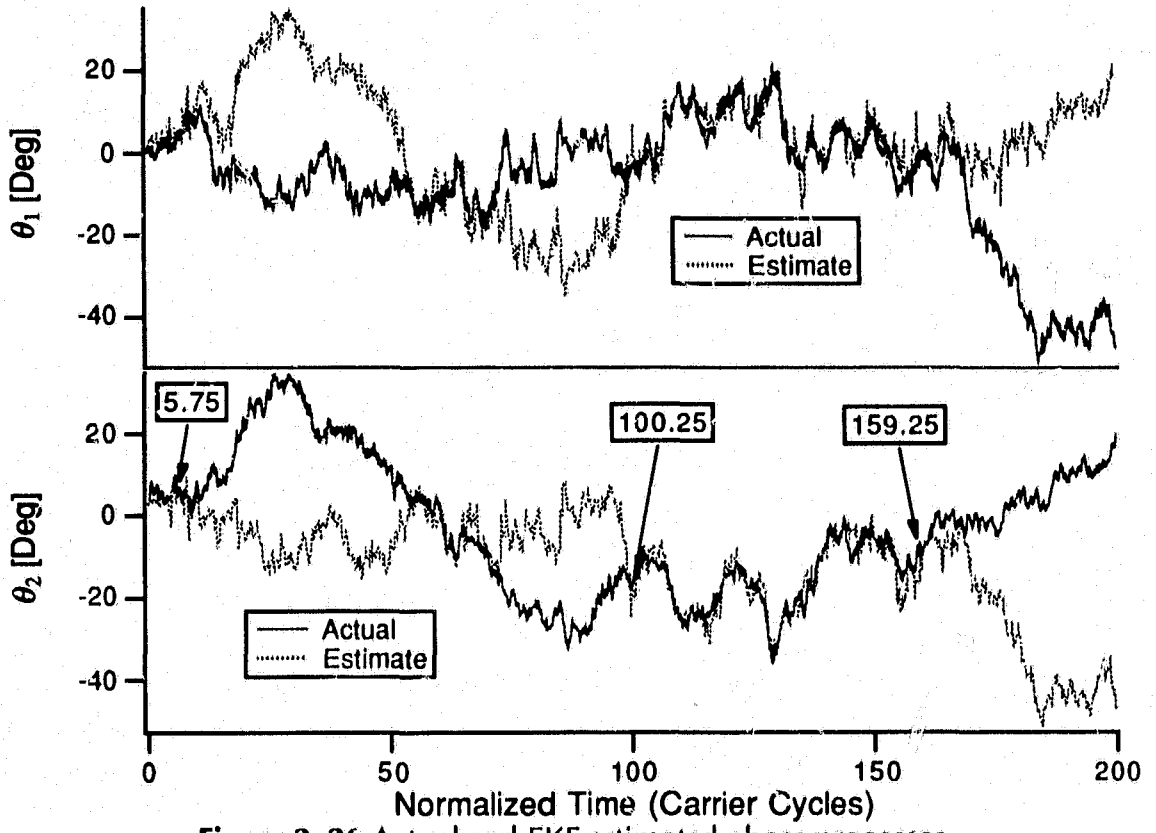

Figure 3–26 Actual and EKF estimated phase processes.

corresponds to intervals where the carriers are nearly in-phase in Fig. 3–25. During the intervals 6–100 and 160–200 the phases are not separated even though the carriers are not in phase. This is because during the previous periods of low observability 0–6 and 140–170 the EKF "lost track" of the phases. Interestingly enough, when comparing θ_1 and θ_2 in Fig 3–26 it is evident that during the intervals 6–100 and 160–200 the phase estimates have been "flipped"; that is $\hat{\theta}_2 \approx \theta_1$ and $\hat{\theta}_1 \approx \theta_2$. During the in-phase condition the phases are not locked so once the carriers move out of phase the phases each reacquired by the EKF. If $\hat{\theta}_2 \approx \theta_1$ at the time of reacquisition, then the EKF continues tracking that phase process which may be seen by examination of the squared-error in the phase estimation shown in Fig. 3–27.

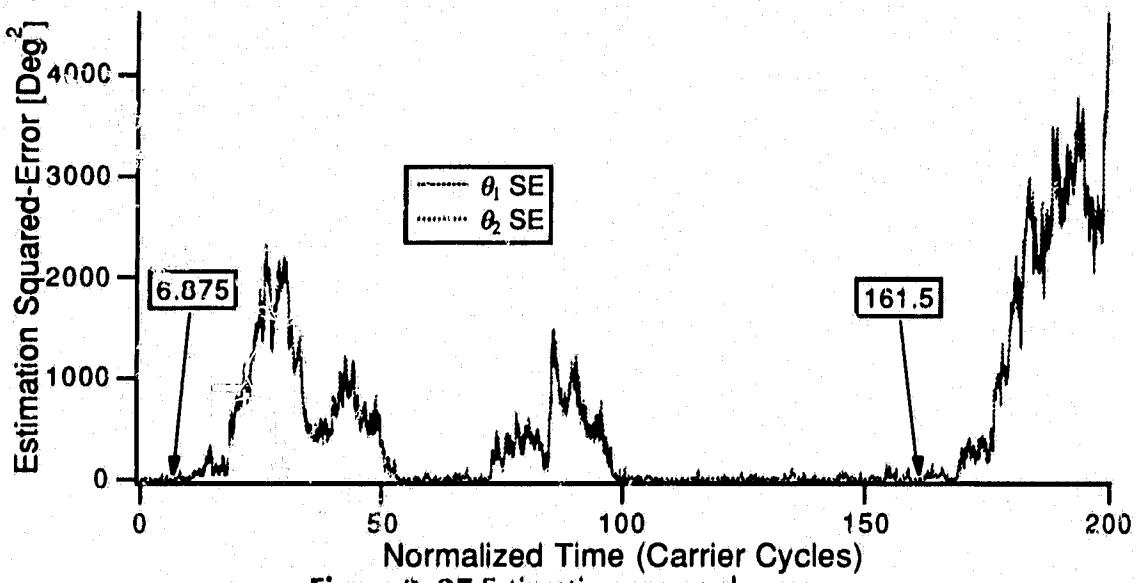

Figure 3–27 Estimation squared-error.

The periods of low observability are quite evident when looking at the estimation error covariance. Fig. 3–28 shows both the auto and cross-covariance terms, the insets are during periods of high observability when the carriers are not in phase. When the carriers are nearly in-phase both auto and cross covariance terms increase substantially which has the effect of increasing the Kalman gain during these intervals. This increase in the Kalman gain effectively increases the closed-loop bandwidth of the phase-locked loop which increases the acquisition capability of the loop. The increase in the cross-covariance terms reflects the apparent increase in the state coupling; since the two independent phase processes cannot be readily observed, they essentially couple to form one process.

Sensitivity to Carrier Phase Difference

To further link observability and separability, the phase estimation error covariance as a function of nominal carrier phase difference is presented. Here again the phase sensitivity has been reduced to $k_p = 0.1$ to maintain nominally constant carrier phase difference. However, as shown in Fig. 3–29, as time progresses, the variance of the phase difference increases. This variance manifests itself by "spreading" the actual phase difference around the desired nomi-

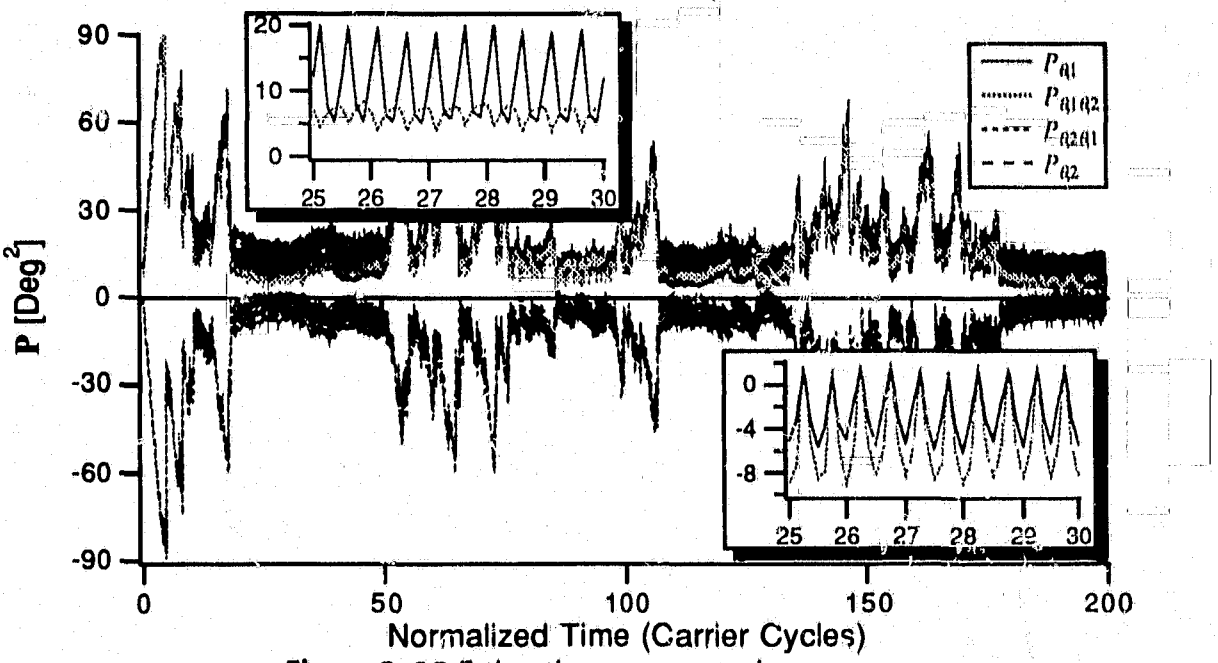

Figure 3–28 Estimation error covariances.

nal phase difference and is thus why the MSE near in-phase case gradually increases from the out-of-phase case. Figs. 3–29 and 3–30 are the results of 100 separate runs.

In the previous section we observed that when two PM sources are in-phase (or nearly so), the EKF may flip the phase estimates. Thus, although the EKF is tracking to two phases, it is not tracking them in the appropriate order. This results in high MSEs even though the EKF is operating "properly." As shown previously, the error covariance is "immune" to this state flipping.

In order to study the EKF tracking accuracy as a function of relative carrier phase difference, an ensemble set of simulations are required for each phase difference $\theta_2 - \theta_1$. For this study, we do not want the state estimate flipping to inflate our measure of EKF tracking error. That is to say for the purpose of this study, we are only concerned if the EKF is tracking the phases at all, the order of the states is unimportant. Therefore instead of using MSE as a metric, the error covariance will be used. This is also backed by Polk [29].

> "...the effectiveness of the DPLL to lock and track depends on the prior phase estimate (that is, the estimate at stage k based on data to stage $k-1$) rather than the

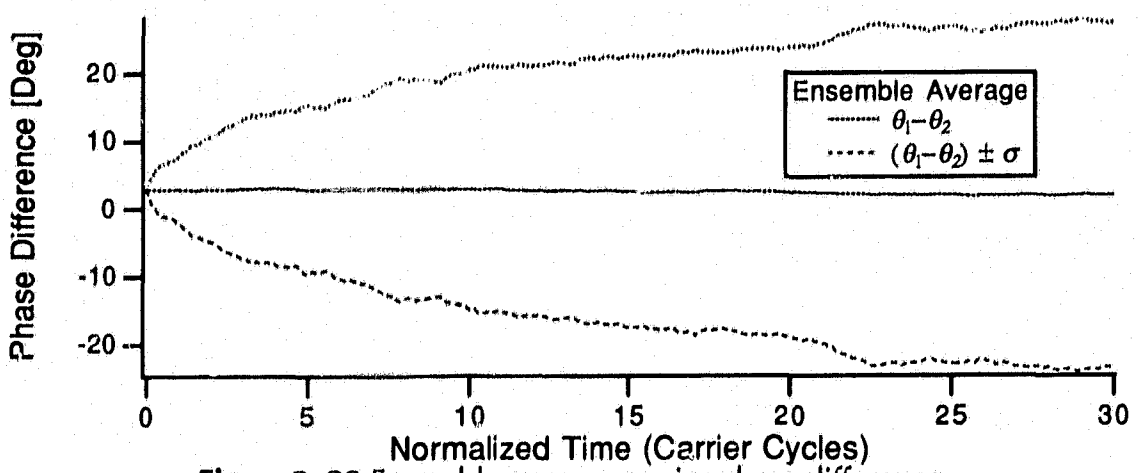

Figure 3–29 Ensemble average carrier phase difference.

phase estimate. Thus, the prior phase error variance should be used to measure the DPLL performance."

Fig. 3–30 shows the prior estimation error covariances $\mathbf{P}_{\theta,1}(k \mid k-1)$ and $\mathbf{P}_{\theta,2}(k \mid k-1)$ over the 360° phase difference range. For each nominal phase difference, the covariances have been normalized by the sample state covariances and are the ensemble average of the steady-state time averaged covariance. The tracking error increases when the states are not observable.

When the phase estimation error covariance, normalized by the sample state covariance (see Fig. 3–30), is compared with the eigenvalues of the observability Gramian (see Fig. 3–19), it is evident that observability and separability are closely related. When the observability Gramian is ill conditioned, the EKF is not able to separate the two carriers as evidenced by the increase in error covariance. This is further exasperated when the phase processes have equal bandwidths ($\alpha_1 = \alpha_2$). The apparent $-10°$ offset in maximum error covariance and 0°, 180°, and 360° is due to the $\pi/32$ radian initial phase offset required to allow the EKF to initially separate (or acquire) the two sources. At this stage only tracking behavior is being examined; acquisition is deferred to a later chapter.

The difference in the error covariance between the two sources is nominal except for the case of θ_2 where the normalized error covariance increases as α_1/α_2 increases. This is due to

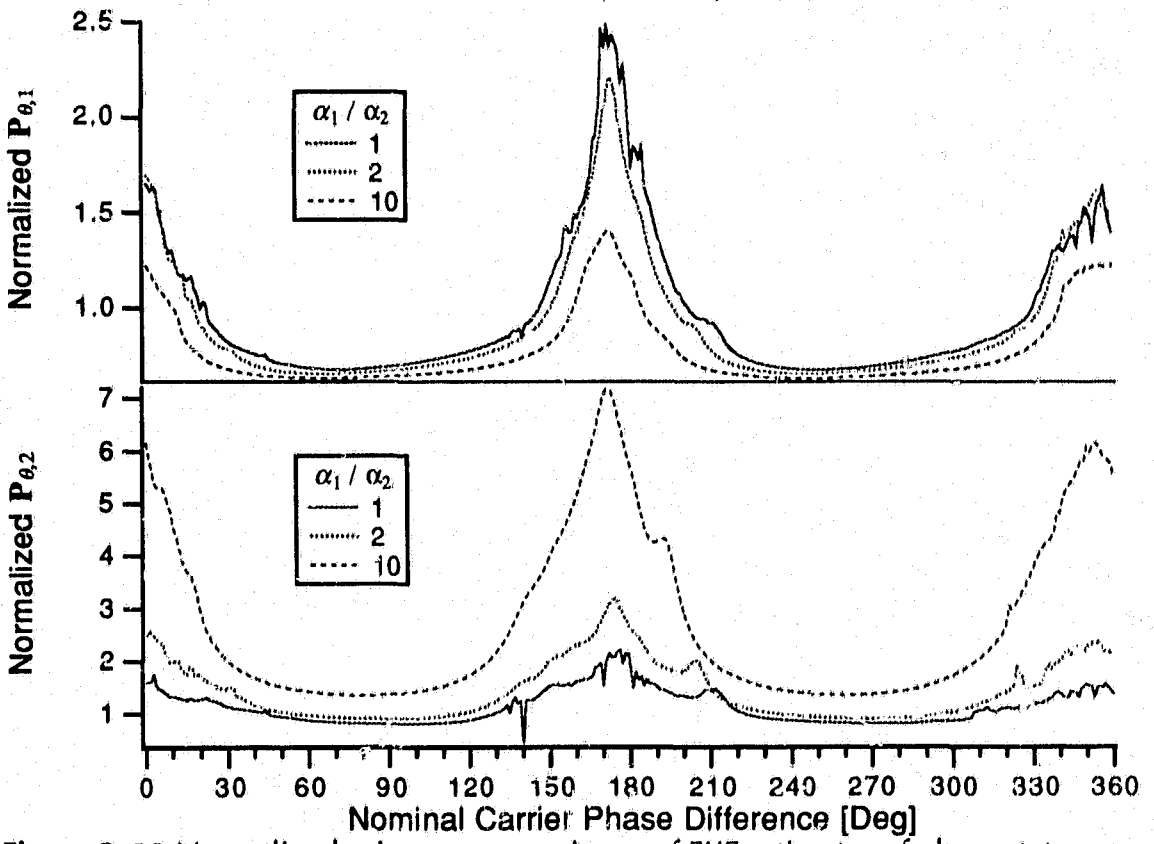

Figure 3–30 Normalized prior error covariance of EKF estimates of phase states as a function of carrier phase difference.

the reduced sample state covariance as α_2 decreases. As shown in (3.5) the state covariance is unity, however the sample state covariance may not be since (3.5) assumes an infinite number of samples. As α decreases, energy is shifted from higher to lower frequencies and thus longer sample records are required to realize this low-frequency energy. If the error covariances are not normalized, there is no difference in the error covariances.

Sensitivity to Carrier Power

All of the above simulation studies assume equal carrier amplitude. This will rarely be the case in practice. Thus the EKF's ability to separate carriers of differing power warrants study.

Fig. 3–31 shows the prior estimation error covariances $\mathbf{P}_{\theta,1}(k \mid k-1)$ and $\mathbf{P}_{\theta,2}(k \mid k-1)$ over a 40 dB range in relative carrier power. For each amplitude ratio, the covariances have

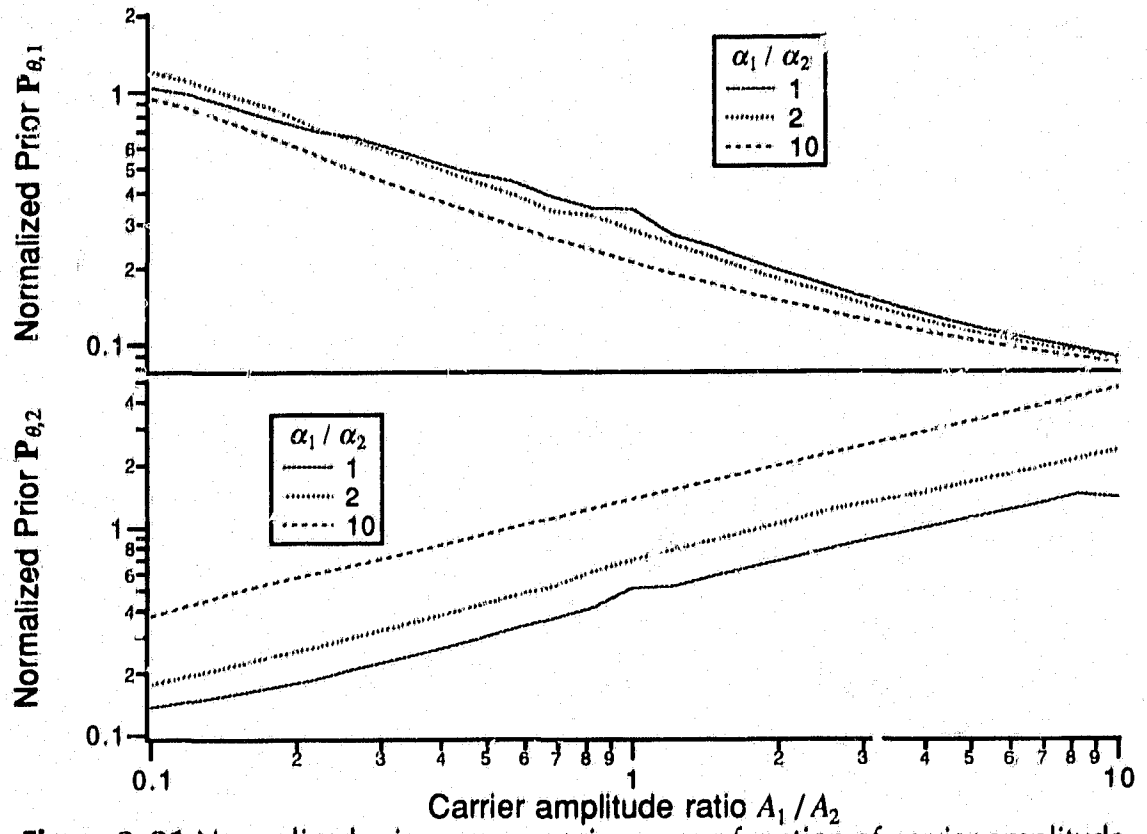

Figure 3–31 Normalized prior error covariance as a function of carrier amplitude ratio.

been normalized by the sample state covariances and are the ensemble average of the steady-state time averaged covariance. The covariances show that the tracking error increases with the increasing power of the "interfering" carrier. This agrees with the corresponding plot of the observability Gramian of Fig. 3–20. Thus $\mathbf{P}_{\theta,1}(k \mid k-1)$ is higher when $A_2 > A_1$ and vice versa. Also at the bandwidth of the interferer is reduced, the phase of the desired signal may be better tracked as shown by smaller $\mathbf{P}_{\theta,1}(k \mid k-1)$ when $\alpha_1 = 10\alpha_2$ and conversely for θ_2.

3.3.6. Two Source Amplitude and Phase Estimation

Next the observability and estimation of two carriers and their respective amplitudes is examined. This is the culmination of the proceeding sections. From (2.150) the state equation for two PM sources is

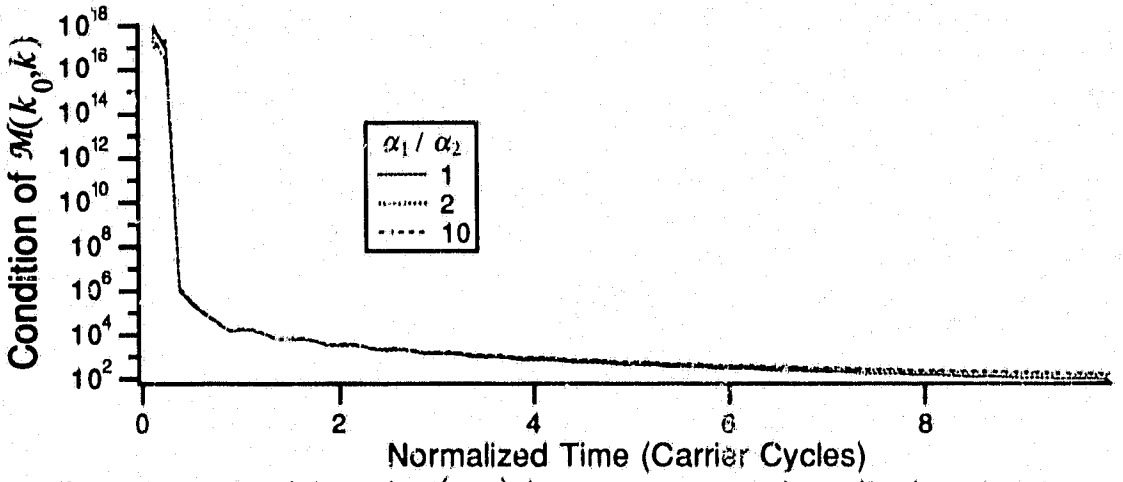

Figure 3–32 Condition of $\mathcal{M}(k_0,k)$ for two sources and amplitude estimation.

$$\begin{bmatrix} \theta_1(k+1) \\ A_1(k+1) \\ \theta_2(k+1) \\ A_2(k+1) \end{bmatrix} = \left[\begin{array}{cc:cc} \phi_{\theta,1} & 0 & \multicolumn{2}{c}{\multirow{2}{*}{$\mathbf{0}$}} \\ 0 & 1 & & \\ \hdashline \multicolumn{2}{c:}{\multirow{2}{*}{$\mathbf{0}$}} & \phi_{\theta,2} & 0 \\ & & 0 & 1 \end{array}\right] \begin{bmatrix} \theta_1(k) \\ A_1(k) \\ \theta_2(k) \\ A_2(k) \end{bmatrix} + \left[\begin{array}{cc:cc} \gamma_{\theta,1} & 0 & \multicolumn{2}{c}{\multirow{2}{*}{$\mathbf{0}$}} \\ 0 & 0 & & \\ \hdashline \multicolumn{2}{c:}{\multirow{2}{*}{$\mathbf{0}$}} & \gamma_{\theta,2} & 0 \\ & & 0 & 0 \end{array}\right] \begin{bmatrix} w_{\theta,1}(k) \\ 0 \\ w_{\theta,2}(k) \\ 0 \end{bmatrix}, \tag{3.65}$$

at the measurement equation is

$$z(k) = \sqrt{2}\left[A_1(k)\sin\left(\omega_c k T_s + \theta_1(k)\right) + A_2(k)\sin\left(\omega_c k T_s + \theta_2(k)\right)\right] + v(k). \tag{3.66}$$

The measurement estimation error is described by

$$\tilde{z}(k) = \mathbf{H}\left(\hat{\mathbf{x}}(k),k\right)\tilde{\mathbf{x}}(k) + v(k), \tag{3.67}$$

where the estimation error observation matrix is

$$\mathbf{H}\left(\hat{\mathbf{x}}(k),k\right) = \sqrt{2}\begin{bmatrix} \hat{A}_1(k)\cos\left(\hat{\Theta}_1(k)\right) \\ \sin\left(\hat{\Theta}_1(k)\right) \\ \hat{A}_2(k)\cos\left(\hat{\Theta}_2(k)\right) \\ \sin\left(\hat{\Theta}_2(k)\right) \end{bmatrix}^{\mathrm{T}}, \tag{3.68}$$

and the state estimation error vector is

$$\tilde{\mathbf{x}}(k) = \begin{bmatrix} \tilde{\theta}_1(k) & \tilde{A}_1(k) & \tilde{\theta}_2(k) & \tilde{A}_2(k) \end{bmatrix}^{\mathrm{T}}. \tag{3.69}$$

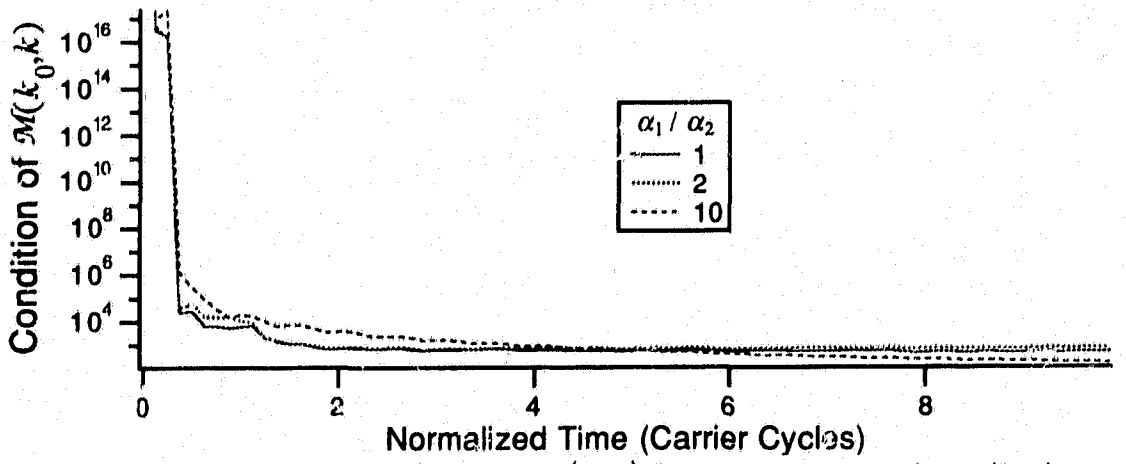

Figure 3–33 Sample condition of $\mathcal{M}(k_0,k)$ for two sources and amplitude estimation.

Since it has been shown in the previous section that carriers in-phase cannot be separated, we will examine the case where the carriers are in quadrature. Analytical evaluation of the eigenvalues of the four sample observability Gramian (3.28) was not carried out because of the complexity (even mathematical computer applications Maple[5] and Mathematica[6] were not able to solve for the eigenvalues). Therefore the condition of the observability Gramian was numerically evaluated for the carriers maintained in quadrature and of equal amplitude. Fig. 3–32 is the case where the phase processes are tones and the phase difference is maintained at approximately 90°. Fig. 3–33 uses the phase processes of (3.65) which results in a nominal 90° phase difference. Although the condition of the matrix is higher than in the previous sections, the condition of $\mathcal{M}(k_0,k)$ does drastically improve after four samples and indicates that the states do become observable.

In both Fig. 3–32 and Fig. 3–33 the condition of the observability Gramian is nearly independent of the relative the bandwidths of the two message processes. In Fig. 3–33 the convergence of the case where $\alpha_1 = 10\alpha_2$ is slower than the other two cases. This is because the

---

[5]Maple® is a registered trademark of Waterloo Maple Software.

[6]Mathematica™ is a trademark of Wolfram Research Inc.

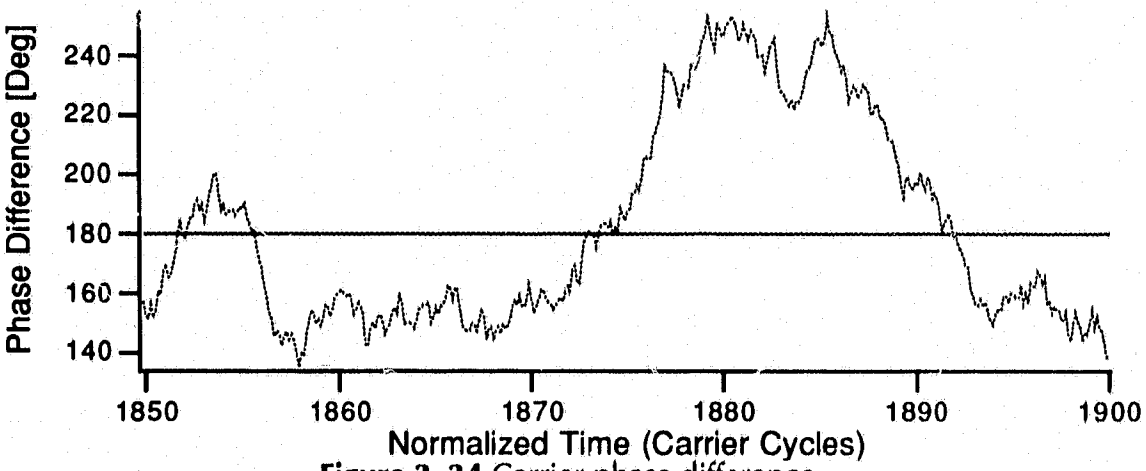

Figure 3–34 Carrier phase difference.

phase difference between the two carriers is slower to change since the frequency of the tones are a function of α.

Next the ability of the EKF to separately track the two sources is examined for $A_1 = A_2$ and $\alpha_1 = 2\alpha_2$. The convergence Kalman gain for the amplitude states is substantially slower than that for the phase states (more on this in a later chapter). Therefore the tracking simulations presented below are after the EKF has run for a long period of time. This is to help separate the transient (acquisition) behavior from that of the steady-state (tracking).

The carrier phase difference for the time interval 1850–1900 is shown in Fig. 3–34. During this interval the carrier are in anti-phase four times. As shown in Fig. 3–35 both phases are successfully tracked with an increase in tracking error during the times where the carriers are in anti-phase. This agrees with the results of Section 3.3.5 where the carrier amplitudes are known.

Fig. 3–36 shows the amplitude estimation. Here $A_1 = A_2$ and the estimates are nearly identical with a scant 3% bias. More interesting is that the amplitude estimates seem unaffected by the periods of low observability when the carriers are in anti-phase. This is due to reduction of the Kalman gain by the near-zero steady-state value of the amplitude error covariances. The estimation error covariance matrix contains 16 elements of greatly differing

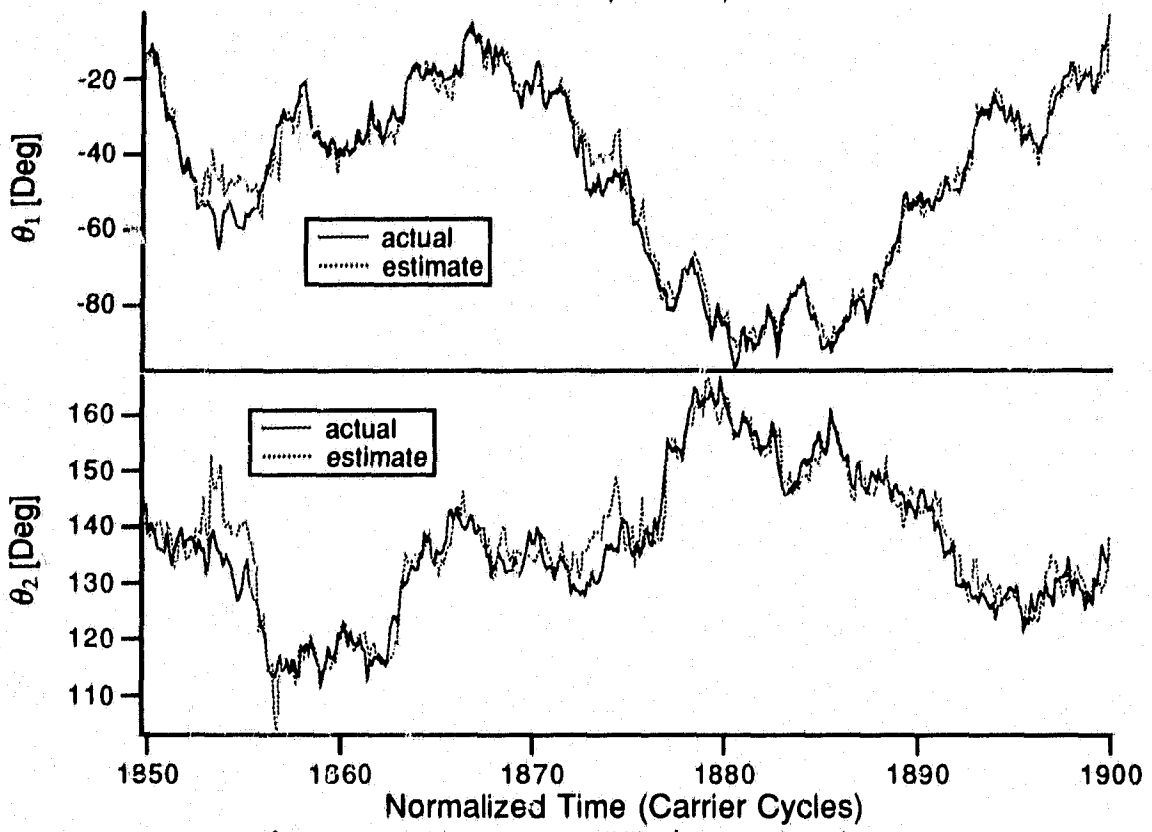

Figure 3–35 Two source EKF phase estimation.

magnitudes. In Fig. 3–37 the elements which are plotted as a function of time are broken into three groups: those related to the phase state, those related to the amplitude state, and those cross-covariance elements related to both phase and amplitude. As in the case of Section 3.3.5, the phase covariances increase during the periods of low observability. However the amplitude covariance terms are nearly zero and are not effected by these periods of low observability. As can be seen in plot $\mathbf{P}_{AA}$ the error covariances are on the order of 10^{-5} and slowly decreasing. The cross-covariance terms are also quite small, order of 10^{-4}.

When these reduced covariance terms are viewed in the context of the EKF realization of Fig. 2–22, it is clear that much the inter-state coupling is effectively zero in the steady-state. Thus only four of the 16 elements of the error covariance matrix actually contribute to the tracking behavior where these four are all related to phase tracking. This is intuitively satisfy-

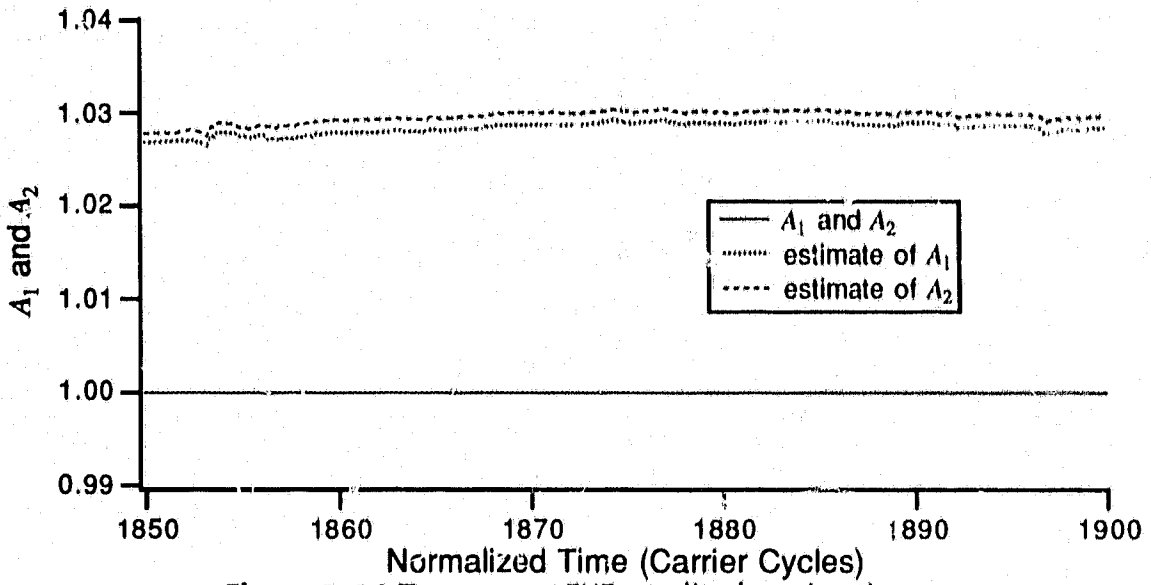

Figure 3–36 Two source EKF amplitude estimation.

ing since the amplitudes do not changed with time and thus, once they have been accurately estimated, need not be updated. Only the phases need to be tracked.

Even when $\alpha_1 = \alpha_2$ the phases and amplitudes are accurately tracked. During the periods of low observability the phase estimate "flipping" described in Section 3.3.5 may occur but since the Kalman gains for the amplitude states are near zero, the amplitude estimated remain unaffected.

To examine the role that relative carrier power plays in state observability, condition of the observability Gramian as a function of relative carrier power is shown in Fig. 3–38. This simulation consisted of 100 separate runs of the ensemble average is shown. To try to minimize the intervals of low observability the phase gain was reduced to $k_p = 0.5$. It is evident that as one carrier's power dominates the second, the state observability of the lower power signal is diminished. In the limiting case where one of the carriers has zero power, its states are certainly not observable.

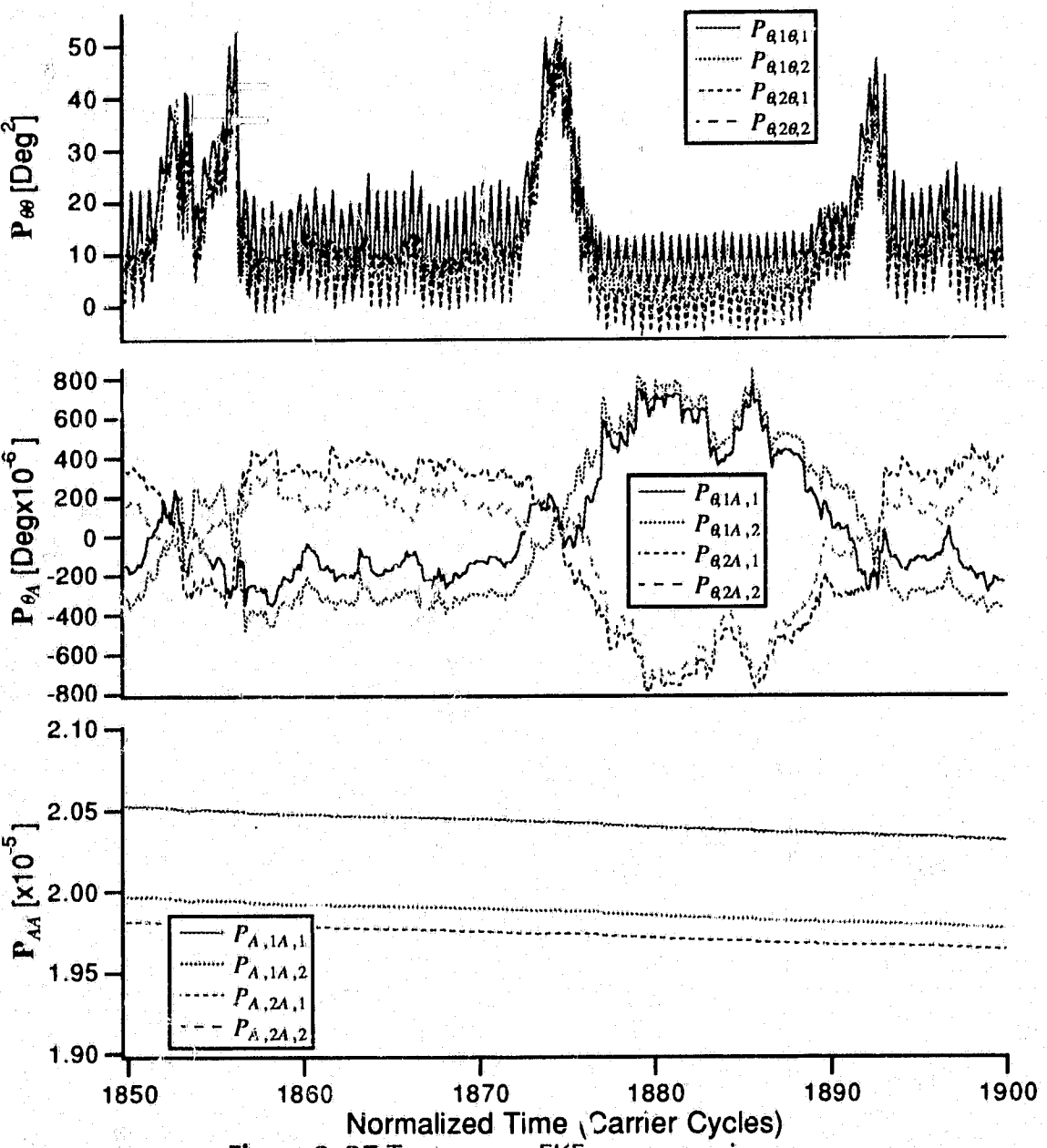

Figure 3–37 Two source EKF error covariance.

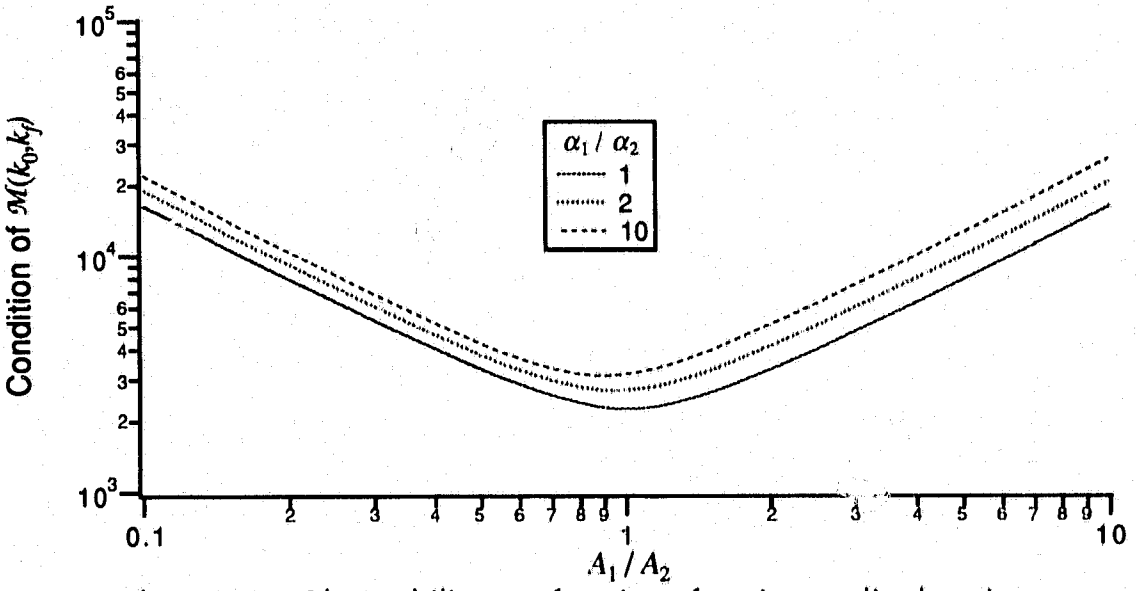

Figure 3–38 Observability as a function of carrier amplitude ratio.

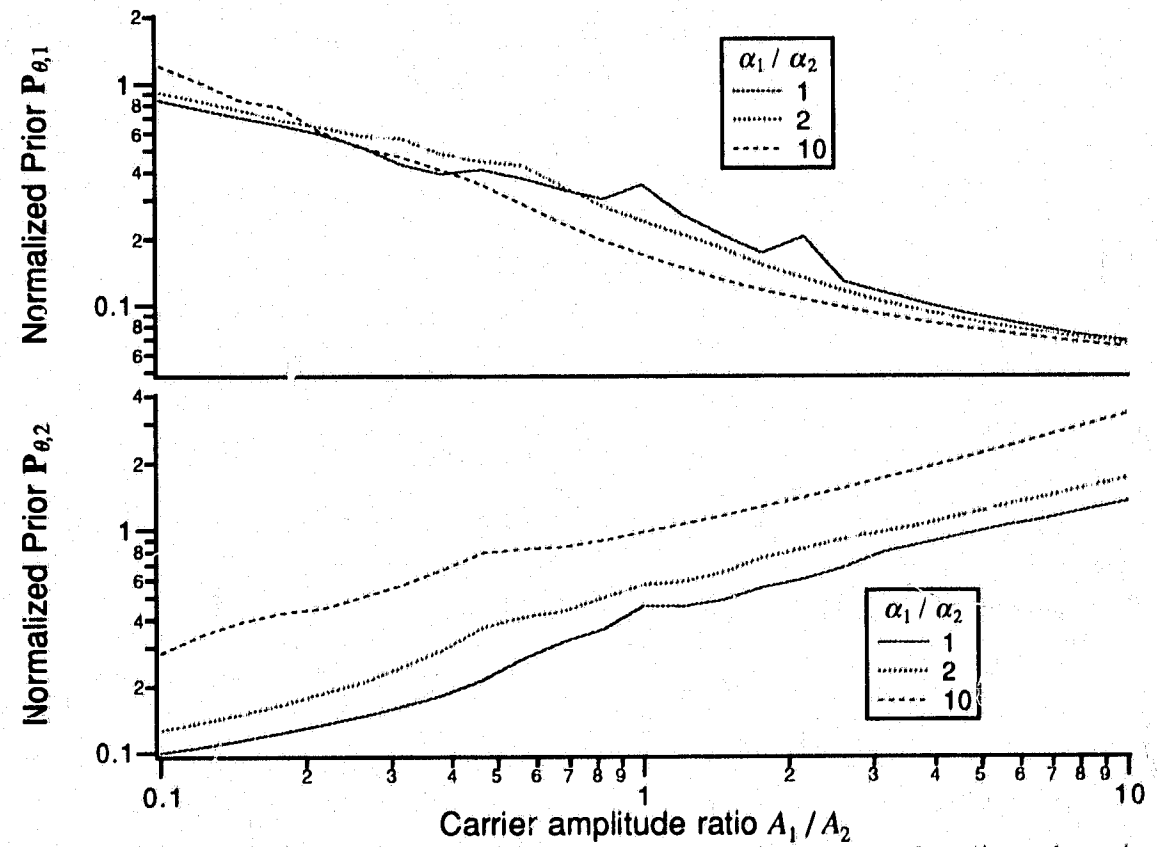

Figure 3–39 Normalized phase estimation error covariance as a function of carrier amplitude ratio.

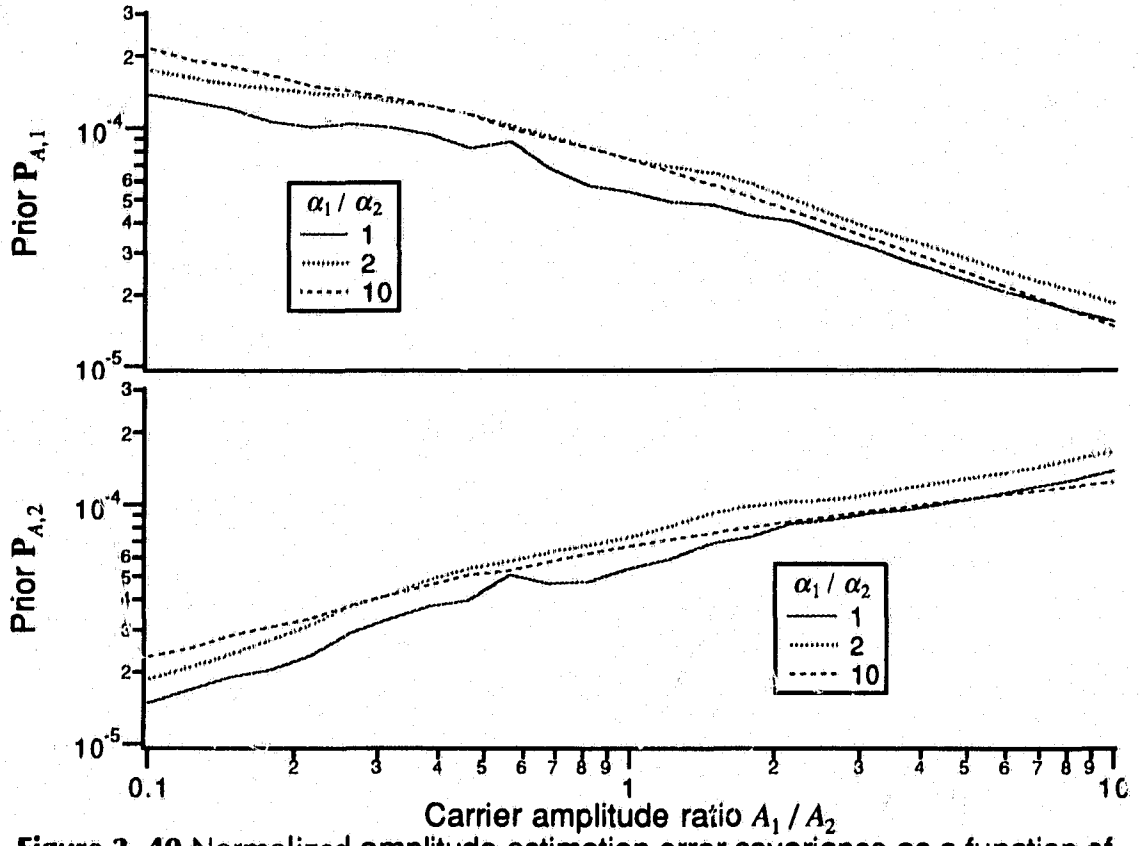

Figure 3–40 Normalized amplitude estimation error covariance as a function of carrier amplitude ratio.

The effect of differing carrier power levels on signal separability may also be studied by examining how accurately the EKF can estimate the states. In Figs. 3–39 and 3–40, the prior error covariances of phase process and carrier amplitude estimates for each carrier are shown as the carrier amplitude ratio is varied. The phase estimation error covariances have been normalized by the sample state covariance and the amplitude estimation error covariances have been normalized by the actual amplitude. It is evident that the EKF is able to track the phase processes and maintain an accurate estimate of the carrier amplitudes over a wide range of relative carrier power levels. It is also evident by the increased error covariance that as one carrier dominates the other, the EKF is less able to accurately estimate the states of the lesser powered carrier. This agrees with Fig. 3–38. It should also be pointed out that if one carrier

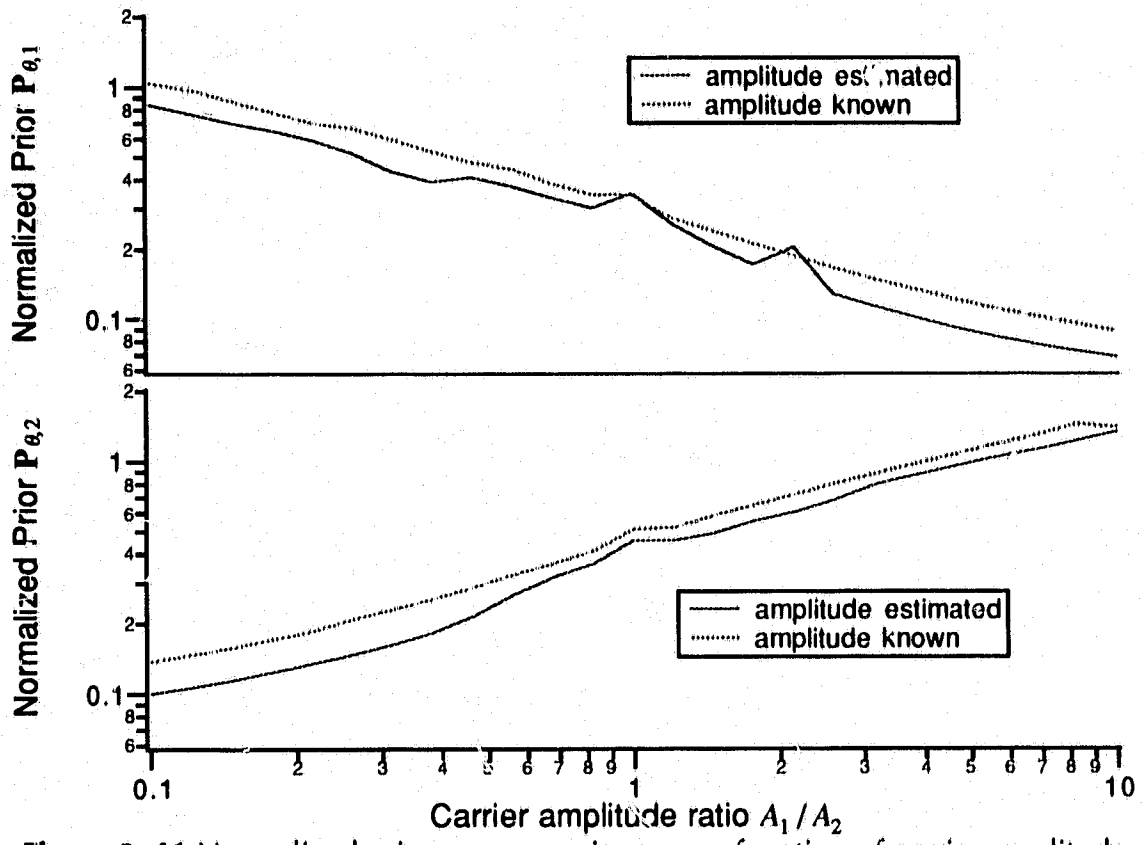

Figure 3–41 Normalized prior error covariance as a function of carrier amplitude ratio.

is at a substantially lower power level than the second, the lower powered signal's contribution to CCI will be substantially reduced.

Fig. 3–41 compares the case where the amplitude is estimated to the case where the amplitude is known (Section 3.3.5). The error covariance is nearly the same for each case with the case where the amplitudes are estimated being slightly less.

3.3.7. Phase, Frequency, and Amplitude Estimation

Finally the two source FM case is examined. This is the scenario which abounds in the literature and will subsequently allow comparisons between the performance of the various estimator structure found therein.

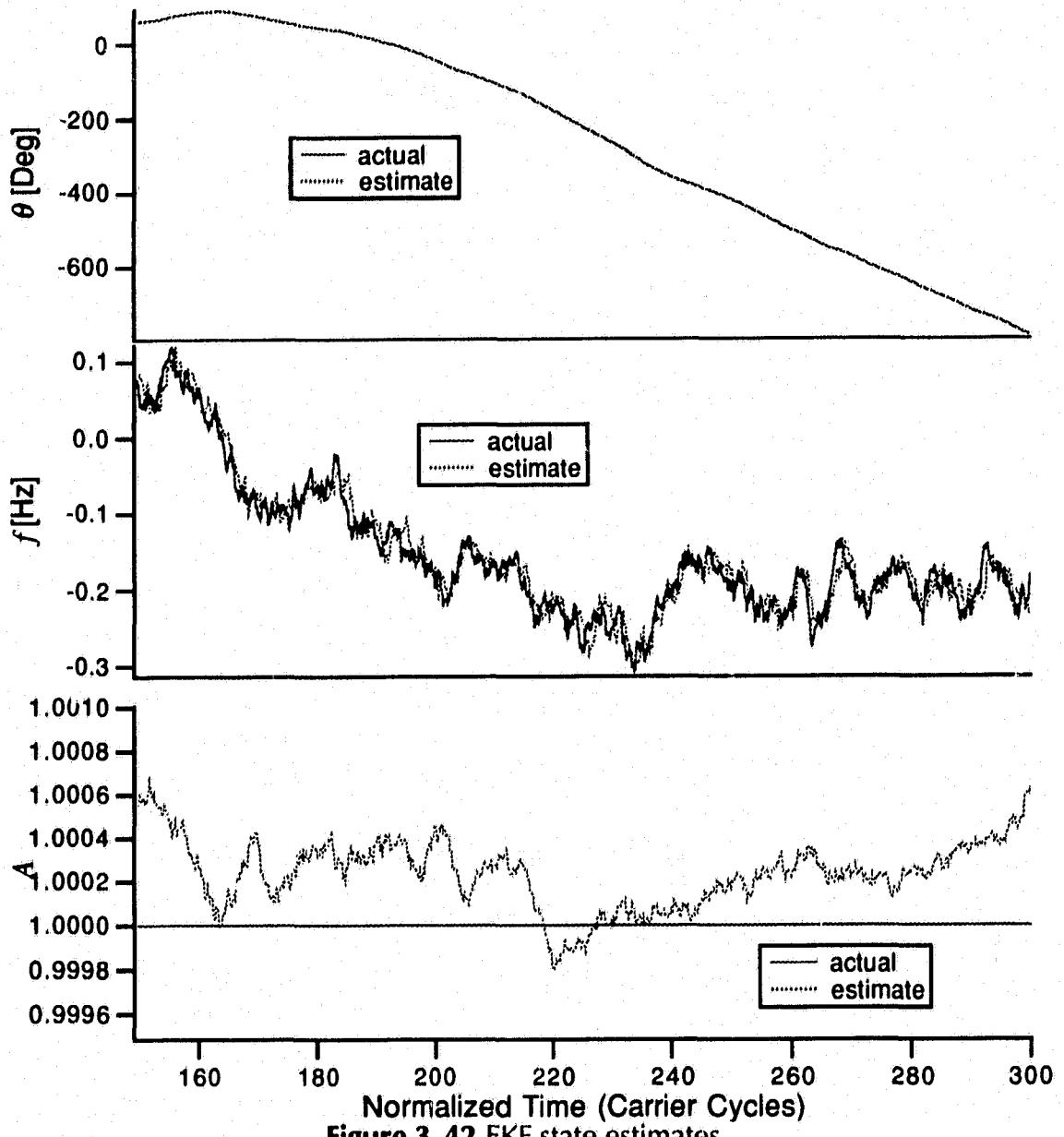

Figure 3–42 EKF state estimates.

Single Source

The state equation for a first-order FM source from (2.159) is

$$\begin{bmatrix} x_\theta(k+1) \\ x_f(k+1) \\ x_A(k+1) \end{bmatrix} = \begin{bmatrix} \theta(k+1) \\ f(k+1) \\ A(k+1) \end{bmatrix} = \left[\begin{array}{cc:c} 1 & \phi_{\theta f} & 0 \\ 0 & \phi_f & 0 \\ \hdashline 0 & 0 & 1 \end{array}\right] \begin{bmatrix} \theta(k) \\ f(k) \\ A(k) \end{bmatrix} + \left[\begin{array}{cc:c} \gamma_\theta & \gamma_{\theta f} & \\ \gamma_{f\theta} & \gamma_f & \mathbf{0} \\ \hdashline & \mathbf{0} & 0 \end{array}\right] \begin{bmatrix} w_\theta(k) \\ w_f(k) \\ \hdashline 0 \end{bmatrix}. \tag{3.70}$$

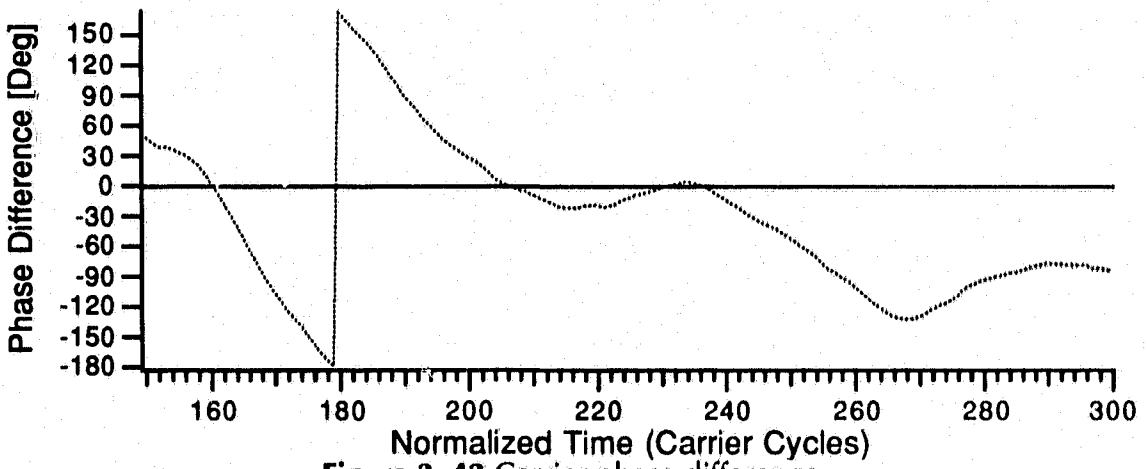

Figure 3–43 Carrier phase difference.

The EKF of Section 2.3.5 is able to accurately track all three states as shown in Fig. 3–42.

The three states result in a 3×3 error covariance matrix. The behavior is much like that in Section 3.3.5 so only the time average of the steady-state **P** is presented (in radians^2)

$$\hat{\bar{\mathbf{P}}} = \begin{bmatrix} 1.5\times10^{-2} & 1.6\times10^{-3} & 3.7\times10^{-9} \\ 1.6\times10^{-3} & 2.4\times10^{-3} & 5.3\times10^{-8} \\ 3.7\times10^{-9} & 5.3\times10^{-8} & 5.9\times10^{-7} \end{bmatrix}, \tag{3.71}$$

which reveals that during tracking only the phase and frequency error auto and cross-covariances contribute to the estimator; the amplitude state estimate is uncoupled.

Two Sources

From (2.181) the state equation describing the two sources is

$$\begin{bmatrix} \theta_1(k+1) \\ f_1(k+1) \\ A_1(k+1) \\ \theta_2(k+1) \\ f_2(k+1) \\ A_2(k+1) \end{bmatrix} = \begin{bmatrix} \Phi_{\theta,1} & 0 & & & & \\ 0 & 1 & 0 & & & \\ & & \Phi_{\theta,2} & 0 & & \\ & 0 & & 0 & 1 & \end{bmatrix} \begin{bmatrix} \theta_1(k) \\ f_1(k) \\ A_1(k) \\ \theta_2(k) \\ f_2(k) \\ A_2(k) \end{bmatrix} + \begin{bmatrix} \Gamma_{\theta,1} & 0 & & & & \\ 0 & 0 & 0 & & & \\ & & \Gamma_{\theta,2} & 0 & & \\ & 0 & & 0 & 0 & \end{bmatrix} \begin{bmatrix} w_{\theta,1}(k) \\ w_{f,1}(k) \\ 0 \\ w_{\theta,2}(k) \\ w_{f,2}(k) \\ 0 \end{bmatrix}. \tag{3.72}$$

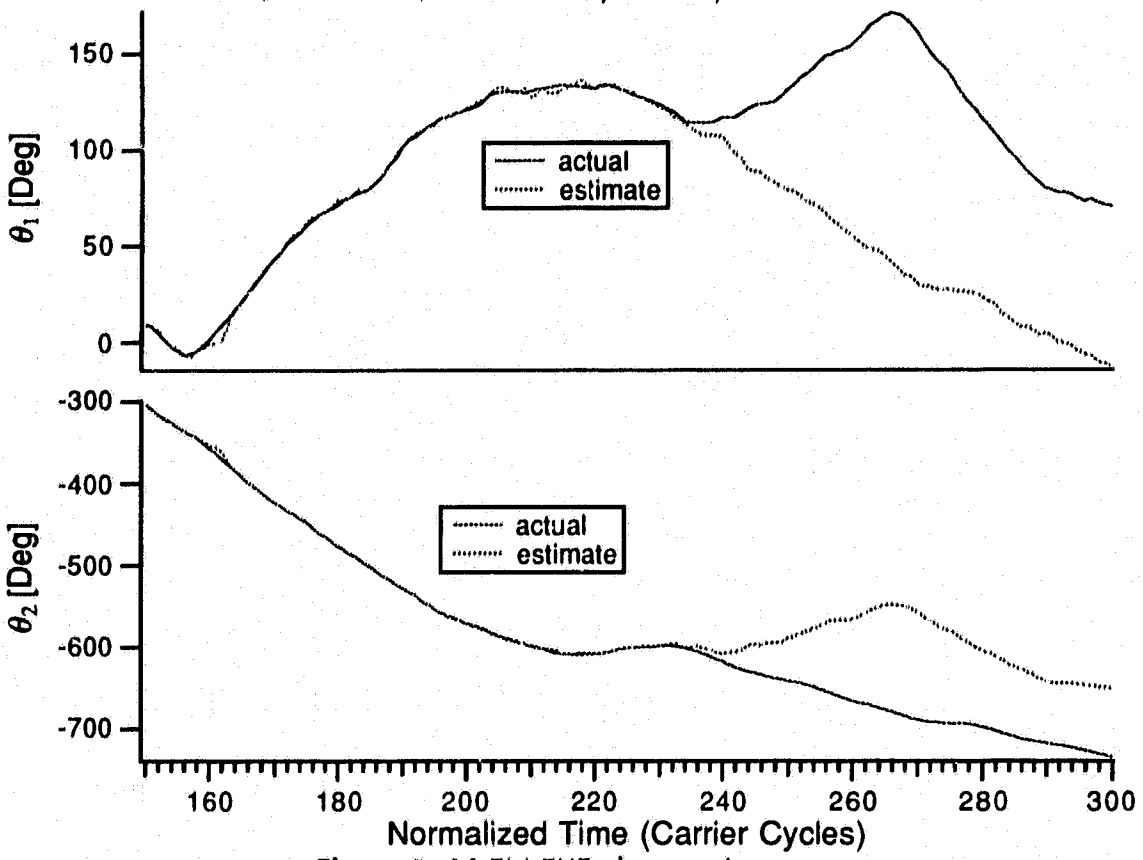

Figure 3–44 FM EKF phase estimates.

The EKF of Section 2.3.5 operates on the sources described by (3.72) where $d_f = 0.1$, $\alpha_1 = 2\alpha_2$, $A_1 = A_2 = 1$, and $\theta_2(0) - \theta_1(0) = 90°$. Of particular interest in the FM case is the relative carrier phase difference. As shown in Fig. 3–43 there is an ever increasing phase difference between the two carriers. When examined modulo-2π, the states repeatedly go through periods of low observability when the carriers are 0° or ±180°. In Fig. 3–43 this happens at times 160, 180, and during 210–240.

In Fig. 3–44 the tracking of the carrier phases is shown. As the carriers approach the anti-phase condition around 160, the tracking error increases. When the carriers again approach the in-phase condition during the 210–240 interval, $\hat{\theta}_1$ and $\hat{\theta}_2$ both lose proper track and eventually the state estimates flip. During these periods the estimate of the frequencies also suffered as evidenced in Fig. 3–45 where the frequency estimates also flip. A relatively small

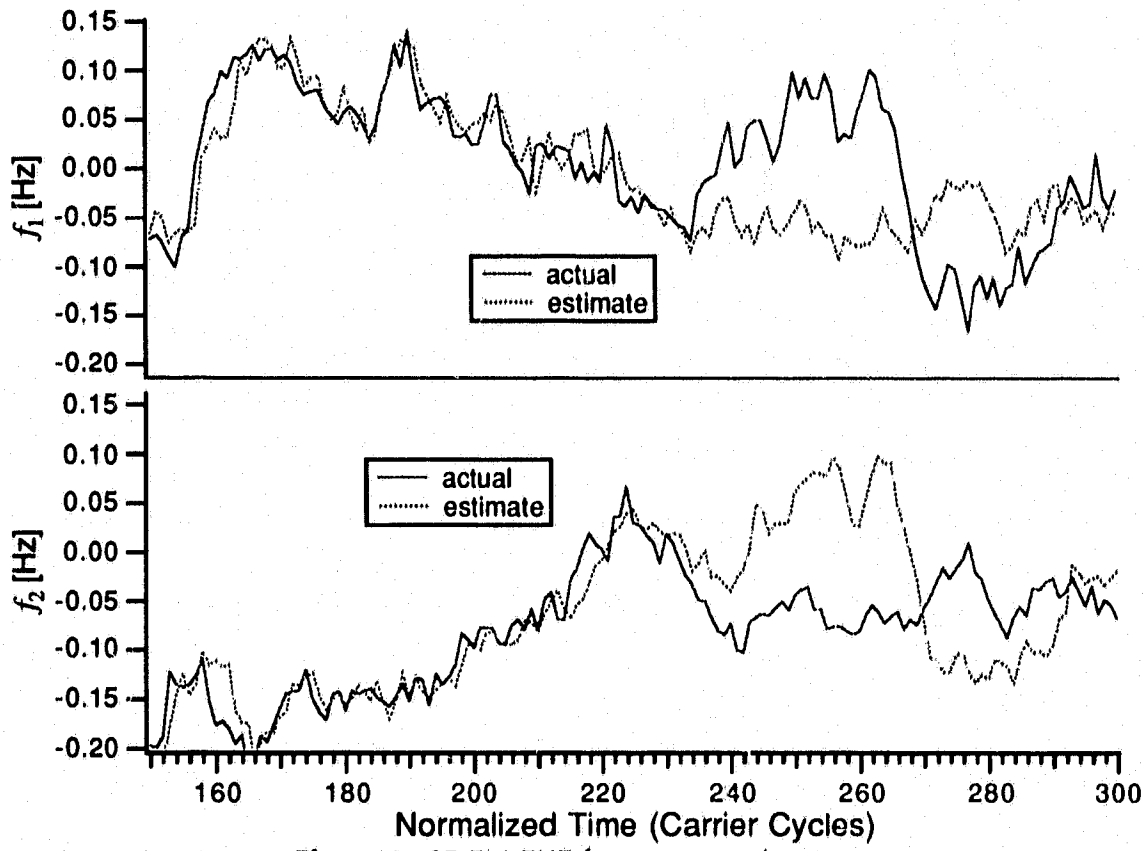

Figure 3–45 FM EKF frequency estimates.

change in the amplitude estimates occurs during the periods of low observability (see Fig. 3–46). There is only a 0.1% change in the amplitude estimates during the anti-phase interval at time 160.

The error covariance matrix is composed of 36 elements so only the time average of the steady-state **P** is presented (in radians^2)

$$\hat{\bar{\mathbf{P}}} = \left[\begin{array}{ccc:ccc} 10^{-3} & 10^{-2} & 10^{-5} & 10^{-3} & 10^{-3} & -10^{-5} \\ 10^{-2} & 10^{-2} & 10^{-5} & 10^{-3} & 10^{-2} & -10^{-6} \\ 10^{-5} & 10^{-5} & 10^{-6} & 10^{-5} & 10^{-6} & -10^{-7} \\ \hdashline 10^{-3} & 10^{-3} & 10^{-5} & 10^{-3} & 10^{-2} & -10^{-5} \\ 10^{-3} & 10^{-2} & 10^{-6} & 10^{-2} & 10^{-2} & -10^{-5} \\ -10^{-5} & -10^{-6} & -10^{-7} & -10^{-5} & -10^{-5} & -10^{-6} \end{array}\right], \tag{3.73}$$

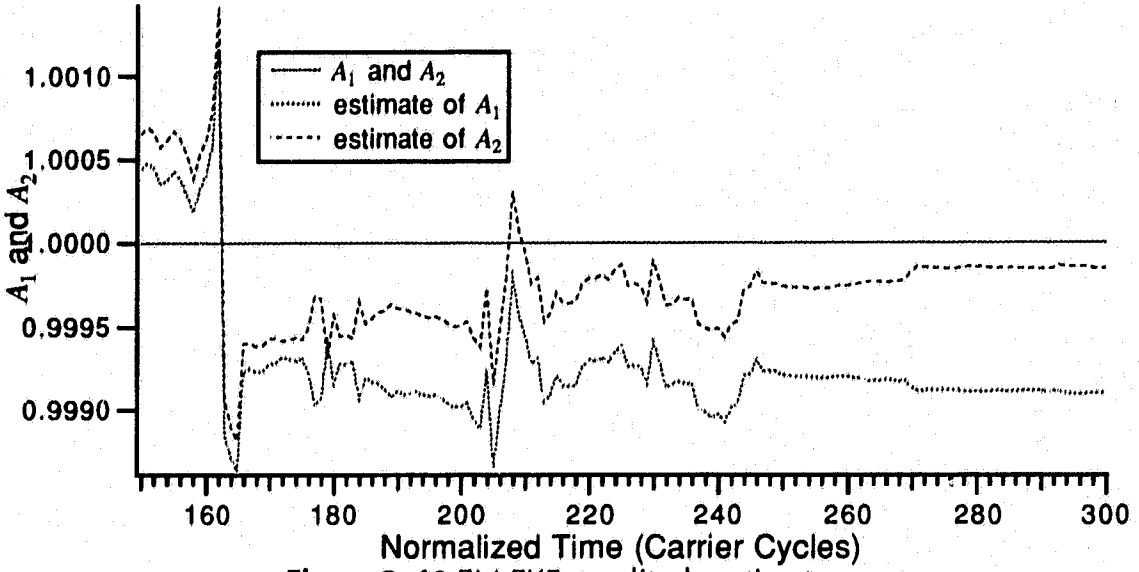

Figure 3–46 FM EKF amplitude estimates.

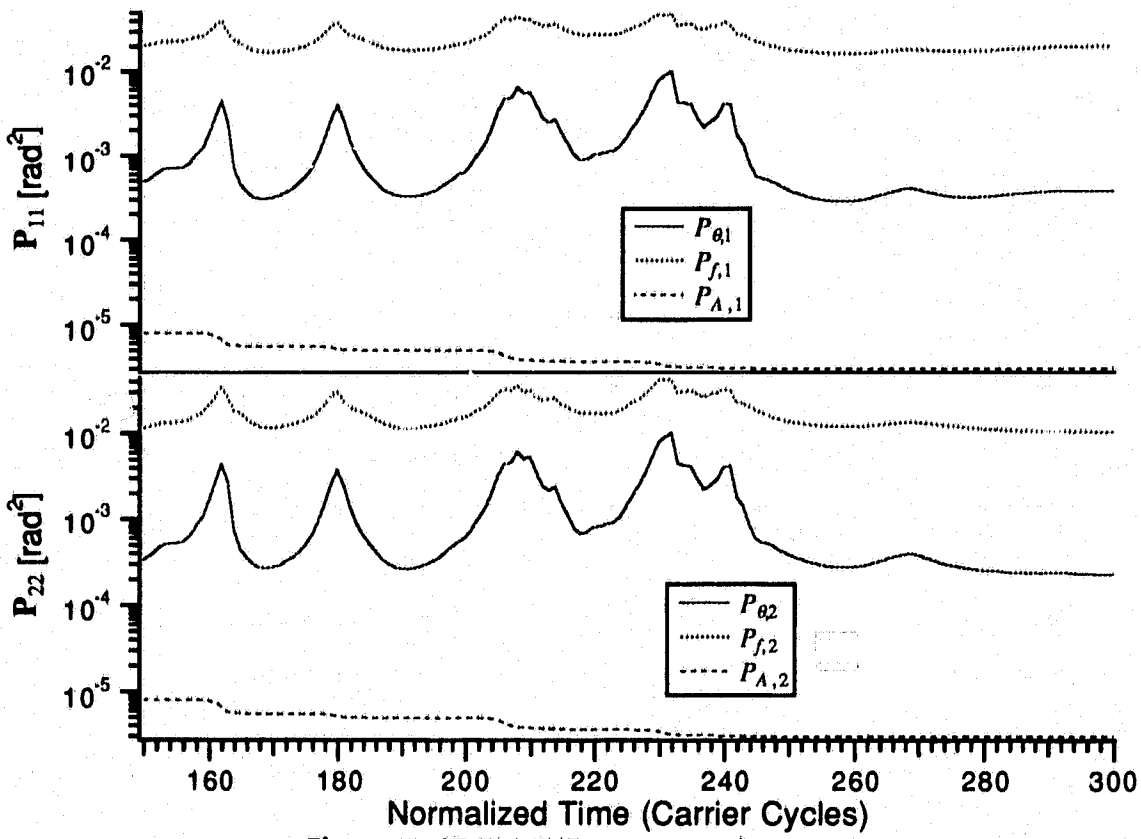

Figure 3–47 FM EKF auto-covariances.

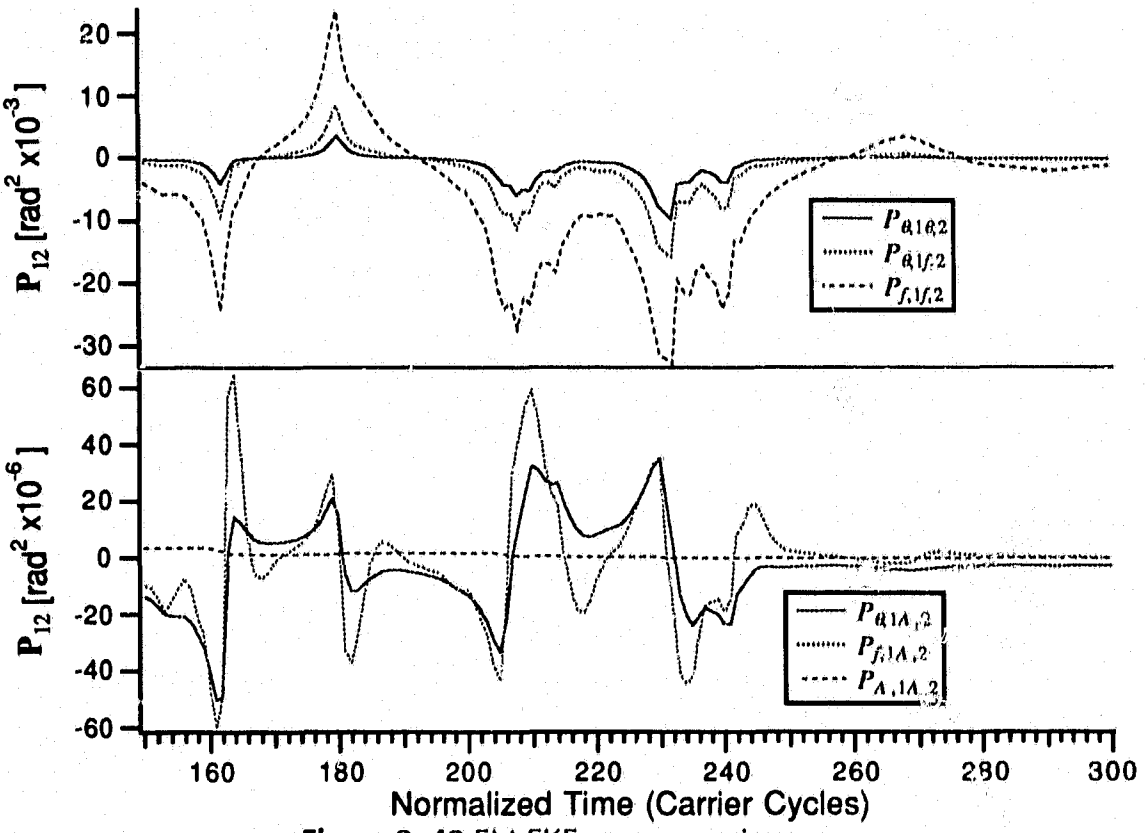

Figure 3–48 FM EKF cross-covariances.

which again shows that the coupling between the amplitude and the phase and frequency states is very small when compared to the coupling between phase and frequency. This why in Fig. 3–46 only a small change in the amplitude estimates occurred when the phase and frequency estimates where more severely effected during the periods of low observability.

Each time the sources pass through these periods of low observability the cross-covariance terms play a part. Fig. 3–47 shows the state auto-covariances and Fig. 3–48 shows the cross-covariances. During periods of high observability, the cross-covariances are normally zero however, as the states become less observable, the contribution of the cross-covariances to the state coupling increases. Whether this is an helps or hinders tracking will be discussed in a subsequent chapter.

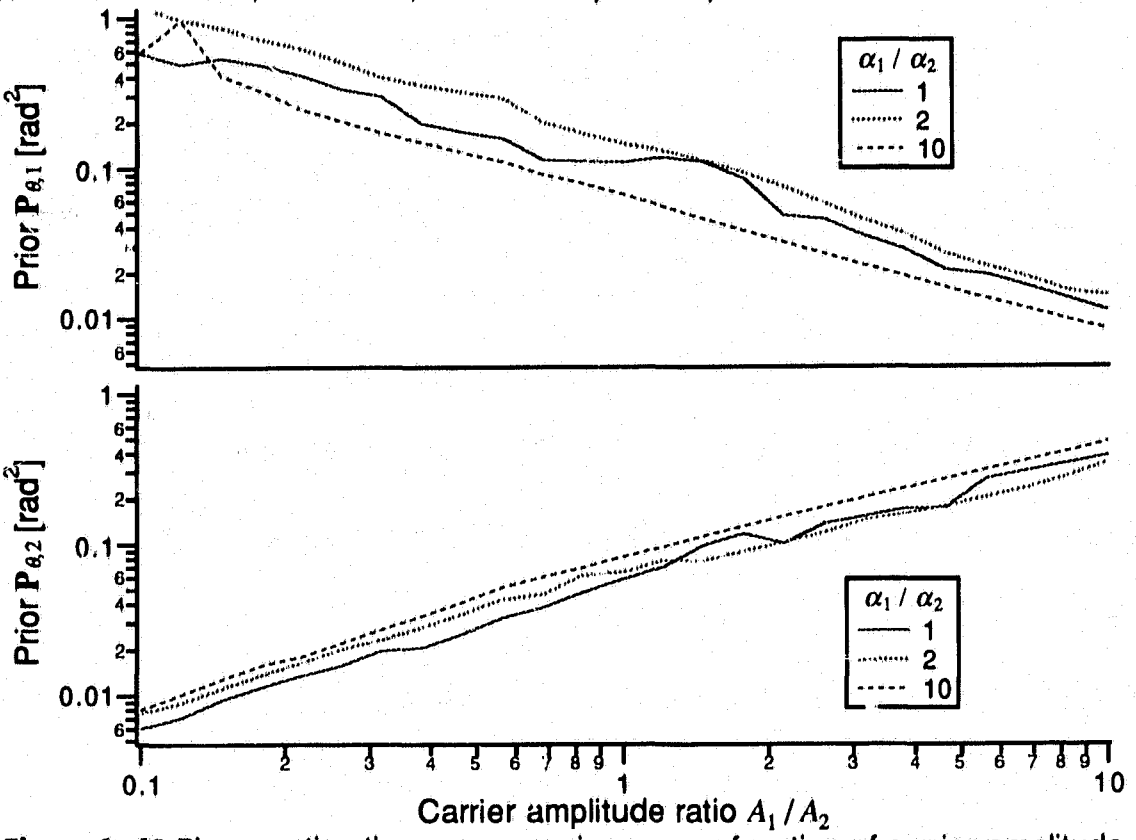

Figure 3–49 Phase estimation error covariance as a function of carrier amplitude ratio.

The relationship between relative carrier power and prior error covariance is essentially the same as in the PM case: the error covariance increases for the lower powered signal (see Figs. 3–49 through 3–51).

3.4. Conclusions

The state observability has been examined in order to address the ability of two similar processes to be separated. This problem is compounded in communications by the inherent nonlinearity of the modulation process. In order to apply the state-space observability criteria, the problem has to be linearized. This is accomplished by the formation of a new state composed of the state estimation error when this error is small. This in effect linearizes the observation function so that the observability Gramian may be formed. The condition of the observability Gramian is examined to study the state observability. Although this is a very re-

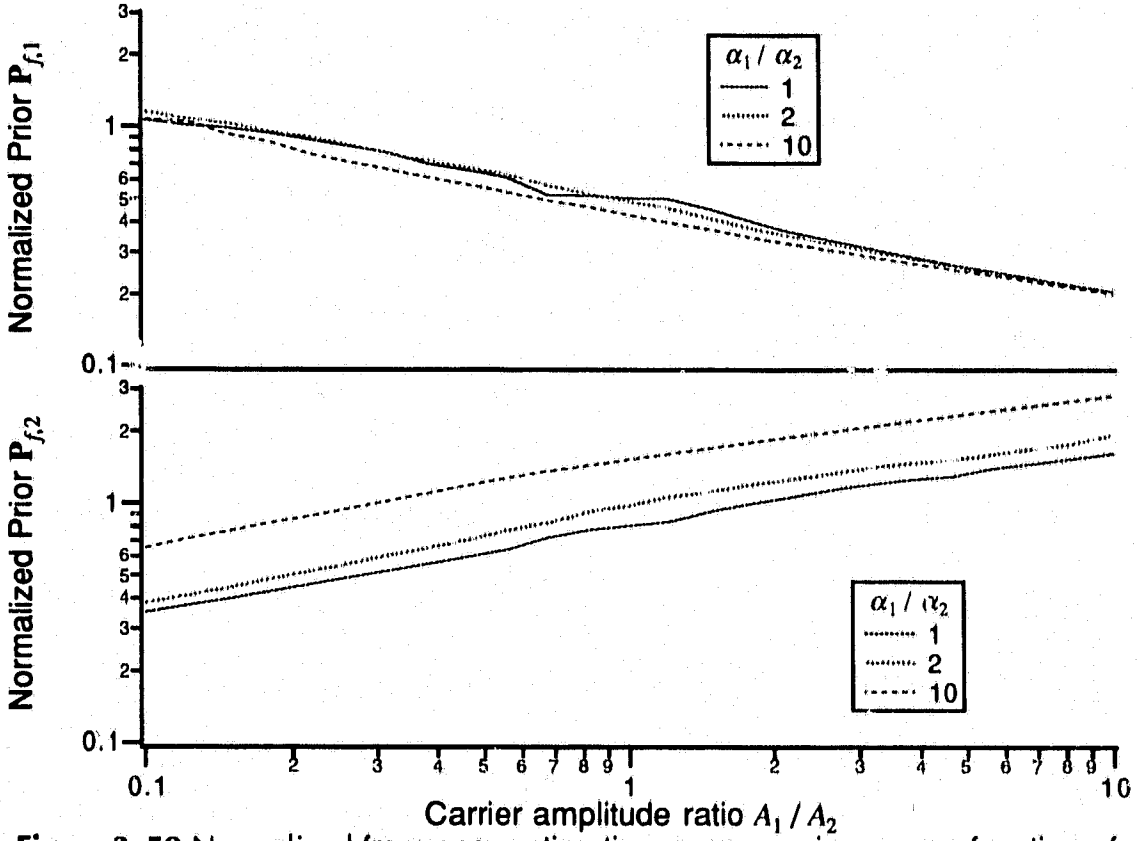

Figure 3–50 Normalized frequency estimation error covariance as a function of carrier amplitude ratio.

strictive case, it is valid for the "locked" condition of the phase-locked loop allowing facilitating the tracking behavior of the estimator.

One of the more important discoveries is that two sources may be separated as long as their carriers are not in phase. The distinctness of the message processes seems to only play a role when the carriers are close to being in phase.

Through extensive simulation of the EKF estimators derived in Chapter 2 demonstrates the connection between state observability and state estimation or separation for high SNR. It has been shown that the states can most accurately be estimated when their "observability" is high, as measured by the condition of the observability Gramian. From this EKF estimators have been shown to track one and two source PM and FM sources with both known and unknown carrier amplitudes. This simulation has also revealed the role of the estimator state

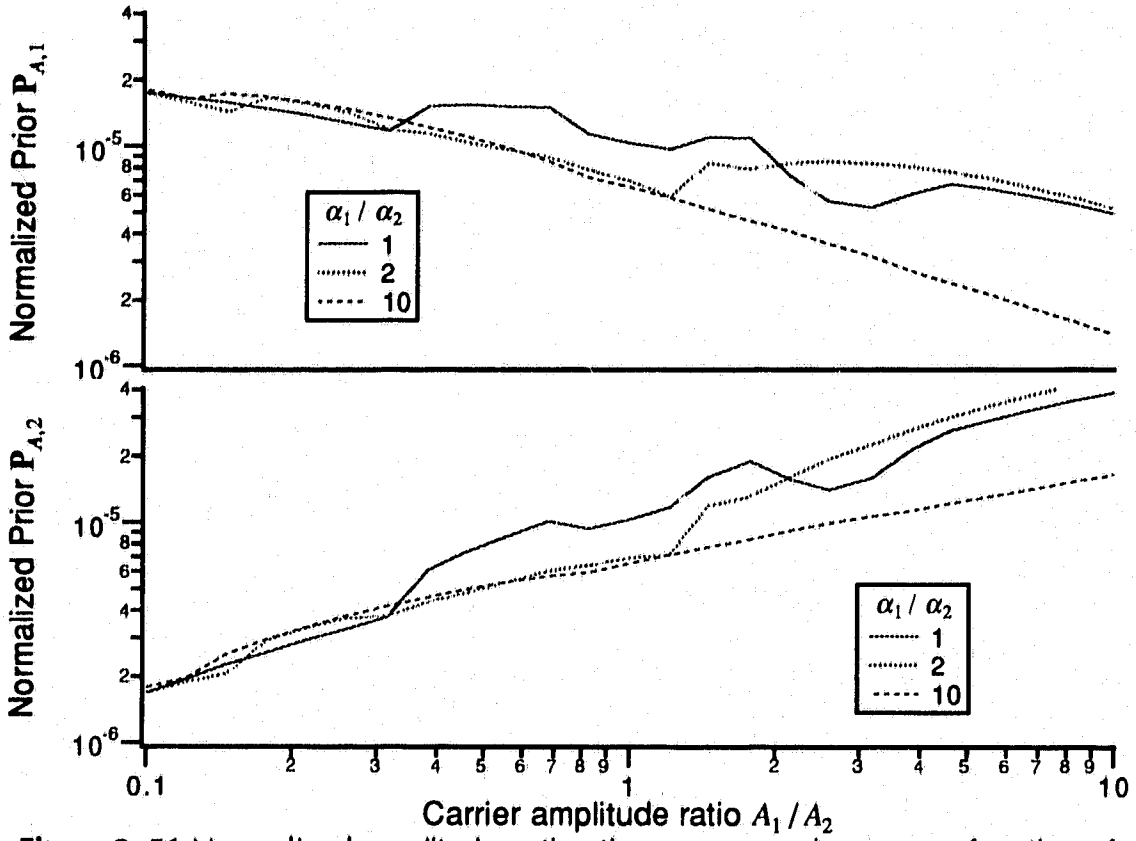

Figure 3–51 Normalized amplitude estimation error covariance as a function of carrier amplitude ratio.

coupling as defined by the error covariance matrix. In particular it has been shown that in the steady-state, the amplitude states are virtually uncoupled with the other states and thus these "connections" in the estimator structures of Section 2.3 are very weak when compared to the phase and frequency state coupling.

4. Coupled Digital Phase-Locked Loop Behavior

In Chapter 2 we presented EKF estimator structures which may be realized by coupled digital phase-locked loops. In Chapter 3 we analyzed how well and under what conditions these EFK estimators could track multiple co-channel sources. In this chapter we elaborate on these CDPLL realizations and examine their acquisition and tracking behavior. These new structures are compared to associated work found in the literature.

We also briefly examine the challenge of determining the signal multiplicity, that is the number of signals present in the channel.

As the DPLL forms the basis of the EKF-based realizations, we will begin by reviewing relevant DPLL theory.

4.1. Digital Phase-Locked Loops

DPLLs are discrete or digital implementations of analog phase-locked loops. The traditional PLL, shown in Fig. 4–1, is composed of three major components: 1) the phase detector, 2) the loop filter, and 3) the voltage controlled oscillator. The PLL is a closed-loop control system that tries to track the phase of the incoming signal by minimizing the difference between the input and the output of the VCO. The output of the phase detector is this error signal, the high frequency components of which are removed by the loop filter. The resulting static error signal allows the VCO to track relatively slow changes in the phase of the input signal, thus it is able to demodulate angle-modulated signals. It has also been shown that the PLL is a realization of the optimum angle-modulation demodulator in the MAP and MMSE sense [22]. Design methods and performance measures for analog PLLs abound in the literature with notable references [8, 9, 22, 10].

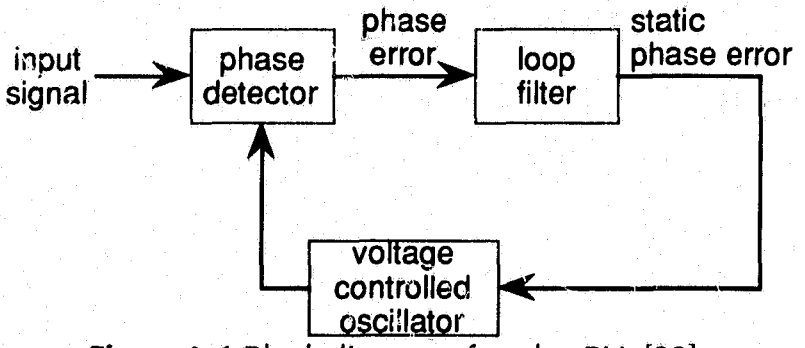

Figure 4–1 Block diagram of analog PLL [20].

During the last two decades DPLLs have received an increasing amount of attention. This may be attributed to two main reasons: 1) the ever increasing strides in function and speed of digital technology and 2) the increased flexibility of the DPLL compared to the PLL. This increased flexibility has left the field wide open for DPLL theory and application research. One result of the diversity in the DPLL research is some ambiguity in the use of the term "digital" in the DPLL context.

In the early days of the DPLL inclusion of any digital components would lead to calling the PLL digital. Thus a digital filter might be used as the loop filter but the phase detector and VCO are still analog as in the case of Gupta [27]. In current parlance, such a PLL would be labeled a hybrid PLL (HPLL); only PLLs with digital implementations of all three major components are referred to as DPLLs.

This has led to two major categories of DPLLs based on the method of sampling. Synchronous DPLLs sample the incoming signal at its zero crossings; thus they sample synchronously with the phase of the input. Since the phase is time-varying, the interval between samples is not constant and thus these types of DPLLs are also known as non-uniform sampling DPLLs. These are by far the most common and most studied as they are relatively easy to implement and their performance and design procedures are quite similar to PLLs. Works of note include Gill [25], Weinberg [26], Holms [43], and Lindsey [20]. Although this is a very straight forward and well understood progression from analog to digital, Gardner [21]

takes great pains to differentiate between hybrid loops and digital loops. By his definition, the synchronous DPLL should be classified as a hybrid loop because the sampling instants are not uniform.

The second category is the asychronous DPLL which samples the incoming signal at uniform intervals. This is the only DPLL that adheres to Gardner's definition. Here the application of PLL theory is not as direct as the synchronous DPLL, however the asychronous DPLL may be studied using digital signal processing theory. Much of the early work took this approach including Kelly [44, 28], McBride [30], and Polk [29].

The majority of the work of the last two decades has focused on the synchronous DPLL. Its close relationship with well-established PLL theory and its relatively light computational load were the main driving factors. As the 1980s drew to a close, the asychronous DPLL started appearing. This may be attributed to the improvements and reduced cost of high-performance digital signal processors and analog-to-digital converters (ADCs). The relatively recent works of Shayan [45] and Statman [46] are examples.

4.1.1. DPLLs in CDPLL Structures

Returning to the topic of this thesis, namely coupled digital PLLs, leads us to the selection of the type of DPLL used in the CDPLL receiver. To address this issue, some review of prior efforts is in order.

Pure Analog (Analog-Analog)

The original coupled PLL work was developed using analog PLLs [13, 14, 15]. In this scenario the signals of interest are analog in nature (e.g. FM voice) as is the CPLL receiver (see Fig. 1–6). The derivation of the canceler is based on phase modulated sinusoids (carriers). Using MAP estimation theory the estimator was found to be in the form of two mutually coupled PLLs.

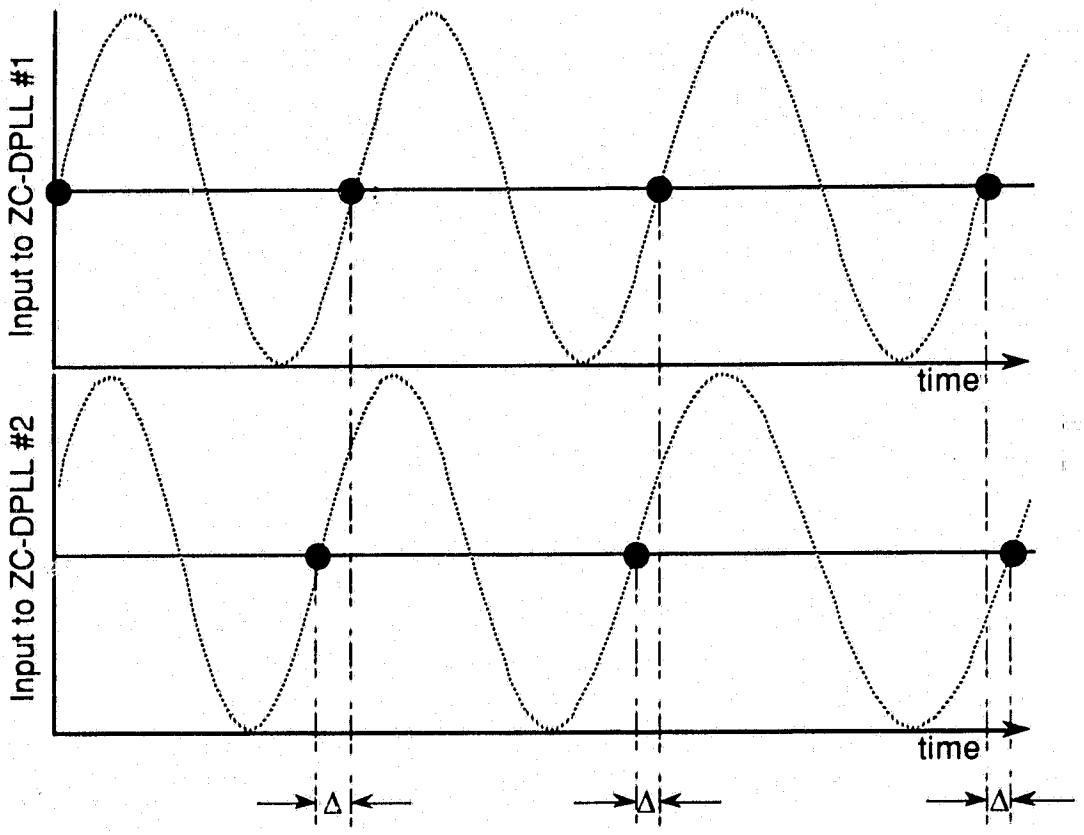

Figure 4–2 Zero-crossing CDPLL timing.

Work relating to synchronized oscillators has also remained in the analog domain. Dessouky [47] and Sayhood [48] examine clock synchronization via mutually coupled PLLs.

Hybrid (Analog-Digital)

The first extension of the strict analog case was to implement the PLL by a digital FLL [3, 17]. In both these initial works the DPLL is in the form of a zero-crossing DPLL (ZC-DPLL) where in the loop tracks the zero crossings (hence the name) of the carrier by sampling the carrier at the estimated zero crossing time and is thus a synchronous DPLL.

An additional problem from the implementation point of view involves coupling the two ZC-DPLLs. The signal recovered from the ZC-DPLL (its output) is in a discrete form where the time between samples is not constant. Thus there exists a synchronization problem between the two ZC-DPLLs since they are sampling their respective carriers at different times

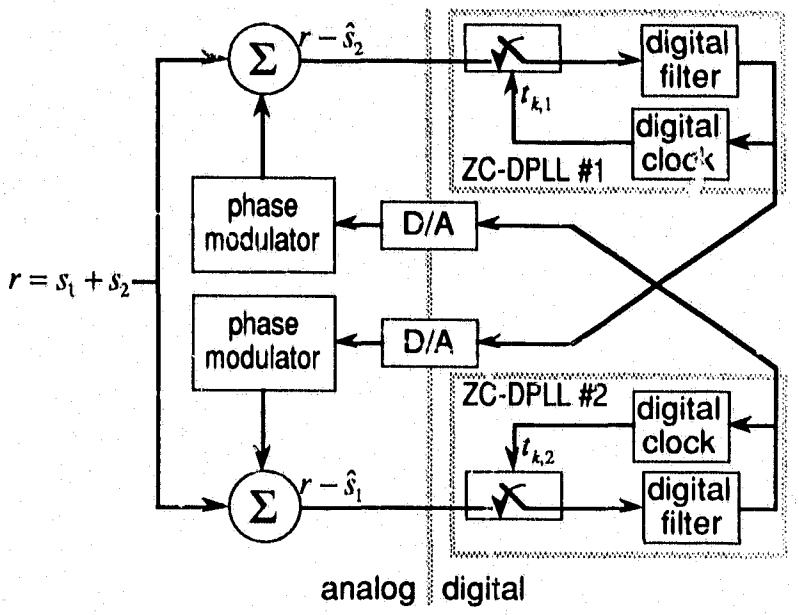

Figure 4–3 Zero-crossing CDPLL implementation.

(see Fig. 4–2). Thus the two ZC-DPLLs must be resychronized with each sample. This may be accomplished by converting the output back to analog form (i.e. regenerating the carrier with proper phase and frequency) and then removing it from the input to the other ZC-DPLL (see Fig. 4–3). This is not an efficient solution. A "purely" digital formulation with asychronous carrier sampling would avoid this problem as the samples would be properly aligned in time.

Pure Digital (Digital-Digital)

In this case both the signals of interest and the DPLLs are digital. Although the carrier and the message process may be analog, sampling is performed external to the DPLL as is recreation of the analog message process if that is even required. In digital communication, the message process would simply be a bit stream and the digital output of the DPLL is the desired form of the information. For a loop to be considered digital by Gardner's definition, the sampling of the carrier must be performed asynchronously to allow the time between sampling instants to be constant. In such a DPLL, also known as a Nyquist rate DPLL (NR-

DPLL) [20], more than two samples per cycle are required depending on the bandwidth as per the Nyquist criterion. In order to make timing corrections (achieve phase-lock), either many samples per carrier cycle are required or the "missing" data samples must be interpolated from the existing data.

The interpolator assumes a known pulse shape of the digital data. This is not the case when the baseband information is analog. However, it may be possible to interpolate the missing analog samples by using a linear predictor and estimating the information (baseband) signal within a Kalman filter.

Bradley employed the NR-DPLL in his CDPLL estimator [18]. The estimator structures derived in Sections 2.3.4 and 2.3.5 also employ the NR-DPLL.

4.1.2. The DPLL and its Relation to Phase Estimation

From this point forward, we restrict ourselves to the study of uniform sampling (Nyquist rate) DPLLs. In Section 2.3 we showed that the derived EKF could be implemented by a DPLL and we have also stated that the PLL is an optimum demodulator in the MAP sense. Here we present in summary form how the PLL is derived from MAP estimates. Most of the summary is from van Trees [22] and although the presentation is based on continuous waveforms, for the purposes of discussion, the mapping to sampled waveforms is a direct one as long as we adhere to the Nyquist sampling criteria.

Let the phase be a filtered version of the random message process $a(t)$ characterized by its covariance function $K_a(t,u)$ where

$$\theta(t) = \int_{T_i}^{T_f} k(t,u)a(u)\,du, \quad T_i \le t \le T_f, \tag{4.1}$$

where $k(t,u)$ is the impulse response of the filter. From (2.1) the output of the phase modulator is

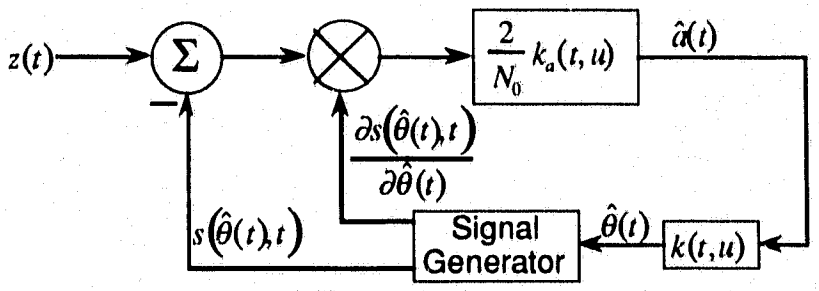

Figure 4–4 Block diagram of MAP estimator [22].

$$s(\theta(t),t) = \sqrt{2}A\sin(\omega_c t + \theta(t)), \quad T_i \le t \le T_f, \tag{4.2}$$

and due to the (Gaussian) measurement noise the received signal is

$$z(t) = s(\theta(t),t) + n(t), \quad T_i \le t \le T_f. \tag{4.3}$$

The objective is to find the MAP estimate of $a(t)$ over the interval $T_i \le t \le T_f$. The MAP estimate is found to be [22]

$$\hat{a}(t) = \tfrac{N_0}{2}\int_{T_i}^{T_f} \frac{\partial s(\hat{\theta}(\zeta),\zeta)}{\partial\hat{\theta}(\zeta)} k_a(t,\zeta)\left[z(\zeta) - s(\hat{\theta}(\zeta),\zeta)\right]d\zeta, \quad T_i \le t \le T_f, \tag{4.4}$$

where

$$k_a(t,\zeta) \equiv \int_{T_i}^{T_f} k(\zeta,\tau)K_a(t,\tau)\,d\tau, \quad T_i \le t \le T_f. \tag{4.5}$$

A block diagram of (4.4) is shown in Fig. 4–4. When compared to the EKF realization of Fig. 2–4 it is clear that they are the same structures where $k_a(t,u)$ is equivalent to the state equation, $2/N_0$ is the inverse of the measurement noise covariance R_v, and the observation function $h(\hat{\mathbf{x}}_\theta)$ and its derivative $\mathbf{H}(\hat{\mathbf{x}}_\theta)$ are present at the output of the signal generator.

Substituting (4.2) and

$$\frac{\partial s(\theta(t),t)}{\partial\theta(t)} = \sqrt{2}A\cos(\omega_c t + \theta(t)) \tag{4.6}$$

and assuming that the filter $k(t,u)$ is time-invariant, (4.4) becomes

$$\hat{a}(t) = \tfrac{2}{N_0}\int_{-\infty}^{\infty} k_a(t-u)\sqrt{2}A\cos(\omega_c u + \hat{\theta}(u))\left[z(u) - \sqrt{2}A\sin(\omega_c u + \hat{\theta}(u))\right]du, \tag{4.7}$$

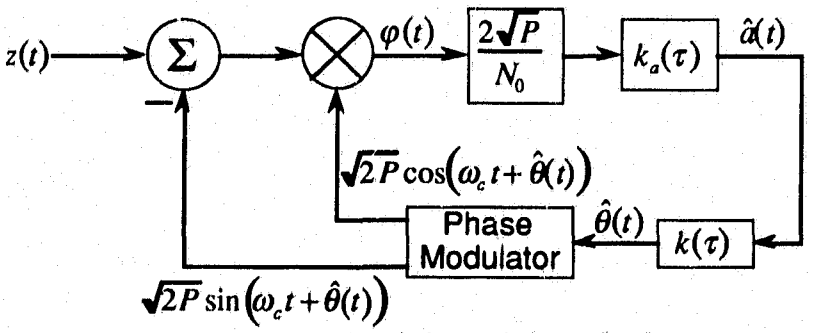

Figure 4–5 Optimal demodulator [22].

for an infinite observation interval. This optimum demodulator is shown in Fig. 4–5. Again when compared to the DPLL portion of Fig. 2–13 the similarities are evident.

When comparing Figs. 4–4 and 4–5 to Figs. 2–4 and 2–13 of particular note is the presence of the innovations process, $z(t) - s\left(\hat{\theta}(t), t\right)$. In Fig. 4–5 the phase error may be written

$$\varphi(t) = \sqrt{P}\sin\left[\theta(t) - \hat{\theta}(t)\right] + n(t)\sqrt{2}\cos\left(\omega_c t + \hat{\theta}(t)\right) + \sqrt{P}\sin\left(2\omega_c t + \theta(t) + \hat{\theta}(t)\right) - \sqrt{P}\sin\left(2\omega_c t + 2\hat{\theta}(t)\right). \tag{4.8}$$

If we assume that the filter $k(\tau)$ has a bandwidth smaller than ω_c then it will be much smaller than $2\omega_c$ and the last two terms on the R.H.S. of (4.8) will not pass through the filter. The term $\sqrt{P}\sin\left(2\omega_c t + 2\hat{\theta}(t)\right)$ is due to the feedback creating the innovations process; since it is not passed through $k(\tau)$ the feedback path may be removed resulting in the familiar PLL structure of Fig. 4–6.

The measurement noise may be decomposed into its in-phase and quadrature components

$$n(t) = \sqrt{2}\left[n_I(t)\cos(\omega_c t) - n_Q(t)\sin(\omega_c t)\right], \tag{4.9}$$

where $n_I(t)$ and $n_Q(t)$ are sample functions from independent low-pass Guassian processes with bandwidth $B_\theta < B_n << \omega_c$. Ignoring double frequency terms, $(t)\sqrt{2}\cos\left(\omega_c t + \hat{\theta}(t)\right)$ may be rewritten as

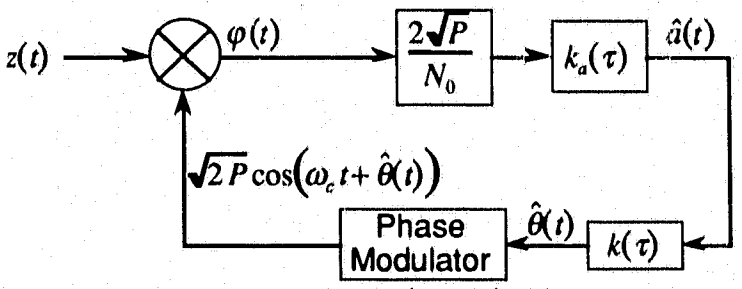

Figure 4–6 MAP derived PLL.

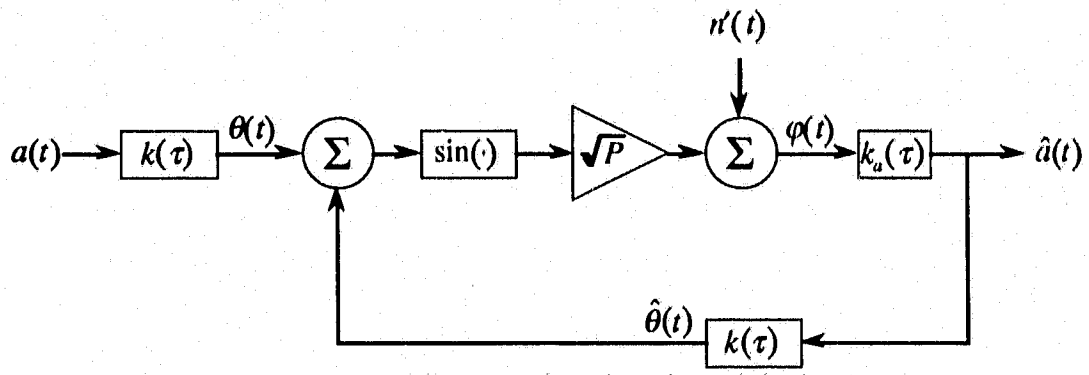

Figure 4–7 "Phase" or baseband model of PLL.

$$n'(t) = n_I(t)\cos\left(\hat{\theta}(t)\right) + n_Q(t)\sin\left(\hat{\theta}(t)\right). \tag{4.10}$$

Substituting (4.10) into (4.8) yields the simplified expression for phase error

$$\varphi(t) = \sqrt{P}\sin\left[\theta(t) - \hat{\theta}(t)\right] + n'(t), \tag{4.11}$$

and a simplified diagram of the angle modulation and demodulation system is shown in Fig. 4–7.

We have shown in the form of a review of [22] that the PLL is the MMSE and the MAP estimator for angle modulated signals; thus the PLL is the optimum demodulator. We now move to the behavior of the DPLL.

4.1.3. DPLL Behavior

The DPLL (and PLL) operate in two "modes": acquisition which is non-linear and tracking which is (very nearly) linear.

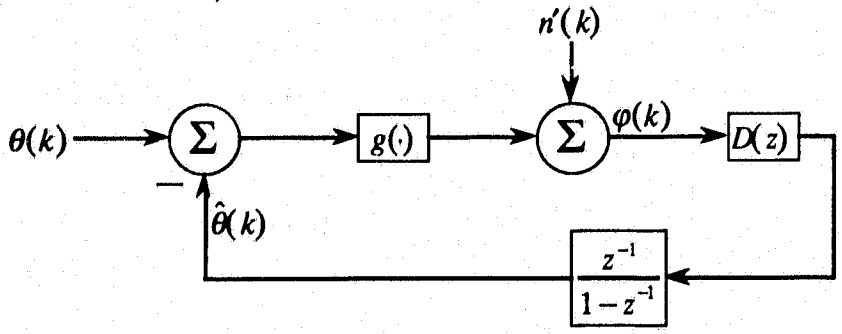

Figure 4–8 Baseband model of DPLL [20].

Linear Behavior

The baseband model of the DPLL shown in Fig. 4–8 is functionally identical to the PLL model. Here the function $g(\cdot)$ defines the phase detector (for example, $g(\cdot) = \sin(\cdot)$ for a sinusoidal phase detector), $D(z)$ is the transfer function of the loop filter, and $1/(z-1)$ is the z-transform representation of the NCO. The measurement noise $n(k)$ has been separated from the input in the same manner as in (4.9) and (4.10).

The local phase estimate in the z-domain is [20]

$$\hat{\theta}(z) = \frac{D(z)}{z-1}\left\{g\left[\tilde{\theta}(z)\right] + V'(z)\right\} \tag{4.12}$$

and the phase error is

$$\tilde{\theta}(z) = \theta(z) - \frac{D(z)}{z-1}\left\{g\left[\tilde{\theta}(z)\right] + V'(z)\right\}, \tag{4.13}$$

where $\theta(z)$, $\tilde{\theta}(z)$, $\hat{\theta}(z)$, and $V'(z)$ are the z-transforms of the sequences $\theta(k)$, $\tilde{\theta}(k)$, $\hat{\theta}(k)$, and $v'(k)$ respectively.

Linear approximations to the PLL may be applied when the PLL is in tracking mode; that is when the phase error is small compared to one radian. In this case the approximation $g[\varphi''(k)] \approx g'(0)\varphi''(k)$ where $g'(k) = \partial g[\varphi''(k)]/\partial\varphi''(k)$ may be used which effectively removes the nonlinear phase detector characteristics in Fig. 4–8 and thus linearizes the model.

Since $g'(0)$ is a constant, it may be lumped in with the loop filter $D(z)$. Thus the linear (tracking) loop equation for the phase error is [20]

$$\tilde{\theta}(z) = [1 - H(z)]\theta(z) - H(z)V'(z), \tag{4.14}$$

where the closed loop transfer function is

$$H(z) = \frac{D(z)}{z - 1 + D(z)}. \tag{4.15}$$

From Appendix B we found that the EKF-derived second-order DPLL has a loop filter with transfer function

$$D(z) = G_1 + \frac{G_2}{1 - z^{-1}} \tag{4.16}$$

where

$$G_1 = P_\theta(k)R_v^{-1}, \tag{4.17}$$

$$G_2 = \phi_{\theta f}P_{f\theta}(k)R_v^{-1}. \tag{4.18}$$

The nonlinear function of the phase detector from Appendix B is $g\left[\tilde{\theta}(k)\right] = 2A^2 \sin\left(\tilde{\theta}(k)\right)$ which is linearized to $2A^2\tilde{\theta}(k)$ where the constant gain $2A^2$ will be included with the loop filter $D(z)$. Substituting (4.16) into (4.15) gives the closed loop transfer function of the second-order DPLL operating in tracking mode

$$\begin{aligned} H(z) &= \frac{2A^2\left[(G_1 + G_2)z - G_1\right]}{(z-1)^2 + 2A^2\left[(G_1 + G_2)z - G_1\right]} \\ &= \frac{(G_1 + G_2)z - G_1}{z^2 + \left[2A^2(G_1 + G_2) - 2\right]z - 2A^2G_1 + 1}. \end{aligned} \tag{4.19}$$

From [49] the one-sided closed-loop bandwidth is defined as

$$B_L[Hz] = \frac{1}{2T_s}\frac{1}{H^2(1)}\frac{1}{2\pi i}\oint_{|z|=1} H(z)H\left(z^{-1}\right)z^{-1}\,dz, \tag{4.20}$$

which, after substitution (4.19) and use of the integral table in [20], reduces to

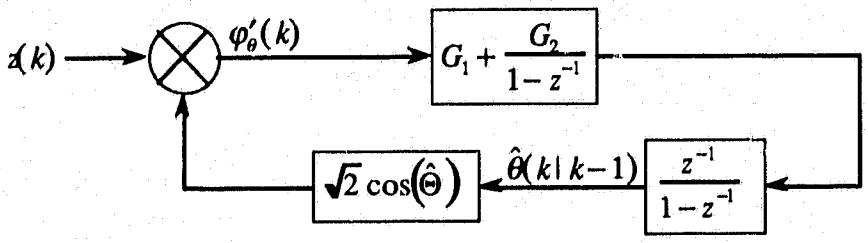

Figure 4–9 Second-order DPLL.

$$B_L[Hz] = \frac{1}{2T_s}\frac{2A^2G_1 + A^2G_1G_2 + G_2}{G_1\left(2 - 2A^2G_1 - A^2G_2\right)}. \tag{4.21}$$

Substituting (4.17) and (4.18) gives

$$B_L(k)[Hz] = \frac{1}{2T_s}\frac{2A^2P_\theta^2(k)R_v^{-1} + \phi_{\theta f}P_{f\theta}(k) + A^2\phi_{\theta f}P_{f\theta}(k)P_\theta(k)R_v^{-1}}{P_\theta(k)\left(2 - 2A^2P_\theta(k)R_v^{-1} - A^2\phi_{\theta f}P_{f\theta}(k)R_v^{-1}\right)}. \tag{4.22}$$

It is important to note that due to the time-varying gains, the loop bandwidth is also a function of time.

The resulting second-order DPLL is shown in Fig 4–9. As shown in Appendix B, inclusion of amplitude estimation results in the DPLL of Fig. 4–10.

When the DPLL is operating in tracking mode, the time dependency exhibited in the error covariance is solely due to the observation matrix $\mathbf{H}_\theta^{\mathrm{T}}(\mathbf{x}(k|k-1),k)$. As noted in Appendix B, the baseband model of the DPLL replaces $\mathbf{H}_\theta^{\mathrm{T}}(\mathbf{x}(k|k-1),k)$ with $\mathbf{c}_\theta^{\mathrm{T}}$. Thus the baseband model of the estimation error covariance recursion (2.88) loses the time dependence of $\mathbf{H}_\theta^{\mathrm{T}}(\mathbf{x}(k|k-1),k)$. Since this linearizes the EKF to simply a Kalman filter, the steady-state (or tracking) solution to the error covariance may be found.

Friedland [50] finds the steady-state solution to a Kalman filter which is very similar to the one we have developed[1]. Starting with $\mathbf{P}(k)$ from (2.67) and the Kalman gain update (2.68)

---

[1]The process noise covariance in [50] is much simpler than that presented in Section 2.1.4.

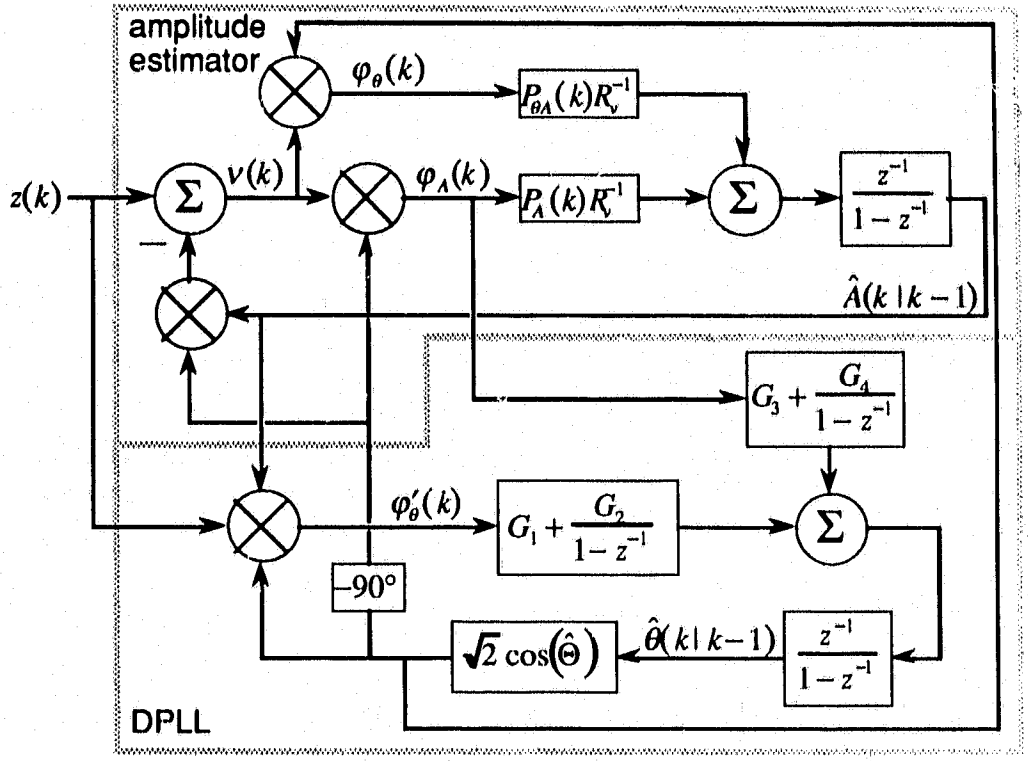

Figure 4–10 Second-order DPLL with amplitude estimation.

$$\mathbf{P}^{-1}(k)=\mathbf{P}^{-1}(k\,|\,k-1)+\mathbf{H}^{\mathrm{T}}R_v^{-1}\mathbf{H} \tag{4.23}$$

where $\mathbf{P}(k\,|\,k-1)$ is from (2.65). In the steady-state $\mathbf{P}(k)=\mathbf{P}(k-1)$ and $\mathbf{P}(k\,|\,k-1)=\mathbf{P}(k-1\,|\,k-2)$ and thus (2.68) and (4.23) may be rewritten

$$\mathbf{P}(k\,|\,k-1)-\mathbf{\Gamma Q}_w\mathbf{\Gamma}^{\mathrm{T}}=\mathbf{\Phi}\left(\mathbf{P}^{-1}(k\,|\,k-1)+\mathbf{H}^{\mathrm{T}}R_v^{-1}\mathbf{H}\right)\mathbf{\Phi}^{\mathrm{T}}. \tag{4.24}$$

Each side may be expanded and the element-by-element equality will result in a system of equations which may be solved. Although this has been done for our EKF using Maple™ the results are not presented here as they would take several pages to repeat.

An alternative approach is that taken by Ekstrand [51] which uses the method reported by Vaughan [52]. Here the solution of the error covariances (4.23) and (2.65) is determined from the eigenvectors of the matrix

$$\kappa=\begin{bmatrix}\mathbf{\Phi}^{-\mathrm{T}} & \mathbf{\Phi}^{-\mathrm{T}}R_v^{-1}\\ \mathbf{\Gamma Q\Gamma\Phi}^{-\mathrm{T}} & \mathbf{\Phi}+\mathbf{\Gamma Q\Gamma\Phi}^{-\mathrm{T}}R_v^{-1}\end{bmatrix}. \tag{4.25}$$

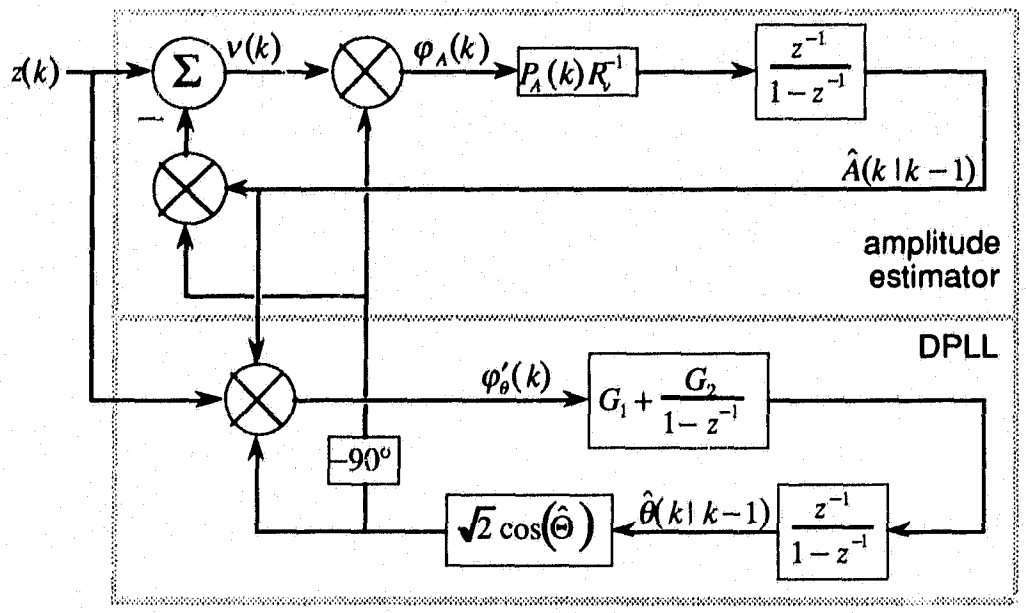

Figure 4–11 Simplified second-order DPLL with amplitude estimation.

The steady-state solution of the error covariance is

$$\mathbf{P}_{ss} = \mathbf{W}_{21}\mathbf{W}_{11}^{-1}, \tag{4.26}$$

where $\mathbf{W}_{21}$ and $\mathbf{W}_{11}$ are from the partitioned eigenvector matrix. Like the previous method, the analytic solution becomes a lesson in bookkeeping and is thus not presented. This method is, however, very well suited for numeric evaluation. In the case of joint phase, frequency, and phase estimation, numeric evaluation of (4.26) reveals that, in the steady-state, the cross-covariance of phase and frequency with amplitude is indeed zero. That is,

$$\mathbf{P}_{ss} = \begin{bmatrix} P_\theta & P_{\theta f} & 0 \\ P_{f\theta} & P_f & 0 \\ 0 & 0 & 0 \end{bmatrix}, \tag{4.27}$$

which agrees with the estimated error covariance of (3.71). Thus, during tracking, there is no coupling of the phase and the frequency states with the amplitude state, and Fig. 4–10 reduces to 4–11 which is of the same form as reported by Bradley [18].

Nonlinear Behavior

The nonlinear behavior of the PLL has been extensively studied and is well understood. Classic references are Viterbi [8], van Trees [72], and Gardner [10]. The nonlinear analysis is generally broken down into two scenarios: noise free and noisy environments where phase-plane and Fokker-Plank techniques are employed. More recently it has been shown that nonlinear behavior of PLLs exhibit chaotic dynamics [53, 54] and have thus become an area of interest in chaos theory circles.

Most of the DPLL literature has focused on the non-uniform sampling DPLL and the ZC-DPLL in particular. Similar techniques to those used in the PLL analysis have been used as well as examination of nonlinear behavior from the chaos perspective have been reported [55].

The acquisition behavior of the joint phase, frequency, and amplitude estimator is examined here by simulation. Results from both the EKF and the DPLL structure of Chapter 2 are presented. Of particular interest is the state coupling of phase and frequency with amplitude. To study acquisition, the EKF is initialized with initial state estimate

$$\hat{\mathbf{x}}(0) = E[\mathbf{x}(0)], \tag{4.28}$$

and initial error covariance estimate

$$\mathbf{P}(0) = E\left[(\mathbf{x}(0) - \hat{\mathbf{x}}(0))(\mathbf{x}(0) - \hat{\mathbf{x}}(0))^{\mathrm{T}}\right]. \tag{4.29}$$

Since the EKF may have to acquire the signal at any time, the initial state of the source should be random. The phase is uniformly distributed between $-\pi$ and π radians. We will let the variance of the initial frequency be equal to the frequency covariance γ_f. Finally we will let the amplitude be χ_1^2; that is, Chi-squared with one degree of freedom. For these initial conditions of the source's state, (4.28) is

$$\hat{\mathbf{x}}(0) = [0 \quad 0 \quad 1]^{\mathrm{T}} \tag{4.30}$$

and (4.28) is

$$\mathbf{P}(0) = \begin{bmatrix} \frac{\pi^2}{3} & \mathbf{0} & \\ & \gamma_f & \\ \mathbf{0} & & 2 \end{bmatrix}. \tag{4.31}$$

A sample run of the EKF during acquisition is shown in Fig. 4–12. Here as in the case of [18] $\alpha = f_c/100$, $d_f = 1$, the effective sampling rate is $f_s = 25f_c$, and the input SNR is 22 dB. The amplitude is accurately estimated within four carrier cycles. Frequency acquisition and phase locking occur within two carrier cycles. The estimation error covariances during acquisition are shown in Fig. 4–13. The auto-covariances P_θ and P_f attain their steady-state values found in Chapter 3 within one carrier cycle. P_A decays exponentially showing that the amplitude is estimated quickly and subsequent measurements improve the estimate little. Of interest are the error cross-covariances. The phase and frequency cross-covariance $P_{\theta f}$ reaches its non-zero steady-state value as quickly as the phase and frequency auto-variances do. This shows that the coupling between phase and frequency is important during all time. However, the cross-covariances including amplitude, $P_{\theta A}$ and P_{fA}, are non-zero only during the initial amplitude estimation. This indicates that this coupling is important for accurate amplitude estimation. In a similar simulation $P_{\theta A}$ and P_{fA} were maintained at zero (effectively decoupling the state estimates) and the DPLL could not acquire the states. Once the amplitude is correctly estimated, $P_{\theta A}$ and P_{fA} approach zero which effectively decouples the amplitude from phase and frequency estimation.

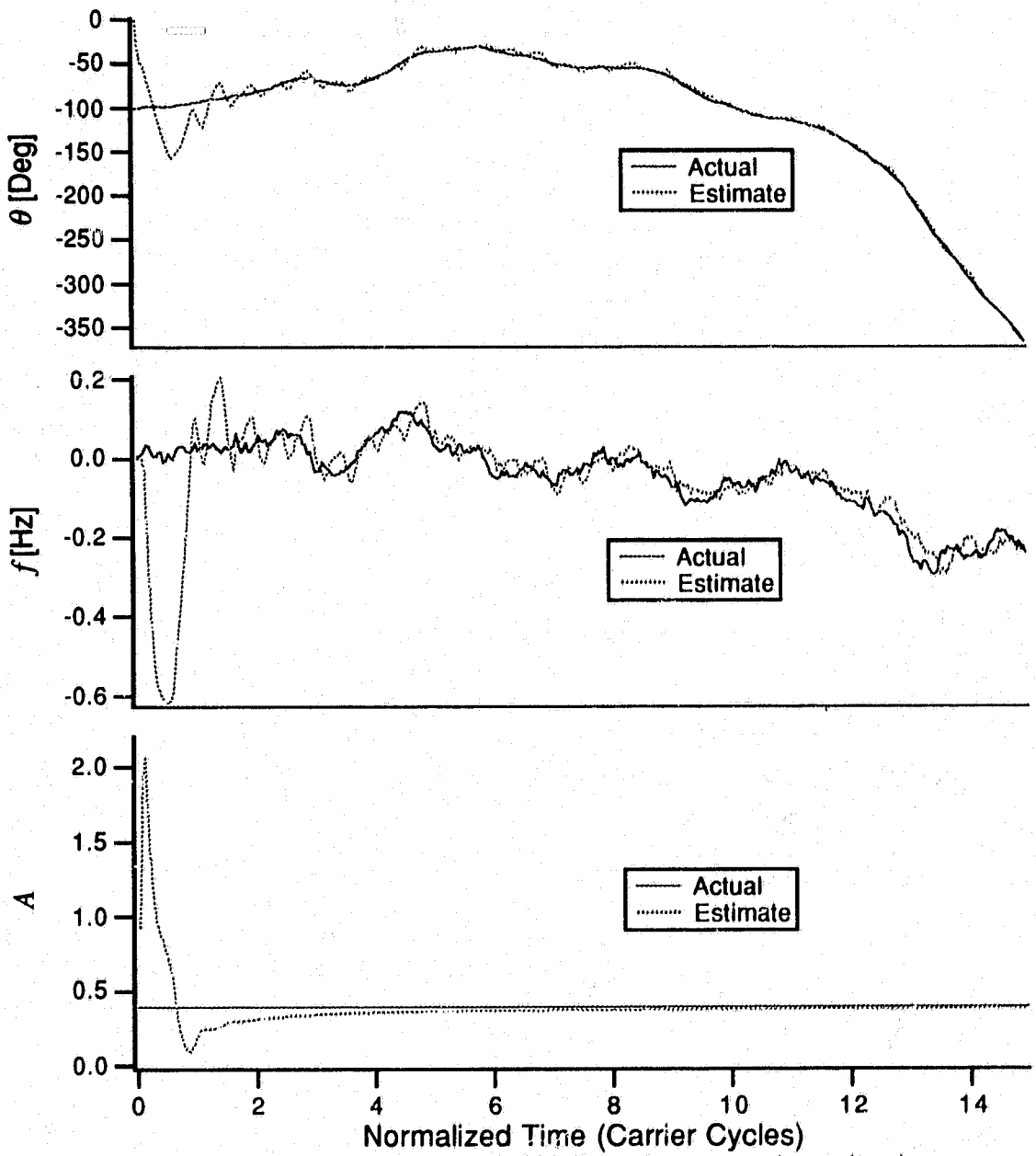

Figure 4–12 EKF acquisition of phase, frequency, and amplitude.

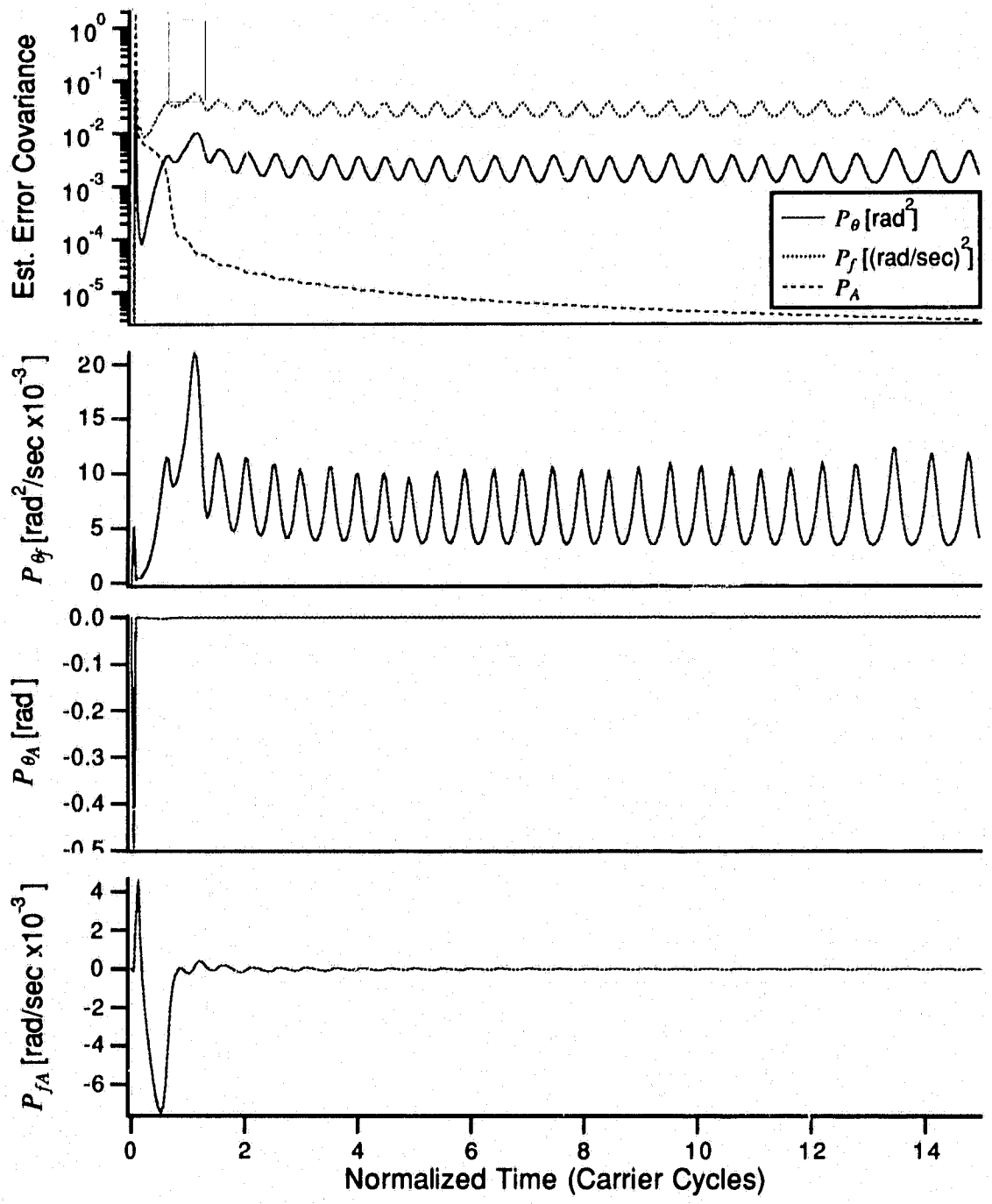

Figure 4–13 EKF estimator error covariance during phase, frequency, and amplitude acquisition.

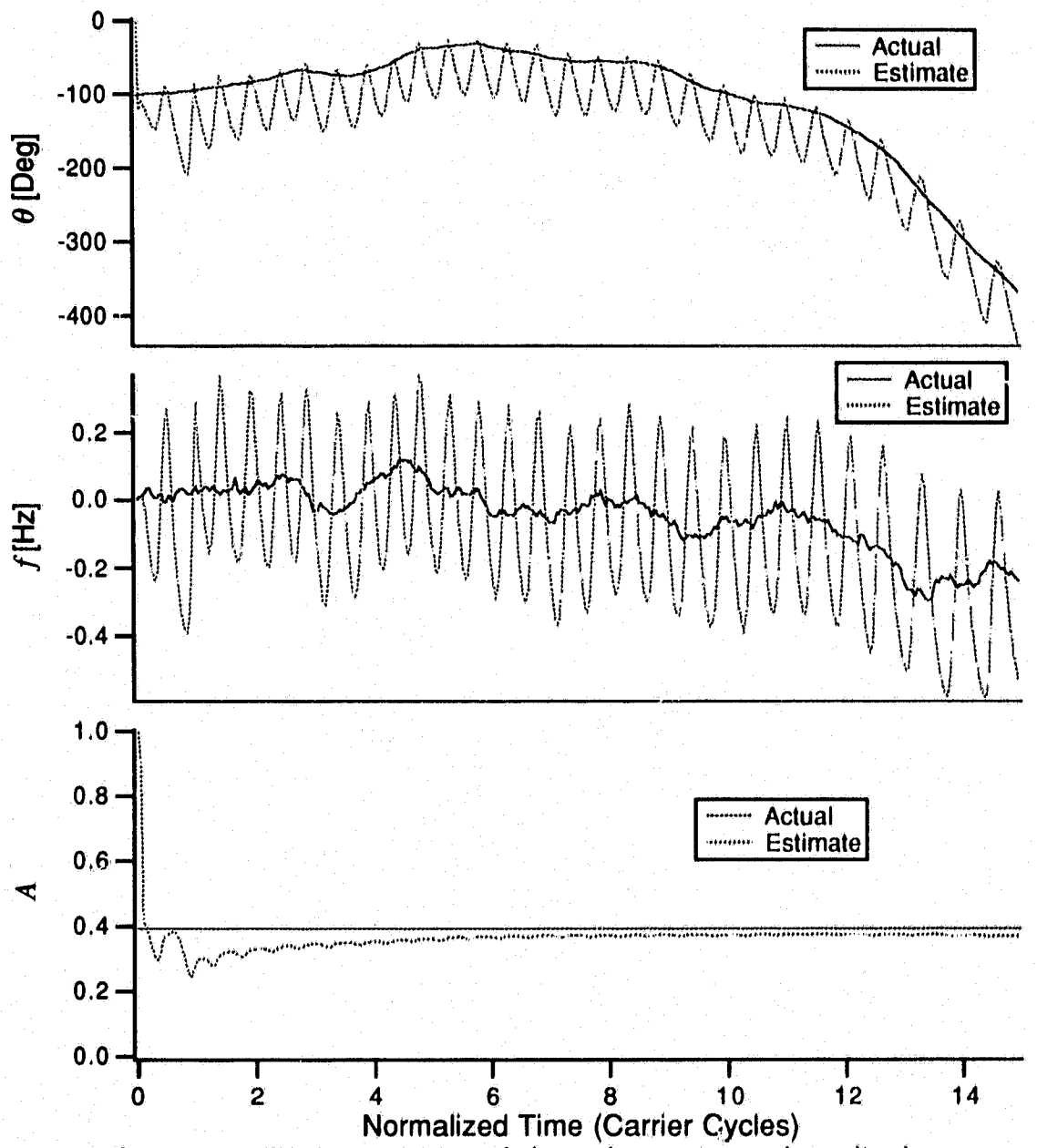

Figure 4–14 DPLL acquisition of phase, frequency, and amplitude.

The same data was processed by the EKF-derived DPLL of Section 2.3.4, the results of which are shown in Figs. 4–14 and 4–15. The increased ripple is due to the double frequency terms that are not completely removed by the loop filter. The DPLL exhibits faster

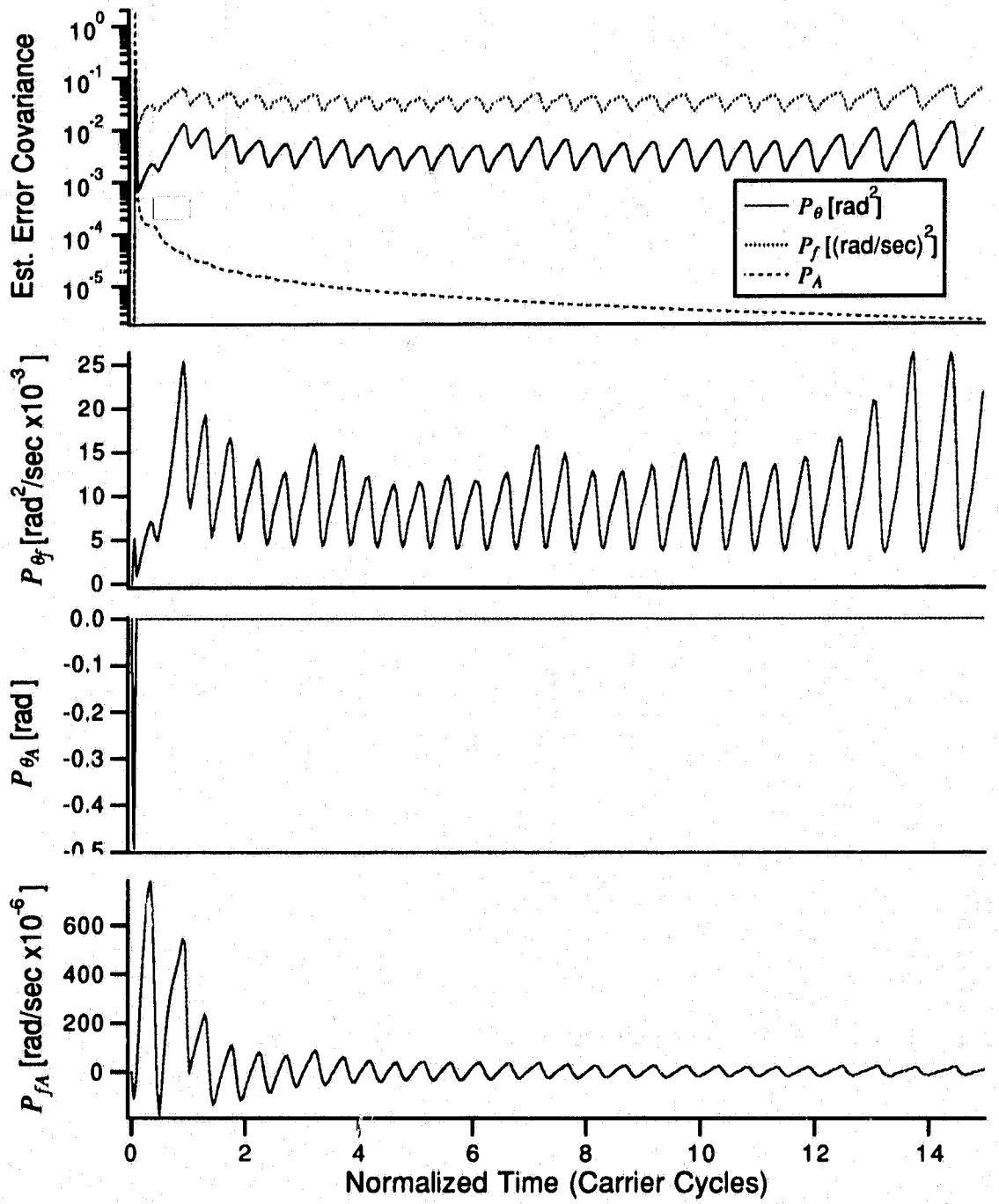

Figure 4–15 DPLL estimator error covariance during phase, frequency, and amplitude acquisition.

acquisition than the EKF from which is was derived, however the estimates of phase and of the amplitude are biased.

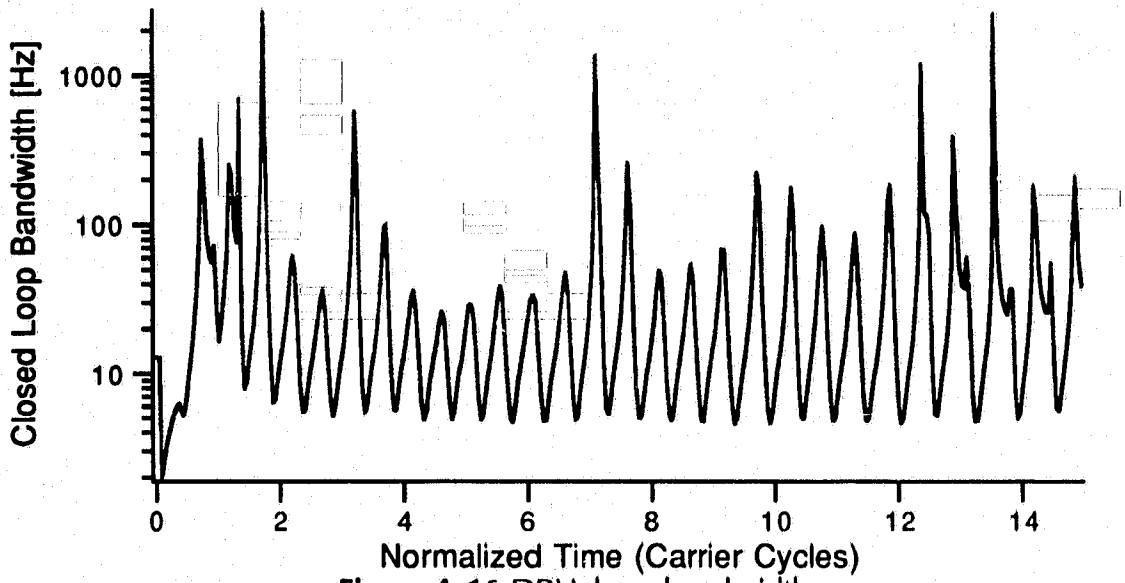

Figure 4–16 DPLL loop bandwidth.

Fig 4–16 shows the loop bandwidth as a function of time where the loop bandwidth is calculated from (4.22). Initially the loop bandwidth is zero since the cross-covariance terms are zero. The loop bandwidth quickly increases during acquisition and then settles down during tracking. The ripple is due to the double frequency terms present in the error covariance matrix.

4.2. Coupled Digital Phase-Locked Loops

With the exception of the work by Bradley [18] and Lagunas [19] neither of which treated acquisition behavior, the literature related to coupled phase-locked loops has remained in the analog world. One of the most complete treatments to date of CPLL acquisition behavior is presented in [14]. Based on the work presented in [13] stability regions for the CPLL system described by coupled nonlinear differential equations were found via computer simulation. Specific cases were simulated: first order loops with continuous wave (CW) interference, first and second order loops with a frequency offset interferer, and second order loops with FM

interferer. The stability regions for these cases were determined resulting in general design guidelines. It was assumed that the carriers are not of equal power.

Of note was a high sensitivity to initial conditions and relatively volatile stability regions. For example, changing a particular loop constraint by less than 10% resulted in an inability of the CPLL to successfully acquire. In their paper a decade later Endo and Chua [56] show that CPLLs operating in a marginal out-of-lock condition exhibit chaotic behavior. One characteristic of chaotic systems is high sensitivity to initial conditions and system parameters [57].

4.2.1. Linear Analysis

Although the DPLLs comprising the CDPLL receiver may individually be linearized, the CDPLL itself cannot. Kumar [36, 37] was able to linearize his receiver because his signal model did not include ACI or CCI, thus no RF coupling was present. Neither Bradley [18] nor Lagunas [19] presented linear analysis of their CDPLLs.

The problem of linearization lies in the RF coupling of the independent sources. Continuing with the derivation of Section 2.3.3., the baseband phase error for the i^{th} estimator from (4.32) is

$$\varphi'_{\theta,i}(k) = \mathbf{c}_{\theta,i}\left[\sqrt{2}A_i\cos\left(\hat{\Theta}_i\right)z(k) - 2A_i\cos\left(\hat{\Theta}_i\right)\sum_{j=1,j\neq i}^{N}A_j\sin\left(\hat{\Theta}_j\right)\right], \tag{4.32}$$

where the measurement from (2.76) is

$$z(k) = \sqrt{2}\sum_{i=1}^{N}A_i\sin\left(\omega_c kT_s + \theta_i(k)\right) + v(k). \tag{4.33}$$

Substituting (4.33) and rewriting (4.32)

$$\varphi'_{\theta,i}(k) = \mathbf{c}_{\theta,i}\left[2A_i\cos\left(\hat{\Theta}_i\right)\sum_{j=1}^{N}A_j\sin\left(\Theta_j\right) + v'_i(k) - 2A_i\cos\left(\hat{\Theta}_i\right)\sum_{j=1,j\neq i}^{N}A_j\sin\left(\hat{\Theta}_j\right)\right] \tag{4.34}$$

where from (B.10)

$$v'_i(k) = A_i\left[v_I(k)\cos\left(\hat{\theta}_i(k\mid k-1)\right) + v_Q(k)\cos\left(\hat{\theta}_i(k\mid k-1)\right)\right]. \tag{4.35}$$

Expanding (4.34) and neglecting double frequency terms yields

$$\begin{aligned}\varphi''_{\theta,i}(k) = \mathbf{c}_{\theta,i}\left[A_i^2 \sin\left(\theta_i(k) - \hat{\theta}_i(k \mid k-1)\right) + v'_i(k)\right] \\ + \mathbf{c}_{\theta,i} A_i \sum_{j=1, j\neq i}^{N} A_j \left[\sin\left(\Theta_i - \hat{\Theta}_j\right) - \sin\left(\hat{\Theta}_i - \hat{\Theta}_j\right)\right]\end{aligned} \tag{4.36}$$

It is evident that the first term is the same as in the single DPLL case as shown in (B.11) of Appendix B. The $\sin(\beta) \approx \beta$ linearizing approximation for high input SNR is valid for the first term. Unfortunately in the CDPLL case, the coupling between the loops, $\sin\left(\Theta_i - \hat{\Theta}_j\right) - \sin\left(\hat{\Theta}_i - \hat{\Theta}_j\right)$ cannot be linearized since the i^{th} and j^{th} sources are uncoupled and small angle approximations cannot be made for either $\Theta_i - \hat{\Theta}_j$ or $\hat{\Theta}_i - \hat{\Theta}_j$. Given this, CDPLLs cannot be linearized.

4.2.2. Tracking Behavior

The tracking behavior of two coupled DPLLs was studied in the previous chapter. Since we have shown that the DPLL may be derived from the EKF realizations of Section 2.3, the simulation study presented in Section 3.3 is in effect the CDPLL operating in tracking mode.

4.2.3. Acquisition Behavior

As previously mentioned, the acquisition behavior will be examined by simulation. We will begin with two FM sources with known amplitude and then include amplitude estimation. In both cases the acquisition of the EKF will be discussed before the EKF-derived CDPLLs.

The EKFs and CDPLLs are initialized as above in (4.28)–(4.31). However, the initial phases of the EKFs and CDPLLs are not all zero as would be expected from (4.28). As discovered in the previous chapter, the states are not observable when the carriers are in phase; initializing the local oscillators with the same phase and frequency would make the state estimated unobservable. Simulation reveals that the EKF is not able to acquire the states if the local oscillators are started in-phase. Therefore the two local oscillators are initialized so that

they have the same frequency but are in quadrature. The message bandwidths are $\alpha_1 = f_c/100$, $\alpha_2 = f_c/200$, $d_{f,1} = d_{f,2} = 1$, the effective sampling rate is $f_s = 25f_c$.

Known Amplitudes

A sample acquisition run for the EKF derived in Section 2.3.4 (see Fig. 2–21) is shown in Fig. 4–17. As shown, the frequencies are acquired and the phases locked within the first cycle and subsequently tracked.

The gains that contribute to state coupling are shown in Fig. 4–18. The gains quickly attain their steady-state value as the states are acquired. The auto-covariances $P_{\theta,1}$ and $P_{\theta,2}$ as well as the phase and frequency cross-covariances *for the same signal* $P_{f,1\theta,1}$ and $P_{f,2\theta,2}$ have a non-zero DC component. However the cross-covariances *between the signals* have zero or near-zero DC component. If these cross-covariance terms are set to zero, the EKF is not able to acquire the states. All covariance terms increase during the periods of low state observability.

As shown in the previous section and in Appendix B, the EKF for an FM signal my be realized by a second-order phase-locked loop with closed loop bandwidth (4.21). Therefore, to a close approximation, (4.22) may be used to approximate the bandwidths of the EKFs. Thus we approximate the closed-loop bandwidth of the i^{th} EKF source estimator as

$$B_{L,i}(k)[Hz] = \frac{1}{2T_s}\frac{2A^2P_{\theta,i}^2(k)R_v^{-1} + \phi_{\theta f,i}P_{f\theta,i}(k) + A^2\phi_{\theta f,i}P_{f\theta,i}(k)P_{\theta,i}(k)R_v^{-1}}{P_{\theta,i}(k)\left(2 - 2A^2P_{\theta,i}(k)R_v^{-1} - A^2\phi_{\theta f,i}P_{f\theta,i}(k)R_v^{-1}\right)}, \tag{4.37}$$

However, the derivation in Appendix B is based on a single DPLL and does not include coupling between DPLLs. The closed-loop bandwidth of a CDPLL requires a linear baseband model which, as previously stated, is not available due to the nonlinear coupling between the DPLLs.

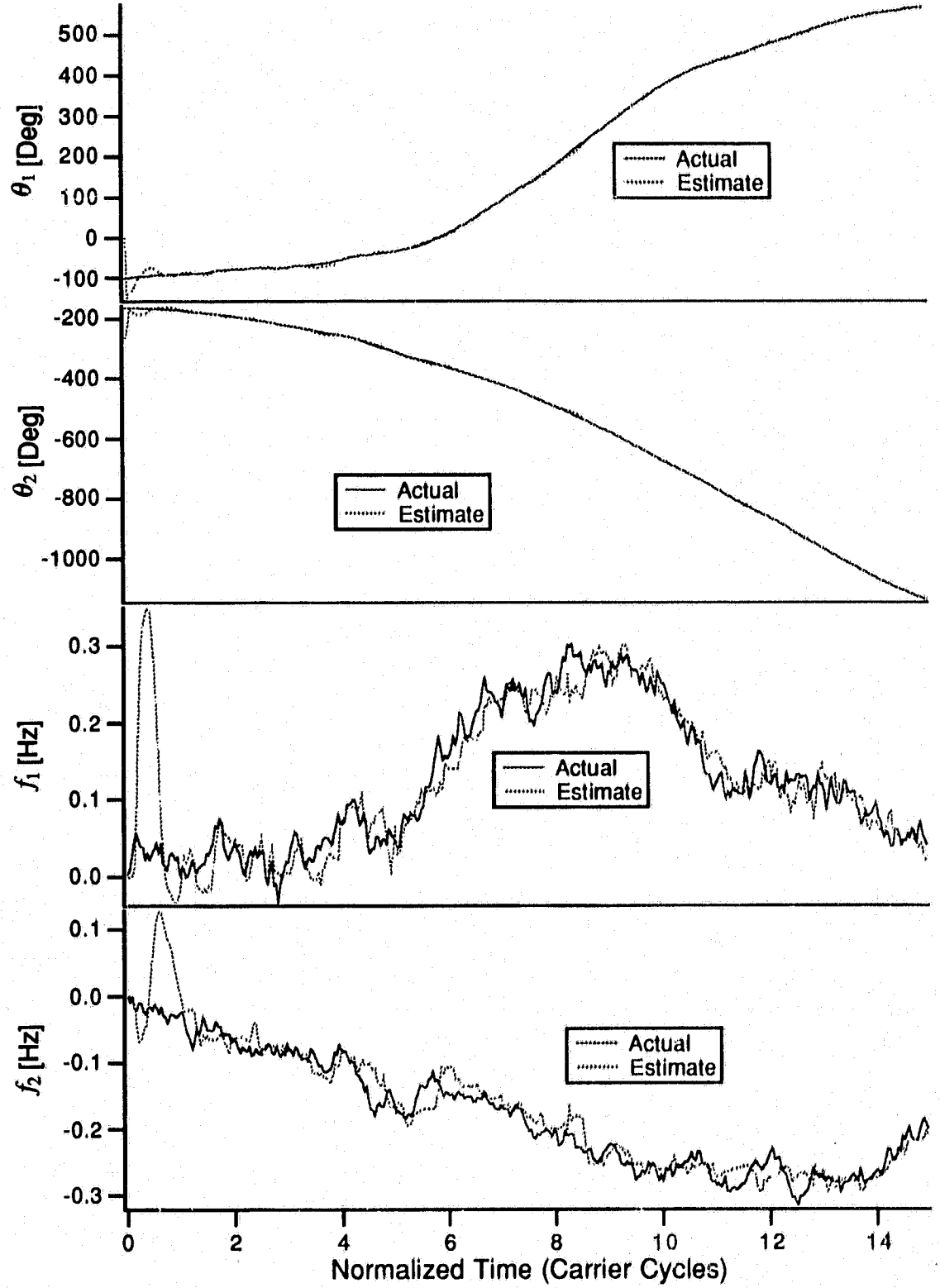

Figure 4–17 State acquisition of two-source EKF.

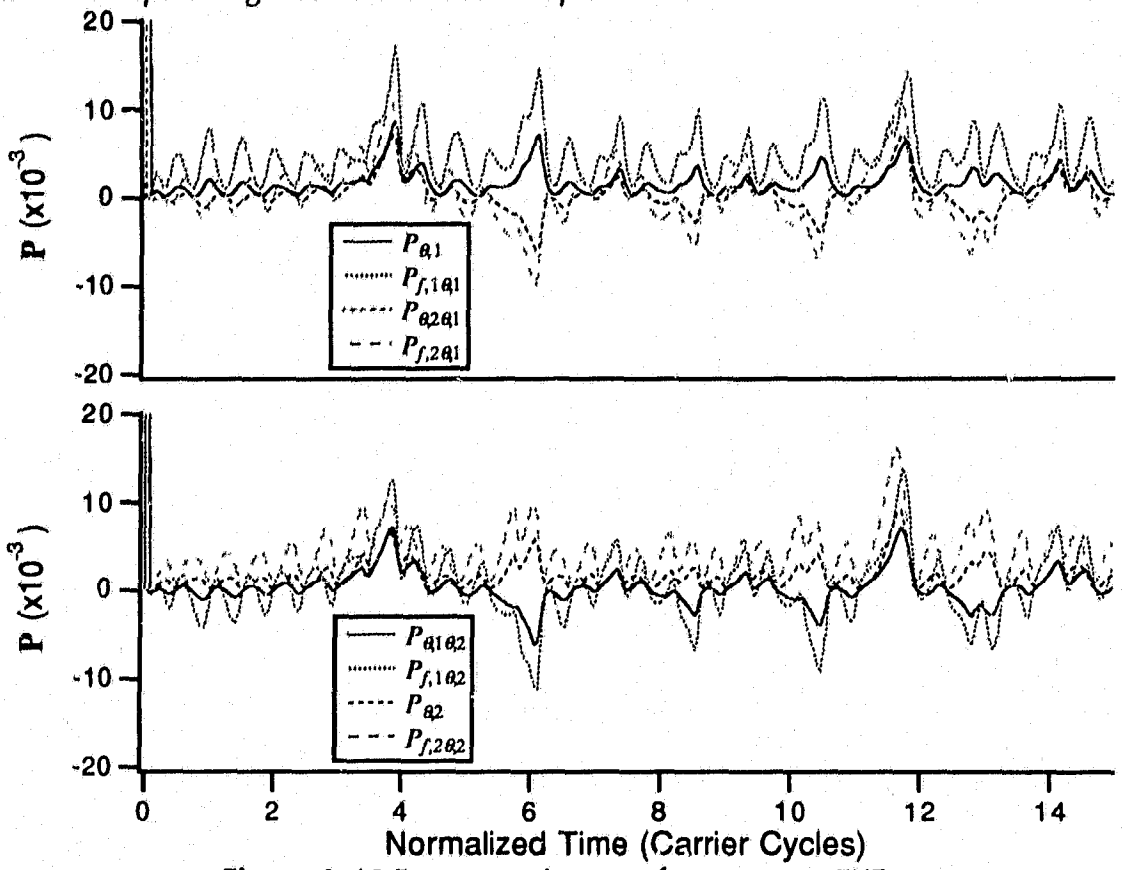

Figure 4–18 Error covariances of two-source EKF.

In Fig. 4–19, the carrier phase difference and the EKF closed loop bandwidths are shown. In Chapter 3 it was shown that the estimation error covariance increased as the carrier phases moved to in-phase and anti-phase condition. By use of (4.22) it is revealed that the closed loop bandwidths decrease during these periods of low observability. This is due to the greater weight put on the state predictions as opposed to the state measurements. By reducing the closed loop bandwidth, the EKF is rejecting the majority of the input, which it sees as noise, and follows the state predictions. In this manner the EKF is better able to "track" the states when they are not observable. Also shown in Fig. 4–19 the closed loop bandwidths are greater just before and just after the interval of low observability. This is a very desirable behavior for the DPLL since the closed-loop bandwidth is directly related to the acquisition and lock-in ranges of the DPLL. Since the DPLL must re-acquire the states at

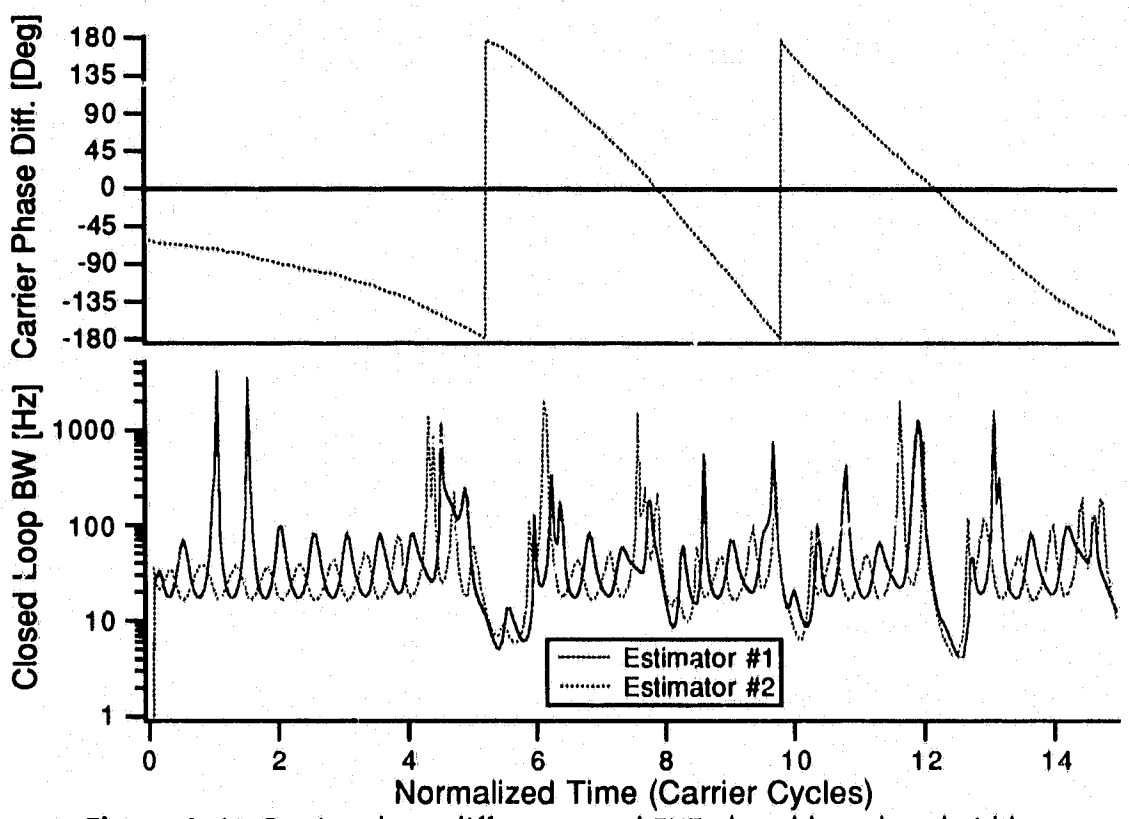

Figure 4–19 Carrier phase difference and EKF closed loop bandwidths.

the end of these unobservable periods, a wide loop bandwidth increases the loops' acquisition and lock ranges.

So far we have examined the acquisition behavior of the EKF. Similar simulation with the resulting EKF-derived CDPLL revealed that it rarely, if ever, was able to acquire the states. There are two differences between the EKF and its derived CDPLL: 1) the loop filter and 2) the input to the phase detectors. The loop filters differ by a lossy integrator in the EKF, $\left(1-\phi_f z^{-1}\right)^{-1}$ being replaced by a perfect integrator in the CDPLL, $\left(1-z^{-1}\right)^{-1}$. This is valid since for practical values of α, $\phi_f \approx 1$. Simulation of the EKF using the perfect integrator shows very little difference when compared to using the lossy integrator. Thus the reduced loop filter is not the culprit in the CDPLL's inability to correctly estimate the states. This leaves the inputs to the phase detectors as the problem's source.

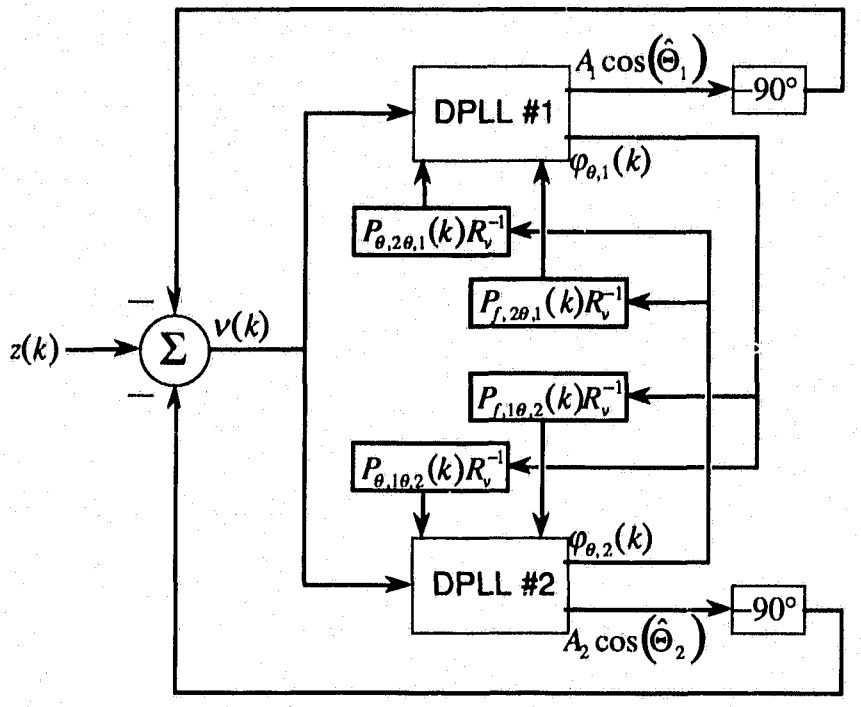

Figure 4–20 Simplified block diagram of "new" CDPLL structure.

As discussed in Section 2.3, the innovations process from the EKF may be simplified by neglecting the double frequency terms present in the innovations process as they will be removed by the loop filter. However, as shown in Fig. 4–19, the closed loop bandwidth, which is a function of the bandwidth of the loop filter, is dynamic especially during acquisition. Thus, neglecting the double frequency terms during acquisition may not be valid in the case of multiple sources. This poses little problem actually. The EKFs may still realized by DPLLs, however the input to the phase detector of each DPLL becomes the EKF innovations process, that is $z(k)-h(\mathbf{x}(k\,|\,k-1),k)$, unlike the case of Fig. 2–16 where a different phase detector input is created for each DPLL. A simplified block diagram of this new CDPLL is shown in Fig. 4–20. This is functionally the same as the EKF.

Unknown Amplitudes

The final situation is the case where phase, frequency, and amplitude of two FM sources are to be estimated. The phase and frequency estimation are handled as above. The amplitude

estimated differs from the single DPLL case in that the χ_1^2 random carrier amplitude is replaced by specific amplitude ratios; in this case $A_1 = A_2 = 1$. This facilitates acquisition study for a controllable range of interference levels. The initial estimate of carrier amplitude is zero for all cases. The initial error covariance for the amplitude estimate is set equal to the measurement noise covariance R_v.

Fig. 4–21 shows the state estimates for a sample run. Here it is evident that the state estimates "flipped" twice during the 30 carrier cycles. Initially each DPLLs lock onto the "wrong" source; that is DPLL #1 acquires source #2 and visa versa. In Fig. 4–22 the amplitude estimates show that A_2 is accurately estimated during this time while A_1 is much less so. The state estimates "flip" during the fifth carrier cycle and DPLL #1 tracks source #1. During this time the amplitude estimates jump to 80% of their actual value and then slowly approach their true value. The phase and frequency state are tracked until the fifteenth carrier cycle when they "flip" again. During the initial acquisition, the first two carrier cycles, the auto and cross-covariances are quite high as shown in Figs. 4–23 and 4–24. The covariance terms related to amplitude quickly drop to zero as the amplitudes are correctly estimated and provide little coupling after the first five carrier cycles. The covariance terms related to phase and frequency remain quite active especially during the periods of low state observability. This is reflected in the reduced closed loop bandwidths during these times as evidenced by Fig. 4–25.

The closed loop bandwidths of Fig. 4–19 differ slightly from those of Fig. 4–25. In the case of the former, the carrier amplitudes are a known constant and the closed loop bandwidth is given by (4.37). However, in the case of the latter the amplitude is an unknown constant and (4.37) becomes

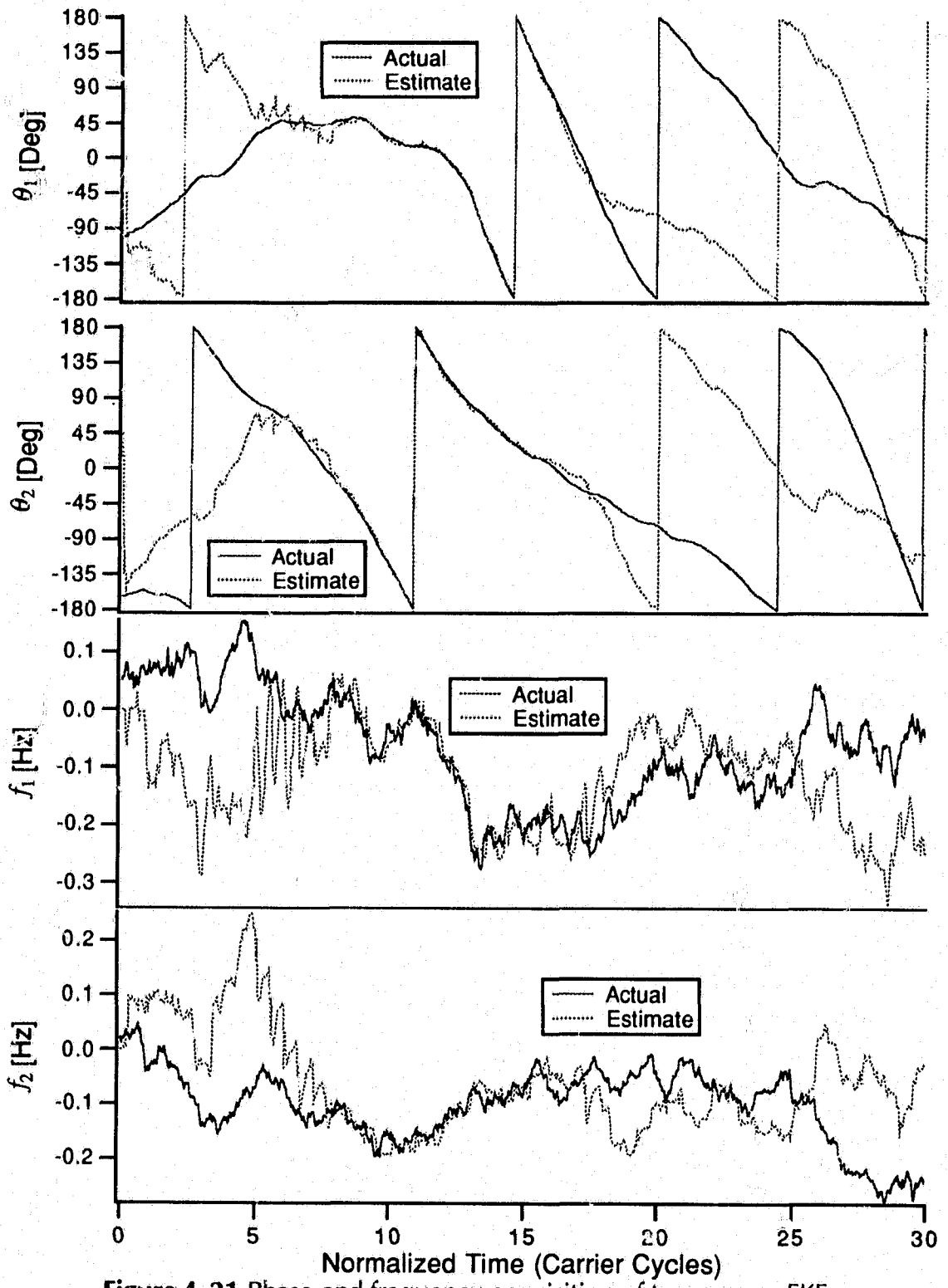

Figure 4–21 Phase and frequency acquisition of two-source EKF.

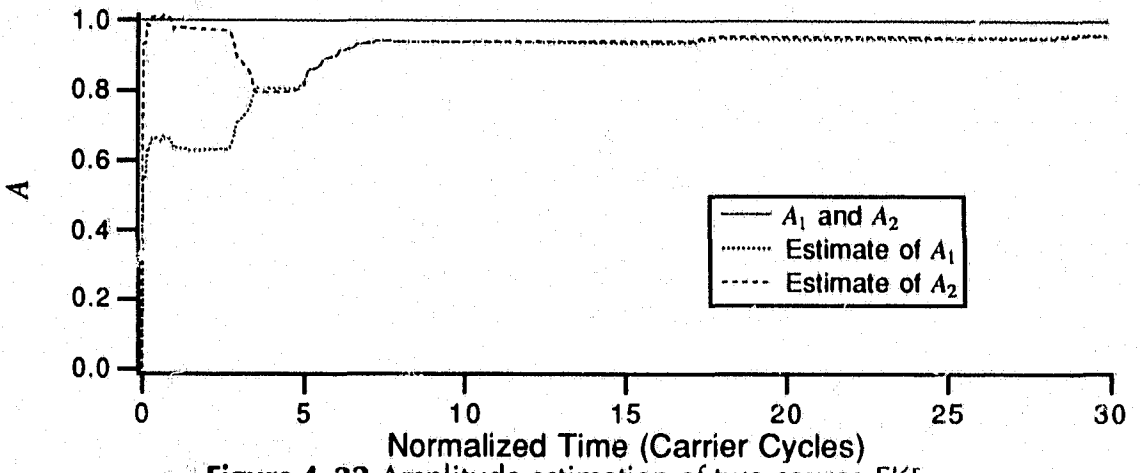

Figure 4–22 Amplitude estimation of two-source EKF.

$$B_{L,i}(k)[Hz] = \frac{1}{2T_s}\frac{2A_i\hat{A}_iP_{\theta,i}^2(k)R_v^{-1} + \phi_{\theta f,i}P_{f\theta,i}(k) + A_i\hat{A}_i\phi_{\theta f,i}P_{f\theta,i}(k)P_{\theta,i}(k)R_v^{-1}}{P_{\theta,i}(k)\left(2 - 2A_i\hat{A}_iP_{\theta,i}(k)R_v^{-1} - A_i\hat{A}_i\phi_{\theta f,i}P_{f\theta,i}(k)R_v^{-1}\right)}, \tag{4.38}$$

where $\hat{A}_i = \hat{A}_i(k \mid k-1)$.

4.2.4. Acquisition Performance

An important performance measure from the world of phase-locked loops is the time to phase lock or the acquisition time. By definition, phase-lock occurs when the phase error is zero [10]. However, when used as a demodulator, the phase error contains the message process and will thus never be zero. According to Gupta, "the acquisition time or lock time is the time before the system stops skipping cycles" [24].

Although this appears to be a simple statistic to measure, it becomes much less so when dealing with CDPLLs and their simulation. The source (state) model and its resulting EKF estimator include the instantaneous frequency as a state and it is assumed in the derivation that the source and the estimator are operating at the same carrier frequency. Although the states of the CDPLLs are initialized with random phase and frequency, the local oscillator is initially at the same frequency as the source. Therefore when the first sample is processed by the estimator, there is no Doppler frequency offset between the source and the local

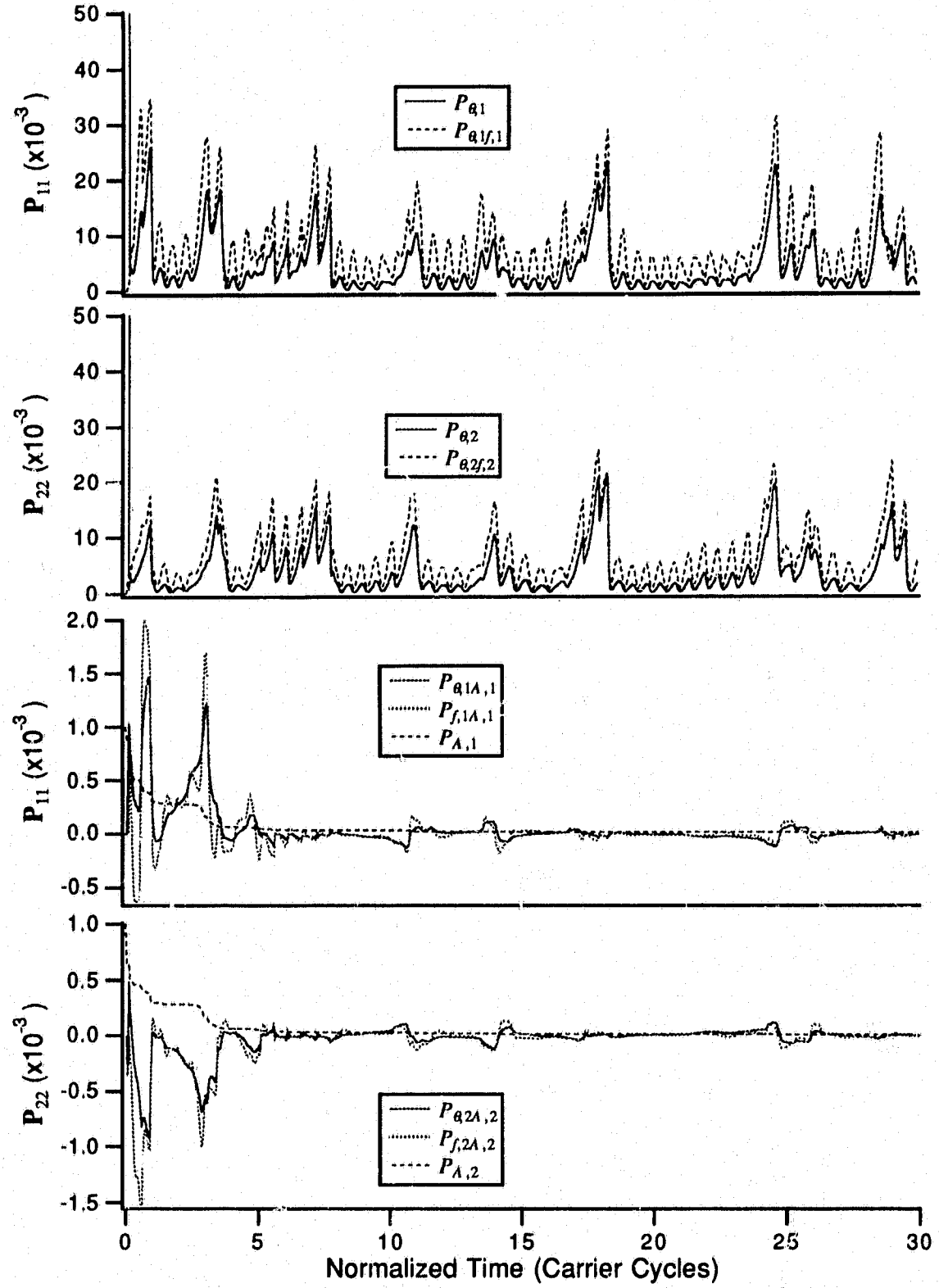

Figure 4–23 Error auto-covariances of two-source EKF with amplitude estimation.

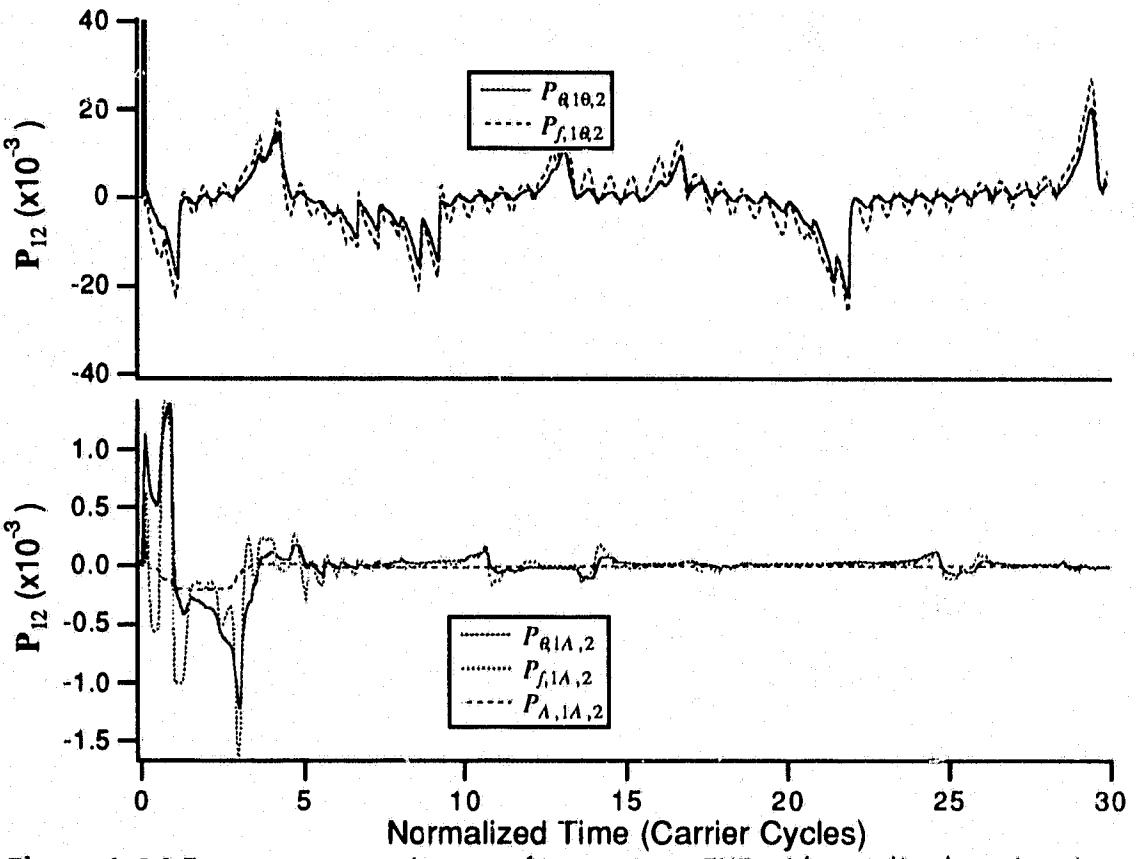

Figure 4–24 Error cross-covariances of two-source EKF with amplitude estimation.

oscillator. Since the phase is a function of the frequency state, the local oscillator may drift with respect to the source after this first sample. Therefore cycle slipping during initial acquisition is not exhibited in the simulations; the CDPLL either "acquires" within the first two samples or fails to acquire. However, slipping may be exhibited if the CDPLLs lose lock as may happen during a period of low state observability. Also as previously mentioned the DPLL may acquire and track the "wrong" signal and "flip" these estimates with time. From the simulation standpoint this makes it difficult to declare if the DPLL has acquired the signal since, we do not know which signal it acquired.

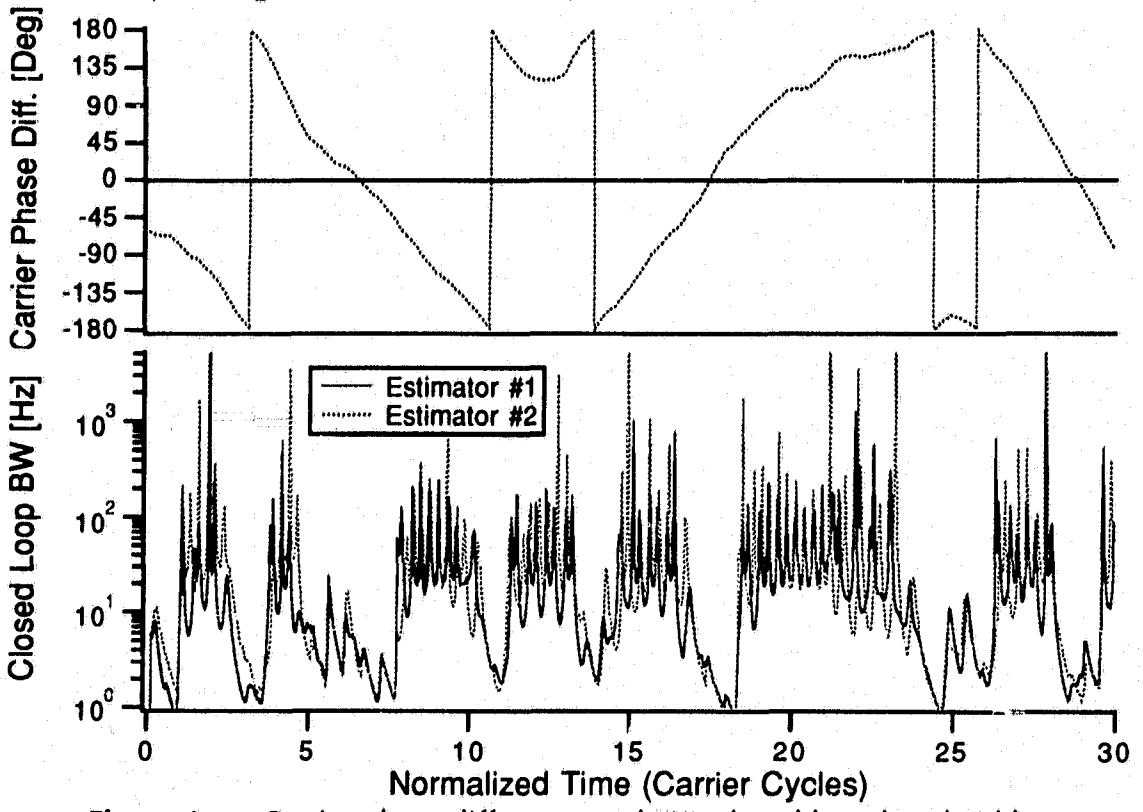

Figure 4–25 Carrier phase difference and EKF closed loop bandwidths.

To provide some investigation into the acquisition behavior, we examine some statistics which are not common in the DPLL world but will shed some light on the CDPLLs ability to acquire the sources. We first estimate the probability of phase lock by examining the phase error of each DPLL for each cycle of the carrier; if the change in phase error is less than π radians for the duration of the carrier cycle, phase lock is declared for that cycle. Similarly the probability of frequency acquisition is estimated by examining the frequency error for each carrier cycle; if the frequency error is less than the frequency deviation d_f, frequency lock is declared. For each of the 500 runs, the percentage of time that the DPLL is locked is recorded.

The results for the case where joint phase, frequency, and amplitude is presented; the results for known carrier amplitude were very similar.

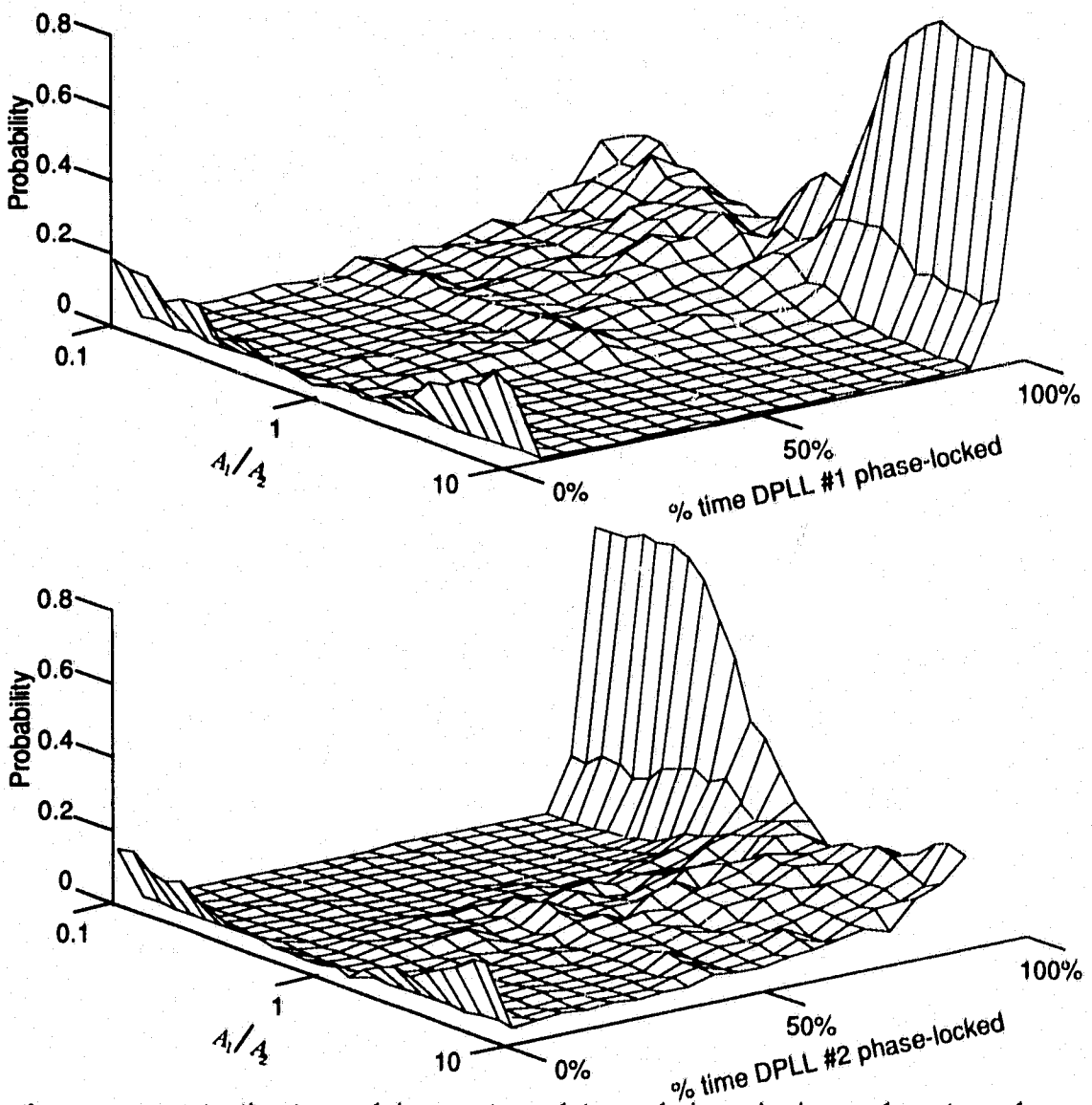

Figure 4–26 Distributions of the portion of time of phase lock as a function of carrier amplitude ratio.

Fig. 4–26 shows the normalized histograms of the portion of time that the DPLLs were phase-locked as a function of carrier amplitude ratio. For example, the case when source #1 is 20 dB stronger than source #2 ($A_1/A_2 = 10$) shows that in about 80% of the runs DPLL #1 was phase locked at least 95% of the time. It also shows that nearly 20% of the time DPLL #1 was not able to lock at all. In general the DPLLs are better able to lock on the stronger source.

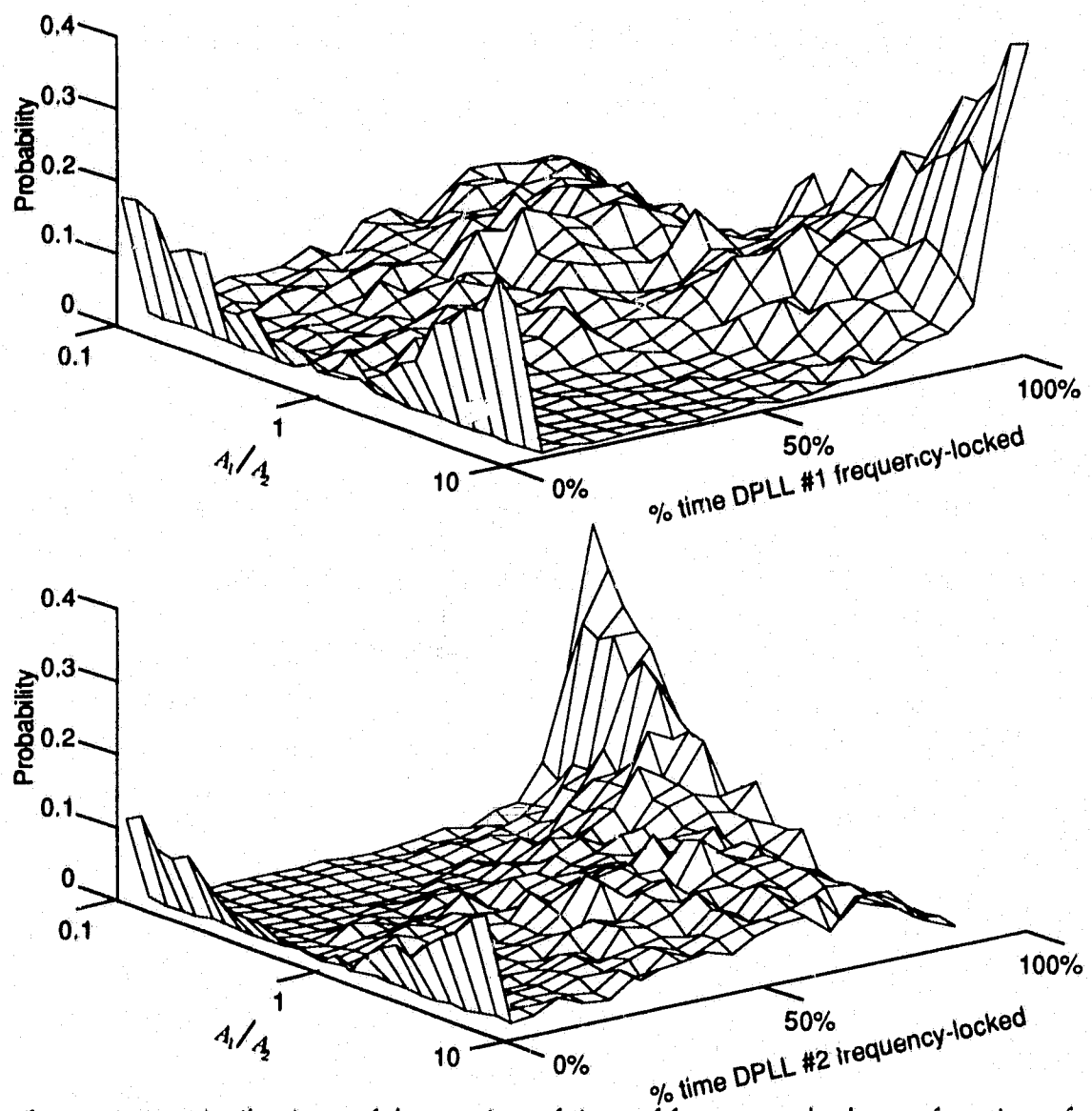

Figure 4–27 Distributions of the portion of time of frequency lock as a function of carrier amplitude ratio.

Fig. 4–27 shows the normalized histograms of the portion of time that the DPLLs were frequency-locked as a function of carrier amplitude ratio. When $A_1/A_2 = 10$ DPLL #1 was frequency-locked least 95% of the time in about 40% of the runs. It again shows that nearly 20% of the time DPLL #1 was not able to frequency lock at all. As the power of the interfer-

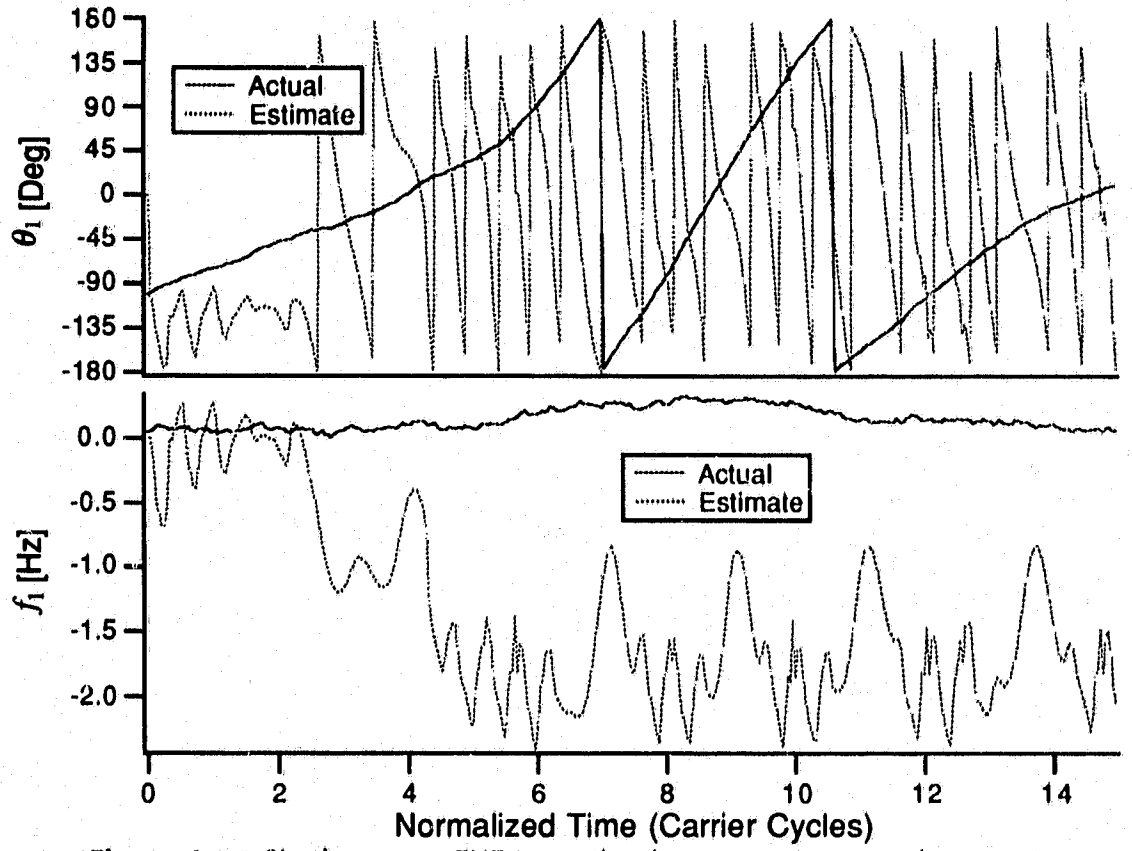

Figure 4–28 Single source EKF operating in a two source environment.

ing carrier increases the frequency estimation error increasing causing the loop to fall out of frequency lock more often.

4.2.5. Signal Improvement

The final, but perhaps the most important, performance measure that we examine is how well the new system separates and tracks the signals. In Chapter 3 we examined the ability of the EKF to separate the signals by looking at the state error covariance as a function of message process bandwidth and carrier amplitude. Here we will examine the improvement of the EKF CDPLL over a single EKF derived DPLL operating in the same multi-source environment.

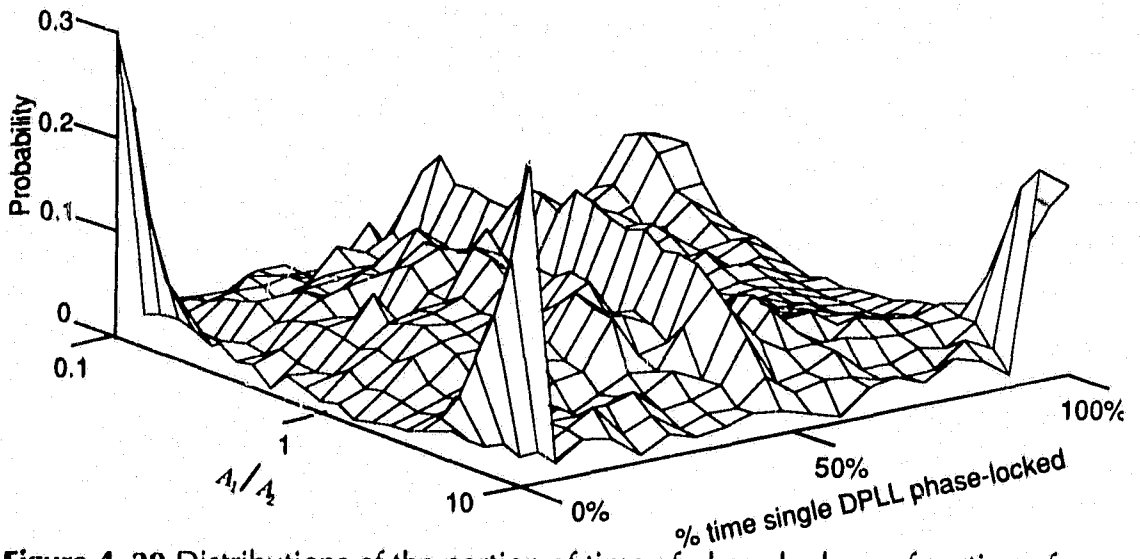

Figure 4–29 Distributions of the portion of time of phase lock as a function of carrier amplitude ratio for single DPLL.

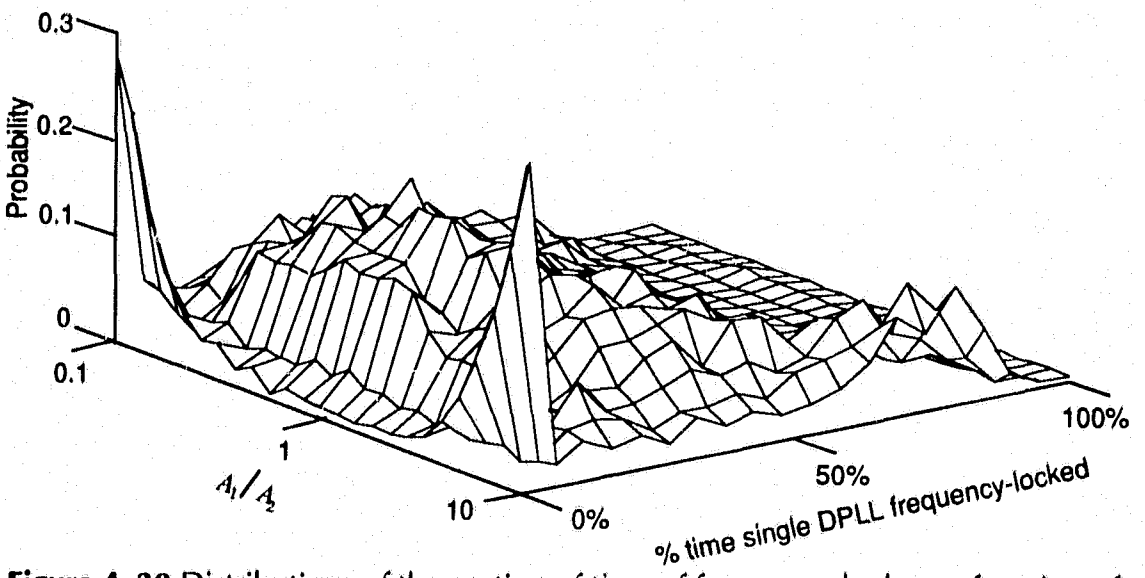

Figure 4–30 Distributions of the portion of time of frequency lock as a function of carrier amplitude ratio for single DPLL.

Simple qualitative analysis shows that the single source EKF is not able to acquire either of the two sources. Fig. 4–28 shows that the single source EKF is not able to accurately estimate the phase or the state when operating on the same signals as in Fig. 4–17 where the multi-source EKF was able to separate the signals. This is also reflected in the acquisition be-

havior. Fig. 4–29 shows the portion of time the DPLL is in phase lock and Fig. 4–30 shows the portion of time the DPLL is in frequency lock. Comparison of Figs. 4–29 and 4–30 to Figs. 4–26 and 4–26 shows that the single DPLL operating in a multi-source environment is much less able to acquire the desired signal.

A more quantitative analysis uses the level of improvement of the multi-source EKF over the single source EKF. The improvement is defined as

$$\text{signal improvement} = \frac{\text{MSE of DPLL}}{\text{MSE of CDPLL}}, \tag{4.39}$$

where in the simulations, the EKF is used to implement the DPLLs. This removes any post-filtering required to remove the double frequency terms present after the loop filter. Also, the new CDPLL uses the EKF's innovations process (see Fig. 4–20) so the same advantage is given to the single DPLL operating in the multi-source environment.

Fig. 4–31 shows the state estimate improvement of the two source EKF over the single source EKF as defined in (4.39). The most useful measure of the improvement of the CDPLL over the DPLL is that of the frequency state as this is the information bearing signal that is the final output of the receiver. Over the 40 dB carrier power ratio, the CDPLL provides at least 20 dB of signal improvement over the DPLL. Maximum improvement appears when the interfering carrier is about 10 dB less than the desired carrier. The phase improvement appears somewhat marginal, however this is primarily due to the modulo-2π nature of the phase and the resulting phase error.

Initially disconcerting is the rapid fall-off of improvement as the carrier amplitude ratio increases. This is due to the capture effect of the DPLL. When $A_1/A_2 < 1$ the single DPLL tends to capture the stronger signal (signal #2, the "wrong" signal) and thus estimates its amplitude. The CDPLL is able to estimate each source and each sources' amplitude; thus the improvement in amplitude estimation is quite high. However as A_1/A_2 increases, the single DPLL begins capturing the "correct" signal and thus estimating the correct amplitude result-

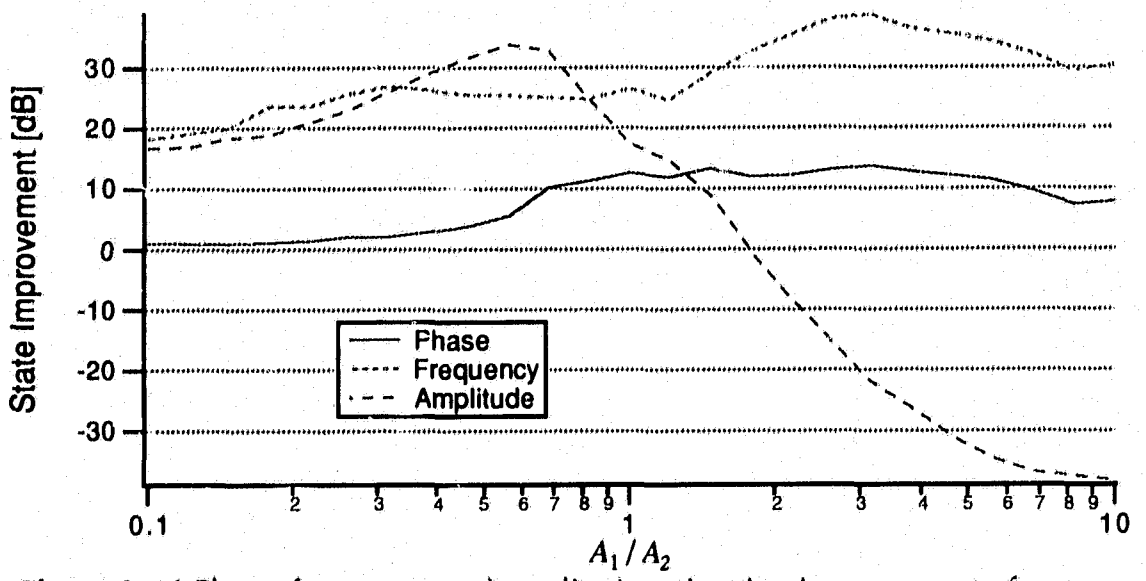

Figure 4–31 Phase, frequency, and amplitude estimation improvement of new estimator.

ing in a reduction of the amplitude improvement. When $A_1/A_2 > 1$ the single DPLL captures and estimates the "correct" single most of the time and correctly estimates its amplitude. As previously shown, the CDPLL tends to "split" the amplitude estimate between the two DPLLs. Although the CDPLL is correctly tracking each of the signals, the amplitude estimates may not be extremely accurate resulting in the state estimate degradation of 4–31.

As mentioned in Chapter 3, there is a difficulty in accurately measuring the state estimation error for the two source EKF due to the "state flipping." In the above simulations, the estimation error for each condition (source #1 tracked by estimator #1 and source #1 tracked by estimator #2) was calculated and the lesser was used in the MSE calculation. This takes into account the case where source #1 is always tracked by estimator #2 (and vice versa) however if the state estimates flip multiple times, the estimation error is artificially inflated.

4.3. Dynamic Source Enumeration

The main issue of this dissertation deals with multiple signals in a common, or nearby, channel. Thus an important issue is the number of signals in the channel. The previous

chapter deal mainly with two co-channel signals. However the number of sources *actually* present is often unknown. Therefore it is important to be able to quantify the co-channel signal multiplicity.

It is doubtful that the number of sources in a channel remain fixed with time. For example, if the sources are mobile phones, they will be moving from cell to cell and thus the number of sources may vary considerably with time. Thus it is desirable to investigate the effect on the derived estimators of sources "appearing" and "disappearing" with time.

In the preceding chapter various EKF-based estimators were derived for specific problem scenarios. This treatment assumes *a priori* knowledge of the number of co-channel signals present. There are many applications where this information is not available. Since the estimator structures derived this far assume *a priori* knowledge of the co-channel signal multiplicity, using these estimators three possible scenarios exist:

Scenario 1 There are more co-channel signals than for which the estimator is designed.

Scenario 2 There are the same number co-channel signals than for which the estimator is designed.

Scenario 3 There are fewer co-channel signals than for which the estimator is designed.

The first difficulty is deciding what constitutes a signal's presence in a channel. This decision may be based in the level of interference a signal is introducing, or its SIR. Since the SIR is a continuous function of amplitude ratio and spectral proximity, arbitrary thresholds need to be established before a particular signal is included as an interfering signal. The choice of a threshold depends on the specific application. An example in digital radio would be to look at the Bit Error Rate (BER) introduced by a particular source and declare that source to be an interferer if the BER exceeds a certain level.

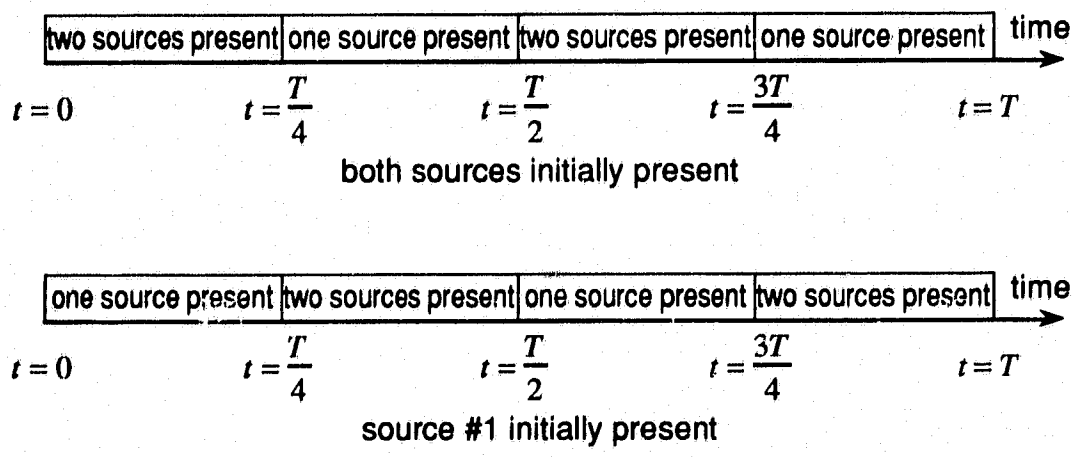

Figure 4–32 Channel multiplicity as a function of time.

We set up the two signal EKF of Section 3.3.7 (that is phase, frequency, and amplitude estimation) for two cases:

Case 1 both signals are present for only part of the time (Scenario 3).

Case 2 both signals are present all of the time (Scenario 2).

Case 2 corresponds to the two-source analysis that has been presented thus far. Case 1 corresponds to times when the "second" signal is not present in the channel. Switching the source off and on is accomplished by setting the states to zero for times when the signal is not present. The two-source EKF operates on a received signal that contains two sources one-half of the time and one sources the rest of the time (see Fig. 4–32). Two possibilities exist: one is that both signals are present initially and the other is where only one signal is present at start and the second appears later.

The estimator is first run for the case where the two signals are always present as a basis for comparison (see Figs. 4–33 and 4–34). In this case the EKF is able to acquire the states

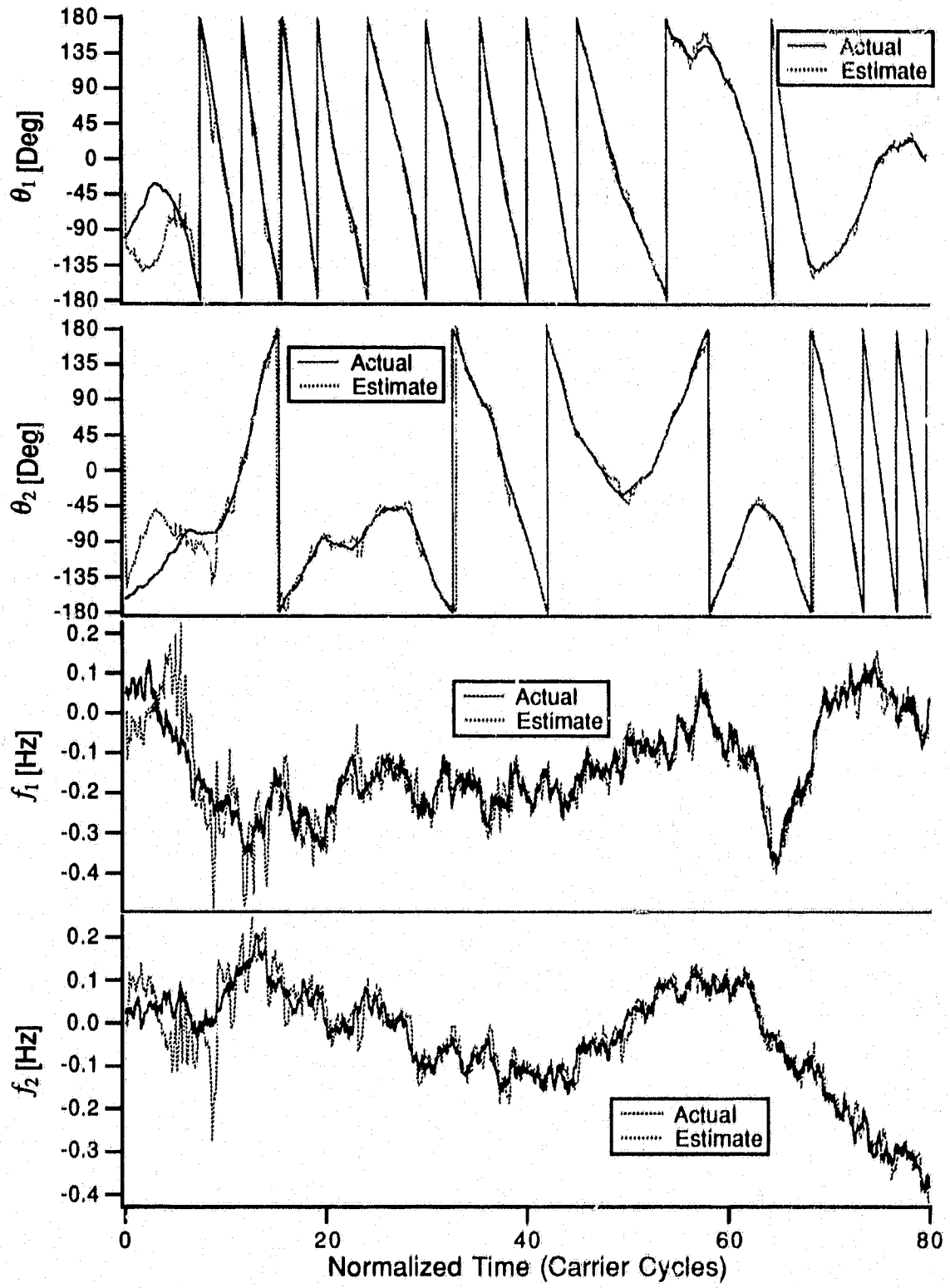

Figure 4–33 Phase and frequency estimates when both sources always present.

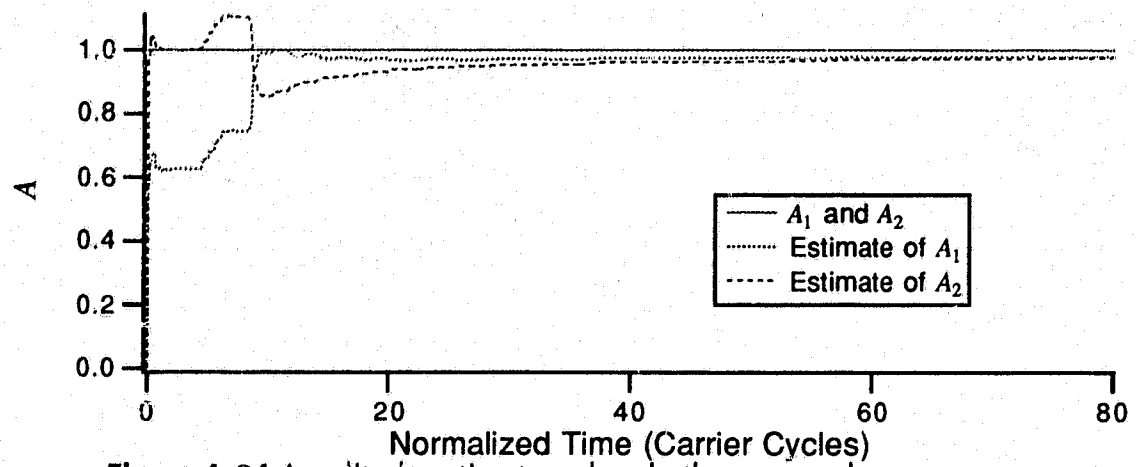

Figure 4–34 Amplitude estimates when both sources always present.

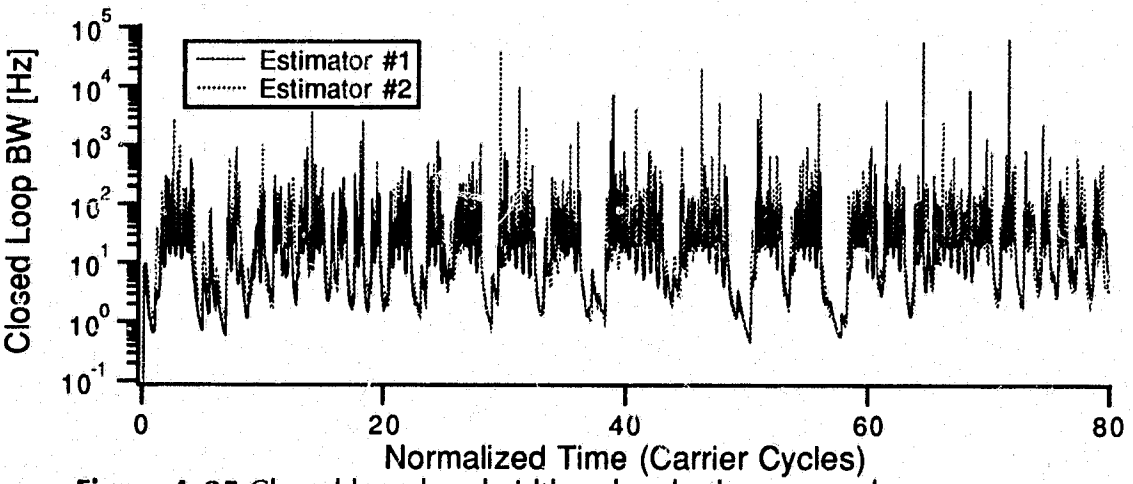

Figure 4–35 Closed loop bandwidths when both sources always present.

within 10 cycles and track them for the remainder of the run. Fig. 4–35 shows the closed loop bandwidth of each DPLL. As previously discussed, the bandwidths decrease when the carrier are in phase but have a "constant" average value for the remainder of the time.

The estimator then operates in the environment where both signals are initially present but then source #2 disappears and reappears as shown in Fig. 4–32. Fig. 4–36 shows the phase and frequency states and Fig. 4–37 shows the amplitude when source #2 is turned off during time 20–40 and 60–80. Since both signals are present from times 0–20, Figs. 4–36 through 4–38 are the same as Figs. 4–33 through 4–35 for this interval. As soon as source #2

disappears the behavior changes drastically from the case where both signals are always present. When source #2 disappears, phase and frequency lock of source #1 immediately is lost and neither is regained until well after source #2 reappears. Examination of Fig. 4–37 shows that the estimator is not able to "track" the changing amplitude. This is due to the model of the carrier amplitude which is simply a random constant. Thus the EKF does not expect the amplitude to change once it has been estimated. Therefore for the estimator to handle time-varying signal multiplicity, the amplitude model must be changed to reflect the time-varying nature of the carrier amplitude in this environment.

Looking back at Fig. 4–36, it may be seen that the estimator is able to reacquire the phase and frequency states for each source at approximately time 50. At time 60 the second source disappears again but this time source #1 is still tracked. Interestingly enough, the estimator for source #2 also tracks source #1 during this time.

Probably the most important discovery made from this experiment is the effect of time varying signal multiplicity on the closed loop bandwidths of the estimators (see Fig. 4–38). During the intervals where only one source is present the closed loop bandwidth of the second source's estimator is substantially reduced. This is a reflection of the increase in the error covariance during these times. The importance of this discovery lies in its possible use as a "detector" which would indicate if redundant estimators are present.

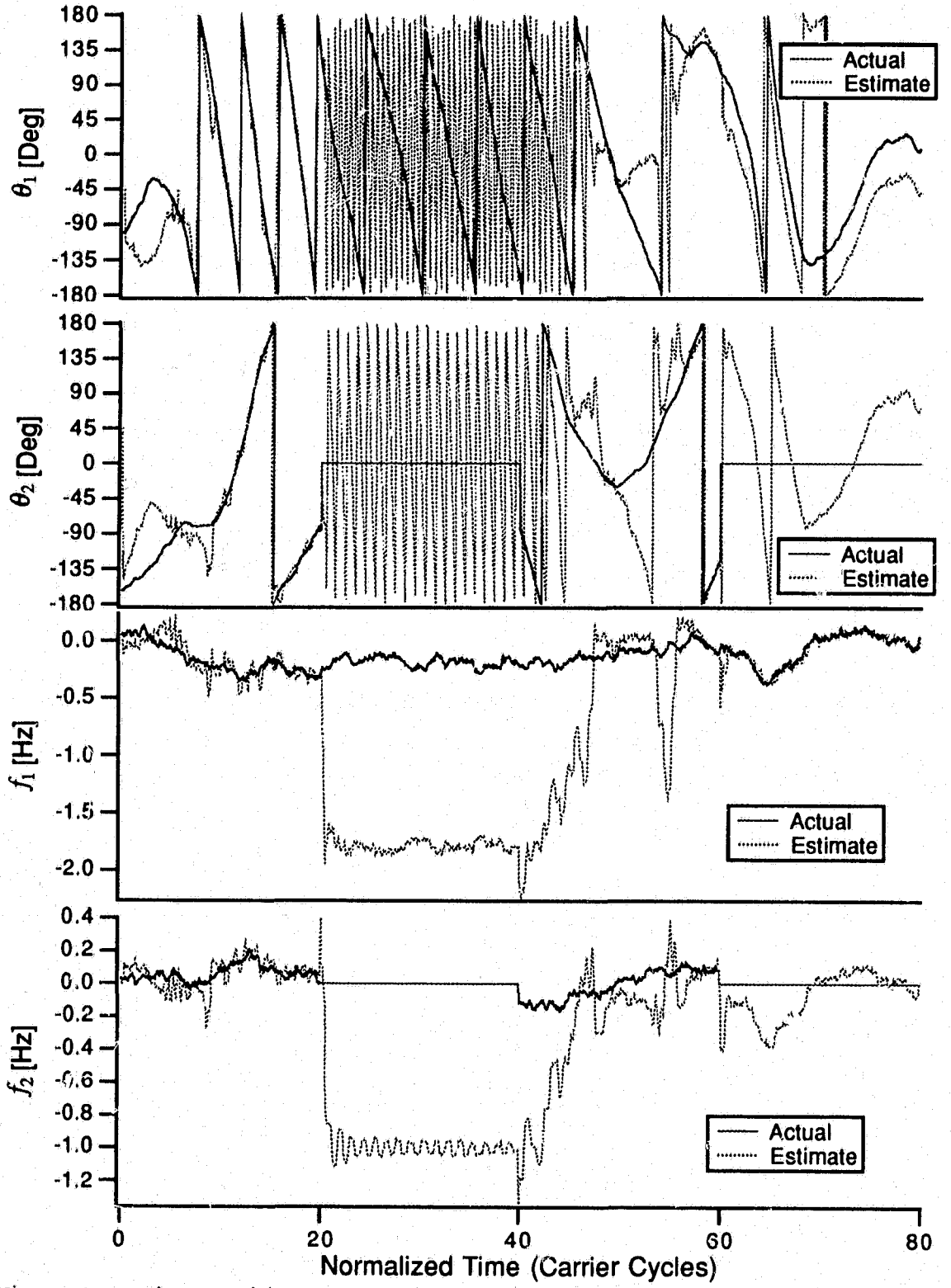

Figure 4–36 Phase and frequency estimates when both sources are initially present.

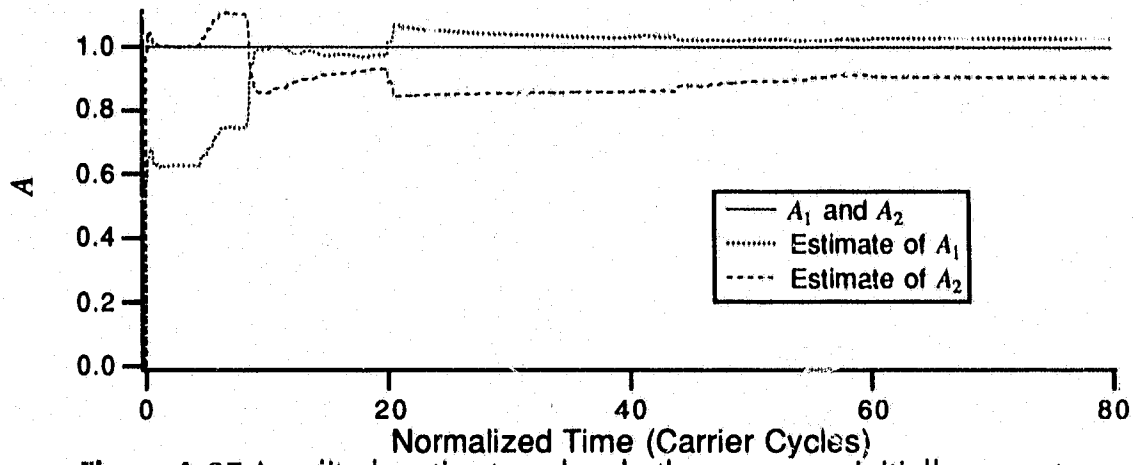

Figure 4–37 Amplitude estimates when both sources are initially present.

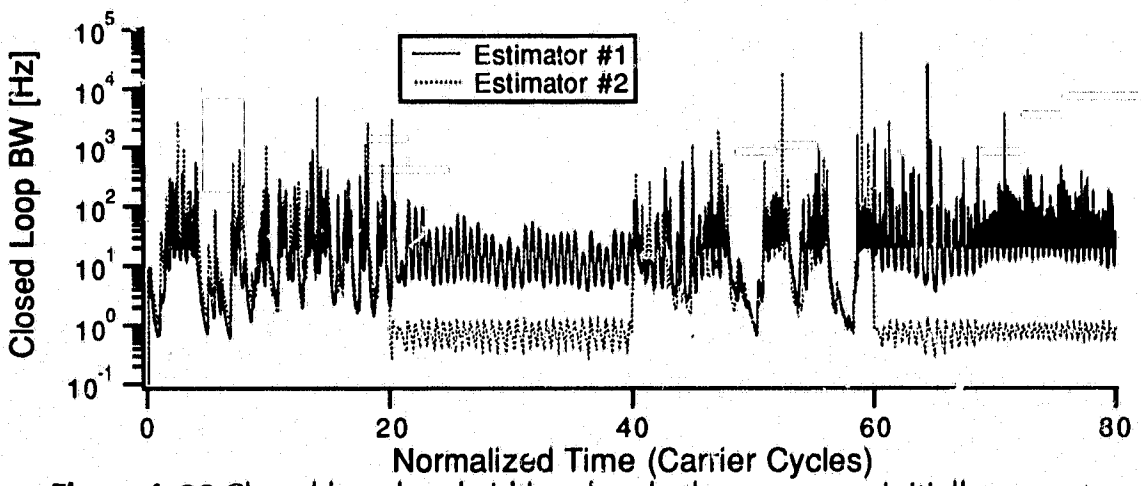

Figure 4–38 Closed loop bandwidths when both sources are initially present.

As a final experiment the estimator operates in an environment where only one source is present initially and then the second one appears. Looking at the state estimates (Fig. 4–39) shows that source #1 is successfully acquired and tracked by *both* estimators for the interval 0–20. Fig. 4–40 shows that with only one source present during acquisition, the amplitude estimator is not able to determine that only one signal exists and "splits" the amplitude between the two estimates.

When source #2 appears at time 20 both estimators are able to maintain phase lock on each signal, however the phase error is increased. At about time index 35 frequency lock is

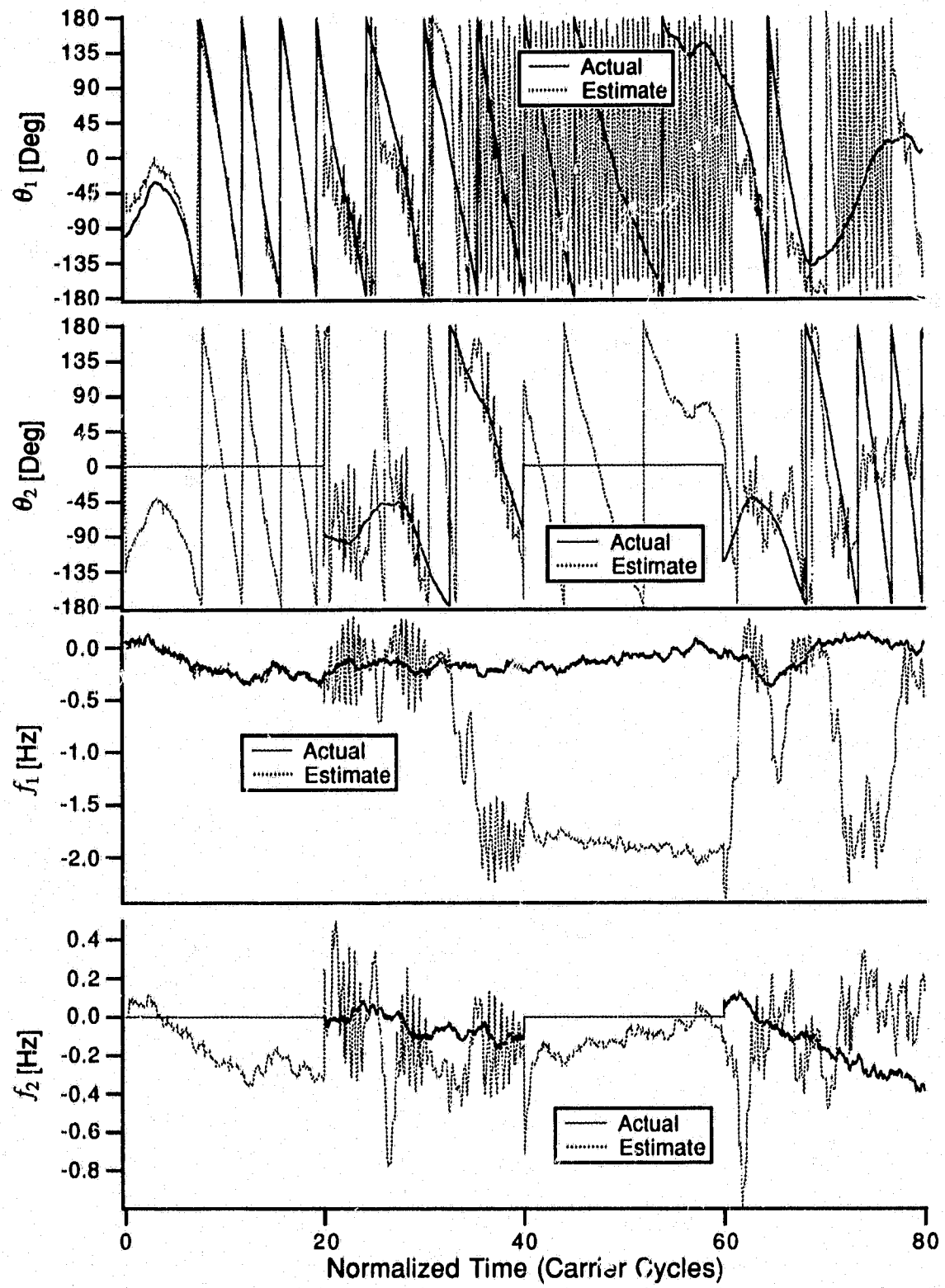

Figure 4–39 Phase and frequency estimates when only source #1 is initially present.

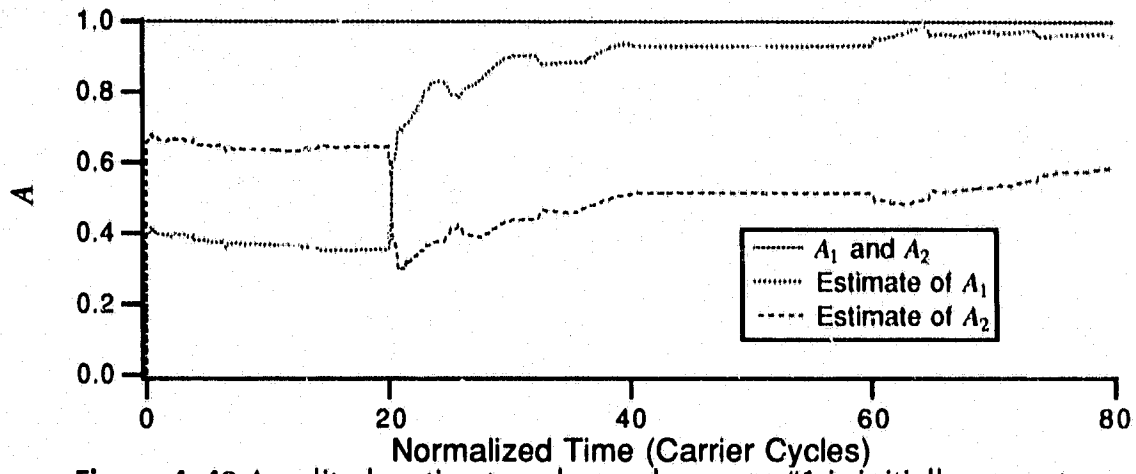

Figure 4–40 Amplitude estimates when only source #1 is initially present.

lost for both signals and not regained until about time index 60 resulting in cycle slipping. However, at time 40 when signal #2 disappears, its estimator begins tracking source #1 (the state estimate has "flipped") until source #2 again appears at time 60 at which time neither signal is successfully tracked. The estimate of the amplitude of source #1 improves when source #2 appears at time 20 (see Fig. 4–40) however source 2's amplitude estimate remains poor.

Looking at the closed loop bandwidths (see Fig. 4–41) again shows the reduced bandwidth when only one signal is present. However, during the first interval when only source #1 is present, both bandwidths are low relative to the intervals where both signals are present. This may be due to the fact that both estimators are tracking the same source and are in a sense "sharing" it.

The previous example demonstrates the need to know the number of signals present in the channel. As the number of sources changes, additional coupled DPLLs will need to be created and destroyed so that the number of DPLLs is equal to the number of sources. Thus there ought to be a method of determining the signal multiplicity.

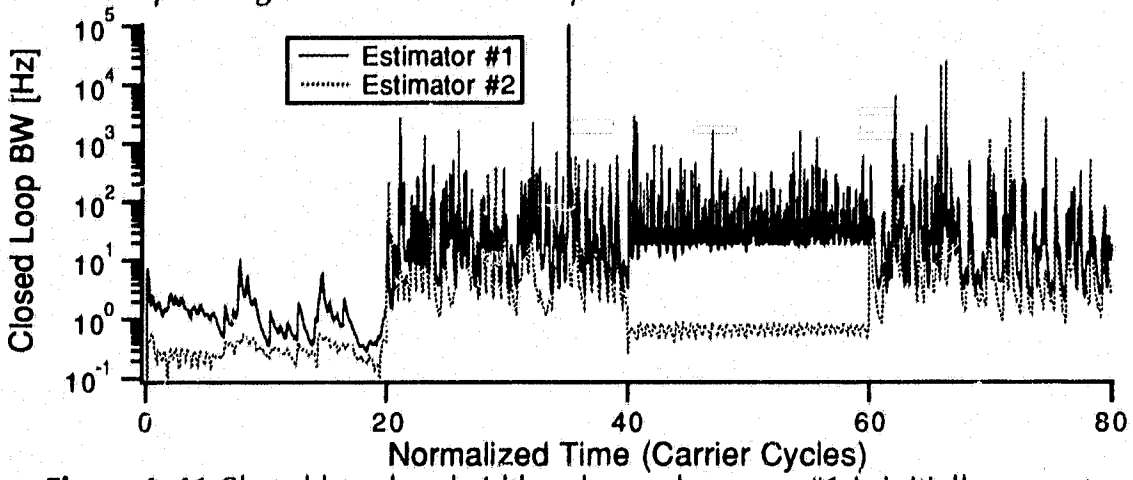

Figure 4–41 Closed loop bandwidths when only source #1 is initially present.

4.4. Summary

We began this chapter with a review of PLL and DPLL theory. We presented the analog, hybrid, and digital PLLs as they have been used in literature relating to coupled PLL structures. We followed this by presenting an overview of how the PLL and DPLL are derived from the optimal phase estimator including the EKF. Finally we characterized the linear and nonlinear behavior of the DPLL from established literature.

Next we turned our attention to the CDPLLs as derived in Chapter 2 and analyzed in Chapter 3. We showed that the coupling between DPLLs could not be linearized even when the DPLLs could be because the small angle approximation is not valid due to the multiple carriers. Much of the analysis of the tracking behavior had been previously presented in Chapter 3. Due to the nonlinear coupling and nonlinear behavior of the DPLLs the acquisition behavior analysis was all carried out by simulation. Out of the acquisition behavior came our new CDPLL where the inputs to the DPLLs is the EKF innovations process instead of simply the measurement of the state. This differs from methods proposed in related literature. Acquisition time is difficult to define with this new estimator structure so the probability of lock was presented. Finally the state MSEs and level of signal improvement over the single EKF were presented.

The last section examined signal multiplicity. The ability (or inability) of the multiple source EKF to track when the true number of signals was not known was briefly discussed. The framework for a possible signal multiplicity detector was established using the closed-loop bandwidths of the DPLLs.

5. Polarization Diversity for Frequency Reuse

In the previous three chapters the phenomenon of co-channel interference was examined from the perspective of a single receiving antenna. The measurement models and estimators were derived for scalar measurements. While this model is valid for many environments, vector measurements are also prevalent. An example is the use of polarization diversity to increase channel capacity of a microwave link. This method of frequency reuse is very common in satellite communications [58].

Frequency reuse by polarization diversity relies on the spatial orientation of the transmitted electromagnetic waves. Two waves, with the same carrier frequency, are transmitted with orthogonal spatial orientations of the electric fields which we will denote as *horizontal* and *vertical* polarization. The transmitter and receiver each have two antennas: one oriented to receive the horizontal wave and the other oriented to receive the vertical wave. If the antennas are perfectly aligned and the medium isotropic, the two waves are perfectly separated. However, in practice the antennas are not perfectly aligned and, a far more troublesome problem, the medium is anisotropic. Thus the received waves may no longer be orthogonally polarized.

In this chapter we present discrete-time process and measurement models for a polarization diversity communication system from which estimators are derived. Our goal here is to show that the general development of Chapter 2 may be applied to other application areas. However, no analysis or simulation is performed based on these models; our objective is to show that the work presented in the previous chapters may be extended to other application areas.

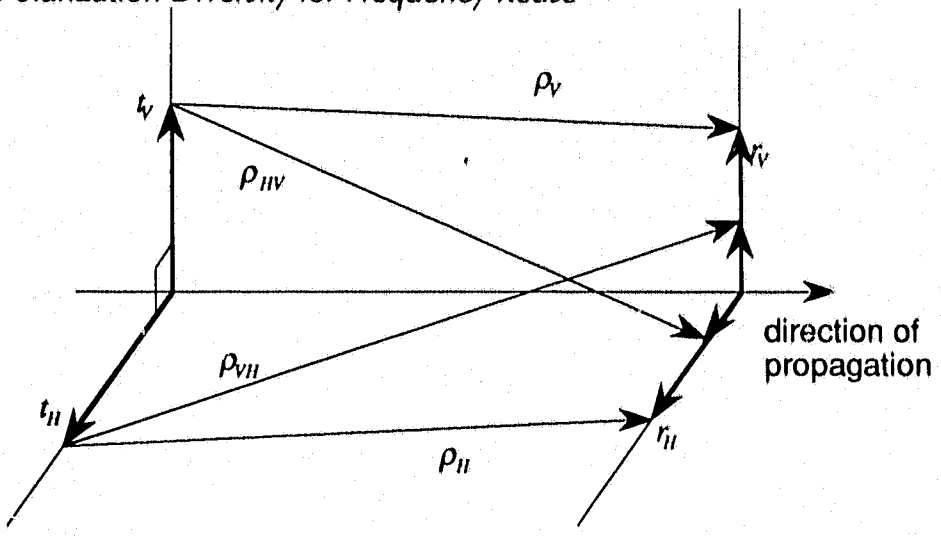

Figure 5–1 Depolarization of cross-polarized waves due to anisotropic medium [59].

5.1. Polarization Diversity

Polarization diversity relies on orthogonal spatial orientation of the electromagnetic wave which carries the information. In theory if two waves are orthogonally polarized, they may be separately received by orthogonally polarized antenna even though they occupy the same communications channel. In practice perfectly orthogonal polarization is not possible.

There are a number of factors which effect cross-polarization, one of the most predominant in satellite communications being the anisotropic medium though which the electromagnetic waves travel [58]. An example of this anisotropy is the presence of raindrops in the atmosphere. Depending on the angle of incidence that the wave has with the rain drop, the wave is attenuated, phase shifted, and depolarized. Thus, even if the transmitter is able to send perfectly cross-polarized waves, the waves will suffer various depolarization effects and the received wave will no longer be perfectly cross-polarized [58, 59]. This is shown graphically in Fig. 5–1. The result of depolarization is *crosstalk* between the horizontal and vertical components which may be expressed by the transform [58]

$$\begin{bmatrix} r_V \\ r_H \end{bmatrix} = \begin{bmatrix} \rho_V & \rho_{VH} \\ \rho_{HV} & \rho_H \end{bmatrix} \begin{bmatrix} t_V \\ t_H \end{bmatrix}, \tag{5.1}$$

where t_H and t_V are the horizontal and vertical transmitted waves and r_H and r_V are the horizontal and vertical received waves. The coefficients in the transform matrix describe the attenuation and depolarization effects of the medium.

5.2. State and Measurement Model

Having defined the crosstalk due to depolarization; we now expand the communication model derived in Chapter 2 to include 1) vector measurement via two sensors and 2) crosstalk between sensors. The sensors are the horizontally and vertically aligned antennas. The crosstalk is due to the off-diagonal elements in the transformation matrix of (5.1).

As in Chapter 2, the two sources are independent FM message processes defined from (2.53)

$$\begin{bmatrix} \theta_H(k+1) \\ f_H(k+1) \\ \rho_H(k+1) \end{bmatrix} = \begin{bmatrix} 1 & \phi_{\theta f,H} & 0 \\ 0 & \phi_{f,H} & 0 \\ 0 & 0 & 1 \end{bmatrix} \begin{bmatrix} \theta_H(k) \\ f_H(k) \\ \rho_H(k) \end{bmatrix} + \begin{bmatrix} \gamma_{\theta,H} & \gamma_{\theta f,H} & \mathbf{0} \\ \gamma_{f\theta,H} & \gamma_{f,H} & \\ \mathbf{0} & & 0 \end{bmatrix} \begin{bmatrix} w_{\theta,H}(k) \\ w_{f,H}(k) \\ 0 \end{bmatrix}, \tag{5.2}$$

for the horizontal component and

$$\begin{bmatrix} \theta_V(k+1) \\ f_V(k+1) \\ \rho_V(k+1) \end{bmatrix} = \begin{bmatrix} 1 & \phi_{\theta f,V} & 0 \\ 0 & \phi_{f,V} & 0 \\ 0 & 0 & 1 \end{bmatrix} \begin{bmatrix} \theta_V(k) \\ f_V(k) \\ \rho_V(k) \end{bmatrix} + \begin{bmatrix} \gamma_{\theta,V} & \gamma_{\theta f,V} & \mathbf{0} \\ \gamma_{f\theta,V} & \gamma_{f,V} & \\ \mathbf{0} & & 0 \end{bmatrix} \begin{bmatrix} w_{\theta,V}(k) \\ w_{f,V}(k) \\ 0 \end{bmatrix}, \tag{5.3}$$

for the vertical component. The γ's are as defined in (2.54)–(2.56). Here we have replaced the carrier amplitude with the copolarized signal attenuations ρ_H and ρ_V. Like the carrier amplitudes these are constants to be estimated, so the carrier amplitudes are included as part of the transform coefficients.

The state vector describing both components as well as the crosstalk is formed by augmenting (5.2) and (5.3) with the state equations describing the crosstalk. In our simple model the cross-polarization coefficients are random constants and we add these to the state

vector. We acknowledge the fact that the channel characteristics change with time and thus the transformation matrix of (5.1) would be time-varying, however our goal is to show that polarization diversity may be modeled in a manner similar to our treatment of scalar measurements. The model framework presented here readily supports inclusion of time-varying channel characteristics. The total state equation then becomes

$$\begin{bmatrix} \mathbf{x}_V(k+1) \\ \mathbf{x}_H(k+1) \\ \rho_{HV}(k+1) \\ \rho_{VH}(k+1) \end{bmatrix} = \begin{bmatrix} \mathbf{\Phi}_V & \mathbf{0} & & \\ \mathbf{0} & \mathbf{\Phi}_H & \mathbf{0} & \\ & & 1 & 0 \\ & \mathbf{0} & 0 & 1 \end{bmatrix} \begin{bmatrix} \mathbf{x}_V(k) \\ \mathbf{x}_H(k) \\ \rho_{HV}(k) \\ \rho_{VH}(k) \end{bmatrix} + \begin{bmatrix} \mathbf{\Gamma}_V & \mathbf{0} & \\ \mathbf{0} & \mathbf{\Gamma}_H & \mathbf{0} \\ \mathbf{0} & & \mathbf{0} \end{bmatrix} \begin{bmatrix} \mathbf{w}_V(k) \\ \mathbf{w}_H(k) \\ \mathbf{0} \end{bmatrix}. \tag{5.4}$$

The state measurement has many similarities to that presented in Chapter 2. The main difference is that the scalar measurement equation (2.76) is replaced by the vector measurement equation

$$\mathbf{z}(k) = \begin{bmatrix} z_V(k) \\ z_H(k) \end{bmatrix} = h(\mathbf{x}(k), k) + \begin{bmatrix} v_V(k) \\ v_H(k) \end{bmatrix} \tag{5.5}$$

where the $\mathbf{v}$ is the $N[\mathbf{0}, \mathbf{R}_v]$measurement noise present at the horizontal and vertical antennas respectively. The observation function is also a vector. Our observation model is defined for a separate FM transmission on each polarization component. Thus using the notation of (5.1) and Fig. 5–1, the transmitted signal is

$$\begin{bmatrix} t_V \\ t_H \end{bmatrix} = \begin{bmatrix} \sin(\omega_c kTs + \theta_V(k)) \\ \sin(\omega_c kTs + \theta_H(k)) \end{bmatrix}. \tag{5.6}$$

The effects of the medium are included by use of the transformation matrix of (5.1) with (5.6) resulting in the observation function

$$h(\mathbf{x}(k), k) = \begin{bmatrix} r_V \\ r_H \end{bmatrix} = \begin{bmatrix} \rho_V & \rho_{VH} \\ \rho_{HV} & \rho_H \end{bmatrix} \begin{bmatrix} \sin(\omega_c kTs + \theta_V(k)) \\ \sin(\omega_c kTs + \theta_H(k)) \end{bmatrix}. \tag{5.7}$$

When this is substituted into (5.5) the complete measurement equation is given

$$\begin{bmatrix} z_V(k) \\ z_H(k) \end{bmatrix} = \begin{bmatrix} \rho_V & \rho_{VH} \\ \rho_{HV} & \rho_H \end{bmatrix} \begin{bmatrix} \sin(\omega_c kTs + \theta_V(k)) \\ \sin(\omega_c kTs + \theta_H(k)) \end{bmatrix} + \begin{bmatrix} v_V(k) \\ v_H(k) \end{bmatrix}. \tag{5.8}$$

5.3. Estimator Formulation

With the state and measurement models defined, we can now derive an estimator. We use the Extended Kalman Filter. We begin our derivation assuming that the depolarization effects of the channel are known; that is the coefficients of the transformation matrix are known. This allows examination of the phase and frequency estimation separately from channel parameter estimation. We then extend the estimator to estimate the channel parameters as well.

5.3.1. Medium Known

If the medium is known, the depolarization coefficients need not be included in the state equation (5.4) and it simplifies to

$$\begin{bmatrix} \theta_V(k+1) \\ f_V(k+1) \\ \theta_H(k+1) \\ f_H(k+1) \end{bmatrix} = \begin{bmatrix} 1 & \phi_{\theta f,V} & & \mathbf{0} \\ 0 & \phi_{f,V} & & \\ & \mathbf{0} & 1 & \phi_{\theta f,H} \\ & & 0 & \phi_{f,H} \end{bmatrix} \begin{bmatrix} \theta_V(k) \\ f_V(k) \\ \theta_H(k) \\ f_H(k) \end{bmatrix} + \begin{bmatrix} \gamma_{\theta,V} & \gamma_{\theta f,V} & & \mathbf{0} \\ \gamma_{f\theta,V} & \gamma_{f,V} & & \\ & \mathbf{0} & \gamma_{\theta,H} & \gamma_{\theta f,H} \\ & & \gamma_{f\theta,H} & \gamma_{f,H} \end{bmatrix} \begin{bmatrix} w_{\theta,V}(k) \\ w_{f,V}(k) \\ w_{\theta,H}(k) \\ w_{f,H}(k) \end{bmatrix}. \quad (5.9)$$

The measurement equation remains the same.

The EKF observation matrix from (2.70) is

$$\mathbf{H}(\mathbf{x}(k \mid k-1),k) = \begin{bmatrix} \mathbf{H}_V(\mathbf{x}_V(k \mid k-1),k) \\ \mathbf{H}_H(\mathbf{x}_H(k \mid k-1),k) \end{bmatrix}^{\mathrm{T}} = \begin{bmatrix} \rho_V \cos\left(\hat{\Theta}_V\right) & \rho_{HV} \cos\left(\hat{\Theta}_V\right) \\ 0 & 0 \\ \rho_{VH} \cos\left(\hat{\Theta}_H\right) & \rho_H \cos\left(\hat{\Theta}_H\right) \\ 0 & 0 \end{bmatrix}^{\mathrm{T}}. \quad (5.10)$$

The Kalman filter equation from (2.86) is

$$\hat{\mathbf{x}}(k) = \mathbf{\Phi}\hat{\mathbf{x}}(k-1) + \mathbf{P}(k)\mathbf{H}^{\mathrm{T}}\left(\hat{\mathbf{x}}(k \mid k-1)\right)\mathbf{R}_{\mathbf{v}}^{-1}(k)\mathbf{v}(k), \quad (5.11)$$

where

$$\mathbf{v}(k) = \mathbf{z}(k) - h\left(\hat{\mathbf{x}}(k \mid k-1)\right). \quad (5.12)$$

In the case of the scalar measurement, expansion and analysis of the Kalman filter equation revealed an underlying structure shown to be similar to the DPLL. However (5.11) dif-

fers from the scalar measurement case in that the measurement noise covariance is now a matrix, not a scalar, and thus the term $\mathbf{P}(k)\mathbf{H}^{\mathrm{T}}(\hat{\mathbf{x}}(k\,|\,k-1))\mathbf{R}_{\mathbf{v}}^{-1}(k)\mathbf{v}(k)$ may not be reordered. The EKF observation matrix $\mathbf{H}$, while a vector in the scalar measurement case, becomes a matrix for vector measurements. Thus expanding (5.11) does not reveal a simple underlying structure due to the cross-coupling between the two measurements brought about by $\mathbf{R}_{\mathbf{v}}^{-1}$ and $\mathbf{H}$. If the noise present that the horizontal and vertical antennas is not correlated, then $\mathbf{R}_{\mathbf{v}}^{-1}$ is diagonal. Although this does simplify (5.11) to some extent, no obvious structures are evident.

5.3.2. Medium Unknown

When the medium is unknown the co and cross-polarization coefficients are unknown constants and must be included in the state equation as in (5.4). In this case the EKF observation matrix is

$$\mathbf{H}(\mathbf{x}(k\,|\,k-1),k)=\begin{bmatrix}\rho_V\cos\left(\hat{\Theta}_V\right) & \rho_{IIV}\cos\left(\hat{\Theta}_V\right)\\ 0 & 0\\ \sin\left(\hat{\Theta}_V\right) & 0\\ \rho_{VII}\cos\left(\hat{\Theta}_{II}\right) & \rho_{II}\cos\left(\hat{\Theta}_{II}\right)\\ 0 & 0\\ 0 & \sin\left(\hat{\Theta}_{II}\right)\\ 0 & \sin\left(\hat{\Theta}_V\right)\\ \sin\left(\hat{\Theta}_{II}\right) & 0\end{bmatrix}^{\mathrm{T}}. \tag{5.13}$$

When substituted into (5.11) the estimator equation for each state becomes even more complex. There is coupling among all of the states and between the states and the measurements and again no simpler structures are evident from the expansion of (5.11).

5.4. Summary

In this chapter we have briefly outlined an approach to the problem of crosstalk in polarization diversity frequency reuse communication systems. No analysis was presented as our goal

was to demonstrate a level of versatility in the work presented in the previous chapters. Using the above derived framework the same analysis presented in Chapters 2 and 3 could be carried out on the polarization crosstalk problem. Concepts such as state observability would play a similar role. For example, the observability would be a function of the level of cross-polarization in the polarization diversity scenario instead of the carrier phase difference as it was in the scalar measurement case.

6. Conclusions

In this dissertation we have examined the problem of co-channel interference and proposed a new method to combat it. The need to operate in adjacent and co-channel interference environments is due to the ever increasing demands placed on the limited electromagnetic spectrum. We have concentrated on the scalar measurement FM scenario as it applies to mobile radio and telephony as it is the most difficult problem. We have also shown that similar interference may be found in polarization diversity systems.

We have begun the investigation by developing models for the types of signals encountered in the FM and we have extended models found in the literature to adequately describe the multiple source communications environment. Although derived from continuous-time, our model is described by discrete time state-space equations, because any eventual implementation will most likely be digital. An Extended Kalman Filter estimator using the state-space model was derived and upon further examination was found to be implementable by coupled digital phase-locked loops.

Using different methods several authors have also derived coupled phase-locked loop receivers. However, their approaches and performance analyses of the behavior of these structures were to a great extent heuristic. In an effort to carry out a more methodical analysis, we have employed tools appropriate for our state-space model. Of principle interest is the investigation of the multiple source separability by examination of the state observability. In concert with numerous simulations of the estimator, this has provided the framework to allow us to better predict and explain the behavior of the derived estimator.

We then expanded on the relationship between the EKF and the CDPLL. The linear and nonlinear behavior of the CDPLL has been discussed and the difficulties in a complete ana-

lytic treatment were presented. Acquisition behavior of the estimator has been examined by simulation as an analytic approach is not feasible. Our estimator has been compared and contrasted with similar works in the literature. Finally the problems associated with time-varying source multiplicity were presented and an avenue of further research opened.

The scope of the thesis has been slightly broadened by briefly examining polarization diversity crosstalk. Here the scalar measurement was replaced by a vector measurement which was shown to be adequately described by our communication model.

6.1. Summary of Findings

Several discoveries have been made in various parts of this work that have not been found in related literature. We briefly highlight each of them here.

EKF-derived CDPLLs have been previously shown in the literature. However these do not include all of the state coupling that optimally should be present due to the estimation error covariance matrix. As we have shown, it is not valid to assume that particular states are not coupled because during acquisition coupling exists between all states. Once the estimator has acquired the signals, the states related to carrier amplitude become uncoupled with the phase and frequency states. However, during periods of low observability, the interstate coupling does increase.

The study of state observability revealed that the states are observable when the carriers are not completely in phase. The bandwidth differences of the individual signals effects the state observability only when the carriers are nearly in phase or in antiphase. Simulations of the derived EKF reveal that the state coupling is low when the states are observable but increases drastically when the observability decreases. During these intervals the EKF ignores the measurement and tries to predict the states. This has the effect of reducing the bandwidth of the DPLLs during the periods of low observability and increasing the bandwidths during the transition between observable and unobservable conditions. In this manner the

EKF is able to reacquire the states once the measurements again hold useful information. We also showed that the estimator is able to operate over a wide range of carrier amplitude ratios but noted that there is a limit where one carrier overwhelms the other and the lower powered signal is not recoverable. We also show that the DPLL bandwidths *may* be of use in determining the source multiplicity.

In the treatment of the relationship between the EKF and the CDPLL, we have shown that many of the estimators presented in the literature are special cases of our more general development. Some have included the bandpass coupling but not the baseband coupling while others include the baseband but not the bandpass coupling. We have also shown that unlike the DPLL, it is not appropriate to neglect the innovations process as all of its components are not removed by the loop filters. Therefore our final CDPLL uses two DPLLs each of which use the innovations process as their input, not the measurement itself.

We have noted that the DPLLs sometimes lock onto the "wrong" signal and will "flip" which signal is being tracked during the periods of low observability. Although this leads to frustration from the simulation point of view, it not an insurmountable obstacle from the implementation point of view. One possible solution would use two antennas (spatial diversity) since it is very unlikely that the carriers will be in-phase at both antennas at the same time. The measurement with the greater observability would be used. An alternative would be to include some distinguishing characteristics into the modulating signals: for example a distinct sub-audible tone could be added to the message process of each co-channel signal.

Finally we have shown that our communications model is general enough to describe polarization diversity crosstalk. This allows for the derivation of an EKF estimator, however, unlike the scalar measurement case, no underlying familiar estimator structures were found in the expansion of the Kalman filter equation.

6.2. Further Work

Like most research this work as answered some questions while creating others. There are several avenues of research that could be carried out from this thesis.

- The separability of more than two sources has not been addressed in the literature or in this work. Are three sources separable? Four? Is there a limit? Under what conditions may N sources be separated? It would seem that there is a limit since we have shown that carriers that are nearly in-phase cannot be separated. The work presented in Chapters 2 and 3 provides the foundation for such an investigation.
- This work has used a first order Gaussian random process as the modulation or message process. The order of the model could be increased. Also the estimator assumes *a priori* knowledge of the bandwidth of the process. Process parameter estimation can be included in the estimator. A model for deterministic modulation was outlined but not examined. Separability of multiple deterministic modulations or a mix of random and deterministic modulations is also of interest.
- The measurement noise has been kept to a minimum. We have chosen to concentrate on the signal separability as an issue unto itself and inclusion of measurement noise would introduce yet another unknown into the problem. The effects of a noisy co-channel environment are of great interest and would be a logical next step in the investigation of the problem.
- A method to determine or to control the state estimate "flipping" is also required. The two above proposed solutions would be a starting point..
- The polarization diversity problem was set-up but not analyzed. A similar treatment could be given to that problem as the ideas of state observability and separability apply there also. A more detailed examination of the resulting EKF may reveal some hidden receiver structure like the CDPLL.

- Implementation of the CDPLL was not addressed. Given today's digital signal processing technology, it should be possible to devise a real-time implementation of the CDPLL.

Bibliography

[1] G. Vincent, "Personal Communications: The Dream and the Reality," *IEE Review*, 299–303, September 1990.

[2] S.L. Marple, Jr, *Digital Spectral Analysis with Applications*, Englewood Cliffs, New Jersey: Prentice-Hall, Inc., 1987.

[3] R.L. Kirlin and Y. Su, "Maximum -Likelihood Multiple Source Tracking Utilizing Multiple Coupled PLL's," in *Proceedings ICASSP 90*, 1990, pp. 2851–2854.

[4] G. Calhoun, *Digital Cellular Radio*, Norwood, MA: Artech House, Inc., 1988.

[5] R.J. Holbeche, *Land Mobile Radio Systems*, IEE Telecommunications Series 14, London, U.K.: Peter Peregrinus, Ltd, 1985.

[6] W.C.Y. Lee, *Mobile Communications Engineering*, New York: McGraw-Hill Book Co., 1982.

[7] R.L. Kirlin, "A Sequential Maximum-Likelihood Multiple Source Tracker and the Relation of Phase-Locked Loop Theory to Eigenstructure Methods," in *Proceedings ISCAS '89*, vol. 3, 1989, pp. 1762–1767.

[8] A.J. Viterbi, *Principles of Coherent Communication*, New York: McGraw-Hill, Inc., 1966.

[9] J.J. Stiffler, *Theory of Synchronous Communication*, Englewood Cliffs, New Jersey: Prentice-Hall, 1971.

[10] F.M. Gardner, *Phaselock Techniques*, Second Edition, New York: John Wiley & Sons, 1979.

[11] *Phase-Locked Loops*, Edited by C.M. Chie and W.C. LindseyIEEE Press, 1986.

[12] P.J. Parker and B.D.O. Anderson, "Frequency Tracking of Nonsinusoidal Periodic Signals in Noise," *Journal of the European Association for Signal Processing*, vol. 20, no. 2, 127–152, June 1990.

[13] T.S. Sundresh, F.A. Cassara, and H. Schachter, "Maximum A Posteriori Estimation for Suppression of Interchannel Interference in FM Receivers," *IEEE Transactions on Communications*, vol. COM-25, no. 12, 1480–1485, December 1977.

[14] F.A. Cassara, H. Schackter, and G.H. Simowitz, "Acquisition Beharvior of the Cross-Coupled Phase-Locked Loop FM Demodulator," *IEEE Transactions on Communications*, vol. COM-28, no. 6, 897–904, June 1980

[15] Y. Bar-ness, F.A. Cassara, H. Schachter, and R. DiFazio, "Cross-Coupled Phase-Locked Loop with Closed Loop Amplitude Control," *IEEE Transactions on Communications*, vol. COM-32, no. 2, 195–199, February 1984.

[16] S. Say, "Vector-Locked Loop Interference Canceller," Ph.D. thesis, Polytechnic Institute of New York, 1985.

[17] J.N. Bradley, R.L. Kirlin, and B. Maranda, "Phase-Locked Loop Cancellation of Interfering Tones," Technical Report, Canadian Defence Research Establishment Pacific, , 1990.

[18] J. Bradley, "Suppression of Adjacent-channel and Cochannel FM Interference via Extended Kalman Filtering," in *Proceedings of ICASSP-92*, vol. IV, 1992, pp. 693–696.

[19] M.A. Lagunas and A. Pages, "Multitone Tracking with Coupled EKFs and High Order Learning," in *Proceedings of ICASSP-92*, vol. V, 1992, pp. 153–156.

[20] W.C. Lindsey and C.M. Chie, "A Survey of Digital Phase-Locked Loops," *Proceedings of the IEEE*, vol. 69, no. 4, 410–431, April 1981.

[21] F.M. Gardner, "Demodulator Reference Recovery Techniques Suited for Digital Implementation," Technical ReportFinal Report, , Gardner Research Company, 1755 University Ave., Palo Alto, CA 94301 (USA), 16 May , 1988, European Space Agency, ESTEC Contract No. 6847/86/NL/DG.

[22] H.L. van Trees, *Detection, Estimation, and Modulation Theory, Part II*, New York: John Wiley and Sons, Inc., 1971.

[23] H.L. van Trees, *Detection, Estimation, and Modulation Theory, Part I*, New York: John Wiley and Sons, Inc., 1968.

[24] S.C. Gupta, "Phase-Locked Loops," *Proceedings of the IEEE*, vol. 63, no. 2, 291–306, February 1975.

[25] G.S. Gill and S.C. Gupta, "First-Order Discrete Phase-Locked Loop with Applications to Demodulation of Angle-Modulated Carrier," *IEEE Transactions on Communications*, 454–462, June 1972.

[26] A. Weinberg and B. Liu, "Discrete Time Analyses of Nonuniform Sampling First- and Second-Order Digital Phase Locked Loops," *IEEE Transactions on Communications*, vol. COM-22, 123–137, February 1974.

[27] S.C. Gupta, "On Optimum Digital Phase-Locked Loops," *IEEE Transactions on Communication Technology*, vol. COM-16, no. 2, 340–344, April 1968.

[28] C.N. Kelly and S.C. Gupta, "Discrete-Time Demodulation of Continuous-Time Signals," *IEEE Transactions on Information Theory*, vol. IT-18, no. 4, 488–493, July 1972.

[29] D.R. Polk and S.C. Gupta, "Quasi-Optimum Digital Phase-Locked Loops," *IEEE Transactions on Communications*, vol. COM-21, no. 1, 75–82, January 1973.

[30] A.L. McBride. "On Optimum Sampled-Data FM Demodulation," *IEEE Transactions on Communications*, vol. COM-21, no. 1, 40–50, January 1973.

[31] S. Haykin, *Communication Systems*, Second Edition, Toronto: John Wiley and Sons, 1983.

[32] *Applied Optimal Estimation*, Edited by A. GelbThe M.I.T. Press, 1974.

[33] R.E. Ziemer and R.L. Peterson, *Digital Communications and Spread Spectrum Systems*Macmillan Publishing Company, 1985.

[34] A.P. Sage and J.L. Melsa, *Estimation Theory with Applications to Communications and Control*, New York: McGraw-Hill Book Co., 1971.

[35] B.D.O. Anderson and J.B. Moore, *Optimal Filtering*, Englewood Cliffs, New Jersey: Prentice-Hall, 1979.

[36] R. Kumar, "A Novel Multireceiver Communications System Configuration Based on Optimal Estimation Theory," Technical ReportTDA Progress Report 90-9, , National Aeronautics and Space Administration, Jet Propulsion Laboratory, Pasadena, California, 1990.

[37] R. Kumar, "Novel Multireceiver Communication System Configurations Based on Optimal Estimation Theory," in *The Third International Conference on Advances in Communicaiton and Control Systems (COMCON)*, vol. 1, 1992, pp. 217–228.

[38] A.V. Oppenheim and R.W. Schafer, *Digital Signal Processing*, Englewood Cliffs, New Jersey: Prentice-Hall, Inc., 1975.

[39] L.L. Scharf, *Statistical Signal Processing: Detection, Estimation, and Time Series Analysis*Addison-Wesley Publishing Co., 1991.

[40] M. Lagunas, *The Combination of Two Time-Varying Systems and High Order Unsymmetrical Learning*, 1991, Escuela Tehnica Superior, Ingenieros Telecommunicacion, Barcelona, Spain Adpo 30.2. Personal correspondence. Also sumbitted to ICASSP-92.

[41] T. Kailath, *Linear Systems*, Englewood Cliffs, New Jersey: Prentice-Hall, Inc., 1980.

[42] G.W. Stewart, *Introduction to Matrix Computations*, Computer Science and Applied MathematicsAcademic Press, Inc., 1973.

[43] J.K. Holms and C.R. Tegnelia, "A Second-Order All-Digital Phase-Locked Loop," *IEEE Transactions on Communications*, 62–68, January 1974.

[44] C.N. Kelly and S.C. Gupta, "The Digital Phase-Locked Loop as a Near-Optimum FM Demodulator," *IEEE Transactions on Communications*, vol. COM-20, no. 6, 406–411, June 1972.

[45] Y.R. Shayan and T. Le-Ngoc, "All Digital Phase-Locked Loop: Concepts, Design, and Applications," *IEE Proceedings, Part F*, vol. 136, no. 1, 53–56, February 1989.

[46] J.I. Statman and W.J. Hurd, "An Estimator-Predictor Approach to PLL Loop Filter Design," *IEEE Transactions on Communications*, vol. 38, no. 10 1667–1669, October 1990.

[47] K. Dessouky and W.C. Lindsey, "Phase and Frequency Transfer Between Mutually Sychronized Oscillators," *IEEE Transactions on Communications*, vol. COM-32, no. 2, 110–117, February 1984.

[48] K.H. Sayhood, "Synchronous Behaviour of Mutually Coupled Phase-Locked Loops in the Presence of Continuous Wave Interferece," *International Journal on Electronics*, vol. 72, no. 4, 631–640, 1992.

[49] S. Hinedi, "An Extended Kalman Filter Based Automatic Frequency Control Loop," Technical ReportTDA Progress Report 42-95, , National Aeronautics and Space Administration, Jet Propulsion Laboratory, Pasadena, CA, USA, July–September, 1988.

[50] B. Friedland, "Optimum Steady-State Position and Velocity Estimation Using Noisy Sampled Position Data," *IEEE Transactions on Aerospace and Electronic Systems*, vol. AES-9, no. 6, 906–911, November 1973.

[51] B. Ekstrand, "Analytical Steady State Solution for a Kalman Tracking Filter," *IEEE Transactions on Aerospace and Electronic Systems*, vol. AES-19, no. 6, 815–819, November 1983.

[52] D.R. Vaughan, "A Nonrecursive Algebraic Solution for the Discrete Riccati Equation," *IEEE Transactions on Automatic Control*, vol. AC-15, 597–599, October 1970.

[53] T. Endo and L.O. Chua, "Chaos from Phase-Locked Loops," *IEEE Transactions on Circuits and Systems*, vol. 35, no. 8, 987–1003, August 1988.

[54] T. Endo and L.O. Chua, "Chaos from Phase-Locked Loops—Part II: High-Dissipation Case," *IEEE Transactions on Circuits and Systems*, vol. 35, no. 2, 255-263, February 1989.

[55] G.M. Berstein, M.A. Lieberman, and A.J. Lichtenberg, "Nonlinear Dynamics of a Digital Phase Locked Loop," *IEEE Transactions on Communications*, vol. 37, no. 10, 1062–1069, October 1989.

[56] T. Endo and L.O. Chua, "Chaos from Two-Coupled Phase-Locked Loops," *IEEE Transactions on Circuits and Systems*, vol. 37, no. 9, 1183–1187, September 1990.

[57] T.S. Parker and L.O. Chua, "Chaos: A Tutorial for Engineers," *Proceedings of the IEEE*, vol. 75, no. 8, 982–1008, August 1987.

[58] T.T. Ha, *Digital Satellite Communications*, Second EditionMcGraw-Hill, Inc., 1990.

[59] D.C. Cox and H.W. Arnold, "Comparison of Measured Cross-polarization Isolation and Discrimination for Rain and Ice on a 19 GHz Space-Earth Path," *Radio Science*, vol. 19, no. 2, 617–628, March–April 1984.

Appendix A
Derivation of Discrete State-Space Message Model

The discrete state equation defining the message model is derived from the analog message model presented in Section 2.1.1 where the analog state equation is

$$\dot{\mathbf{x}}(t) = \mathbf{F}\mathbf{x}(t) + \mathbf{G}\mathbf{d}(t) \tag{A.1}$$

for which we wish to derive an equivalent discrete state equation

$$\mathbf{x}(k+1) = \mathbf{\Phi}(k+1,k)\mathbf{x}(k) + \mathbf{\Gamma}(k)\mathbf{w}(k). \tag{A.2}$$

The state vector $\mathbf{x}(t)$ is simply replaced by the discrete state vector $\mathbf{x}(k)$. The relationship between $\mathbf{F} \leftrightarrow \mathbf{\Phi}(k,k-1)$ and $\mathbf{G} \leftrightarrow \mathbf{\Gamma}(k)$ depends on the system being described. The continuous-time driving noise $\mathbf{d}$ is replaced by the discrete-time driving noise $\mathbf{w}$.

A.1. Frequency Modulation

The continuous state equation, repeated from (2.23), is

$$\begin{bmatrix} \dot{x}_\theta(t) \\ \dot{x}_f(t) \\ \dot{x}_A(t) \end{bmatrix} = \begin{bmatrix} 0 & d_f & 0 \\ 0 & -\alpha & 0 \\ 0 & 0 & 0 \end{bmatrix} \begin{bmatrix} x_\theta(t) \\ x_f(t) \\ x_A(t) \end{bmatrix} + \begin{bmatrix} 0 \\ \sqrt{2\alpha} \\ 0 \end{bmatrix} d(t). \tag{A.3}$$

The state transition matrix may be found by using (2.31) resulting in

$$\mathbf{\Phi}(t_k, t_{k-1}) = \mathcal{L}^{-1}\left\{ \begin{bmatrix} s & -d_f & 0 \\ 0 & s+\alpha & 0 \\ 0 & 0 & s \end{bmatrix}^{-1} \right\} = \mathcal{L}^{-1}\left\{ \begin{bmatrix} \frac{1}{s} & \frac{d_f}{s(s-\alpha)} & 0 \\ 0 & \frac{1}{s-\alpha} & 0 \\ 0 & 0 & \frac{1}{s} \end{bmatrix} \right\} \tag{A.4}$$

and (2.46) is formed by performing the inverse Laplace transform and defining $T_s = t_k - t_{k-1}$.

The discrete process driving noise is related to the continuous case by the matrix superposition integral (2.32)

$$\boldsymbol{\Gamma}(k)\mathbf{w}(k) = \int_{t_{k-1}}^{t_k} \boldsymbol{\Phi}(t_k,\tau)\mathbf{G}(\tau)d(\tau)\,d\tau, \tag{A.5}$$

however (A.5) does not directly provide a means for finding $\boldsymbol{\Gamma}$. We have defined $\mathbf{w}$ as a vector of i.i.d. zero mean Gaussian samples such that $E\{\mathbf{w}\mathbf{w}^{\mathrm{T}}\} = \mathbf{I}$. The covariance of the discrete process driving noise is

$$\mathbf{Q}_{\boldsymbol{\Gamma}} = E\{\boldsymbol{\Gamma}\mathbf{w}\mathbf{w}^{\mathrm{T}}\boldsymbol{\Gamma}^{\mathrm{T}}\} = \boldsymbol{\Gamma}E\{\mathbf{w}\mathbf{w}^{\mathrm{T}}\}\boldsymbol{\Gamma}^{\mathrm{T}} = \boldsymbol{\Gamma}\mathbf{I}\boldsymbol{\Gamma}^{\mathrm{T}} = \boldsymbol{\Gamma}\boldsymbol{\Gamma}^{\mathrm{T}}. \tag{A.6}$$

Using (A.5) the covariance of the discrete process driving noise may also be found from (2.33)

$$\mathbf{Q}_{\Gamma\mathrm{w}} = \int_{t_{k-1}}^{t_k} \boldsymbol{\Phi}(t_k,\tau)\mathbf{G}(\tau)\mathbf{R}_{\mathrm{d}}(\tau)\mathbf{G}^{\mathrm{T}}(\tau)\boldsymbol{\Phi}^{\mathrm{T}}(t_k,\tau)\,d\tau. \tag{A.7}$$

Substituting (A.3) into (A.7) yields

$$\mathbf{Q}_{\Gamma\mathrm{w}} = \begin{bmatrix} q_0 & q_{0f} & \vdots & \mathbf{0} \\ q_{f0} & q_f & & \\ \cdots & \cdots & \cdots & \cdots \\ \mathbf{0} & & \vdots & 0 \end{bmatrix}, \tag{A.8}$$

where

$$\begin{aligned} q_0 &= 2\alpha^2\beta^2\int_{t_{k-1}}^{t_k}\left(1-e^{-\alpha(t_k-\tau)}\right)^2 d\tau \\ &= \beta^2\left(2\alpha T_s + 4e^{-\alpha T_s} - e^{-2\alpha T_s} - 3\right) \end{aligned} \tag{A.9}$$

$$\begin{aligned} q_{0f} = q_{f0} &= 2\alpha^2\beta\int_{t_{k-1}}^{t_k}\left(e^{-\alpha(t_k-\tau)} - e^{-2\alpha(t_k-\tau)}\right)d\tau \\ &= \beta\left(1-e^{-\alpha T_s}\right)^2 \end{aligned} \tag{A.10}$$

$$\begin{aligned} q_f &= 2\alpha^2\int_{t_{k-1}}^{t_k} e^{-2\alpha(t_k-\tau)}d\tau \\ &= 1-e^{-2\alpha T_s} \end{aligned} \tag{A.11}$$

$\boldsymbol{\Gamma}$ may then be found by equating the two expressions for the discrete process driving noise covariance (A.6) and (2.33),

$$\mathbf{Q}_{\Gamma w} = \begin{bmatrix} q_\theta & q_{\theta f} & \mathbf{0} \\ q_{f\theta} & q_f & \\ \mathbf{0} & & 0 \end{bmatrix} = \begin{bmatrix} \gamma_\theta & \gamma_{\theta f} & \mathbf{0} \\ \gamma_{f\theta} & \gamma_f & \\ \mathbf{0} & & 0 \end{bmatrix} \begin{bmatrix} \gamma_\theta & \gamma_{\theta f} & \mathbf{0} \\ \gamma_{f\theta} & \gamma_f & \\ \mathbf{0} & & 0 \end{bmatrix}^{\mathrm{T}} = \mathbf{Q}_\Gamma, \tag{A.12}$$

allowing the elements of $\mathbf{\Gamma}$ to be readily found. Thus

$$\gamma_\theta = \beta\left(2\alpha T_s + 4e^{-\alpha T_s} - e^{-2\alpha T_s} - 3\right)^{\frac{1}{2}} \tag{A.13}$$

$$\gamma_{\theta f} = \gamma_{f\theta} = \sqrt{\beta}\left(1 - e^{-\alpha T_s}\right) \tag{A.14}$$

$$\gamma_f = \left(1 - e^{-2\alpha T_s}\right)^{\frac{1}{2}} \tag{A.15}$$

for $\alpha \geq 0$.

A.2. Phase Modulation

The model for phase modulation is contained in that of frequency modulation; the state equation for PM is (A.3) less the state variable $x_\theta(t)$. Thus the PM state transition matrix is simply the lower 3×3 submatrix of (2.46) which is (2.41). Only one discrete noise process is needed and $\mathbf{\Gamma}$ becomes the column vector

$$\mathbf{\Gamma} = \begin{bmatrix} \left(1 - e^{-2\alpha T_s}\right)^{\frac{1}{2}} & 0 \end{bmatrix}^{\mathrm{T}}. \tag{A.16}$$

Appendix B. Second-Order DPLL Derived from EKF

In this appendix we derive the "traditional" second-order digital phase lock loop from the Extended Kalman Filter estimator.

B.1. Phase and Frequency Estimator

Our objective is to derive a DPLL with a baseband model of Fig. 4–8 starting from the Kalman filter equation for the single FM source case. For a single FM source with known amplitude, the EKF estimator from (2.162) is

$$\begin{bmatrix}\hat{\theta}(k)\\ \hat{f}(k)\end{bmatrix}=\begin{bmatrix}1 & \phi_{\theta f}\\ 0 & \phi_f\end{bmatrix}\begin{bmatrix}\hat{\theta}(k-1)\\ \hat{f}(k-1)\end{bmatrix}+\begin{bmatrix}P_\theta(k) & P_{\theta f}(k)\\ P_{f\theta}(k) & P_f(k)\end{bmatrix}R_v^{-1}\begin{bmatrix}\varphi'_\theta(k)\\ \varphi'_f(k)\end{bmatrix}, \tag{B.1}$$

where from (2.163)

$$\boldsymbol{\varphi}'(k)=\begin{bmatrix}\varphi'_\theta(k)\\ \varphi'_f(k)\end{bmatrix}=\begin{bmatrix}\sqrt{2}A\cos\left(\hat{\Theta}\right)z(k)\\ 0\end{bmatrix}, \tag{B.2}$$

with measurement

$$\begin{aligned} z(k) &= \sqrt{2}A\sin(\Theta)+v(k)\\ &= \sqrt{2}A\sin\left(\omega_c kT_s+\theta(k)\right)+v(k)\end{aligned} \tag{B.3}$$

For notational convenience, (B.1) is rewritten as

$$\hat{\mathbf{x}}(k)=\hat{\mathbf{x}}(k\mid k-1)+\mathbf{P}(k)R_v^{-1}\boldsymbol{\varphi}'(k), \tag{B.4}$$

with state prediction

$$\hat{\mathbf{x}}(k\mid k-1)=\boldsymbol{\Phi}\hat{\mathbf{x}}(k-1). \tag{B.5}$$

This results in the general DPLL realization of Fig 2–5. The auto-regressive part of the loop filter, shown in Fig. B–1, is

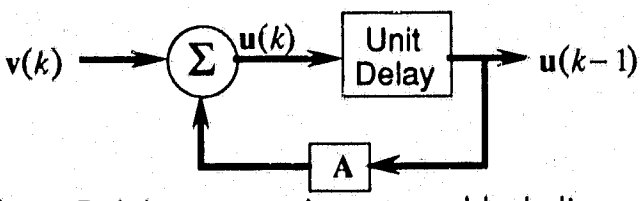

Figure B–1 Auto-regressive process block diagram.

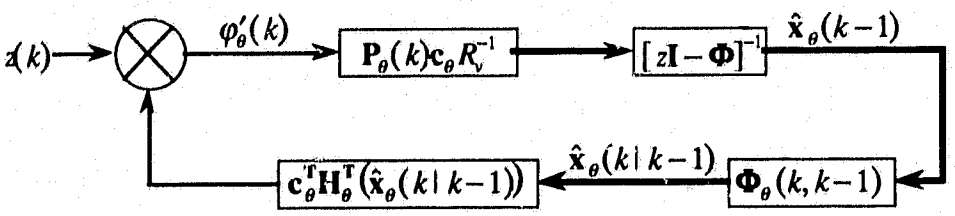

Figure B–2 Simplified EKF phase and frequency estimator.

$$\mathbf{u}(k) = \mathbf{A}\mathbf{u}(k-1) + \mathbf{v}(k) \tag{B.6}$$

which may be written in the z-domain as

$$\begin{aligned} \mathbf{U}(z) &= \mathbf{A}z^{-1}\mathbf{U}(z) + \mathbf{V}(z) \\ \mathbf{U}(z) - \mathbf{A}z^{-1}\mathbf{U}(z) &= \mathbf{V}(z) \\ z\mathbf{U}(z) - \mathbf{A}\mathbf{U}(z) &= z\mathbf{V}(z) \\ \mathbf{U}(z) &= z\mathbf{V}(z)[z\mathbf{I} - \mathbf{A}]^{-1} \end{aligned} \tag{B.7}$$

However, the output of interest in Fig. B–1 is $\mathbf{u}(k-1)$, not $\mathbf{u}(k)$. Multiplying both sides of (B.7) by the unit delay z^{-1} yields

$$\begin{aligned} z^{-1}\mathbf{U}(z) &= z^{-1}z\mathbf{V}(z)[z\mathbf{I} - \mathbf{A}]^{-1} \\ &= \mathbf{V}(z)[z\mathbf{I} - \mathbf{A}]^{-1} \end{aligned} \tag{B.8}$$

Thus Fig 2–5 simplifies to Fig. B–2.

To transform Fig. B–2 to the baseband model, (B.3) and (B.2) are substituted into (4.8)

$$\begin{aligned} \varphi'_\theta(k) &= \sqrt{2}A\cos\left(\hat{\Theta}\right)\sqrt{2}A\sin(\Theta) + \sqrt{2}A\cos\left(\hat{\Theta}\right)v(k) \\ &= 2A^2\left[\sin\left(\theta(k) - \hat{\theta}(k\,|\,k-1)\right) + \sin\left(2\omega_c kT_s + \theta(k) + \hat{\theta}(k\,|\,k-1)\right)\right] + v'(k) \end{aligned} \tag{B.9}$$

where from (4.10)

$$v'(k) = v_I(k)\cos\left(\hat{\theta}(k\,|\,k-1)\right) + v_Q(k)\sin\left(\hat{\theta}(k\,|\,k-1)\right). \tag{B.10}$$

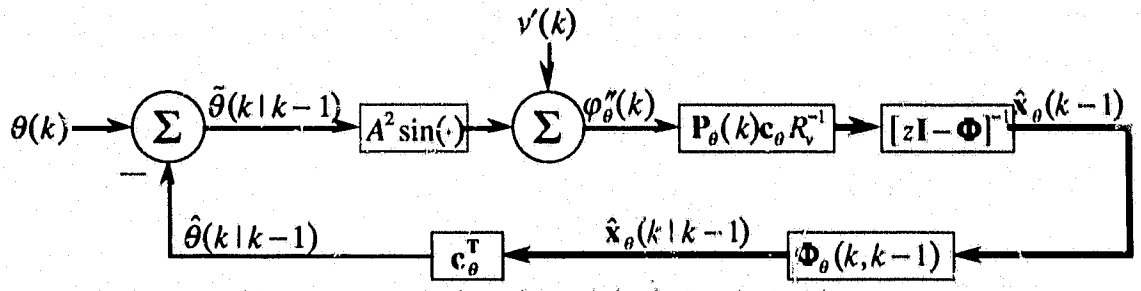

Figure B–3 Baseband model of EKF derived DPLL.

The double frequency term will be removed by the loop filter. Thus the baseband form becomes

$$\varphi''_\theta(k) = 2A^2\sin\Big(\theta(k)-\hat{\theta}(k)\Big)+\nu'(k) \tag{B.11}$$

In effect, the baseband model reduces the observation matrix $\mathbf{H}_\theta^{\mathrm{T}}\big(\mathbf{x}(k\,|\,k-1),k\big)$ to simply the selection vector $\mathbf{c}_\theta^{\mathrm{T}}$. This results in the baseband representation of Fig. B–3.

From the baseband model

$$\hat{\theta}(k\,|\,k-1) = \mathbf{c}_\theta^{\mathrm{T}}\mathbf{\Phi}[z\mathbf{I}-\mathbf{\Phi}]^{-1}\mathbf{P}(k)R_\nu^{-1}\mathbf{c}_\theta\varphi''(k), \tag{B.12}$$

which results in the transfer function

$$\begin{aligned}\frac{\hat{\theta}(k\,|\,k-1)}{\varphi''(k)} &= \mathbf{c}_\theta^{\mathrm{T}}\mathbf{\Phi}[z\mathbf{I}-\mathbf{\Phi}]^{-1}\mathbf{P}(k)R_\nu^{-1}\mathbf{c}_\theta \\ &= \begin{bmatrix}1 & 0\end{bmatrix}\begin{bmatrix}1 & \phi_{\theta f}\\ 0 & \phi_f\end{bmatrix}\begin{bmatrix}\dfrac{1}{z-1} & \dfrac{\phi_{\theta f}}{(z-1)(z-\phi_f)}\\ 0 & \dfrac{1}{z-\phi_f}\end{bmatrix}\begin{bmatrix}P_\theta(k) & P_{\theta f}(k)\\ P_{f\theta}(k) & P_f(k)\end{bmatrix}\begin{bmatrix}1\\0\end{bmatrix}R_\nu^{-1},\end{aligned} \tag{B.13}$$

which simplifies to

$$\frac{\hat{\theta}(k\,|\,k-1)}{\varphi''(k)} = \underbrace{\frac{1}{z-1}}_{\text{clock}}\underbrace{\frac{\big[P_\theta(k)+\phi_{\theta f}P_{f\theta}(k)\big]R_\nu^{-1}z-P_\theta(k)R_\nu^{-1}\phi_f}{z-\phi_f}}_{\text{loop filter}}. \tag{B.14}$$

When (B.14) is compared to Fig. 4–8, the tranfer function may be decomposed into the clock and the loop filter.

The second order DPLL has a first order loop filter with transfer function [20]

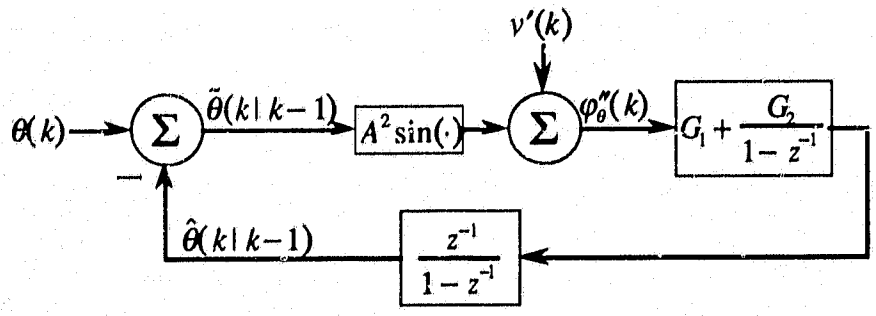

Figure B–4 Baseband model of EKF derived second-order DPLL.

$$D(z)=\frac{(G_1+G_2)z-G_1}{z-1}. \tag{B.15}$$

which is very similar to the loop filter of (B.14). The presense of the ϕ_f term in (B.14), due to the state transition term for the state f, may be set equal to unity since from (2.48) $\phi_f = e^{-\alpha T_s}$ where $\alpha T_s << 1$. So replacing this imperfect integrator (or summer) in (B.14)

$$\frac{\hat{\theta}(k|k-1)}{\varphi''(k)}=\frac{1}{z-1}D(z)=\frac{1}{z-1}\frac{\left[P_\theta(k)+\phi_{\theta f}P_{f\theta}(k)\right]R_v^{-1}z-P_\theta(k)R_v^{-1}}{z-1}. \tag{B.16}$$

where

$$G_1=P_\theta(k)R_v^{-1}, \tag{B.17}$$

$$G_2=\phi_{\theta f}P_{f\theta}(k)R_v^{-1}, \tag{B.18}$$

resulting in the baseband model of the second order DPLL of Fig. B–4.

B.2. Phase, Frequency, and Amplitude Estimator

The inclusion of amplitude estimation is an easy progression from the previous section. Staring from (2.168)

$$\begin{bmatrix}\varphi'_\theta(k)\\ \varphi'_f(k)\\ \varphi'_A(k)\end{bmatrix}=\begin{bmatrix}\sqrt{2}\hat{A}(k|k-1)\cos\left(\hat{\Theta}\right)z(k)\\ 0\\ \sqrt{2}\sin\left(\hat{\Theta}\right)z(k)-\hat{A}(k|k-1)\end{bmatrix}, \tag{B.19}$$

substituting (B.3) and simplifying gives

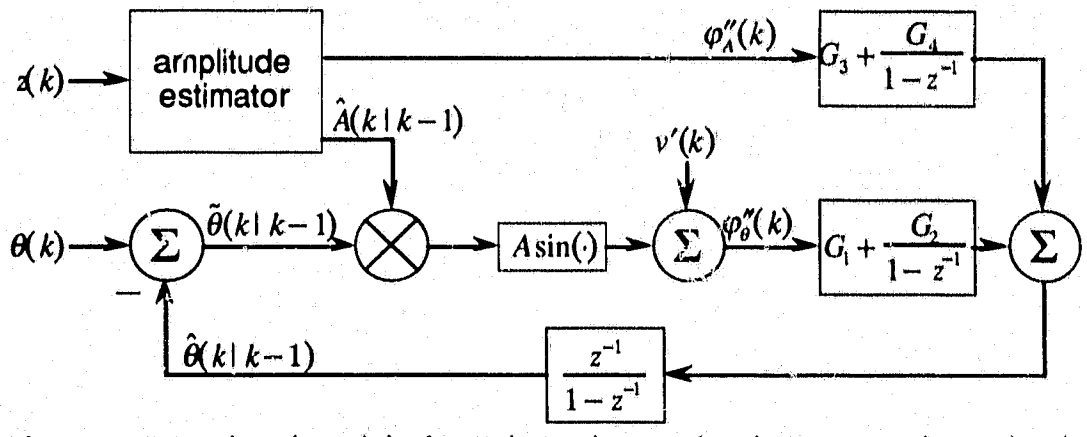

Figure B–5 Baseband model of EKF derived second-order DPLL with amplitude estimator.

$$\begin{bmatrix} \varphi''_\theta(k) \\ \varphi''_f(k) \\ \varphi''_A(k) \end{bmatrix} = \begin{bmatrix} \hat{A}(k|k-1)A\sin\left(\theta(k) - \hat{\theta}(k|k-1)\right) + v'(k) \\ 0 \\ A - \hat{A}(k|k-1) + v'_A(k) \end{bmatrix}, \tag{B.20}$$

where $\varphi''_\theta(k)$ is the same as in (B.11) and

$$v'_A(k) = v_Q(k)\cos\left(\hat{\theta}(k|k-1)\right) - v_I(k)\sin\left(\hat{\theta}(k|k-1)\right). \tag{B.21}$$

As in (B.12),

$$\hat{\theta}(k|k-1) = \mathbf{c}^{\mathrm{T}}\boldsymbol{\Phi}[z\mathbf{I} - \boldsymbol{\Phi}]^{-1}\mathbf{P}(k)R_v^{-1}\boldsymbol{\varphi}''(k) \tag{B.22}$$

which reduces to

$$\hat{\theta}(k|k-1) = \frac{1}{z-1}\left[\frac{[G_1+G_2]R_v^{-1}z - G_1}{z-1}\varphi''_\theta(k) + \frac{[G_3+G_4]R_v^{-1}z - G_3}{z-1}\varphi''_A(k)\right], \tag{B.23}$$

where G_1 and G_2 are defined in (B.17) and (B.18) respectively. Similarly

$$G_3 = P_{\theta A}(k)R_v^{-1}, \tag{B.24}$$

$$G_4 = \phi_{\theta f}P_{fA}(k)R_v^{-1}. \tag{B.25}$$

As the amplitude estimator has an all-pass loop filter, the baseband approximations are not valid for $\hat{A}(k|k-1)$ as given in (2.166). The baseband form of the DPLL with amplitude estimation is shown in Fig. B–5. The DPLL implementation is shown in Fig. 2–20.